Chronic meningeal inflammation as a cause of cortical grey matter pathology in multiple sclerosis

Renée Maria Schalks

September 2014

A thesis submitted for the degree of Doctor of Philosophy of Imperial College London

Wolfson Neuroscience Laboratories

Division of Brain Sciences

Imperial College Faculty of Medicine

Hammersmith Hospital Campus

Burlington Danes Building

Du Cane Road

London W12 0NN

Declaration of originality

I hereby declare that the work described herein is solely that of the author except where otherwise acknowledged. This work has not previously been submitted for any other degree at this or other institutions.

Renée Maria Schalks

September 2014

Copyright declaration

Abstract

Subpial demyelination in cerebral cortical grey matter is associated with clinical progression in multiple sclerosis and is suggested to result from diffusion of pro-inflammatory cytokines from areas of meningeal inflammation into the cortex.

In order to test this hypothesis we have developed an animal model of subpial demyelination driven by meningeal inflammation, involving delivery of cytokines into the subarachnoid space (SAS). Dark Agouti rats were immunised with a subclinical dose (10μg) of recombinant mouse myelin oligodendrocyte glycoprotein followed 21-24 days later by injection of TNF (1.25-5μg) and IFN-γ (75-300ng) into the SAS of the sagittal sulcus. The presence of the cytokines in the SAS resulted in acute demyelination and inflammation followed by resolution of pathology. This supports the hypothesis that cytotoxic/pro-inflammatory molecules diffuse from areas of meningeal inflammation into the underlying cortex resulting in microglial activation and subpial demyelination. Increasing the doses of TNF and IFN-γ resulted in increased extent, but not duration, of pathology due to the acute presence of the cytokines. We conclude that a chronic inflammatory milieu in the CSF/meningeal compartment is required to achieve chronic microglial activation and subpial demyelination and neuronal loss.

In order to achieve the chronic presence of the cytokines in the SAS a high titre VSV-G-pseudotyped lentiviral vector carrying the enhanced green fluorescent protein (eGFP) gene under control of the CMV promoter was tested. It induced extensive and long-term, up to 12 weeks, eGFP expression in the sagittal sulcus in the absence of long-term microglial activation in naïve animals. Expression was localised to astrocytes, leptomeningeal cells and a small number of pyramidal neurons. The vector did not induce non-specific demyelination

and inflammation in animals immunised with a subclinical dose of rmMOG. In order to achieve more localised expression, the vector was injected with collagen hydrogel. The hydrogel delayed eGFP expression but increased its spread along the anteroposterior axis. The distribution and duration of expression appeared optimal for achieving the chronic presence of TNF and IFN-γ in the CSF/meningeal compartment required to develop this novel model, if expression at the injection site could be increased using the hydrogel, which requires optimisation. We propose that the chronic presence of the cytokines will result in chronic meningeal inflammation and cortical grey matter pathology, allowing evaluation of the role of cytotoxic/pro-inflammatory molecules.

The identity of several of the cytotoxic/pro-inflammatory molecules suggested to diffuse from areas of meningeal inflammation were also identified in post-mortem MS meninges using PCR arrays. Expression of CXCL13, IL5RA, IFNG and CXCL9 were increased, and that of CXCL1 decreased, in MS patients, consistent with an inflammatory milieu in the CSF/meningeal compartment and suggesting that these molecules may represent novel therapeutic targets for modulating meningeal inflammation and cortical pathology.

Acknowledgements

First and foremost, I would like to thank my supervisor, Professor Richard Reynolds, for taking me on as a PhD student in his lab four years ago and for giving me this project to work on. His advice and assistance has been invaluable.

I have been lucky enough to work closely with my ‘work wife,’ Miss Eleanor Browne, for most of my time in the Reynolds group and I could not have asked for a better person to do this with, I would not be at this stage without her. All other members of the Reynolds group past and present deserve a shout out for their advice and assistance as well as their company in the lab. Dr Owain Howell and Dr Rachel Bates get a special mention, followed, in no particular order, by Dr Daniele Carassiti, Dr Chris Gardner, Dr Paolo Giannetti, Dr Roberta Magliozzi and Dr Joel Raffel, chewing gum dealer. Dr Pascal Durrenberger and Dr Praveen Paul were first ports of call for PCR and other molecular biology issues respectively.

Thanks must go to the staff of Central Biomedical Services at Hammersmith Hospital for processing rat orders and for ensuring happy rats. There are too many names to mention but I am grateful to every one of the staff, although particular thanks go to Mrs Maeve Harrison and Mr Reece Williams.

The experiments described in Chapter 4 were performed in collaboration with Professor Nicholas Mazarakis and Dr Stuart Ellison of the Gene Therapy group at Imperial College London and with Professor Abhay Pandit and Dr Ben Newland of the Network of Excellence for Functional Biomaterials at National University of Ireland, Galway. I am grateful for the opportunity I had to work with these groups and to those mentioned for their help.

Aliquots of CSF and tissue blocks used in Chapter 5 were obtained from the UK Multiple Sclerosis Tissue Bank. The staff, including Dr Djordje Gveric, Mrs Sue Fordham, Mrs Louisa McGuinness and Miss Julia Steele, were incredibly helpful and ensured speedy access to samples and case details.

I must mention Mr Colin Rantle, laboratory manager, for his endless assistance with health and safety issues and for processing Reynolds groups orders on what seemed like a daily basis, and Mrs Hadeel Abdeen for processing orders in Colin's absence.

My PhD studentship was provided by the Medical Research Council via the Centre for Integrative Mammalian Physiology and Pharmacology at Imperial College London, with further funding provided by the British Pharmacological Society, for which I am very thankful.

Last but by no means least, I could not have done this without the encouragement and support of my family, in particular my parents, and my friends, including those I have made on the fourth floor of the Burlington Danes Building. My church family at Duke Street Church, especially the brilliant Kew home group, has also played a huge role and reminded me regularly of God's faithfulness through the ups as well as downs of the last four years.

Dedication

This thesis is dedicated to all the people with MS that I have had the pleasure of meeting, they have moved and motivated me over the last four years.

Table of contents

List of figures

Chapter 5 - Expression of inflammatory cytokines and receptors in meninges in F+ SPMS

Appendix

List of tables

Abbreviations

4S-StarPEG	Poly(ethylene glycol) ether tetrasuccinimidyl glutarate
ABC	Avidin-biotin-peroxidase complex
ANOVA	Analysis of variance
APC	Antigen presenting cell
BAFF	B cell activating factor
BBB	Blood-brain barrier
BSA	Bovine serum albumin
CD	Cluster of differentiation
cDNA	Complementary deoxyribonucleic acid
CBS	Central Biomedical Services
CCL	Chemokine (C-C motif) ligand
CCR	Chemokine (C-C motif) receptor
CFA	Complete Freund's adjuvant
CIS	Clinically isolated syndrome
CMV	Cytomegalovirus
CNS	Central nervous system
CSF	Cerebrospinal fluid
C_T	Threshold cycle
DA	Dark Agouti
DAB	3, 3'-diaminobenzidine
DAPI	4',6-diamidino-2-phenylindole
dpi	Days post immunisation
EAE	Experimental autoimmune encephalomyelitis
EBV	Epstein-Barr virus
ECL	Electrochemiluminescence
EDSS	Expanded Disability Status Scale
EDTA	Ethylenediaminetetraacetic acid
eGFP	Enhanced green fluorescent protein
ELISA	Enzyme-linked immunosorbent assay
FC	Fold change
F- SPMS	Follicle-negative secondary progressive multiple sclerosis

F+ SPMS	Follicle-positive secondary progressive multiple sclerosis
gDNA	Genomic deoxyribonucleic acid
GM	Grey matter
GML	Grey matter lesion
GOI	Gene of interest
HEK	Human embryonic kidney
HIV-1	Human immunodeficiency virus type 1
HLA	Human leukocyte antigen
HKG	Housekeeping gene
H&E	Haematoxylin and eosin
Iba1	Ionized calcium binding adaptor molecule 1
IF	Immunofluorescence
IFA	Incomplete Freund’s adjuvant
IFN-γ	Interferon-γ
Ig	Immunoglobulin
IHC	Immunohistochemistry
IL	Interleukin
i.p.	Intraperitoneal
IPTG	Isopropyl β-D-1-thiogalactopyranoside
IR	Immunoreactivity
KO	Knockout
LB	Lysogeny broth
LV	Lentivirus / lentiviral
MBP	Myelin basic protein
MHC	Major histocompatibility complex
MMP	Matrix metalloproteinase
MOG	Myelin oligodendrocyte glycoprotein
MRI	Magnetic resonance imaging
mRNA	Messenger ribonucleic acid
MS	Multiple sclerosis
NAGM	Normal appearing grey matter
NF-κB	Nuclear factor-kappa B
NGS	Normal goat serum
NHS	Normal horse serum
NK	Natural killer
NNC	Non-neurological control

NO	Nitric oxide
NOS	Nitric oxide synthase
OPC	Oligodendrocyte precursor cell
PAS	Periodic acid-Schiff
PBS	Phosphate buffered saline pH7.4
PBST	Phosphate buffered saline pH7.4 with 0.1% (v/v) Triton X-100
PCR	Polymerase chain reaction
PFA	Paraformaldehyde
PLP	Proteolipid protein
PMD	Post-mortem delay
PPMS	Primary progressive multiple sclerosis
REST	Relative expression software tool
RIN	RNA integrity number
rmMOG	Recombinant mouse myelin oligodendrocyte glycoprotein
RNA	Ribonucleic acid
rm	Recombinant mouse
rr	Recombinant rat
RRMS	Relapsing remitting multiple sclerosis
RT	Reverse transcription
SAS	Subarachnoid space
s.c.	Subcutaneous
SEM	Standard error of the mean
SOB	Super Optimal Broth
SPMS	Secondary progressive multiple sclerosis
sTNF	Soluble tumour necrosis factor
TBST	Tris-buffered saline pH7.4 with 0.1% (v/v) Tween 20
Tc	Cytotoxic T (lymphocyte)
TCR	T cell receptor
TGF-β	Transforming growth factor-β
Th	Helper T (lymphocyte)
tmTNF	Transmembrane tumour necrosis factor
TNF	Tumour necrosis factor
TNFR	Tumour necrosis factor receptor
TU	Transducing units
VSV-G	Vesicular stomatitis virus glycoprotein
WM	White matter
WML	White matter lesion

Chapter 1

General introduction

1.1 Multiple sclerosis

1.1.1 Introducing multiple sclerosis

Multiple sclerosis (MS) is the most common neurological condition that affects young adults, with approximately 2.3 million people affected worldwide (Multiple Sclerosis International Federation, 2013). It is characterised by foci of demyelination (lesions), astrocyte proliferation (gliosis), inflammation and neuronal/axonal loss in the central nervous system (CNS). It is thought to be an immune-mediated disease that results in the loss of the insulating myelin sheath that surrounds axons that is required for fast saltatory axonal conduction. This in turn results in a wide variety of cognitive, motor and sensory symptoms depending on the site of the pathology.

1.1.2 MS epidemiology and aetiology

The mean age of onset is approximately 30 years, with 70% of patients showing symptoms between the ages of 20 and 40 years and with onset being rare under the age of 10 years and above the age of 60 years (O'Connor, 2002). The sex ratio of MS is dependent on incidence, latitude, and year but is approximately 2:1 female:male (Voskuhl and Gold, 2012), the reason for which is not clear despite extensive research (Compston and Coles, 2002). However, this ratio is in keeping with immune-mediated diseases as a whole; approximately 78% of patients are women (Fairweather *et al.*, 2008). Meta-analysis has confirmed studies that showed positive associations between latitude and prevalence, for areas of European descent and worldwide, with the disease being rare in tropical areas (Simpson *et al.*, 2011). However, systematic review of incidence studies published between 1966 and 2007 showed that this positive association was decreased after 1980, associated with increased incidence at lower latitudes (Alonso and Hernán, 2008), while another meta-analysis of studies published between 1980 and 1998 showed that the association between latitude and incidence was not significant when incidence was adjusted for age (Zivadinov *et al.*, 2003).

These studies, however, are all limited by a lack of incidence studies in Africa, Asia and Central and South America.

Susceptibility appears to have both genetic and environmental components. The genetic component is demonstrated by twin concordance, values of which are approximately 25% and approximately 3% for monozygotic and dizygotic twins respectively in high prevalence areas such as Canada, Denmark and Great Britain (Ebers *et al.*, 1986, Hansen *et al.*, 2005, Mumford *et al.*, 1994). Multiple variants in the human leukocyte antigen (HLA) regions, which encode proteins involved in antigen presentation, have been found to contribute to susceptibility (Jersild *et al.*, 1972, Gourraud *et al.*, 2012). The strongest susceptibility locus is the HLA DRB1*15:01 haplotype, which is carried by 28-33% of Northern Caucasian MS patients compared with 9-15% of healthy controls, corresponding to a mean odds ratio of 3.08 (Sawcer *et al.*, 2011). A large genome-wide association study involving 9,772 cases identified genes implicated by proximity to single nucleotide polymorphisms showing evidence of association with MS, which were found to be enriched with genes related to lymphocyte function, in particular those involved in T helper (Th) cell differentiation. It also identified a receptor for the pro-inflammatory cytokine tumour necrosis factor (TNF), TNFR1, which is discussed in detail in 1.3.3.4 (Sawcer *et al.*, 2011). A recent study determined that there are 110 non-HLA risk genes, which, together with HLA effects, explain 28% of the sibling recurrence risk (Beecham *et al.*, 2013). However, a study that compared the genomes, epigenomes and transcriptomes of discordant monozygotic twins found no differences in HLA regions, single nucleotide polymorphisms shown to contribute to MS susceptibility, copy number variations or gene expression in cluster of differentiation (CD) 4+ T cells that explained discordance (Baranzini *et al.*, 2010), indicating the contribution of the environmental component.

Migration studies, however, have shown that the timing of exposure to the environmental component may determine subsequent susceptibility. For example, migration from high to

low prevalence areas before the age of 15 years decreases susceptibility, whereas migration after the age of 15 years does not (Kurtzke *et al.*, 1970), hence studies investigating the environmental component are difficult to perform and interpret.

One of the proposed explanations for the positive association between latitude and prevalence is the decreased exposure to sunlight at higher latitude. Decreased ultraviolet B exposure has been associated with prevalence (Orton *et al.*, 2011, Ramagopalan *et al.*, 2011), thought to result from vitamin D deficiency. Prevalence increased with decreasing 25-hydroxyvitamin D concentrations in serum (Munger *et al.*, 2006), which are associated with higher Expanded Disability Status Scale (EDSS) scores and lower brain parenchymal fraction (Weinstock-Guttman *et al.*, 2011). Sequence analysis has localized a vitamin D response element to the promoter region of HLA-DRB1 (Ramagopalan *et al.*, 2009), supporting a connection between the main genetic and environmental components of susceptibility.

Epstein-Barr virus (EBV) is one of the infectious agents thought to be involved in MS aetiology. EBV infects approximately 95% of people worldwide but usually remains asymptomatic. Meta-analysis of 13 case control studies showed that 99.5% of MS cases were EBV seropositive compared to 94% of control cases (Ascherio and Munger, 2007). Cellular and humoral responses to the EBV-encoded nuclear antigen 1 were increased in clinically isolated syndrome (CIS) cases, and were correlated with the number of T2 lesions on magnetic resonance imaging (MRI) scans at baseline and with the number of new T2 lesions on MRI and EDSS after a mean of 7 years follow-up (Lünemann *et al.*, 2010). The same study showed that increased specific immunoglobulin (Ig) G responses predicted conversion of CIS to MS (Lünemann *et al.*, 2010), suggesting a role for infectious aetiology.

1.1.3 Clinical features of MS

1.1.3.1 Symptoms

The characteristic symptoms of MS are Lhermitte's symptom (electrical sensation running down the limbs or spine when the head is bent forward) and Uhtoff's phenomenon (worsening of symptoms when the body gets overheated as a result of exercise, fever or hot bath or weather). The remaining symptoms also result from demyelination and depend on the site of the pathology. They include impaired speech and swallowing, vertigo, paroxysmal symptoms, ataxia, tremor, cognitive impairment, motor symptoms, unilateral loss of vision, bladder and erectile dysfunction, spasticity and weakness (Compston and Coles, 2008). Other symptoms include fatigue and pain. Affective symptoms are relatively common, although it is unclear whether they are a consequence of pathology or psychological reaction (Minden, 2000).

1.1.3.2 Diagnosis

Diagnosis requires the demonstration of dissemination of lesions in space and time and the exclusion of alternative diagnoses and can be made based on clinical presentation alone. However, MRI scans can replace some clinical criteria as described by the 2010 revisions to the McDonald Criteria (Polman *et al.*, 2011). When a patient presents with at least 2 episodes but objective clinical evidence of only 1 lesion, dissemination of lesions in space can be demonstrated with at least 1 T2 lesion on MRI in at least 2 of 4 areas considered to be characteristic for MS (infratentorial, juxtacortical, periventricular, spinal cord). Alternatively, when a patient presents with only 1 episode but objective clinical evidence of at least 2 lesions, dissemination in time can be demonstrated with a new T2 and/or gadolinium-enhancing (inflammatory activity) lesion on follow-up MRI when compared to baseline or simultaneous asymptomatic gadolinium-enhancing and non-enhancing lesions at any time. Positive cerebrospinal fluid (CSF) findings (increased IgG index or isoelectric focusing evidence of oligoclonal bands) may be used to support diagnoses (Polman *et al.*,

2011). Meta-analysis of 71 studies showed that oligoclonal bands were present in 87.7% of 12,253 MS and 68.6% of 2,685 CIS patients and predicted conversion of CIS to MS (Dobson *et al.*, 2013) and may hence be used to supplement clinical criteria and MRI scans.

1.1.3.3 Clinical course

In 80% of patients, MS initially presents as one acute episode of neurological dysfunction (CIS), followed by a period of recovery (remission) and subsequent further episode (relapse), termed relapsing-remitting MS (RRMS). The frequency of relapses is on average approximately 1.5 per year (Compston and Coles, 2008), but is highly variable from patient to patient. More relapses in the first 2 years and a shorter interval between the first 2 relapses have been shown to be associated with shorter intervals between disease onset and disease milestones (Scalfari *et al.*, 2010). After approximately 10 years the recovery from relapses becomes incomplete resulting in an accumulation of chronic symptoms. This occurs in approximately 65% of RRMS patients and is termed secondary progressive MS (SPMS; Compston and Coles, 2008). Approximately 11% of patients will present with an accumulation of symptoms from onset (Reynolds *et al.*, 2011). This is termed primary progressive MS (PPMS).

Disease milestone data from 431 cases in the UK MS Tissue Bank population-based cohort established a median age of onset of 31.5 years, age at progression to SPMS of 44 years, age at which patients required the use of a wheelchair of 50 years and age of death of 62 years (Reynolds *et al.*, 2011). The median disease duration is 23-30.5 years (Scalfari *et al.*, 2010, Reynolds *et al.*, 2011), resulting in a decrease in life expectancy of 5-10 years (Brønnum-Hansen *et al.*, 2004). MS is cited as the cause of death in 60% of MS patients (Reynolds *et al.*, 2011), with the resulting increased frequency of infections and suicides contributing to the remainder (Compston and Coles, 2008).

It has been shown that relapses are associated with acute inflammation and accompanying demyelination involving cytotoxic T cells and activated macrophages/microglia (Kuhlmann *et al.*, 2002), whereas progression is associated with an accumulation of axonal and neuronal loss and a relative lack of inflammation (Figure 1.1; Compston and Coles, 2008, Reynolds *et al.*, 2011).

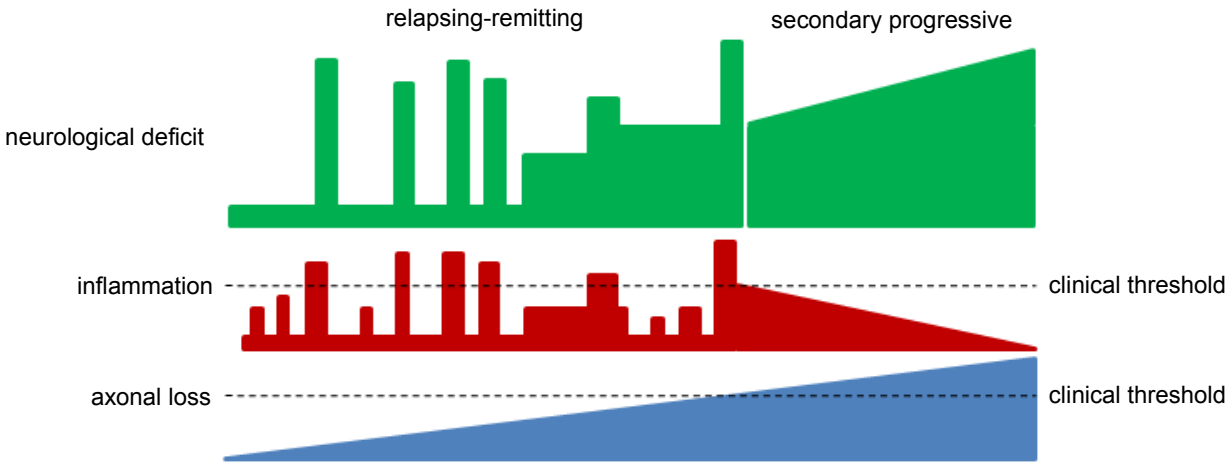

Figure 1.1. Representation of the relationship between neurological deficit, inflammation and axonal loss in RRMS and SPMS. Adapted from Compston and Coles, 2008.

1.2 MS pathology

1.2.1 White matter lesions

1.2.1.1 Destruction of myelin

The pathological hallmark of MS is the presence of foci of inflammation, consisting of perivascular cuffs of T lymphocytes and monocytes/macrophages. These are associated with changes in blood-brain barrier (BBB) permeability and oligodendrocyte loss and demyelination (Reynolds *et al.*, 2011) and are termed lesions, which can be observed on macroscopic observation in major white matter (WM) tracts. Although lesions may occur anywhere in the CNS parenchyma, the WM lesions (WMLs) considered to be characteristic of MS for diagnostic purposes as stated in the 2010 revisions to the McDonald Criteria and described in 1.1.3.2, are infratentorial, juxtacortical, periventricular and spinal cord lesions (Polman *et al.*, 2011). Astrocytes respond to active inflammation and demyelination with hypertrophy and proliferation, which persist in chronic lesions resulting in gliosis and the formation of a glial scar in the majority of WMLs (Brosnan and Raine, 2013). Multiple small WMLs may merge to form large confluent plaques (Popescu and Lucchinetti, 2012) and slowly expanding demyelination surrounding WMLs has also been identified in both clinical MRI and neuropathological studies. These WMLs exhibit a rim of activated microglia at their border, some of which contain early myelin degradation products (Lassmann, 2008) and may be observed surrounding old, gliotic WMLs lacking perivascular cuffs in autopsy samples from SPMS patients (Prineas *et al.*, 2001).

Remyelination of axons by oligodendrocyte lineage cells was first identified using electron microscopy in 1965 (Périer and Grégoire, 1965) by sharply demarcated areas of uniformly thin myelin sheaths. It starts early during lesion formation (Prineas *et al.*, 1993a, Lucchinetti *et al.*, 1999, Goldschmidt *et al.*, 2009) and is variable, but may be extensive (Patrikios *et al.*, 2006, Patani *et al.*, 2007). For example, a study using autopsy samples showed

remyelination of 60-96% of the total lesion area in 20% of all 51 patients, including SPMS and PPMS as well as RRMS patients, whereas remyelination of 0-25% was observed in 67% of all patients (Patrikios *et al.*, 2006). However, remyelinated areas may be more susceptible to repeated demyelination than normal appearing WM (Prineas *et al.*, 1993b).

1.2.1.2 WML classification

WMLs may be classified into stages in order to determine the sequence of events in pathogenesis. Several systems have been proposed, including those based on lesion distribution and location, inflammation extent and pattern, presence of myelin/myelin degradation products in macrophages, extent of remyelination, pattern of oligodendrocyte loss and presence of complement deposition, and which system is used depends to some extent on the area of research.

WMLs are usually classified as active, chronic active or chronic inactive based on the extent and pattern of inflammation. Active lesions are defined as those with macrophage infiltration throughout the lesion; macrophages contain myelin degradation products positive for all myelin proteins including the minor components, such as myelin oligodendrocyte glycoprotein (MOG) and CNPase (2',3'-cyclic-nucleotide 3'-phosphodiesterase). Chronic active lesions are defined as those with infiltration at the lesion edge but little at the centre; myelin degradation products are positive for major myelin proteins, such as myelin basic protein (MBP) and proteolipid protein (PLP), only. Finally, chronic inactive lesions are defined as those with little infiltration throughout; macrophages contain empty vacuoles or myelin degradation products positive for periodic acid-Schiff (PAS; Bö *et al.*, 1994, Brück *et al.*, 1994, Trapp *et al.*, 1998, van der Valk and De Groot, 2000). Two remyelinating WML stages have also been proposed. Early remyelinating lesions are defined as those with macrophage infiltration and some axons surrounded by thin myelin sheaths; macrophages contain empty vacuoles or myelin degradation products positive for PAS. Late remyelinating lesions or shadow plaques are defined as those with few macrophages and myelinated

axons; myelin sheaths are thinner and axon density is lower than in surrounding WM and gliosis is present (Brück *et al.*, 1994).

A study using mainly biopsy samples taken shortly after disease onset found heterogeneity in active lesions between cases, resulting in their further classification based on the proposed mechanism of demyelination. Type I lesions were defined as those with lesional oligodendrocyte loss without complement activation, Type II as those Type I lesions with complement activation, Type III as those with lesional and perilesional oligodendrocyte apoptosis without complement activation and with an intact BBB and Type IV as those with lesional and perilesional oligodendrocyte loss but not apoptosis (Lucchinetti *et al.*, 2000). All active lesions in one case were of the same type. However, a later study using autopsy samples from cases with established MS found homogeneity in active lesions between cases, hence it was proposed that the initial heterogeneity found in the early stages of pathogenesis may disappear as different mechanisms converge into one general mechanism (Breij *et al.*, 2008).

1.2.1.3 WML pathogenesis

The proposed mechanism of demyelination in the WM involves the inflammation-induced destruction of the myelin sheath that surrounds axons (Lassmann *et al.*, 2001). Briefly, myelin-reactive T (Th CD4+ and T cytotoxic (Tc) CD8+) cells are activated in the periphery, expand and traffic to the CNS (Hafler and Weiner, 1987), which they enter across an activated BBB expressing adhesion molecules (Minagar and Alexander, 2003) or across the blood-CSF barrier that constitutively expresses adhesion molecules (Ransohoff *et al.*, 2003). These T cells become reactivated on encountering their specific myelin epitope presented by microglia and perivascular macrophages, the antigen presenting cells (APCs) of the CNS, proliferate and form perivascular cuffs in the WM and accumulate in the meninges (Compston and Coles, 2008). They release pro-inflammatory cytokines including TNF and interferon-γ (IFN-γ), which results in the upregulation of adhesion molecules on the BBB,

facilitating further entry of T and B cells, plasma cells and macrophages to the CNS (Hellings *et al.*, 2002), as well as direct cytotoxicity to oligodendrocytes (Buntinx *et al.*, 2004). Although the phagocytosis of myelin by macrophages results in demyelination, additional immune effector mechanisms have been proposed. The sustained presence of auto-antibodies against the myelin antigens MBP and MOG in CSF and sera from MS patients has been detected (Reindl *et al.*, 1999) and antibody deposition is thought to be a major mechanism of demyelination. Ig deposition in active, demyelinating lesions was found in approximately 50% of MS patients (Lucchinetti *et al.*, 2000) and myelin-oligodendrocyte complexes may be damaged by complement activation as well as antibody-dependent cytotoxicity (Lassmann *et al.*, 2001).

The partially demyelinated axons that result from this inflammation-induced demyelination have a decreased capacitance and are not able to transmit fast action potential trains. Depolarisation, though able to traverse lesions, does so at a decreased velocity. These axons may also discharge spontaneously and are more sensitive to mechanical stimuli, resulting in distortion of sensations and symptoms including Lhermitte's symptom and Uhtoff's phenomenon (Compston and Coles, 2008).

Although most lesions are characterised by a relative sparing of axons, it has been shown that axonal damage and loss within lesions in both the brain and spinal cord does occur (Trapp *et al.*, 1998, Lovas *et al.*, 2000) and that it is associated with both demyelination and inflammation in all lesion types and at all disease stages (Lassmann *et al.*, 2001, Frischer *et al.*, 2009). Acute axonal damage, determined by the presence of amyloid precursor protein in axon end bulbs and spheroids indicating impaired axonal transport, is observed in active WMLs regardless of disease duration but is most apparent 1 year after disease onset and decreases more than 10 years after disease onset (Kuhlmann *et al.*, 2002). However, other studies have shown a 58-61% reduction in axonal density in spinal cord lesions in progressive MS patients with long disease duration (Bjartmar *et al.*, 2000,

Lovas *et al.*, 2000). Axonal damage and loss appear to be highly variable and correlated with infiltration of activated macrophages/microglia and B and T (mainly CD8+) cells (Trapp *et al.*, 1998, Frischer *et al.*, 2009, Kuhlmann *et al.*, 2002), which release, for example, nitric oxide (NO; Hill *et al.*, 2004) that results in decreased ATP (adenosine triphosphate) production in demyelinated axons and induce calcium-mediated axonal degeneration (Dutta *et al.*, 2006). The level of N-acetylaspartate in the brain can be used as a neuronal and axonal marker *in vivo.* It is age-dependently decreased in RRMS patients compared to healthy controls (Gonen *et al.*, 2000) and, as well as being correlated with WML volume, is also correlated with EDSS score in RRMS but not progressive MS patients (De Stefano *et al.*, 1998). Hence, although axonal damage and loss are present in WMLs in progressive MS patients with long disease duration and correlate with disability, indicating a role for axonal pathology in progression, they are not able to account for the accumulation of chronic symptoms that are not attributable to WMLs (Reynolds *et al.*, 2011).

1.2.2 Grey matter lesions

1.2.2.1 Grey matter lesion prevalence historically underestimated

Established cortical grey matter (GM) lesions (GMLs) are characterised by microglial activation, oligodendrocyte loss and demyelination in GM characteristically associated with only mild peripheral immune cell infiltration. Studies using autopsy samples have shown that the density of CD4+ and CD8+ T cells is lower in GMLs than WMLs (Bø *et al.*, 2003a) and is not different to that in normal appearing GM (NAGM), which was also the case for the density of macrophages/microglia (Peterson *et al.*, 2001). However, a study using biopsy samples from early MS patients showed that T cells and microglia are present in 82% and 100% of GMLs respectively, while macrophages containing myelin were present in GMLs from 66% of patients (Lucchinetti *et al.*, 2011). A subsequent study using autopsy samples from SPMS patients showed that activated microglia and perivascular cuffs, consisting of CD8+ T cells, CD20+ B cells and Ig+ plasmablasts/plasma cells, are present in a subset of

cases (Magliozzi *et al.*, 2013), suggesting a role for immune cell infiltration in established in addition to early GMLs. Additionally, the integrity of the BBB appears to be preserved in GMLs, indicated by a lack of plasma protein leakage and basement membrane and tight junction changes (van Horssen *et al.*, 2007). However, another study showed a thinning, and in some places a loss, of the glia limitans as a result of astrocyte loss in GMLs (Magliozzi *et al.*, 2010) and gliosis does not appear to be a feature of GMLs (van Horssen *et al.*, 2007). Neuronal and synapse loss has been detected in GMLs (Wegner *et al.*, 2006), as have transected axons and dendrites displaying spheroids, which were in contact with activated microglia and associated with the level of inflammation in the lesion (Peterson *et al.*, 2001). This study also showed the presence of neuronal apoptosis, mainly that of pyramidal neurons, in cortical layers 3 and 5. Neuronal loss of pyramidal neurons in cortical layers 3 and 5 was confirmed in a subset of cases in a subsequent study (Magliozzi *et al.*, 2010).

MS has always been regarded as predominantly a WM disease due to the macroscopic observation of lesions in major WM tracts. Although GMLs have been observed in neuropathological studies since 1892 (Taylor, 1892; reviewed in Kutzelnigg and Lassmann, 2005), their pathological importance has been underestimated, perhaps because conventional histochemical stains, such as Luxol Fast Blue that detects myelin lipids, miss the superficial GMLs (Geurts *et al.*, 2012), which are also not visible on MRI scans using conventional sequences (Kidd *et al.*, 1999). However, studies have since shown that GML burden may be greater than that of WMLs.

MBP immunohistochemistry using autopsy samples from chronic MS patients demonstrated a mean demyelinated area in the cerebral cortex of 25% compared to 5% in subcortical and periventricular WM (Bø *et al.*, 2003b). Subsequent studies have shown similar mean demyelinated areas; PLP immunohistochemistry demonstrated areas of 28.8% in motor cortex, cingulate gyrus, cerebellum, thalamus and spinal cord GM compared to 15.6% in corresponding WM (Gilmore *et al.*, 2009). Additionally, GM rather than WM fraction volume

relative to total intracranial volume has been correlated with EDSS and regression modelling has shown that GM fraction volume is able to explain more of the variability in clinical symptoms over 20 years following presentation with CIS than WM fraction volume (Fisniku *et al.*, 2008).

1.2.2.2 GML classification

Initial studies identified 7 different GML types based on their location relative to the venous supply of the cerebral cortex (Kidd *et al.*, 1999), but further studies proposed a simpler classification based on their location within the layers of the cortex (Figure 1.2; Peterson *et al.*, 2001, Bø *et al.*, 2003b). Type I lesions (leukocortical) involve deep GM layers as well as the WM at the GM/WM border but not superficial GM or WM, Type II (intracortical) are confined to GM, do not involve superficial GM or WM and are usually small and centred on a blood vessel, Type III extend from the pial surface into GM layer III or IV and Type IV extend the width of the cortex without entering WM. Type III and IV lesions are known as subpial lesions and may involve multiple gyri. Subpial lesions account for up to 50-70% of all GMLs followed by Type 1 lesions, which account for 25-34% (Peterson *et al.*, 2001, Bø *et al.*, 2003a, Magliozzi *et al.*, 2007).

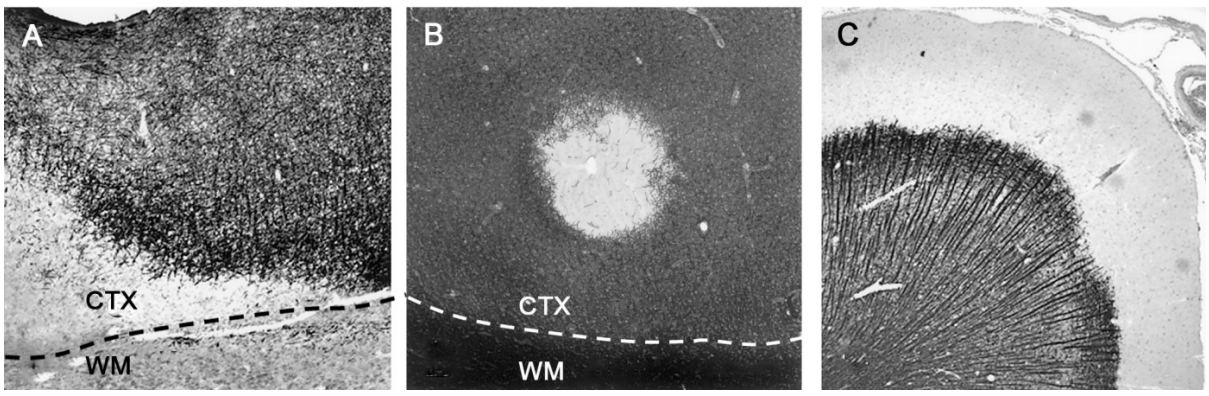

Figure 1.2. Current GML classification based on location within the layers of the cortex. Type I lesions (A) involve both WM and GM (CTX), Type II lesions (B) involve only the GM and are usually small and centred on a blood vessel and subpial lesions (Type III and Type IV; C) extend from the pial surface into the GM. Adapted from Peterson *et al.*, 2001.

1.2.2.3 GMLs occur throughout the CNS in progressive MS

The development of sensitive immunohistochemical stains using antibodies to myelin has led to increased understanding of the prevalence and spatiotemporal patterns of GMLs. Periventricular WMLs were found to be characteristic of acute MS and RRMS, whereas GMLs and more diffuse WM inflammation were characteristic of PPMS and SPMS (Kutzelnigg *et al.*, 2005). One study using post-mortem samples from mainly SPMS cases found that 28.8% of GM was demyelinated compared to 15.6% of WM, with demyelination in GM being greater than that in WM in cingulate gyrus, motor cortex, thalamus, cerebellum and spinal cord (Gilmore *et al.*, 2009). This study showed particularly prominent GM demyelination in cingulate gyrus and spinal cord. The hippocampus is another area affected by GM demyelination in progressive MS, with one study showing 30.4% GM demyelination (Papadopoulos *et al.*, 2009) and another showing decreased expression of neuronal proteins required for learning and memory (Dutta *et al.*, 2011), which may explain the memory impairments seen in MS. In the cerebellum in progressive MS, a mean of 38.7% and a maximum of 92% GM demyelination have been observed (Kutzelnigg *et al.*, 2007).

1.2.2.4 GMLs detected using MRI

More sensitive MRI techniques, such as double inversion recovery, have led to a five-fold increase in the detection of GMLs compared to conventional T2-weighted sequences (Geurts *et al.*, 2005). However, approximately 80% of GMLs detected using immunohistochemical stains were missed, in particular subpial GMLs (Seewann *et al.*, 2012). Ultra-high field MRI using a field strength of 9.4T, which is not yet widely available, was able to detect 77% of GMLs detected using immunohistochemical stains using post-mortem brains (Schmierer *et al.*, 2010), and the authors suggested that this finding may be translated to high field MRI using field strengths of 3T or 5T.

Nonetheless, recent studies using double inversion recovery have demonstrated a high frequency of GMLs, as well as their presence early in the disease course, including in patients presenting with CIS (Calabrese *et al.*, 2007). Although it is not yet clear how early in the course of MS GMLs appear, several studies suggest that it may be prior to WMLs. Two of these were case studies documenting patients presenting with GMLs (Coebergh *et al.*, 2010, Popescu *et al.*, 2011), while one study described 4 MS patients presenting with symptoms characteristic of MS but having normal appearing WM on MRI, in whom GMLs were observed months or years prior to WMLs (Calabrese and Gallo, 2009).

1.2.2.5 Clinical relevance of GMLs

Studies using autopsy samples have also shown that GML area, determined using PLP immunohistochemistry, is correlated with age at death (Gilmore *et al.*, 2009). It is now widely accepted that GM pathology is involved in clinical progression (Calabrese *et al.*, 2010a) and studies, mainly using clinical MRI, have attempted to correlate GM pathology with motor and cognitive disability.

Recent studies suggest that GMLs are associated with motor disability. The number of GMLs correlated with EDSS score in CIS, RRMS and SPMS patients (Calabrese *et al.*, 2007) and a prospective, longitudinal study showed that GML number and volume increases over 3 years were higher in patients with worsening of clinical symptoms over the 3 years (Calabrese *et al.*, 2010b). Additionally, the baseline GML volume correlated with EDSS score increases in RRMS and SPMS, leading the authors to suggest that baseline GML volume may be an independent predictor of worsening of clinical symptoms. These correlations were also found in PPMS after 2 years follow-up (Calabrese *et al.*, 2009c). Conversely, patients with benign MS (EDSS score ≤3 and disease duration ≥15 years) had a lower number of GMLs than early RRMS patients (EDSS score ≤3 and disease duration ≤5 years) at both baseline and after 1 year follow-up, which did not increase over time (Calabrese *et al.*, 2009b). A recent study has confirmed the stronger association of GM

rather than WM atrophy with clinical progression, defined as an increase in EDSS score of ≥1 compared to baseline, over 5 and 10 years follow-up (Jacobsen *et al.*, 2014).

As well as being associated with motor disability, GMLs have also been associated with cognitive disability. For example, the number and volume of GMLs was higher in RRMS patients defined as cognitively impaired using the Rao Brief Repeatable Battery of Neuropsychological Tests than in those defined as cognitively unimpaired, whereas no difference in the number and volume of WMLs was found (Calabrese *et al.*, 2009a).

The extent of GM pathology is variable and depends on the area examined. The cingulate gyrus, frontal and temporal lobes and hippocampus appear to be more severely affected than the motor cortex and occipital lobe (Kutzelnigg *et al.*, 2005, Gilmore *et al.*, 2009, Papadopoulos *et al.*, 2009), which may explain the greater prevalence of cognitive disability resulting from GM pathology than motor disability (Reynolds *et al.*, 2011). One study showed that cognitive disability had been noted in the medical records for all cases with extensive subpial demyelination identified using PLP immunohistochemistry (Bö *et al.*, 2007).

1.2.2.6 GML pathogenesis

Although the exact mechanism of demyelination in the GM remains unclear, several mechanisms have been proposed. These must take into account the mild peripheral immune cell infiltration observed in GMLs compared to WMLs, which are characterised by microglial activation and in which perivascular infiltrates are characteristically rare (Peterson *et al.*, 2001, Magliozzi *et al.*, 2010) as discussed in 1.2.2.1 and the density of B and T cells is the same as that in NAGM (Bø *et al.*, 2003a), as well as the high prevalence of subpial lesions. Additionally, although BBB integrity is compromised in WMLs (Kirk *et al.*, 2003), it appears to be preserved in GMLs (van Horssen *et al.*, 2007), suggesting that the mechanism of GML development may differ from that of WMLs.

One theory is that demyelination and degeneration of axons in the WM result in the same pathology, and the formation of lesions, in the GM by anterograde or retrograde degeneration (Klaver *et al.*, 2013). For example, a study combining whole brain post-mortem MRI with autopsy sample immunohistochemistry found correlation between neurodegeneration in connected cortical areas, WM tracts and thalamus. Neuronal or axonal loss in one area appeared to result in anterograde or retrograde degeneration in connected areas (Kolasinski *et al.*, 2012), which is suggested to result in microglial activation and subsequent oligodendrocyte damage (Lassmann, 2012).

However, one of the leading theories regarding GML pathogenesis is that they result from meningeal inflammation and associated release of pro-inflammatory cytokines. Several studies using autopsy samples have shown that diffuse inflammatory infiltrates are present in the meninges of PPMS and SPMS cases (Guseo and Jellinger, 1975, Howell *et al.*, 2011, Choi *et al.*, 2012, Kutzelnigg *et al.*, 2005) as well as in a study using cortical biopsy samples from early MS patients (Lucchinetti *et al.*, 2011), particularly in those with extensive subpial GM demyelination. Additionally, recent studies have shown that as well as these diffuse inflammatory infiltrates, ectopic lymphoid follicle-like structures are also present in the meninges, particularly those of the sulci, in a significant proportion of SPMS cases (41.4%, 54% and 40% in Magliozzi *et al.*, 2007, Magliozzi *et al.*, 2010 and Howell *et al.*, 2011 respectively), and were associated with subpial lesions. These cases have been defined as F+ SPMS. These lymphoid-like structures consist of aggregates of CD20+ B cells, together with CD35+ follicular dendritic cells, Ki67+ proliferating CD20+ B cells, IgA, -G or -M+ plasmablasts/plasma cells and CD3+ T cells. Their presence in the deep sulci has led to the hypothesis that the decreased flow of CSF in the sulci results in a protected environment that allows the homing and retention of immune cells, which in turn results in an inflammatory milieu in the CSF (Reynolds *et al.*, 2011). Lymphoid-like structures have also been found in the target organs of several other autoimmune and chronic inflammatory conditions, such as atherosclerosis (Houtkamp *et al.*, 2001), autoimmune thyroiditis

(Armengol *et al.*, 2001), myasthenia gravis (Roxanis *et al.*, 2002), rheumatoid arthritis (Magalhães *et al.*, 2002) and Sjögren's syndrome (Salomonsson *et al.*, 2003), where they are associated with disease progression. The development of lymphoid-like structures, or tertiary lymphoid organs, is thought to depend mainly on CXCL13 (chemokine (C-X-C motif) ligand 13), CCL21 (chemokine (C-C motif) ligand 21) and the cytokine lymphotoxin-$\alpha_1\beta_2$ (Aloisi and Pujol-Borrell, 2006).

The presence of lymphoid-like structures in the cerebral meninges of F+ SPMS cases has been correlated with increased GM atrophy as well as increased subpial demyelination, in the absence of any significant change in the number of WMLs (Magliozzi *et al.*, 2010). Their presence is associated with gradients of neuronal loss and microglial activation in cortical layers, with the greatest loss or activation in cortical layer I, as well as with a gradient of astrocyte loss that resulted in a thinning, or loss, of the glia limitans (Magliozzi *et al.*, 2010). These gradients were observed not only in GMLs but also in NAGM. Finally, their presence is associated with a younger age at onset, age at wheelchair dependence and age at death (Magliozzi *et al.*, 2007). A later study using a large, representative sample of 123 SPMS cases showed that diffuse inflammatory infiltrates in the meninges are similarly associated with GM demyelination and a younger age at onset, time to disease progression, time to wheelchair dependence and age at death (Howell *et al.*, 2011). The authors suggest that the presence of lymphoid-like structures represents a more substantial inflammation at one end of a continuum of diffuse meningeal inflammation that may result in a shorter, more aggressive disease (Howell *et al.*, 2011). These findings support the hypothesis that meningeal inflammation results in increased concentrations of pro-inflammatory cytokines in the CSF, which diffuse from the pial surface into the cortex resulting in GM pathology, directly or indirectly through the activation of microglia, and a more severe clinical course (Peterson *et al.*, 2001, Reynolds *et al.*, 2011). This hypothesis remains controversial, however, as another study failed to show a correlation between the extent of subpial demyelination and the extent of meningeal inflammation and also failed to show the

presence of lymphoid-like structures. Additionally, meningeal inflammation was no different in meninges overlying subpial GMLs than in meninges overlying NAGM in autopsy samples from progressive MS cases (Kooi *et al.*, 2009).

However, it has recently been shown in this laboratory that the number of cells expressing the pro-inflammatory cytokines TNF and IFN-γ and the gene expression of these cytokines are increased in the meninges of F+ SPMS patients. TNF was expressed by cells in the meninges with monocyte/macrophage morphology as well as some microglia in superficial GM, whereas IFN-γ was expressed by a proportion of cells in meninges, mainly CD3+ T cells (Gardner *et al.*, 2013). TNF gene expression was significantly increased in meninges of both F+ and F- SPMS cases compared with non-neurological controls (NNCs), with greater upregulation in F+ SPMS, and IFN-γ gene expression was also increased in F+ SPMS cases compared with NNCs, but not in F- SPMS (Gardner *et al.*, 2013). Additionally, the levels of these cytokines in post-mortem CSF of F+ SPMS cases are increased. TNF concentration was increased in CSF from F+ SPMS cases compared with both F- SPMS cases and NNCs whereas this increase did not reach significance for IFN-γ (Gardner *et al.*, 2013). These findings were in agreement with previous studies that showed the presence of monocytes expressing TNF (Magliozzi *et al.*, 2010) and CD8+ T cells expressing IFN-γ (Serafini *et al.*, 2007) in inflamed meninges, and studies that showed increased levels of TNF and IFN-γ in CSF, particularly in that obtained from RRMS patients at relapse (Obradović *et al.*, 2012 and Romme Christensen *et al.*, 2012 respectively).

It has also been proposed that lymphoid-like structures may be sites of EBV infection in MS (Serafini *et al.*, 2007), consistent with serological studies such as that described in 1.1.2 that suggest that EBV is involved in MS aetiology (Ascherio and Munger, 2007). EBV infects naïve B cells, causing them to express viral proteins and become activated. They then become proliferating blasts and undergo germinal centre reactions to differentiate into resting memory B cells, which undergo the transition into long-lived memory B cells

(Thorley-Lawson and Gross, 2004). CD8+ T cells may target these B cells resulting in damage to the underlying GM (Serafini *et al.*, 2007). A study using autopsy samples showed the presence of perivascular cuffs, which appeared to be sites of EBV infection, in subpial GMLs from a subset of F+ SPMS cases (Magliozzi *et al.*, 2013). However, this hypothesis remains controversial, as several studies showed no or rare EBV infection in MS brain (Torkildsen *et al.*, 2010, Willis *et al.*, 2009 respectively).

In summary, there is increasing evidence from clinical MRI and neuropathological studies to support a major role for cortical GM pathology in driving progression in MS (Reynolds *et al.*, 2011). Models will be required to study the relationship between GM pathology and progression in greater detail.

1.3 Lessons learned from *in vivo* and *in vitro* models

1.3.1 Limitations of human tissue studies

The studies using human tissue described above have increased understanding of the pathogenesis of MS and have allowed clinicopathological correlations to be made, leading to the identification of new drug targets. The main benefit of studies using human tissue is that the results obtained are directly relevant to humans. Brain banks operating prospective donor schemes, such as the UK MS Tissue Bank, supply well-characterised brain, spinal cord and CSF samples from population-based cohorts invaluable for research.

The main limitation of studies using human MS tissue is that the majority is obtained at autopsy and hence each case represents only a single time point after variable disease duration, therefore it is not possible to study the development of pathology over time. Researchers also have only limited access to early and immunologically active MS tissue and hence it is difficult to study the earliest stages in the development of pathology. Additionally, due to the variable nature of the clinical course and pathology of MS between patients, clinicopathological correlations require the study of well-characterised tissue from a large number of cases with detailed medical records, the availability of which is limited. As the majority of human MS tissue is obtained at autopsy, several factors may compromise the tissue and molecular preservation of the samples. Both pre-mortem factors, including prolonged agonal state, hypoxia, acidosis, fever and seizures, and post-mortem factors, including long post-mortem delay between death and sample processing, temperature of the cadaver, fixative and sample processing are of concern (Ferrer *et al.*, 2008). Finally, the alteration of experimental conditions is limited in studies using MS tissue compared to those using *in vivo* or *in vitro* models.

The main *in vivo* models that are used are those induced by toxic agents such as the copper chelator cuprizone, those induced by Theiler's murine encephalomyelitis virus and the most widely studied, experimental autoimmune encephalomyelitis (EAE) (Batoulis *et al.*, 2011).

1.3.2 EAE models of MS

EAE involves the immunisation of susceptible animals with a myelin protein, or peptide thereof, together with an adjuvant, or alternatively antigen-specific T cells, resulting in an autoimmune disease with antigen specificity for the endogenous myelin protein, and a demyelinating inflammatory disease similar to MS. Studies using EAE models have led to the view of MS as a T cell-mediated autoimmune disease and have also allowed the development of effective anti-inflammatory and immunomodulatory treatments, although several effective treatments in EAE have failed in clinical trials (Lassmann and van Horssen, 2011).

The exact pathology and clinical course of the disease depends on the species, strain, sex, age and season of the animal, the identity, concentration and species origin of the myelin protein, the physical structure of the myelin protein/adjuvant emulsion and epigenetic factors (Schreiner *et al.*, 2009). The Dark Agouti (DA) rat, Lewis rat and C57BL/6 mouse are the most common animals used, while MOG and MBP are two of the most common myelin proteins used in the induction of EAE. These antigens are emulsified in adjuvant, such as complete or incomplete Freund's adjuvant (CFA and IFA respectively), and pertussis toxin may be required. Animals present with ascending paralysis, as current EAE models typically target the spinal cord (Sriram and Steiner, 2005), which initially affects the tail, followed by hind limbs and then fore limbs, leading to quadriplegia and subsequent death depending on disease severity. The clinical course may be relapsing-remitting, chronic or monophasic (Batoulis *et al.*, 2011). Additionally, the antigen specificity of CD4+ T cells has been shown to affect the location of lesions following their adoptive transfer, with those specific for MOG

resulting in a high number of lesions in the periventricular and cerebellar WM compared to those specific for MBP resulting in pathology mainly in the spinal cord (Berger *et al.*, 1997).

1.3.2.1 Spontaneous models of EAE

Spontaneous EAE models have been developed that allow studies to be performed without the requirement for adjuvants or adoptive transfer. For example, opticospinal encephalomyelitis mice are double transgenic animals on a C57BL/6 background that have transgenic B cells that bind native MOG and produce antibodies to it as well as transgenic T cells specific for amino acids 35-55 of MOG. Approximately half of these animals developed opticospinal encephalomyelitis, a variant of MS, with lesions in the optic nerve and spinal cord (Krishnamoorthy *et al.*, 2006).

1.3.2.2 T cell and antibody-mediated demyelination in EAE

Studies that transferred T cells to naïve animals have shown that T cells are responsible for the induction of EAE (Paterson, 1960, Ben-Nun *et al.*, 1981), inducing acute monophasic disease in most species and strains, characterised by high levels of inflammation and little or no demyelination. The transfer of encephalitogenic T cells may, however, in some animals induce relapsing-remitting or chronic disease again characterised by high levels of inflammation but associated with some demyelination (Mokhtarian *et al.*, 1984). Chronic disease characterised by extensive demyelination may be induced by immunisation with whole spinal cord tissue in CFA (Snyder *et al.*, 1975). Antibodies against components of myelin also appear to be involved in the pathogenesis of this chronic demyelinating disease. For example, the injection of a monoclonal antibody against MOG at disease onset in rats that had received encephalitogenic T cells resulted in extensive demyelination associated with increased duration and severity of clinical symptoms (Linington *et al.*, 1988). The titres of anti-MOG antibody in serum have also been found to correlate with demyelination (Linington and Lassmann, 1987).

1.3.2.3 MOG-EAE in the Dark Agouti rat

The clinical course and pathology of MS may be modelled in female DA rats by immunisation with a recombinant protein corresponding to the N-terminal amino acids 1-125 of rat MOG. Immunisation induced mainly a chronic relapsing disease, resulting in both a B and T cell response and lesions in the optic nerves and spinal cord. Spinal cord demyelination was accompanied by inflammatory infiltrates around blood vessels as well as in the meninges, with spread into the underlying parenchyma (Storch *et al.*, 1998b). The immunisation of DA rats with recombinant mouse (rm) MOG results in similar inflammatory lesions and is accompanied by increased axonal loss associated with a more severe clinical course in rats at the chronic stage of relapsing-remitting EAE (Reynolds *et al.*, 2002, Papadopoulos *et al.*, 2006).

1.3.2.4 GMLs in EAE

Pathology in the majority of EAE models is focused on spinal cord WM, with lesions in the cerebellum and optic nerves occasionally being observed. In addition to spinal cord lesions, all three types of GML have been identified in the cortex of marmosets with MOG-induced EAE (Pomeroy *et al.*, 2005). However, the ethical and husbandry considerations and lack of molecular tools make this model impractical. GMLs have also been identified in MOG-induced EAE in the Lewis rat (Storch *et al.*, 2006) and PLP-induced EAE in the SJL mouse (Rasmussen *et al.*, 2007), but their frequency, localisation, size and type is random and hence these models lack the necessary consistency.

1.3.2.5 Limitations of EAE models

Although studies using EAE models have increased understanding of the inflammatory aspects of MS, they have been poor in predicting the success of treatment for MS (Ransohoff, 2012). Their value is limited as a result of being induced by immunisation with strong adjuvants with the myelin protein or peptide. Additionally, EAE models only approximate some features of the clinical course and pathology of MS. For example, it is not

possible to study progression or make clinicopathological correlations, as animals with EAE do not display accumulation of chronic symptoms. It is also not possible to study relapses when using C57BL/6 mice, which are most commonly used because of the availability of transgenic models on this background, or remyelination, as lesions appear randomly with regard to localization and time. Pathology in the majority of EAE models is also focused on spinal cord WM, whereas MS affects the brain with prominent involvement of cerebral and cerebellar cortical GM. Finally, there is a lack of data regarding the roles of particular immune cells in EAE, including CD8+ T cells and B cells, which are discussed below and which appear to be involved in the pathogenesis of MS.

1.3.3 Role of immune cells in MS and EAE

As discussed in 1.2.1.3, MS is suggested to be initiated by activation and entry to the CNS of T cells, with a subsequent involvement of B cells. Additionally, EAE can be induced by the adoptive transfer of activated myelin-specific CD4+ T cells from mice with EAE to naïve mice (Stromnes and Goverman, 2006), hence understanding of the roles of these immune cells in mediating inflammation in the CNS in MS and EAE is necessary.

1.3.3.1 T cells

T cells respond to infection by clonal expansion of cells with receptors specific for molecular components of the infectious agent that are presented by APCs. Many different T cells have been identified and can be grouped into various subsets, including helper, follicular helper, regulatory, natural killer (NK), gamma delta and cytotoxic T cells (Fletcher *et al.*, 2010), based on the cell surface markers they express and the effector molecules they produce. Most of the data regarding the role of T cells in the pathogenesis of MS and EAE concern helper and cytotoxic T cells.

CD4+ Th cells

Th cells are a subtype of T cells characterised by the expression of CD4. They are activated by recognition of antigen presented by major histocompatibility complex (MHC) class II on APCs through the T cell receptor (TCR) and expand and differentiate into one of three subtypes, Th1, Th2 and Th17 (Kaiko *et al.*, 2008), depending on the predominant cytokine microenvironment (Dittel, 2008). Th1 cells secrete IFN-γ, interleukin (IL) 2, lymphotoxin-α and TNF and are involved in the response to intracellular infection (Dittel, 2008, Zhu *et al.*, 2010), resulting in the activation of macrophages/microglia and upregulation of adhesion molecules on the BBB as discussed in 1.2.1.1. Th2 cells secrete IL4, IL5, IL10 and IL13, resulting in the activation of B cells and the upregulation of antibody production (Kaiko *et al.*, 2008). A third subtype of Th cells has recently been identified. Th17 cells secrete IL17, IL17F, IL6, IL22 and TNF and are involved in the response to extracellular infection through the activation of neutrophils as well as tissue inflammation (Langrish *et al.*, 2005, Kaiko *et al.*, 2008).

MS has historically been regarded as a Th cell-mediated disease due to its association with MHC class II alleles as described in 1.1.2, with Th1 cells being the main pathogenic cells. This view was based on the finding that the adoptive transfer of Th1 cells to SJL/J mice caused severe EAE, whereas that of Th2 cells did not, for example (Khoruts *et al.*, 1995).

However, findings from human tissue studies are controversial. Although the presence of CD4+ T cells in MS lesions from biopsy samples has been reported (Fritzsching *et al.*, 2011), this is not a consistent finding. For example, another study using biopsy samples from early MS patients showed that CD4+ T cells are not the dominant subset in lesions. This study also investigated the TCR repertoire in lesions but failed to show clonal expansion in the CD4+ T cell population (Skulina *et al.*, 2004). The administration of recombinant IFN-γ however, a Th1 effector cytokine, to RRMS patients induced exacerbations, which were

associated with increased numbers of peripheral macrophages expressing MHC class II (Panitch *et al.*, 1987).

Th17 cells have also recently been implicated. PLP-specific T cells cultured with IL23, which is required for differentiation into Th17 cells, induced EAE following their transfer to SJL mice, whereas cells cultured with IL12, which is required for differentiation into Th1 cells, did not (Langrish *et al.*, 2005). However, a subsequent study showed that myelin-specific Th1 cells without Th17 cell contamination induced EAE following their transfer to C57BL/6 mice, whereas Th17 cells without IFN-γ-positive cells did not. This study also found that only Th1 cells were able to enter the CNS initially, but that once demyelinated lesions had developed, Th17 cells appeared in the CNS (O'Connor *et al.*, 2008). The relative roles of Th1 and Th17 cells in the pathogenesis of EAE and MS have not yet been resolved.

Additionally, studies have investigated the role of natural and induced regulatory CD4+ T cells. These cells downregulate the activity of B, T, NK and dendritic cells by the secretion of the anti-inflammatory cytokines IL10, IL35 and transforming growth factor-β (TGF-β), the induction of apoptosis and the inhibition of dendritic cell maturation (Buc, 2013). Studies using EAE models support a role for regulatory T cells in reducing the incidence and severity of clinical and pathological EAE (Kohm *et al.*, 2002, Reddy *et al.*, 2004). However, the inhibitory effect of regulatory T cells on antigen-specific T cell proliferation is reduced in these cells from MS patients (Haas *et al.*, 2005), as is their migration across primary human brain endothelium (Schneider-Hohendorf *et al.*, 2010).

CD8+ Tc cells

Tc cells are characterised by the expression of CD8. They are activated by recognition of antigen presented by MHC class I on APCs through the TCR, and since most nucleated cells express MHC class I, they can function as APCs (Mars *et al.*, 2011). Tc cells are cytotoxic through the release of either lytic enzymes, including granzymes and perforin, or

Fas ligand, which induces apoptosis by binding its receptor Fas. Additionally, Tc cells secrete cytokines, including TNF and IFN-γ, which contribute to the response to intracellular infection by increasing the recruitment and activation of macrophages/microglia (Harty and Bevan, 1999).

As well as being associated with MHC class II alleles, studies have shown the presence of a risk locus for MS in the class I allele independent of those in class II alleles (Rubio *et al.*, 2007). Tc cells are more common than Th cells in acute and chronic lesions (Hauser *et al.*, 1986) and their oligoclonal expansion in blood (Skulina *et al.*, 2004), CSF (Jacobsen *et al.*, 2002) and active lesions (Babbe *et al.*, 2000) has been demonstrated, which is not the case for Th cells, suggesting a role for Tc cells in the pathogenesis of MS.

A $CD161^{high}CD8+$ T cell subset has recently been described, which expresses natural killer receptor protein 1a/CD161. The expression of this protein was increased in peripheral blood from MS patients and $CD161^{high}CD8+$ T cells producing IFN-γ were detected in perivascular cuffs in WMLs as well as in diffuse inflammatory infiltrates and lymphoid-like structures in the meninges in autopsy samples from SPMS cases (Annibali *et al.*, 2011). This T cell subset has been shown to produce pro-inflammatory IL17 as well as IFN-γ, but not anti-inflammatory IL10, and is also depleted following autologous haematopoietic stem cell transplantation (Abrahamsson *et al.*, 2013), which results in improvements in cognitive and motor disability (Burt *et al.*, 2009). These findings further support a role for Tc cells.

A similar role in EAE has been suggested based on the finding that the adoptive transfer of MBP-specific Tc cells to C3H mice caused EAE, characterised by atypical symptoms rather than ascending paralysis, and by lesions in the brain rather than spinal cord, which was dependent on IFN-γ (Huseby *et al.*, 2001). However, a regulatory role has also been suggested. Th cells have been found to be more common than Tc cells in the CNS of

C57BL/6 mice immunised with MOG and the percentage of Tc cells was inversely correlated with clinical score (Weiss *et al.*, 2007).

1.3.3.2 B cells

B cells are activated in response to infection in a T cell dependent or independent manner. Activation results in differentiation into plasma cells, and the production of antigen-specific antibodies, or memory B cells and a more specific and stronger antibody response on subsequent exposure to the same antigen. B cells, which express MHC class II, can also function as APCs and activate Th cells (Rodríguez-Pinto, 2005) as well as secreting cytokines, including IFN-γ (Harris *et al.*, 2005), lymphotoxin and TNF (Bar-Or *et al.*, 2010).

Oligoclonal bands and high levels of the B cell chemokine CXCL13, indicative of abnormal B cell activity, are present in the CSF in early MS and have been shown to predict conversion from CIS to MS (Brettschneider *et al.*, 2010). Additionally, these markers of B cell presence and activation are correlated with disease activity and progression. For example, mature B cell and plasma blast numbers in CSF and levels of CXCL13 in CSF and serum were correlated with MRI activity (Kuenz *et al.*, 2008, Festa *et al.*, 2009). Further evidence for a role for B cells in disease progression came from studies that showed the presence of lymphoid-like structures, consisting mainly of B cells, in the meninges of a significant proportion of SPMS cases that were associated with a younger age at onset, age at wheelchair dependence and age at death (Magliozzi *et al.*, 2007) as discussed in 1.2.2.6. Taken together, these studies using MS tissue and CSF/serum suggest an important role for B cells in the pathogenesis of MS.

Studies in EAE have yielded conflicting results, with one study showing that B cell-deficient mice were susceptible to MOG peptide-induced EAE and developed chronic disease characterised by demyelinating inflammatory lesions in optic nerves, spinal cord and brain (Hjelmström *et al.*, 1998). However, another study showed that B cell-deficient mice were

resistant to recombinant MOG-induced EAE, although not to encephalitogenic MOG peptide-induced EAE (Lyons *et al.*, 1999).

As for Tc cells, a regulatory role for B cells has been suggested. These cells secrete the anti-inflammatory cytokine IL10 (Kala *et al.*, 2010). Antibody-mediated depletion of B cells prior to the induction of EAE has been found to result in more severe clinical and pathological EAE due to the depletion of regulatory B cells, whereas depletion at the peak of EAE resulted in less severe EAE due to the depletion of antibody producing and antigen presenting B cells (Matsushita *et al.*, 2008). A better understanding of the roles of B cells, in particular regulatory B cells, in EAE and MS is required.

Despite this, the targeting of B cells has been shown to be a promising treatment strategy. A phase II trial of rituximab, a monoclonal antibody against CD20, showed that B cell depletion resulted in decreased numbers of new and total inflammatory lesions and fewer relapses in the two year follow-up in RRMS patients receiving rituximab compared to placebo (Hauser *et al.*, 2008).

1.3.3.3 Microglia

Microglia are the resident macrophages of the CNS and have a wide variety of effector functions. Their main role is as components of the innate immune system in the CNS, where they function as the first line of defence against infection and injury (Ransohoff, 2009). In the healthy, mature CNS 'resting' microglia have a ramified morphology characterised by a small cell soma and the presence of numerous fine, branched processes that are covered with fine, shorter protrusions (Ransohoff, 2009). *In vivo* two-photon imaging of mouse cortex has shown that 'resting' microglia are highly active, continuously surveying their microenvironment with their processes and protrusions, without movement of their soma, and making contact with astrocytes, neurons and vasculature (Nimmerjahn *et al.*, 2005). These functions are enabled by the constitutive and inducible expression of a wide variety of

surface receptors, including pattern recognition receptors, which identify pathogen-associated molecular patterns, as well as receptors for both pro- and anti-inflammatory cytokines (Aloisi, 2001). Activated microglia have an amoeboid morphology characterised by a larger cell soma and shorter, thicker processes and express MHC class II, allowing them to function as APCs, as well as secreting cytokines including the pro-inflammatory TNF and anti-inflammatory IL10 (Aloisi, 2001).

Studies using biopsy samples from early MS patients have shown that early active WMLs are characterized by the infiltration of a combination of haematogenous microglia and monocytes, whereas late active WMLs are characterized by a monomorphic population of phagocytic macrophages (Brück *et al.*, 1995). The number of cells of the mononuclear phagocyte system in early and late active WMLs is the same, suggesting that the phagocytic macrophages in late active WMLs arose from the microglia and monocytes in early active WMLs. It has been estimated that between one half and one third of phagocytic macrophages arise from microglia (Brück *et al.*, 1995, Trebst *et al.*, 2001). Early GMLs, however, are characterized by the infiltration of phagocytic macrophages as well as microglia (Lucchinetti *et al.*, 2011, Popescu *et al.*, 2011), whereas the majority of phagocytic cells in GMLs from chronic progressive MS patients have the morphology of activated microglia (Peterson *et al.*, 2001, Bø *et al.*, 2003a, Bø *et al.*, 2003b, Kutzelnigg *et al.*, 2007).

As described in 1.2.1.2, active lesions in MS and EAE are defined as those with infiltration of activated macrophages/microglia containing myelin/myelin degradation products and expressing the phagocytosis marker CD68, associated with antibody deposition on myelin sheaths, throughout the lesion (Lucchinetti *et al.*, 2000, Storch *et al.*, 1998b). Phagocytosis of myelin, opsonised by antibody or complement, is mediated by Fc and complement receptors, the expression of which is increased in activated macrophages/microglia (Mosley and Cuzner, 1996). Additionally, these macrophages/microglia express MHC class II (Bö *et al.*, 1994, Nikodemova *et al.*, 2007), resulting in the differentiation of naïve T cells into Th1

cells (Aloisi *et al.*, 1999b). They have also been shown to express inducible NO synthase (NOS) in chronic active WMLs in MS and EAE (Hill *et al.*, 2004, Tran *et al.*, 1997), and the NO radicals produced are cytotoxic to oligodendrocytes *in vitro* (Merrill *et al.*, 1993) and result in conduction block of both myelinated and demyelinated axons *in vivo* (Redford *et al.*, 1997). Finally, activated macrophages/microglia secrete TNF, the autocrine signalling of which results in increased messenger ribonucleic acid (mRNA) expression levels of the enzyme glutaminase and subsequent increased release of glutamate by microglia *in vitro*. This in turn results in neuritic beading, focal swellings of axons and dendrites and neuronal death (Takeuchi *et al.*, 2006).

Studies in EAE support a role for microglia in MS pathogenesis. The prophylactic and therapeutic treatment of rats with chronic relapsing-remitting EAE with the anti-inflammatory tetracycline, minocycline, resulted in decreased disease severity and progression, associated with inhibition of microglial activation in the spinal cord (Popovic *et al.*, 2002). This effect has been shown to be mediated in part by decreased IFN-γ-induced expression of MHC class II on microglia (Nikodemova *et al.*, 2007). Although several mechanisms of action for minocycline have been proposed (Plane *et al.*, 2010), and hence its effect in EAE may not be mediated solely by the inhibition of microglial activation, the finding of Popovic *et al.* (2002) was confirmed in a subsequent study using mice and the macrophage/microglia activation inhibitor MMIF (macrophage migration inhibitory factor). However, only a modest effect on disease progression was observed with prophylactic treatment compared to a substantial effect with therapeutic treatment. This effect was associated with a shift in the expression of the transcription factors T-bet and GATA-3 from T-bet, which controls the transcription of Th1 cell markers, to GATA-3, which controls the transcription of Th2 markers (Bhasin *et al.*, 2007). The selective paralysis of microglia by ganciclovir treatment of transgenic mice expressing herpes simplex virus thymidine kinase under the control of the CD11b promoter in macrophages/microglia, followed by bone marrow transfer to restore peripheral macrophages, resulted in delayed onset and decreased severity of disease

associated with decreased inflammation. Ganciclovir treatment of brain slice cultures from these mice showed that this effect was likely mediated by abolished release of nitrite and TNF in response to IFN-γ (Heppner *et al.*, 2005).

However, a protective as well as a damaging role for microglia in MS pathogenesis has been suggested. Microglia can release the anti-inflammatory cytokines IL10 and TGF-β *in vitro*, which inhibit further microglial activation by decreasing their release of pro-inflammatory cytokines, chemokines and nitrogen and oxygen radicals (Aloisi, 2001, Qian *et al.*, 2006) and their expression of MHC class II molecules (O'Keefe *et al.*, 1999). Additionally, a phenotype of microglia that supports remyelination has been described. Genome-wide gene expression analysis of microglia during demyelination and remyelination in the mouse cuprizone model was used to show that microglia are involved in the phagocytosis of myelin/myelin degradation products and apoptotic cells during demyelination but that they express cytokines and chemokines that allow them to activate and recruit oligodendrocyte precursor cells (OPCs) to the lesion during remyelination (Olah *et al.*, 2012). This explains the finding that the inhibition of microglial activation decreases remyelination, using minocycline in a rat ethidium bromide model (Li *et al.*, 2005). Finally, activated microglia have also been shown to express brain-derived neurotrophic factor and glial cell line-derived neurotrophic factor (Batchelor *et al.*, 1999) and hence may also have a neuroprotective role.

1.3.3.4 Cytokines

Cytokines are soluble proteins released by immune cells that mediate their interactions and regulate their immune functions. Gene expression studies using brain tissue, peripheral blood mononuclear cells and whole blood from MS patients have shown that the expression of cytokines is dysregulated in MS (Sospedra and Martin, 2005). They have also been implicated in the pathogenesis of EAE, with the pro-inflammatory cytokines TNF and IFN-γ having received particular attention. It has recently been shown in this laboratory that the number of cells expressing TNF and IFN-γ and the gene expression of these cytokines in the

meninges, as well as their levels in post-mortem CSF, are increased in F+ SPMS cases (Gardner *et al.*, 2013).

TNF

TNF is synthesised as a monomeric transmembrane (tmTNF) precursor protein with a molecular weight of 26kDa, the cytoplasmic tail of which may be cleaved by TNF-α converting enzyme to release a soluble (sTNF) cytokine. Both tmTNF and sTNF must form homotrimers to function (Caminero *et al.*, 2011). TNF is mainly produced by activated macrophages, but also by B and T cells and several other immune cells (Caminero *et al.*, 2011), and in the CNS it may be produced by some neurons (Villarroya *et al.*, 1997). Its effects are mediated by two TNF receptors, TNFR1 and TNFR2. Although sTNF and tmTNF can bind to both TNFR1 and TNFR2, sTNF binds preferentially to TNFR1 whereas tmTNF binds preferentially to TNFR2 (Grell *et al.*, 1998, Grell *et al.*, 1995 respectively). TNFR1 is coupled to one of three distinct signalling pathways by binding of the adaptor protein TRADD (TNFR-associated via death domain) to the death domain in its cytoplasmic region. The main pathway results in the formation of complex I and subsequent transcription of pro-inflammatory genes by activation of the transcription factor family nuclear factor-kappa B 1 (NF-κB) (Tracey *et al.*, 2008). A distinct pathway results in the formation of complex II, the composition of which determines outcome. Complex IIa results in apoptosis mediated by caspases 8 and 3, whereas complex IIb results in necroptosis, which requires the activity of RIPK1 and RIPK3 (receptor-interacting protein kinase) IFN-γ (Vanlangenakker *et al.*, 2012). TNFR2 lacks a death domain in its cytoplasmic region, and its binding results in the activation of inflammatory and cell survival signalling pathways (Yang *et al.*, 2002).

Studies using autopsy samples from RRMS and SPMS cases have demonstrated the presence of TNF in astrocytes and microglia in chronic active lesions (Hofman *et al.*, 1989), while a more recent study using autopsy samples from F+ SPMS cases demonstrated its presence in activated microglia in active subpial GMLs as well as in macrophages in the

inflamed meninges (Magliozzi *et al.*, 2010). Studies using CSF from chronic progressive MS patients showed high levels of TNF in a majority of cases, which were correlated with disease severity and progression over 24 months of follow-up (Sharief and Hentges, 1991). The incubation of murine brain slices with CSF from progressive MS patients *in vitro* resulted in increased spontaneous excitatory postsynaptic currents and neuronal swelling, which were shown to be dependent on TNF signalling (Rossi *et al.*, 2013). Additionally, TNF messenger RNA expression levels were increased in peripheral blood mononuclear cells from RRMS patients prior to a relapse (Rieckmann *et al.*, 1995).

Studies in EAE support a damaging role of TNF in MS pathogenesis. Treatment of mice with antibodies to TNF or TNFR1-IgG fusion proteins prevented the development of clinical and pathological EAE (Ruddle *et al.*, 1990, Selmaj *et al.*, 1991, Körner *et al.*, 1997a), and the absence of TNF in TNF-deficient mice delayed the onset of disease (Körner *et al.*, 1997b, Kassiotis *et al.*, 1999). Disease severity and progression, however, were comparable to that in wild type mice, suggesting a role in development rather than progression of disease. Conversely, the overexpression of TNF in the CNS of transgenic mice resulted in spontaneous, chronic inflammatory demyelination that could be prevented by treatment with antibodies to TNF (Probert *et al.*, 1995). The absence of sTNF alone in transgenic mice, on the other hand, delayed the onset of disease and prevented progression while tmTNF was able to maintain autotolerance and resistance to infection (Alexopoulou *et al.*, 2006). Additionally, TNFR2 knockout mice developed more severe clinical and pathological EAE than wild type mice, whereas TNFR1 knockout mice were resistant to the development of disease (Suvannavejh *et al.*, 2000). These studies suggest that the selective inhibition of sTNF and its TNFR1 signalling pathway may be a useful therapeutic strategy. Support for this came from two recent studies that used both a selective sTNF and a non-selective TNF inhibitor and found that inhibition of sTNF and TNFR1 alone resulted in protection from EAE and increased remyelination and neuroprotection (Brambilla *et al.*, 2011, Taoufik *et al.*, 2011). A further study showed that prophylactic and therapeutic treatment with a selective

TNFR1 antagonist resulted in less severe clinical disease in mice with MOG-induced EAE, and that the prophylactic treatment resulted in neuroprotection (Williams *et al.*, 2014).

Finally, returning to MS, the gene for TNFR1 has been found to contain two independent susceptibility alleles in a meta-analysis of genome-wide association studies, further supporting a role for sTNF and TNFR1 signalling (De Jager *et al.*, 2009).

The importance of distinguishing between the damaging and protective roles of TNF when considering therapeutic strategies was realised following a clinical trial with lenercept, a fusion protein of the extracellular domain of TNFR1 and a heavy chain fragment of IgG1. This multicentre, double-blind, placebo-controlled and randomised phase II trial was stopped due to a dose-dependent increase in the number and severity of exacerbations in RRMS patients (The Lenercept Multiple Sclerosis Study Group, 1999). Unexpected results such as these have discouraged the use of therapeutic strategies targeting TNF, but have led to increased research into the functions of TNF and TNFRs.

IFN-γ

IFN-γ is produced mainly by Th1 cells and results in the proliferation and differentiation of naïve T cells into Th1 cells (Imitola *et al.*, 2005) as well as the activation of macrophages/microglia by increasing the expression of MHC class II (Vass and Lassmann, 1990) and TNF (Welser-Alves and Milner, 2013) as well as TNFR1 (Veroni *et al.*, 2010).

Studies using autopsy samples have demonstrated the presence of IFN-γ in macrophages/microglia at the margins of chronic active lesions, associated with apoptotic oligodendrocytes (Vartanian *et al.*, 1995). The administration of recombinant IFN-γ to RRMS patients appeared to induce exacerbations, which were associated with increased numbers of peripheral macrophages expressing MHC class II (Panitch *et al.*, 1987), and IFN-γ production in a whole blood mitogen assay preceded exacerbations (Beck *et al.*, 1988).

As for TNF, studies in EAE appear to support a damaging role of IFN-γ in MS pathogenesis. IFN-γ messenger RNA expression levels in the CNS increased during relapse and decreased during remission (Issazadeh *et al.*, 1995) while the overexpression of IFN-γ in oligodendrocytes of transgenic mice resulted in spontaneous demyelination associated with activation of microglia and infiltration of mainly CD8+ T cells accompanied by clinical disease (Horwitz *et al.*, 1997). However, IFN-γ knockout mice were susceptible to EAE and developed massive inflammatory infiltrates in the CNS (Ferber *et al.*, 1996). It has been suggested (Imitola *et al.*, 2005) that this unexpected result may be due to the role of IFN-γ in inhibiting T cell proliferation (Konieczny *et al.*, 1998, Badovinac *et al.*, 2000).

In vitro studies have shown that individual treatment of oligodendrocytes with TNF or IFN-γ induced dose-dependent apoptosis. Combined treatment with these cytokines indicated synergistic actions, resulting in accelerated oligodendroglial apoptosis (Buntinx *et al.*, 2004). Individual treatment of OPCs with TNF induced metabolic changes, driven by mitochondrial defects, resulting in the inhibition of differentiation to mature oligodendrocytes (Bonora *et al.*, 2014). Combined treatment of microglia has indicated similar synergistic actions. Individual treatment did not induce NOS expression or NO production, in contrast to combined treatment, which activated NF-κB resulting in NOS transcription (Mir *et al.*, 2008). Studies have investigated the molecular basis of the synergistic actions of TNF and IFN-γ. One of these studies proposed the model shown in Figure 1.3 based on the actions of TNF and IFN-γ on the expression of MHC class 1 in oligodendrocytes, with IFN-γ inducing the expression of TNFR1 and interferon regulatory factor 1 (IRF1) suggested to be the main common transcription factor (Agresti *et al.*, 1998).

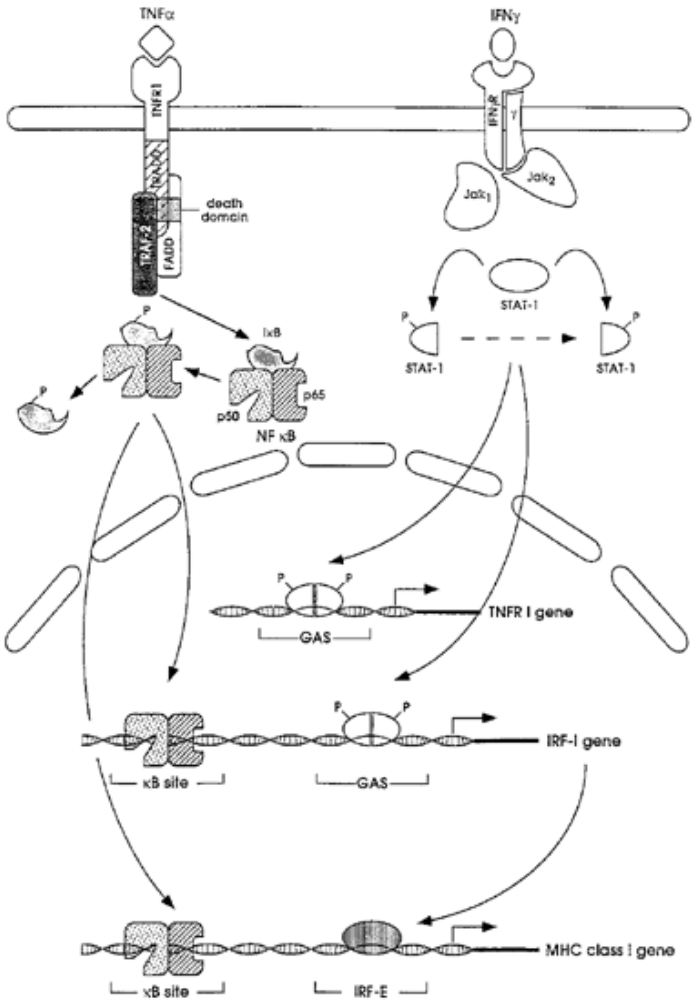

Figure 1.3. Model proposed for the molecular basis of synergistic actions of TNF and IFN-γ. Phosphorylation of the JAK1 and JAK2 kinases following IFN-γ treatment results in phosphorylation of STAT1, homodimers of which bind to GAS sequences in the TNFR1 and IRF1 promoter regions. IRF1 then acts as intermediate transcription factor, resulting in the expression of MHC class I together with the transcription factor NF-κB, activated following binding of TNF to TNFR1 (Agresti *et al.*, 1998).

1.3.4 Targeted EAE

In order to target demyelination and inflammation to specific anatomical locations within the rodent CNS, EAE models have now been developed that involve the immunisation of animals with a subclinical dose of recombinant MOG to prime anti-MOG specific T and B cells followed by the injection of pro-inflammatory cytokines at the desired location to attract the primed auto-reactive T cells and antibodies and induce demyelination (Kerschensteiner *et al.*, 2004). The immunisation of female Lewis rats with a subclinical dose of recombinant rat (rr) MOG followed 18-22 days post immunisation (dpi) by the injection of TNF and IFN-γ

into the dorsal funiculus resulted in large demyelinating inflammatory lesions with axonal damage localised mainly to the WM (Kerschensteiner *et al.*, 2004). These animals developed motor symptoms that were maximal at 3-8 days post injection and correlated with demyelination. The same laboratory subsequently developed a model that shows cortical pathology by injecting the cytokines into the motor cortex. This resulted in all three types of GML in the injected cortex, associated with activated microglia, infiltration of T cells and axonal damage, but not in the contralateral cortex (Merkler *et al.*, 2006). However, the value of this model to study MS is limited by the lack of chronic pathology and by the physical injury and BBB damage induced by the direct injection of cytokines. Demyelination was maximal at 3 days after injection and remyelination was complete at 14 days after injection (Merkler *et al.*, 2006).

In order to test the hypothesis that TNF and IFN-γ produced in the meninges can diffuse from the pial surface into the cortex, resulting in subpial lesions, and avoid the damage caused by injection into the motor cortex, this laboratory has recently developed a model that shows cortical pathology driven by meningeal inflammation (Gardner *et al.*, 2013). The immunisation of female DA rats with a subclinical dose of rmMOG followed 18-22 dpi by the injection of TNF and IFN-γ into the subarachnoid space (SAS) of the sagittal sulcus resulted in subpial lesions similar to those described in SPMS. Microglia with activated morphology (large, rounded cell bodies with short, thick processes) were found associated with the myelin sheaths, particularly at the edge of the lesion, and a gradient of microglial activation was observed, again similar to that described in SPMS. Lesions were associated with B cell, CD4+ and CD8+ T cell and macrophage accumulation in the meninges. No demyelination occurred in rats immunised with IFA and injected with cytokines or in rats immunised with rmMOG and injected with phosphate buffered saline (PBS). This model has been shown to be highly reproducible but, as in the motor cortex model, there is a lack of chronic pathology due to the acute nature of the cytokine delivery. Demyelination was maximal at 7 days after injection and remyelination was complete at 14 days after injection (Gardner *et al.*, 2013).

1.4 Hypothesis

Both human tissue and *in vivo* model studies performed in this laboratory have suggested that cytotoxic and/or pro-inflammatory molecules diffusing from the CSF in the chronically inflamed meninges into the underlying cortical GM may result in subpial GMLs in MS (Gardner *et al.*, 2013).

In this project we test the hypothesis that meningeal inflammation resulting from the presence of increased levels of TNF and IFN-γ in the SAS of animals immunised with a subclinical dose of rmMOG will result in subpial demyelination and microglial activation, and that lentiviral (LV) vectors will be a promising delivery system to achieve the chronic presence of TNF and IFN-γ in the SAS for future studies. In addition, we test the idea that cytotoxic and/or pro-inflammatory molecules other than TNF and IFN-γ are present in the chronically inflamed meninges in MS.

1.5 Aims

We aimed to develop a system that would enable the chronic delivery of TNF and IFN-γ into the SAS of animals immunised with a subclinical dose of rmMOG using LV vectors and to determine the identity of the cytotoxic and/or pro-inflammatory molecules present in the meninges in MS.

To fulfil these aims, the following studies were performed:

- Expression and purification of rmMOG followed by the identification of a suitable subclinical dose in the DA rat.
- Determination of the effect of the dose of TNF and IFN-γ on the duration and extent of pathology in the model of cortical pathology driven by meningeal inflammation.
- Evaluation of LV vectors as a delivery system to achieve the chronic presence of TNF and IFN-γ in the SAS of the DA rat.
- Identification of the cytotoxic and/or pro-inflammatory molecules expressed in the meninges in post-mortem MS brain.

Chapter 2

MOG-EAE in the DA rat

2.1 Introduction

2.1.1 Myelin oligodendrocyte glycoprotein

2.1.1.1 Structure and function

The formation of myelin depends on the expression of myelin-specific proteins, including CNPase, MBP and PLP. MOG is a minor myelin-specific protein, accounting for approximately 0.05% of proteins (Amiguet *et al.*, 1992). It is expressed at the external surface of the myelin sheath and the plasma membrane of oligodendrocytes with low expression in the lamellae of compact myelin and at the border between myelin and axon (Brunner *et al.*, 1989, Scolding *et al.*, 1989). It may be used as a marker of oligodendrocyte maturation, during which it is expressed in the later stages, and its temporal expression parallels subsequent myelination (Pham-Dinh *et al.*, 1993, Johns and Bernard, 1999).

Rat, mouse, bovine and human MOG have been cloned, leading to the identification of mature MOG as a 218 amino acid member of the Ig superfamily (Gardinier *et al.*, 1992, Pham-Dinh *et al.*, 1993, Hilton *et al.*, 1995) that is highly conserved between species (Johns and Bernard, 1999). Western blotting of MOG from several species, including human, revealed two major bands at 28kDa and 55kDa, with the band at 55kDa thought to be a dimer of the band at 28kDa (Slavin *et al.*, 1997). The model for the structure of MOG proposed by Kroepfl *et al.*, 1996 is shown in Figure 2.1.1.

Although the function(s) of MOG in myelin has proved difficult to identify, three possible functions have been proposed (Johns and Bernard, 1999). The structure of MOG indicates that it may function as an adhesion molecule or cellular receptor and it has been suggested that it mediates contact between adjacent myelinated axons during the later stages of myelination (Burger *et al.*, 1993, Bernard *et al.*, 1997). Additionally, a role for MOG as a regulator of microtubule stability has been proposed after it was shown that the treatment of

oligodendrocytes with anti-MOG antibody *in vitro* resulted in microtubule depolymerisation (Dyer and Matthieu, 1994), thought to be due to the degradation of MBP (Johns *et al.*, 1995). Finally, it has been shown that purified native MOG, as well as the recombinant N-terminal extracellular Ig-like domain, bind the C1q component of complement in a dose-dependent and saturating manner, resulting in complement activation (Johns and Bernard, 1997), suggesting a role for MOG in mediating interactions between myelin and immune cells (Johns and Bernard, 1999).

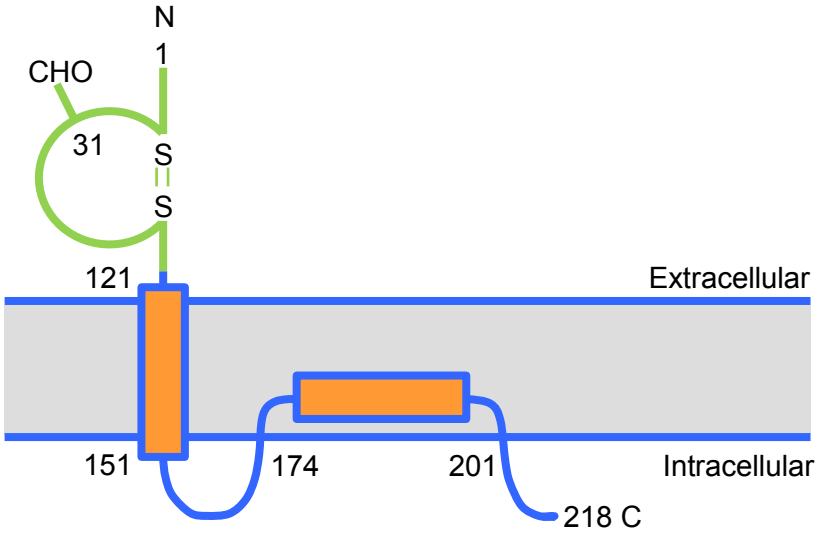

Figure 2.1.1. Model proposed for the structure of native MOG. Kroepfl *et al.*, 1996 proposed that it contains two transmembrane regions, with the second of these thought to be associated with the membrane without spanning it, resulting in the C-terminal domain being intracellular. The 1.8Å crystal structure of the N-terminal extracellular domain, shown in green, confirmed that it assumes a classical Ig fold (Clements *et al.*, 2003), which is expressed and purified for use in EAE models of MS.

However, it is the hypothesised role for MOG as an auto-antigen in MS, rather than its physiological function(s), that has received particular attention.

2.1.2 MOG as an auto-antigen in MS

In contrast to the high affinity antibodies for self-antigens that have been identified in other neurological conditions, including the acetylcholine receptor in myasthenia gravis (Vincent, 2002) and aquaporin 4 in neuromyelitis optica (Lennon *et al.*, 2005), such a self-antigen has proven difficult to identify in MS. In this context, the T cell response to the enzyme transaldolase expressed in oligodendrocytes (Banki *et al.*, 1994), the small heat shock

protein αB-crystallin expressed in oligodendrocytes and astrocytes (van Noort *et al.*, 1995) and the myelin-specific proteins MBP (Warren and Catz, 1993), PLP (Greer and Pender, 2008) and MOG have been investigated. MOG expression is specific to the CNS, consistent with the observation of MS lesions only in the CNS, and its expression at the external surface of the myelin sheath renders it accessible for recognition by components of the immune system. These properties of MOG led to the hypothesis that it is an auto-antigen in MS.

Peripheral T cells obtained from MS patients have been shown to proliferate following treatment with myelin antigens *in vitro*, this response being greatest following treatment with MOG (Kerlero de Rosbo *et al.*, 1993). MOG auto-antibodies have been identified in IgG purified from lesion autopsy samples from SPMS cases, where their levels were higher than those in CSF and serum, indicating the significance of local accumulation/production (O'Connor *et al.*, 2005). They have also been identified bound to disintegrating myelin in lesions of active MS cases (Genain *et al.*, 1999).

MOG auto-antibodies have been detected in serum and CSF obtained from MS patients and shown to persist during the disease course. However, they are not detected in all samples (they are detected in 38% and 33% of serum and CSF samples respectively) and are also detected in samples obtained from other inflammatory neurological disease patients (53% in both serum and CSF samples), although they have been shown to be transient in samples from these patients (Reindl *et al.*, 1999). The binding of MOG auto-antibodies purified from serum from MS patients was investigated using the native MOG Ig-like domain expressed on the cell surface of transfected cells *in vitro*, and was observed in only 1 of 17 MS patients (Haase *et al.*, 2001), indicating that MOG auto-antibodies may only mediate demyelination in a limited subset of MS patients. Given this, the hypothesis that MOG is the sole auto-antigen in MS remains controversial and it has been suggested that there are several auto-antigens (Nylander and Hafler, 2012). Additionally, although the initial auto-reactivity may be specific

for a particular epitope of a particular antigen, epitope spreading may result in subsequent auto-reactivity specific for further epitopes of the particular antigen or further antigens (Tuohy *et al.*, 1999).

2.1.2.1 Mechanisms of antibody-mediated demyelination

Several mechanisms of antibody-mediated demyelination have been proposed. The ability of monoclonal antibodies specific for MOG to induce demyelination in EAE induced by the transfer of MBP-specific T cells has been shown to depend on the ability of the antibody to fix complement (Piddlesden *et al.*, 1993). The co-localisation of immunoglobulins with the complement C9neo antigen on degenerating myelin sheaths and in myelin degradation products has also been observed at the edge of active WMLs (Storch *et al.*, 1998a), suggesting a role for antibody-mediated complement activation and subsequent formation of the complement membrane attack complex. However, studies in EAE have demonstrated no effect of decomplementation on demyelination (Piddlesden *et al.*, 1991), suggesting that mechanisms other than complement activation are involved, although this is a controversial finding (Mead *et al.*, 2002). Myelin phagocytosis by macrophages *in vitro* has been shown to depend on its opsonisation, which was greatest following treatment with a monoclonal antibody specific for MOG (Van der Goes *et al.*, 1999). Phagocytosis induces the production of cytotoxic TNF and NO by the macrophages, further contributing to antibody-dependent cell-mediated cytotoxicity (van der Laan *et al.*, 1996).

2.1.3 MOG-EAE

EAE is the most widely studied *in vivo* model of MS. It involves immunisation with a myelin antigen, typically together with an adjuvant, or adoptive transfer of myelin antigen-reactive T cells, resulting in a disease that is immunologically and pathologically similar to MS (Batoulis *et al.*, 2011). It is purely autoimmune, with antigen specificity for the endogenous myelin antigen, in contrast to the alternative *in vivo* models induced by a toxic agent or virus. The exact pathology and clinical course of the disease depends on the species, strain, sex and

age of the animal, the identity, concentration and species origin of the myelin protein, the physical structure of the myelin protein/adjuvant emulsion and epigenetic factors (Teuscher *et al.*, 2004, Schreiner *et al.*, 2009, Spach *et al.*, 2009).

Unlike the majority of myelin antigens used for immunisation, MOG induces a demyelinating auto-antibody response as well as an encephalitogenic CD4+ T cell response in susceptible species (Gold *et al.*, 2006) and hence more closely reproduces the complex pathology and clinical course associated with MS than other myelin antigens. MOG auto-antibodies result in more severe clinical EAE and induce extensive demyelination in T cell-mediated encephalitis in mouse, rat and primate EAE models as well as in MOG-induced EAE, the auto-antibody response acting synergistically with the T cell response (Schluesener *et al.*, 1987, Linington *et al.*, 1988, Genain *et al.*, 1995, Storch *et al.*, 1998b). It has recently been shown that EAE induced by the Ig-like domain of MOG, amino acids 1-125, is more severe than that induced by the MHC class II-associating domain of MOG, amino acids 35-55. This was associated with increased numbers of CD4+ T cells producing IFN-γ in the CNS (Mony *et al.*, 2014).

The most commonly used murine MOG-EAE model is that induced in C57BL/6 mice by MOG amino acids 35-55 peptide, resulting in chronic progressive EAE. However, the extent of complement activation as well as that of the demyelinating auto-antibody response varies widely between strains, which is particularly important when considering C57BL/6 mice. This strain is most commonly used because of the availability of transgenic models on this background, but gene(s) associated with the H-2^b MHC haplotype in this strain prevent a demyelinating auto-antibody response to conformational-dependent epitopes of the MOG Ig-like domain, hence tissue damage is not mediated by auto-antibodies. Instead, clinical disease, demyelination and inflammation are mediated by T cells, with a role for TNF-dependent mechanisms (Akassoglou *et al.*, 1999, Bourquin *et al.*, 2003).

In contrast to murine MOG-EAE models, demyelination in marmoset and rat appears to be dependent on auto-antibodies and complement only (Adelmann *et al.*, 1995, Genain *et al.*, 1995, Stefferl *et al.*, 1999a). The levels of MOG auto-antibodies in serum from guinea pigs with chronic relapsing EAE are correlated with demyelination and inflammation following administration of the serum to naïve rats (Linington and Lassmann, 1987) and inhibition of complement activation prevents the more severe clinical EAE and the more extensive demyelination observed following treatment with MOG auto-antibodies in MBP-induced EAE (Linington *et al.*, 1989). The rat strains used include Lewis and Brown Norway as well as DA rats while the MOG antigens used include rat amino acids 35-55, 1-125 and 1-118 epitopes of the Ig-like domain (Mannie *et al.*, 2009). The immunisation of Lewis rats with MOG antigen results in meningeal and perivascular inflammation, but no significant demyelination, macrophage recruitment or clinical EAE is observed, suggested to be due to a lack of antigen-specific T cell response (Adelmann *et al.*, 1995, Weissert *et al.*, 1998). In contrast, severe clinical EAE is observed in the more susceptible DA rats (Weissert *et al.*, 1998).

2.1.3.1 MOG-EAE in DA rat

The clinical course and pathology of MS may be modelled in DA rats by immunisation with a recombinant MOG peptide, which is usually the complete N-terminal extracellular Ig-like domain, emulsified in IFA. The onset of clinical EAE is approximately 14 dpi (Papadopoulos *et al.*, 2010), although the clinical and pathological characteristics of the resulting disease depend on the protocol used. The dose of MOG required is approximately 50µg per animal, which induces chronic progressive EAE in some animals, whereas a dose of 200µg induces relapsing-remitting EAE in approximately 50% of animals (Papadopoulos *et al.*, 2006, Reynolds, personal communication, 2014). Differences in the monomer:dimer ratio of individual batches of recombinant MOG have been shown to affect the incidence, clinical course and severity of EAE, with high monomer:dimer ratios thought to be more encephalitogenic (unpublished observations from this laboratory). Additionally, the clinical and pathological characteristics depend on whether precipitated or soluble MOG is used.

The immunisation of female DA rats with 50μg of precipitated MOG emulsified in CFA resulted in a greater demyelination score of brain and spinal cord combined and a high incidence of neuromyelitis optica (80%), whereas immunisation with soluble MOG instead resulted in a high incidence of acute disseminated leucoencephalomyelitis (100%; Storch *et al.*, 1998b). Finally, effects of gender have also been observed. A significant proportion of female DA rats immunised with 75μg of MOG developed neuromyelitis optica, whereas the optic nerves were not affected in equivalent male rats. The inflammatory index of spinal cord and demyelination score were also greater in female rats (Storch *et al.*, 1998b).

The most common distribution pattern of lesions following the immunisation of female DA rats with a soluble recombinant protein corresponding to the N-terminal amino acids 1-125 of rat MOG emulsified in IFA is both the spinal cord and optic system in 44% of lesions, followed by only the spinal cord in a further 38% of lesions, inducing mainly a chronic relapsing disease. Active lesions are characterised by the presence of Ig and complement C9neo antigen on degenerating myelin sheaths and meningeal and perivascular inflammation consisting of activated macrophages and T cells (Storch *et al.*, 1998b), hence reproducing the pathology of the pattern II WMLs observed in MS (Lucchinetti *et al.*, 2000). The immunisation of female DA rats with rmMOG results in similar inflammatory demyelinating lesions and is accompanied by axonal loss. This is observed as early as 5 days from disease onset, is correlated with the density of activated macrophages/microglia and is associated with a more severe clinical course in rats at the chronic stage of relapsing-remitting EAE (Reynolds *et al.*, 2002, Papadopoulos *et al.*, 2006). Again, this reproduces the proposed association between axonal loss and clinical progression in MS (Compston and Coles, 2008, Reynolds *et al.*, 2011), rendering MOG-EAE in the female DA rat a useful model.

2.1.3.2 Targeted MOG-EAE

However, pathology in the majority of EAE models is focused on spinal cord WM and cortical GM pathology is rarely observed. In order to target pathology to specific anatomical locations within the rat CNS, EAE models have now been developed that involve immunisation with a subclinical dose of recombinant MOG to prime anti-MOG specific T and B cells followed by the injection of pro-inflammatory cytokines at the desired location to attract the primed auto-reactive T cells and antibodies and induce demyelination (Kerschensteiner *et al.*, 2004, Merkler *et al.*, 2006, Gardner *et al.*, 2013). The subclinical dose of recombinant MOG used does not result in clinical symptoms, but does result in a peripheral anti-MOG antibody response that is the same as that in animals with clinical symptoms. Additionally, little inflammation and no demyelination are observed in the CNS of animals immunised with this dose.

2.1.4 Aims

We aimed to identify a suitable subclinical dose of rmMOG for subsequent use in the development of the chronic model of cortical pathology driven by meningeal inflammation. This dose should result in a peripheral anti-MOG antibody response in the absence of immune cell infiltration into the CNS, demyelination and clinical symptoms.

To fulfil these aims, the following were performed:

- Expression and purification of rmMOG.
- Induction of EAE in female DA rats and clinical scoring.
- Assessment of EAE pathology using immunostaining.
- Determination of peripheral anti-MOG antibody levels using enzyme-linked immunosorbent assays (ELISAs).
- Identification of a suitable subclinical dose of rmMOG.

2.2 Methods

The methods described in this Chapter were performed with equal contribution by Miss Eleanor Browne (Neuroinflammation and Multiple Sclerosis, Division of Brain Sciences, Imperial College London), who also required a subclinical dose of rmMOG for her studies. Expression and purification of rmMOG were performed together and although one group of animals was used, Miss Browne and the author each performed half of the immunostaining and ELISAs.

2.2.1 Expression and purification of rmMOG

2.2.1.1 Expression vector

E. coli glycerol stocks transformed with complementary DNA coding for the N-terminal amino acids 1-118 of mouse MOG were donated by Dr McMahon, National University of Ireland, Galway. The MOG sequence was cloned into the multiple cloning site of the pRSET A vector (Invitrogen, Paisley, UK) that also contains an N-terminal polyhistidine tag for purification with a nickel-chelating resin (Figure 2.2.1).

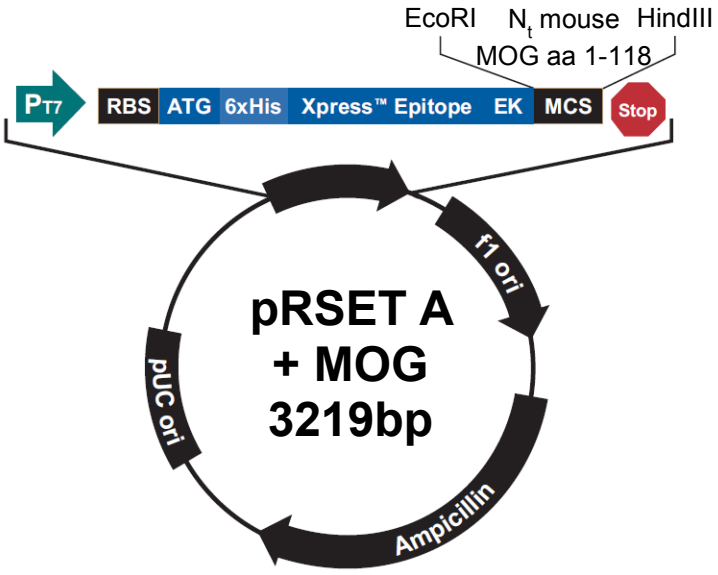

Figure 2.2.1. Vector map of pRSET A. Note the T7 promoter (P_{T7}), N-terminal polyhistidine tag (6xHis) and MOG sequence flanked by EcoRI and HindIII restriction sites in the multiple cloning site.

2.2.1.2 Expression of rmMOG protein

E. coli glycerol stocks were streaked onto Lysogeny broth (LB) agar (Sigma-Aldrich, Poole, Dorset, UK) plates containing ampicillin (100µg/ml, Sigma-Aldrich) and chloramphenicol (35µg/ml, Sigma-Aldrich) and incubated overnight at 37°C. Six single colonies were selected for culture in LB (Sigma-Aldrich) containing antibiotics at the same concentrations and incubated overnight at 37°C in a shaking incubator.

DNA was prepared from the six cultures using a QIAprep Spin Miniprep Kit (Qiagen, Crawley, Sussex, UK) according to manufacturer's instructions. The concentration of eluted DNA was determined using a NanoDrop spectrophotometer (NanoDrop, Wilmington, Delaware, USA). T7 primer (3.2pmol; Life Technologies, Paisley, Renfrewshire, UK) was added to 500-600ng DNA and sequencing was performed by the MRC Genomics Laboratory. Additionally, restriction digestion was performed for 60 minutes in a water bath at 37°C using HindIII in NEBuffer 2 (New England Biolabs, Ipswich, Massachusetts, USA), followed by the addition of EcoRI and sodium chloride (1M) for a further 60 minutes prior to inactivation for 20 minutes at 65°C. Loading buffer (Qiagen) was added to cut and uncut DNA. Samples were run in Tris-borate-ethylenediaminetetraacetic acid (EDTA; all Sigma-Aldrich; 0.5x) buffer on a 1% agarose (Sigma-Aldrich) gel with ethidium bromide (Sigma-Aldrich) for approximately 60 minutes at 109V until the bands of the ladder (Hyperladder 1; Bioline, London, UK) were well separated. Bands were visualised under ultraviolet illumination (BioDoc-It Imaging System; UVP, Cambridge, Cambridgeshire, UK).

Following confirmation that the *E. coli* cultures were transformed with complementary DNA coding for the MOG sequence and polyhistidine tag, a single culture was grown in Super Optimal Broth (SOB) medium (Invitrogen) containing antibiotics at the same concentrations as in LB overnight at 37°C in a rotary incubator. Growth of the culture was monitored by determining the absorbance of the culture at 600nm. Expression of MOG from the P_{T7}

promoter was induced at the mid-logarithmic phase of growth at which the absorbance was approximately 0.3, by the addition of isopropyl β-D-1-thiogalactopyranoside (IPTG; 1mM; Sigma-Aldrich). Growth was allowed to continue for approximately 4 hours until the absorbance was 0.8-1.2, at which point medium was placed on ice.

Cells were harvested by centrifugation at 1,380*g* for 10 minutes at 4°C. Pellets were stored overnight at -20°C. Cells were lysed with pH8 lysis buffer (10mM Tris-HCl, 50mM PO_4, 8M urea, 100mM NaCl; all Sigma-Aldrich) followed by further disruption of membranes and removal of cell debris by repeated sonication and centrifugation (16,100*g*, 25 minutes, 4°C), keeping the supernatant after each round.

2.2.1.3 Purification and concentration of rmMOG protein

Talon metal affinity resin (Clontech, Saint-Germain-en-Laye, France) was washed with a volume of lysis buffer, centrifuged and the supernatant discarded five times. It was added to the supernatant containing protein and allowed to bind the protein by agitation for 60 minutes on a rotary shaker. The resin-protein complex was washed by centrifugation at 700*g* for 5 minutes, removal of the supernatant, addition of lysis buffer (5ml), agitation for a further 15 minutes on a rotary shaker and centrifugation at 700*g* for 5 minutes. The resin-protein complex was added to a gravity flow column and washed on the column with lysis buffer followed by pH7 wash buffer (50mM $NaPO_4$, 300mM NaCl, 8M urea). Elution of protein was induced by adding pH5.3 elution buffer (50mM $NaPO_4$, 300mM NaCl, 8M urea, 20mM MES (2-(N-morpholino)ethanesulfonic acid; Sigma-Aldrich)) and monitored by determining absorbance at 280nm. The eluted protein was diluted with a volume of pH7.4 arginine (1M; Sigma-Aldrich) in PBS (Sigma-Aldrich), added to dialysis tubing (SnakeSkin 3.5K MWCO; Pierce, Rockford, Illinois, USA) and dialysed against 3 volumes of pH7.4 dialysis buffer (1M arginine, 2mM reduced glutathione, 0.2mM oxidised glutathione (both Sigma-Aldrich) in PBS) at 4˚C overnight. The dialysate was concentrated by centrifugation at 4000*g* at 4˚C using Amicon Ultra-15 centrifugal filter units (Millipore, Watford, Hertfordshire, UK), until a

suitable final concentration was achieved, determined using a NanoDrop spectrophotometer at 280nm.

2.2.1.4 SDS-PAGE and western blot

Samples of rmMOG (10µg) were diluted in NuPAGE LDS sample buffer (Life Technologies) with NuPAGE Reducing Agent (Life Technologies) for denaturing gel electrophoresis of reduced samples and heated for 10 minutes at 70°C. Samples were loaded onto a NuPAGE Novex 4-12% Bis-Tris Gel (Life Technologies) with protein molecular weight markers (SeeBlue Plus2 Pre-Stained Standard; Life Technologies) and control samples comprising a sample of rmMOG produced previously in this laboratory and bovine serum albumin (BSA; 2mg/ml) in PBS. NuPAGE Antioxidant (Life Technologies) was added to NuPAGE MES SDS Running Buffer (Life Technologies) in the Upper Buffer Chamber of the XCell *SureLock* Mini-Cell (Life Technologies) and the gel was run for approximately 45 minutes at 200V.

Protein bands were detected by immersion of the gel in Coomassie Brilliant Blue (Sigma-Aldrich) followed by destaining in ethanol (10% (v/v); Sigma-Aldrich) and acetic acid (7.5% (v/v); BDH Chemicals from VWR International Ltd, Lutterworth, Leicestershire, UK) until a clear background was achieved. The monomer:dimer ratio of rmMOG was determined by light intensity measurement using the line profile tool in Image-Pro Plus 7.0 (Media Cybernetics, Rockville, Maryland, USA). The mean of 3 measurements was used. A high monomer:dimer ratio is thought to be more encephalitogenic (unpublished observations from this laboratory).

RmMOG was detected using western blot. SDS-PAGE was performed as described above, followed by equilibration of the gel in NuPAGE Transfer Buffer (Life Technologies) with antioxidant. Protein bands were transferred to a 0.2µm nitrocellulose membrane (Life Technologies), which had been soaked in transfer buffer with antioxidant and methanol

(Sigma-Aldrich) and placed under the gel between filter paper, using semi-dry transfer for 60 minutes at 2V.

The membrane was washed in pH7.4 Tris-buffered saline with 0.1% (v/v) Tween 20 (Sigma-Aldrich; TBST) followed by blocking of non-specific binding sites with 5% w/v dried milk powder (Marvel; Premier Foods, St Albans, Hertfordshire, UK) in TBST for 60 minutes with agitation. It was then washed in TBST for 10 minutes followed by incubation with goat anti-mouse MOG primary antibody (R&D Systems, Abingdon, Oxfordshire, UK) at 1:10,000 in 2% w/v dried milk powder in TBST for 60 minutes with agitation. The membrane was again washed in TBST, for 5 minutes 3 times, and subsequently incubated with donkey anti-goat horseradish peroxidase conjugated secondary antibody (R&D Systems) at 1:10,000 in 2% w/v dried milk powder in TBST for 60 minutes with agitation. Following washing of the membrane in TBST for 30 minutes, bands were detected using electrochemiluminescence (ECL) Western Blotting Detection Reagent (Amersham; GE Healthcare Life Sciences, Little Chalfont, Buckinghamshire) and Hyperfilm ECL (Amersham) according to manufacturer's instructions.

2.2.2 Induction of EAE

2.2.2.1 Animals

Female DA rats (Charles River, Germany) aged 8 to 12 weeks and weighing approximately 160g were housed in groups of 4 or 5 in individually ventilated cages with two levels for environmental complexity (Tecniplast, London, UK) in the Central Biomedical Services (CBS) at the Hammersmith Hospital campus of Imperial College London. They were housed under standard conditions at a temperature of 21-23°C using a 12h light-dark cycle (lights on at 07:00). Identification was by rings marked on the bases of their tails. They were maintained on standard chow pellets and water *ad libitum*. They were allowed to acclimatise to CBS for a minimum of 7 days prior to any regulated procedures being carried out,

following which they were housed in the same room under the same conditions. Animals with clinical EAE were provided with wet mash. Animal work was carried out in compliance with Home Office regulations (project licence 70/7213).

2.2.2.2 Immunisation

Animals were placed under general anaesthesia (isoflurane 2%; Abbott Laboratories, Maidenhead, Berkshire, UK and oxygen 2l/min), the base of the tail was shaved and povidone-iodine antiseptic solution (Videne; Ecolab, Leeds, Yorkshire, UK) was applied. Animals received an intradermal injection into the dorsal aspect of the base of the tail of 2, 5, 10 or 50μg of rmMOG (the batch expressed and purified here, batch pXVII; *n* = 4 per group) diluted in PBS emulsified in an equal volume of IFA (Difco Laboratories, Detroit, Michigan, USA). Control animals received an injection of PBS emulsified in an equal volume of IFA (*n* = 3). The total injection volume was 100μl.

2.2.2.3 Clinical scoring

Following immunisation animals were weighed and scored daily. Clinical scores were based on the level of neurological deficit and were modified from Storch *et al.*, 1998b as in Table 2.2.1, with greater scores representing greater neurological deficit. Animals were removed from the experiment if they reached the humane endpoints of a loss of 25% of their body mass (from the day prior to the development of deficit) for 48 hours or complete weakness of both hind limbs for more than 5 days without weight gain, in compliance with Home Office regulations.

2.2.3 Assessment of EAE pathology

2.2.3.1 Tissue harvesting and treatment

Animals received an intraperitoneal (i.p.) injection of an overdose of 200mg/ml pentobarbital sodium (Euthatal; Merial Animal Health, Harlow, Essex, UK) at the peak of neurological deficit or at 28 or 29 dpi. Respiratory arrest was confirmed, a thoracotomy was performed

Clinical score	Deficit
0	No deficit
0.25	Loss of tone of tip of tail
0.5	Loss of tone of half of tail
1	Complete weakness of tail
2	Partial weakness of one limb
2.5	Complete weakness of one limb
3	Partial weakness of both hind limbs
3.5	Complete weakness of both hind limbs or weakness in limbs on one side
4	Weakness of all limbs or complete weakness in limbs on one side
5	Complete weakness of all limbs/moribund/dead

Table 2.2.1. Animals were scored daily based on the level of neurological deficit.

and animals were perfused through the left ventricle with approximately 50ml of PBS (until the blood from an incision made in the right atrium flowed clear) followed by approximately 100ml of 4% (w/v) paraformaldehyde (PFA; Sigma-Aldrich) in PBS using a 19 gauge needle (BD Biosciences, Oxford, Oxfordshire, UK). The blood from the right atrium was collected and treated as described in 2.2.3.5. The brain and spinal cord were harvested and post-fixed in 4% PFA for 4 hours at 4°C followed by cryoprotection in 30% (w/v) sucrose (Sigma-Aldrich) in PBS for 48 hours or until equilibrium was reached at 4°C.

The spinal cord was cut into 8 sections (approximately 8mm in length) corresponding to two cervical (C2 and C6), four thoracic (T2, T5, T9 and T12) and two lumbar (L2 and L5) segments. Tissue was briefly rinsed in PBS, placed in a mould filled with optimal cutting temperature compound (Tissue-Tek; Sakura, Alphen aan den Rijn, The Netherlands) and frozen in isopentane (Sigma-Aldrich) on dry ice. 10µm sections in the coronal plane were cut using a cryostat (Leica, Wetzlar, Hesse, Germany) and stored at -20°C.

2.2.3.2 Immunofluorescence

In order to identify areas of demyelination and the presence of activated macrophages/microglia in the spinal cord, double immunofluorescence (IF) for MOG and

ionized calcium binding adaptor molecule 1 (Iba1) respectively was performed. Sections were immersed in -20°C methanol (Sigma-Aldrich) for 6 minutes for retrieval of the MOG antigen followed by 3 washes with 0.1% (v/v) Triton X-100 (Sigma-Aldrich) in PBS (PBST). Sections were blocked with 5% (v/v) normal horse serum (NHS; Sigma-Aldrich) in PBST for 60 minutes and incubated with primary antibodies (Table 2.2.2) diluted in 1% (v/v) NHS in PBST overnight at 4°C. Sections were incubated with horse anti-mouse biotinylated secondary antibody (Vector Laboratories, Peterborough, Cambridgeshire, UK) at 1:500 in the same diluent for 60 minutes followed by incubation with goat anti-rabbit Alexa Fluor 546 conjugated secondary antibody (Alexa Fluor Dyes; Life Technologies) and Alexa Fluor 488 conjugated streptavidin (Alexa Fluor Dyes) at 1:1000 for 60 minutes in the dark. Following incubation with 4', 6-diamidino-2-phenylindole (DAPI, 4µg/ml; Sigma-Aldrich) for 5 minutes to identify cell nuclei, sections were mounted in Vectashield mounting medium (Vector Laboratories). PBST washes were performed between incubations, which were performed at room temperature unless otherwise stated.

In order to identify B cells, IF for CD79a was performed using the same protocol as that for MOG but replacing methanol retrieval with heat mediated pH6 citrate buffer (0.1M citric acid, 0.1M sodium citrate (both Sigma-Aldrich)) retrieval using a vegetable steamer.

Antigen	Cell specificity	Species	Dilution	Source
CD3	T cell	Mouse	1 in 750	BD Pharmingen from BD Biosciences
CD79a	B cell	Mouse	1 in 500	Pierce Antibodies from Thermo Scientific, Cramlington, Northumberland, UK
Iba1	Activated macrophages/ microglia	Rabbit	1 in 1000	Wako, Neuss, North Rhine-Westphalia, Germany
MOG	Myelin and oligodendrocytes	Mouse	1 in 20	Reynolds' group, Imperial College London

Table 2.2.2. Primary antibodies used for IF and immunohistochemistry.

2.2.3.3 Immunohistochemistry

In order to identify the presence of T cells, immunohistochemistry (IHC) for CD3 was performed. Heat mediated modified pH6.1 citrate buffer (Dako UK Ltd, Ely, Cambridgeshire, UK) retrieval using a vegetable steamer was followed by immersion in 0.3% (v/v) hydrogen peroxide (Sigma-Aldrich) in PBST for 10 minutes to destroy endogenous peroxidase activity. Sections were blocked with 5% (v/v) NHS in PBST for 60 minutes and incubated with anti-CD3 primary antibody (Table 2.2.2) diluted in 1% (v/v) NHS in PBST overnight at 4°C. Sections were incubated with horse anti-mouse biotinylated secondary antibody at 1:1000 in 1% (v/v) NHS in PBST for 60 minutes followed by avidin-biotin-peroxidase complex (ABC, Vectastain Elite ABC Kit; Vector Laboratories) for 60 minutes. PBST washes were performed between incubations, which were performed at room temperature unless otherwise stated. Sections were developed with 3, 3'-diaminobenzidine (DAB, DAB Peroxidase Substrate Kit; Vector Laboratories) and counterstained with haematoxylin (Haemalum Mayer; TCS Biosciences, Botolph Claydon, Buckinghamshire) for 2 minutes followed by destaining in warm running tap water for 5 minutes. Sections were dehydrated using ethanol gradients and cleared using xylene (VWR International Ltd) followed by mounting in DPX (BDH Chemicals from VWR International Ltd).

2.2.3.4 Imaging and analysis

IF and IHC sections were imaged using a Nikon Eclipse 80i or 50i microscope (Nikon, Kingston upon Thames, Surrey, UK) respectively with a QImaging QICAM digital camera (QImaging, Newcastle under Lyme, Staffordshire, UK) and Image-Pro Plus software (Media Cybernetics, Marlow, Buckinghamshire, UK). This software was able to tile multiple high magnification images to yield high resolution images of complete sections.

Image-Pro Plus 7.0 was used to quantify areas of demyelination (Figure 2.2.2 A) while immune cells were quantified manually using the 20x objective lens. While looking down the

eyepiece, cells were counted in complete sections by moving across them row by row. Quantification was performed by two blinded observers to eliminate bias and ensure accurate, reproducible immune cell counts. ImageJ (NIH, Bethesda, Maryland, USA) was used to quantify areas of Iba1 immunoreactivity (IR; B). Quantification was performed on 3 consecutive sections per animal and a mean calculated.

2.2.3.5 ELISA for peripheral anti-MOG antibodies

Blood was collected at 14 and 21 dpi. Animals were incubated in a hot box at 28°C for 10 minutes before being placed in a restraint tube with tails in warm water at 40°C for 2 minutes. Blood (maximum of 250µl) was collected from a lateral tail vein using a 23 gauge butterfly cannula (Venofix; Medisave, Weymouth, Dorset, UK). EDTA was added at a final concentration of 2.3mg/ml to prevent coagulation. Blood was also collected at termination. Blood was centrifuged at 800*g* for 10 minutes and the serum collected and stored at -20°C.

An ELISA was performed to determine the levels of anti-MOG antibodies. Briefly, 96-well microplates (BD Biosciences) were coated with 50µl per well of 10µg/ml rmMOG (mixed batch pXIV) in PBS overnight at 4°C followed by 5 washes with PBST. Plates were blocked with 200µl per well of 2% (w/v) BSA in PBS for 60 minutes and incubated with 100µl per well of serum, diluted as stated in Table 2.2.3 in 1% (w/v) BSA in PBS, in triplicate for 2 hours. Plates were incubated with 100µl per well of goat anti-rat IgG-specific alkaline phosphatase-linked secondary antibodies, diluted as stated in Table 2.2.3 in the same diluent, for 1 hour. Plates were developed using 200µl per well of p-Nitrophenyl phosphate in Tris buffer (SIGMA*FAST* p-Nitrophenyl phosphate tablets; Sigma-Aldrich) at room temperature in the dark. Optical density was measured at 405nm after 30 minutes using a VersaMax ELISA Microplate Reader (Molecular Devices, Wokingham, Berkshire, UK) and SoftMax Pro software (Molecular Devices). PBST washes were performed between incubations, which were performed at a temperature of 37°C and with shaking unless otherwise stated.

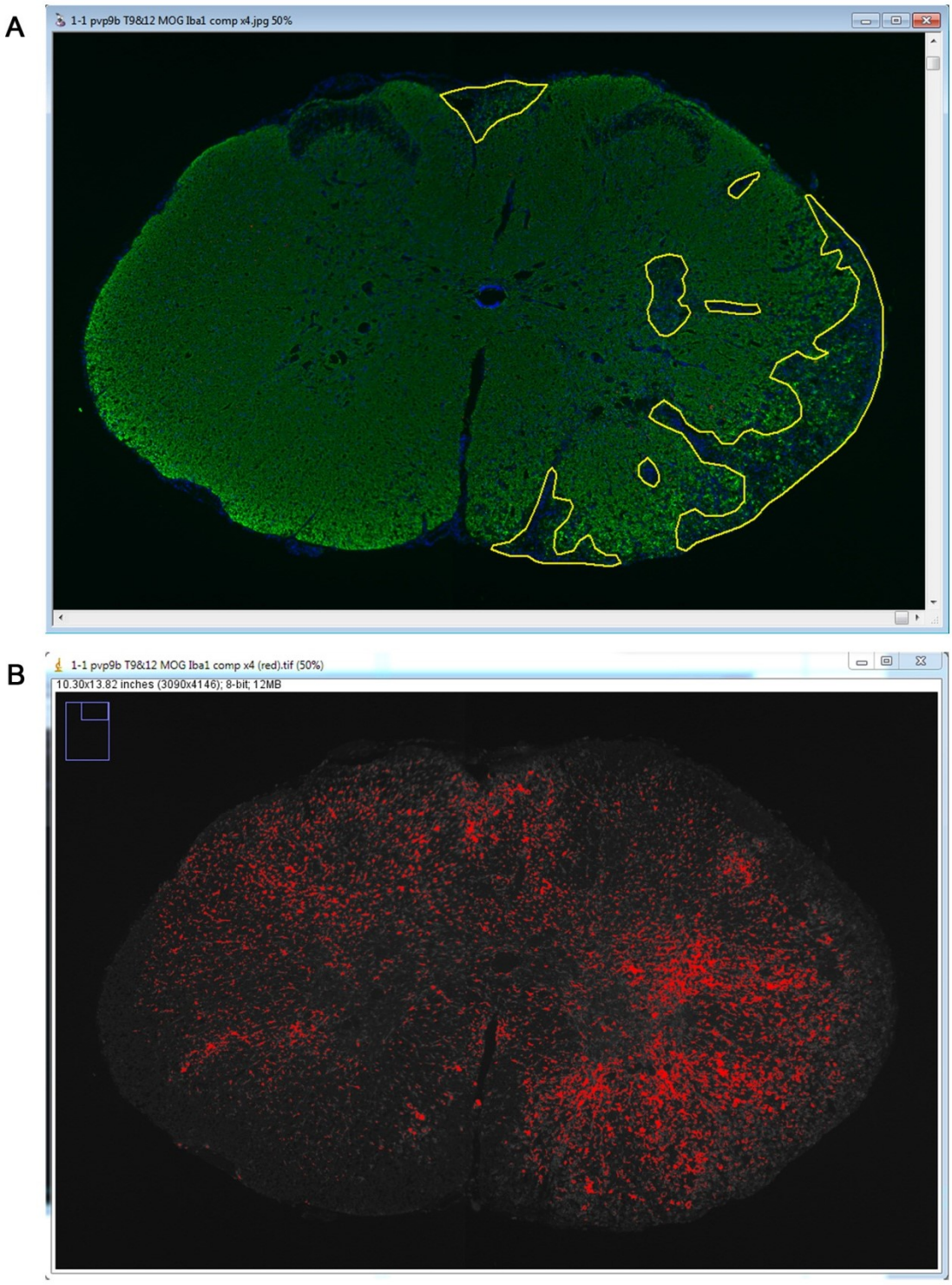

Figure 2.2.2. Quantification of area of demyelination and Iba1 immunoreactivity. The total area of demyelination in each spinal cord section was quantified using tiled images of MOG and Iba1 double IF sections taken using the 4x objective lens and Image-Pro Plus 7.0 software. Iba1 was removed from the composite, individual areas of demyelination were selected (yellow) and calculated areas summed (A). The total area of Iba1 immunoreactivity was quantified using the same images and ImageJ software. All images were taken at the same exposure as far as was possible. The channels were split and the same threshold was applied to Iba1 images to select the Iba1 immunoreactivity and calculate its area (B).

Secondary antibody	Serum dilution	Antibody dilution	Source
Total IgG	1:4000	1 in 5000	Southern Biotech
IgG1	1:1000	1 in 4000	AbD Serotec
IgG2a	1:1000	1 in 4000	AbD Serotec

Table 2.2.3. Secondary antibodies used for ELISA.

2.2.4 Statistical analysis

All data are presented as the mean ± the standard error of the mean (SEM). GraphPad Prism 5 (GraphPad Software, La Jolla, California, USA) was used to construct graphs and perform statistical analysis. Groups were compared using Kruskal-Wallis one-way analysis of variance (ANOVA) with Dunn's multiple comparisons post-hoc test. A p value of <0.05 was considered to be statistically significant.

2.3 Results

2.3.1 Expression and purification of rmMOG

DNA gel electrophoresis was performed to confirm that the colony of transformed *E. coli* selected for expression of the recombinant protein corresponding to the N-terminal amino acids 1-118 of mouse MOG contained the rmMOG insert in the vector (Figure 2.3.1 A). Although the size of the vector containing the rmMOG insert is approximately 3.2kb, it was observed in the uncut lane at approximately 2.2kb. This was due to the supercoiled conformation of the vector, which resulted in its faster electrophoretic mobility than the cut conformation. The cut vector without the rmMOG insert was observed in the EcoR1 + HindIII lane at approximately 2.9kb, while the rmMOG insert was observed at approximately 360bp, as expected. DNA sequencing was also performed, which confirmed that the colony selected contained the rmMOG sequence as well as the polyhistidine tag required for subsequent purification with a nickel-chelating resin.

SDS-PAGE followed by western blotting confirmed that the experimental batch of rmMOG produced in the current study, batch pXVII, was MOG. Bands corresponding to dimer and trimer as well as monomer were observed at approximately 40, 60 and 20kDa respectively (Figure 2.3.1 B). Identical bands were observed for a control batch of rmMOG produced previously, batch pXV. SDS-PAGE followed by Coomassie staining allowed the monomer:dimer ratio to be determined by light intensity measurement. The Coomassie stained gel was used for this purpose rather than the western blot to avoid the introduction of confounding variables. For example, the efficiency of protein transfer from the gel to the membrane depends on the characteristics of the protein, and hence the protein on the membrane may not represent the total protein. Additionally, the antibody used for western blotting may not bind monomer and dimer with equal affinity. The monomer:dimer ratio of batch pXVII was 8.7:1 compared to 12.0:1 for batch pXV. Bands were also observed on the

western blot, as well as on the Coomassie stained gel, at approximately 14kDa. These bands were observed for both batch pXVII and batch pXV.

The total volume of batch pXVII rmMOG obtained was 61.5ml, the concentration of which, determined using a NanoDrop spectrophotometer at 280nm, was 2.46mg/ml (Figure 2.3.1 C). The peak observed at 230nm in the spectrum corresponds to urea, which was present at 8M concentration in the buffers used throughout purification and in the elution buffer in which rmMOG is dissolved.

2.3.2 Induction of EAE

2.3.2.1 Clinical disease in animals immunised with 50µg rmMOG only

Female DA rats were immunised with 2, 5, 10 or 50µg of rmMOG emulsified in an equal volume of IFA (*n* = 8 for 50µg, *n* = 4 for 2, 5 and 10µg of rmMOG). Control animals received an injection of PBS also emulsified in an equal volume of IFA (*n* = 3). Immunisation with 50µg of rmMOG induced relapsing-remitting disease with 100% incidence, with a mean day of disease onset of 16 dpi (Figure 2.3.2 A). Half of these animals (*n* = 4) were culled at the peak of neurological deficit (mean 22 dpi) and half (*n* = 4) were culled at 28 dpi at the same time as animals immunised with 2, 5 or 10µg of rmMOG and IFA only, although one of these animals was culled at 22 dpi due to humane endpoints being reached, with remission followed by a further relapse (B). Ascending paralysis was observed in diseased animals, with initial weakness of the tail followed by weakness of the hind limbs and, in some cases, all limbs. The maximum clinical score was 4, corresponding to weakness of all limbs, typically with complete weakness of both hind limbs. Two diseased animals developed atypical symptoms characterised by disturbances in balance and coordination, including involuntary rotation, and were culled due to humane endpoints being reached. In the remaining diseased animals peak neurological deficit was followed by remission or complete recovery. Immunisation with IFA only and 2, 5 or 10µg of rmMOG did not induce disease (A).

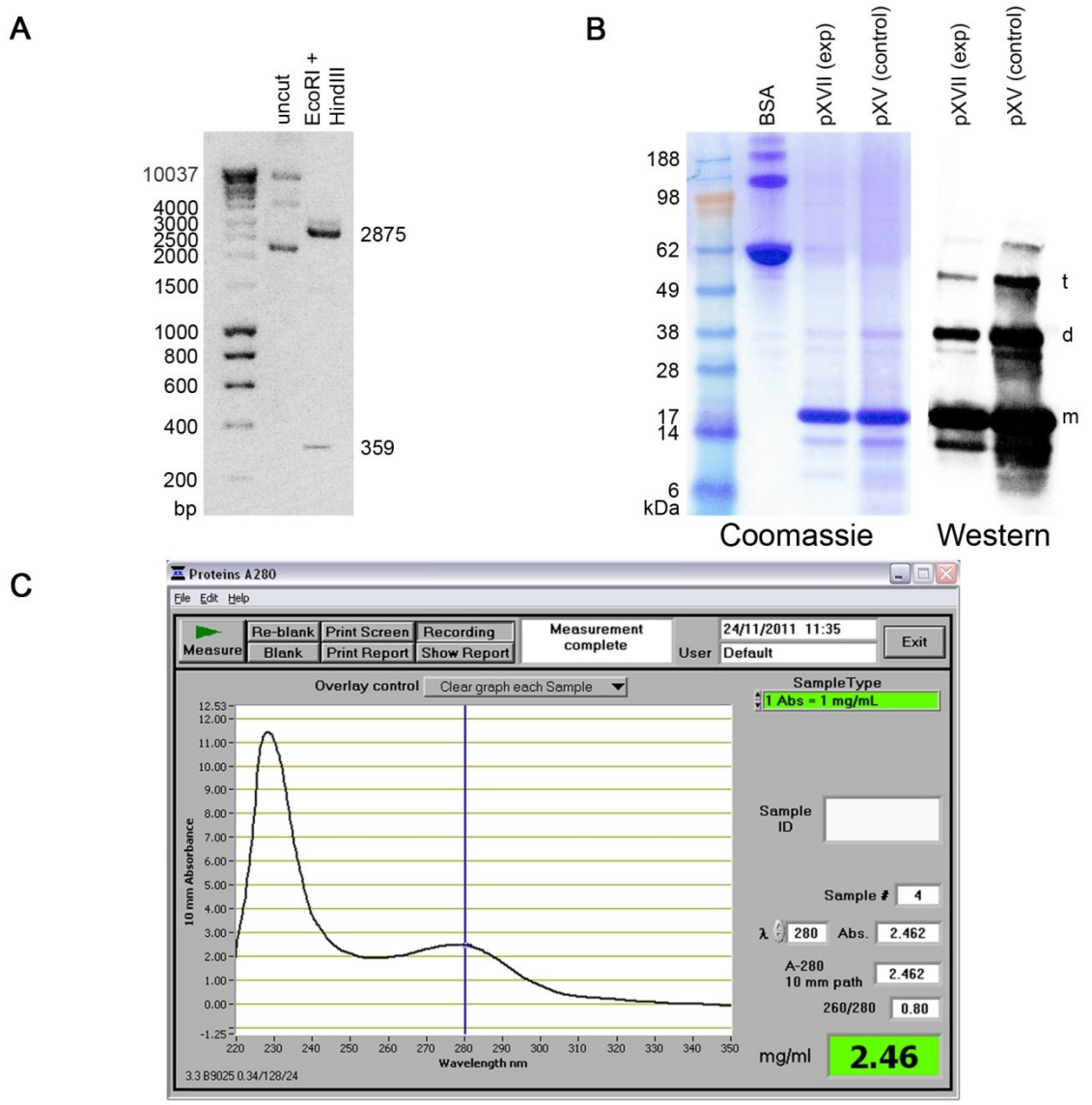

Figure 2.3.1. Expression and purification of rmMOG from transformed *E.coli* glycerol stocks. DNA gel electrophoresis was performed to confirm that colonies contained the correct size of insert. The uncut lane represents the supercoiled vector and the EcoR1 + HindIII lane represents the linearised 2875bp vector and the 359bp rmMOG insert excised following restriction digestion (A). Identical bands corresponding to monomer (m) were observed at ~20kDa on a Coomassie stained gel for both the current experimental batch and a previous control batch (pXV; B). Identical bands corresponding to dimer (d) and trimer (t) were observed on a Western blot, which confirmed that the protein was MOG (B). The concentration of Batch pXVII was determined using a NanoDrop spectrophotometer (C).

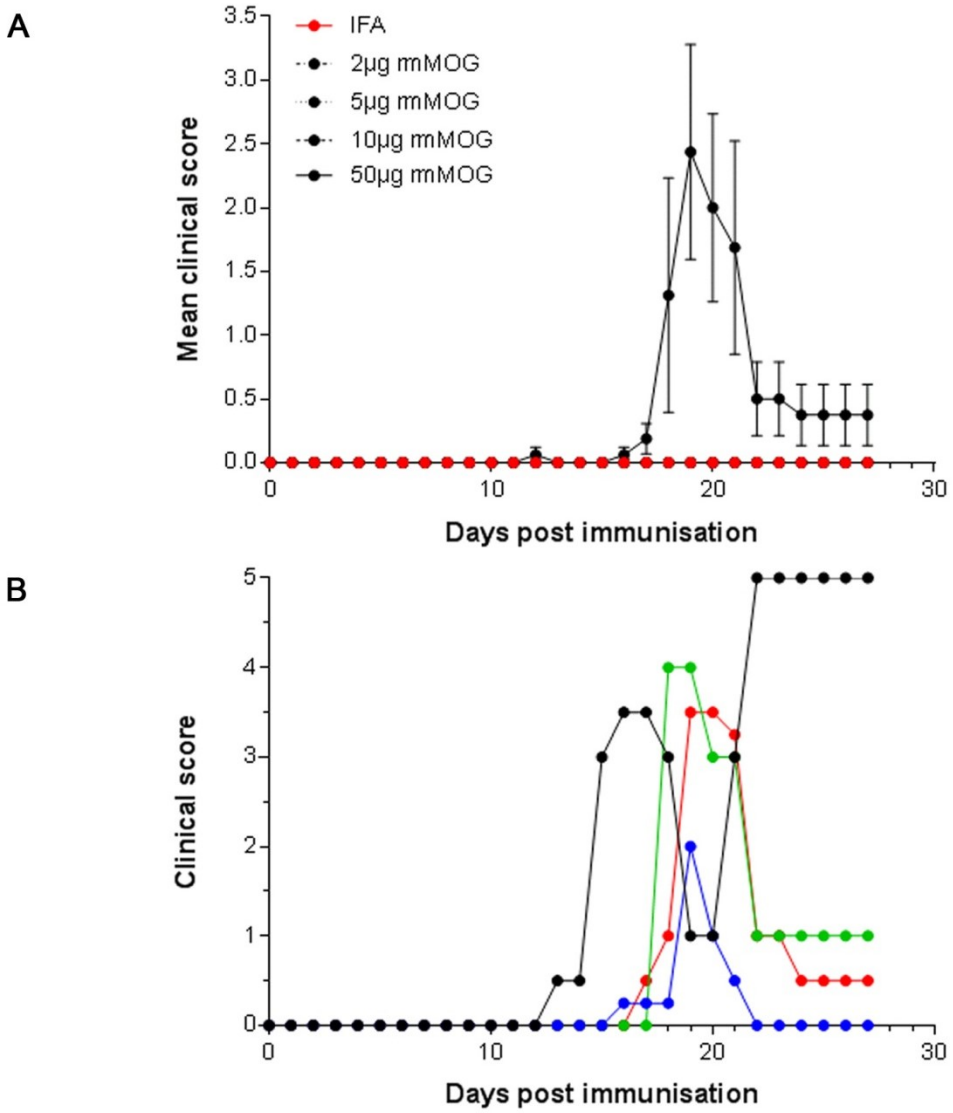

Figure 2.3.2. Development of neurological deficit in animals immunised with 50µg of rmMOG. Animals immunised with IFA only and 2, 5 or 10µg of rmMOG were asymptomatic, whereas animals immunised with 50µg of rmMOG developed neurological deficit, with a mean day of disease onset of 16 dpi (A; mean ± SEM of animals surviving to 28 dpi; *n* = 3 for IFA, 4 for 2, 5, 10 and 50µg). Animals allowed to survive to the end of the experiment developed relapsing-remitting disease, with one episode of neurological deficit followed by remission (clinical scores of individual animals in B). In one of these animals remission was followed by relapse at 22 dpi and this animal was culled (black).

2.3.2.2 Spinal cord demyelination in diseased animals only

In order to identify areas of demyelination and the presence of activated macrophages/microglia in the spinal cord, double IF for MOG and Iba1 respectively was performed, showing demyelination and inflammation in the spinal cord of animals immunised with 50µg of rmMOG culled at the peak of neurological deficit.

Demyelination was present in the spinal cord WM of 75% of animals culled at the peak of neurological deficit. It was most extensive in the lower thoracic and lumbar sections and was observed in the cuneate and gracile fasciculi of the dorsal funiculus as well as in the lateral funiculus. Here, it was observed in the anterior and posterior spinocerebellar tracts, particularly at the exit of the ventral roots, extending into the anterior and lateral spinothalamic tracts, as well as in the lateral corticospinal tract (Figure 2.3.3 Ai, Aiii). Demyelination was not present in the spinal cord GM. Areas of demyelination were associated with the presence of a high number of activated macrophages/microglia, which had an amoeboid morphology characterised by a large cell soma and mostly absent or short, thick processes (Figure 2.3.3 Aii, Aiv). Spinal cord demyelination was not observed in asymptomatic animals immunised with IFA or 2 or 5µg of rmMOG, or in diseased animals immunised with 50µg of rmMOG not culled at the peak of neurological deficit but at 28 dpi (Bi, Ci, Figure 2.3.4 A). Macrophages/microglia in these animals had a ramified morphology characterised by a small cell soma and numerous fine, branched processes and did not contain myelin/myelin degradation products (Figure 2.3.3 Bii, Cii). The density of activated macrophages/microglia in these asymptomatic animals was not significantly different to that in animals immunised with IFA (Figure 2.3.4 B). Despite the absence of demyelination in the diseased animals culled at 28 dpi, activation of macrophages/microglia was observed throughout the spinal cord and, as in animals culled at the peak of neurological deficit, was more severe in the lumbar cord.

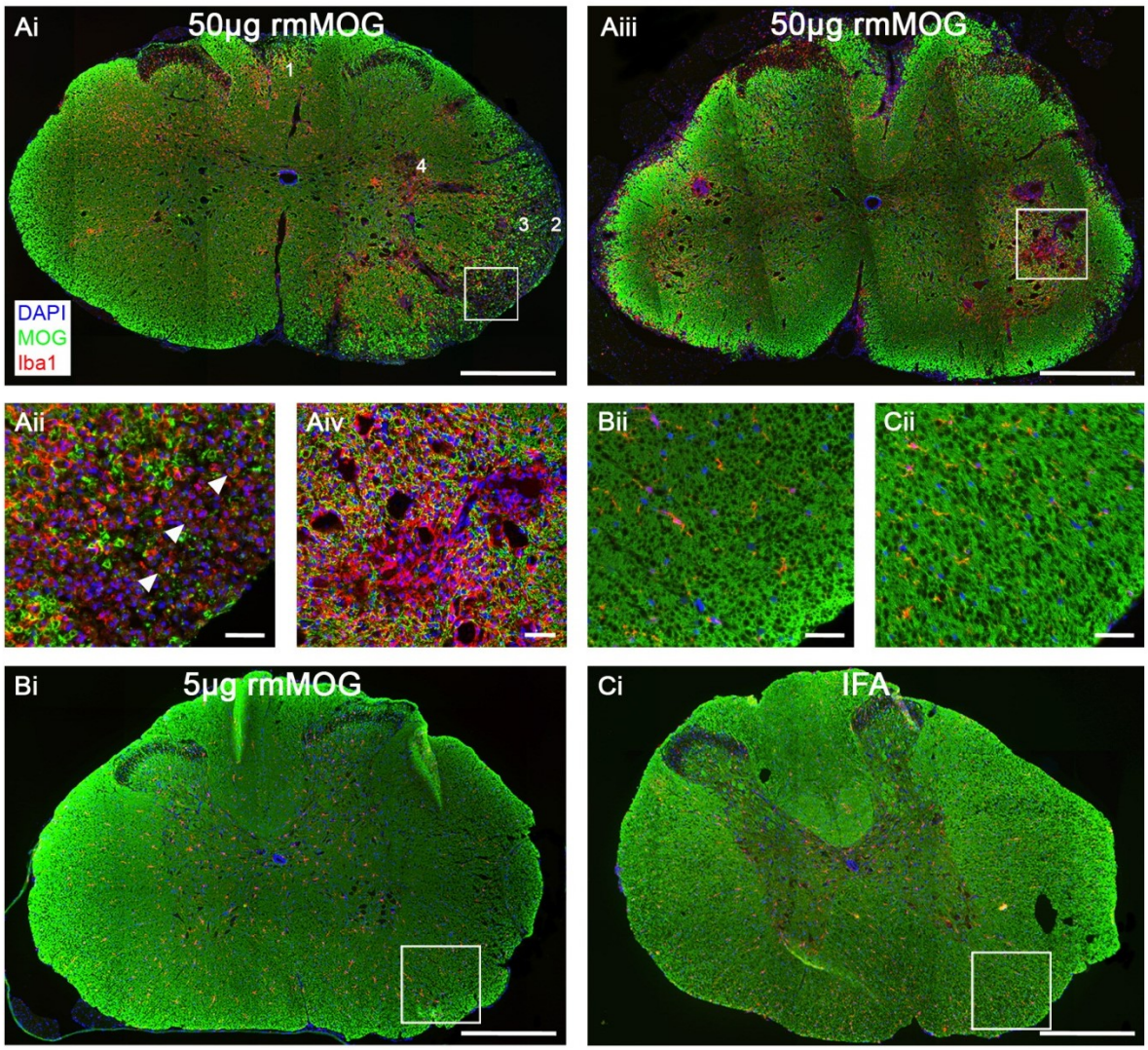

Figure 2.3.3. Double IF for MOG and Iba1 showed demyelination and inflammation in the spinal cord. WMLs were observed in the animals immunised with 50µg of rmMOG culled at the peak of neurological deficit in the dorsal funiculus (1) and spinocerebellar (2), spinothalamic (3) and lateral corticospinal (4) tracts in the lateral funiculus (Ai, Aiii). High numbers of activated macrophages/microglia with amoeboid morphology were present in WMLs (Aii, Aiv) and appeared to contain myelin/myelin degradation products (arrowheads in Aii). Lesions were not observed in asymptomatic animals immunised with 5µg of rmMOG (Bi) or IFA only (Ci). Low numbers of resting macrophages/microglia with ramified morphology were present (Bii and Cii). Images are representative; two animals immunised with 50µg of rmMOG are shown. Images in Aii, Aiv, Bii, and Cii are magnifications of the boxed areas in Ai, Aiii, Bi and Ci respectively. Scale bar: Ai, Aiii, Bi and Ci = 500µm; Aii, Aiv, Bii and Cii = 50µm.

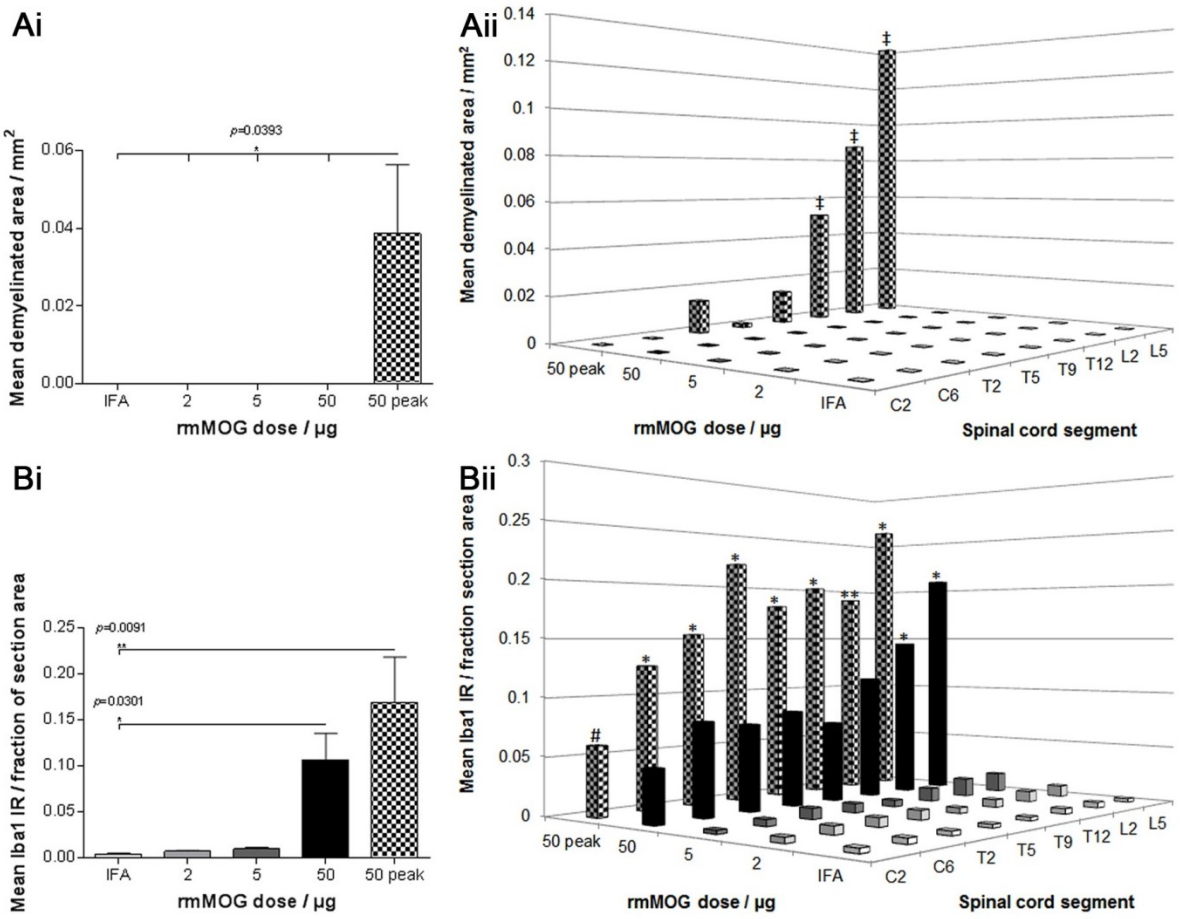

Figure 2.3.4. Quantification of demyelination and inflammation in the spinal cord. Demyelination was observed in animals culled at the peak of neurological deficit (50 peak) only (Ai; Kruskal-Wallis with Dunn's multiple comparisons test; mean ± SEM; * = $p \leq 0.05$; n = 3 for IFA, 4 for remaining groups), the area of which was greatest in the lower thoracic and lumbar sections (Aii; ‡ = $p \leq 0.05$ compared to IFA, 2, 5 and 50). Iba1 immunoreactivity was significantly increased in animals immunised with 50µg of rmMOG culled at 28 dpi as well as in the 50 peak animals, whereas that in asymptomatic animals immunised with 2 or 5µg of rmMOG was not significantly different to that in animals immunised with IFA only (Bi; Kruskal-Wallis with Dunn's multiple comparisons test; mean ± SEM; * = $p \leq 0.05$, ** = $p \leq 0.01$; n = 3 for IFA, 4 for remaining groups). Although inflammation was increased throughout the spinal cord, it was more severe in lumbar sections, particularly in animals immunised with 50µg of rmMOG culled at 28 dpi (Bii; * = $p \leq 0.05$ compared to IFA, ** = $p \leq 0.01$ compared to IFA, # = $p \leq 0.05$ compared to 5).

2.3.2.3 T and B cell infiltration in spinal cords of diseased animals only

The presence of T and B cells in the spinal cord was identified using IHC for CD3 (Figure 2.3.5 Ai) and IF for CD79a (Bi) respectively. Although these cells were observed in the meninges as well as in the parenchyma, only those in the parenchyma were quantified due to variation in meningeal preservation between sections. However, T cell infiltration in the meninges appeared to be greater in diseased than asymptomatic animals and those immunised with IFA only, in which very few T cells were observed. Very few B cells were present in the meninges of both diseased and asymptomatic animals, as well as those immunised with IFA only.

Infiltration of T cells was observed in diseased animals immunised with 50µg of rmMOG, both those culled at the peak of neurological deficit and those culled at 28 dpi (Figure 2.3.5 Aii). T cells were distributed throughout the parenchyma but appeared concentrated in areas in which demyelination had been observed, particularly in the dorsal funiculus and spinocerebellar, spinothalamic and lateral corticospinal tracts in the lateral funiculus. This increase in T cell infiltration was observed throughout the spinal cord and was not greater in the lower thoracic and lumbar sections (Aiii), in contrast to demyelination. The number of T cells in asymptomatic animals immunised with 2 or 5µg of rmMOG was low and not significantly different to that in animals immunised with IFA only. Although only very few B cells, distributed throughout the parenchyma, were present, their number was significantly increased in animals culled at the peak of neurological deficit (Bii). Infiltration of B cells was observed throughout the spinal cord and, like the infiltration of T cells, did not vary between spinal cord sections (Biii). Asymptomatic animals had the same number of B cells as animals immunised with IFA only.

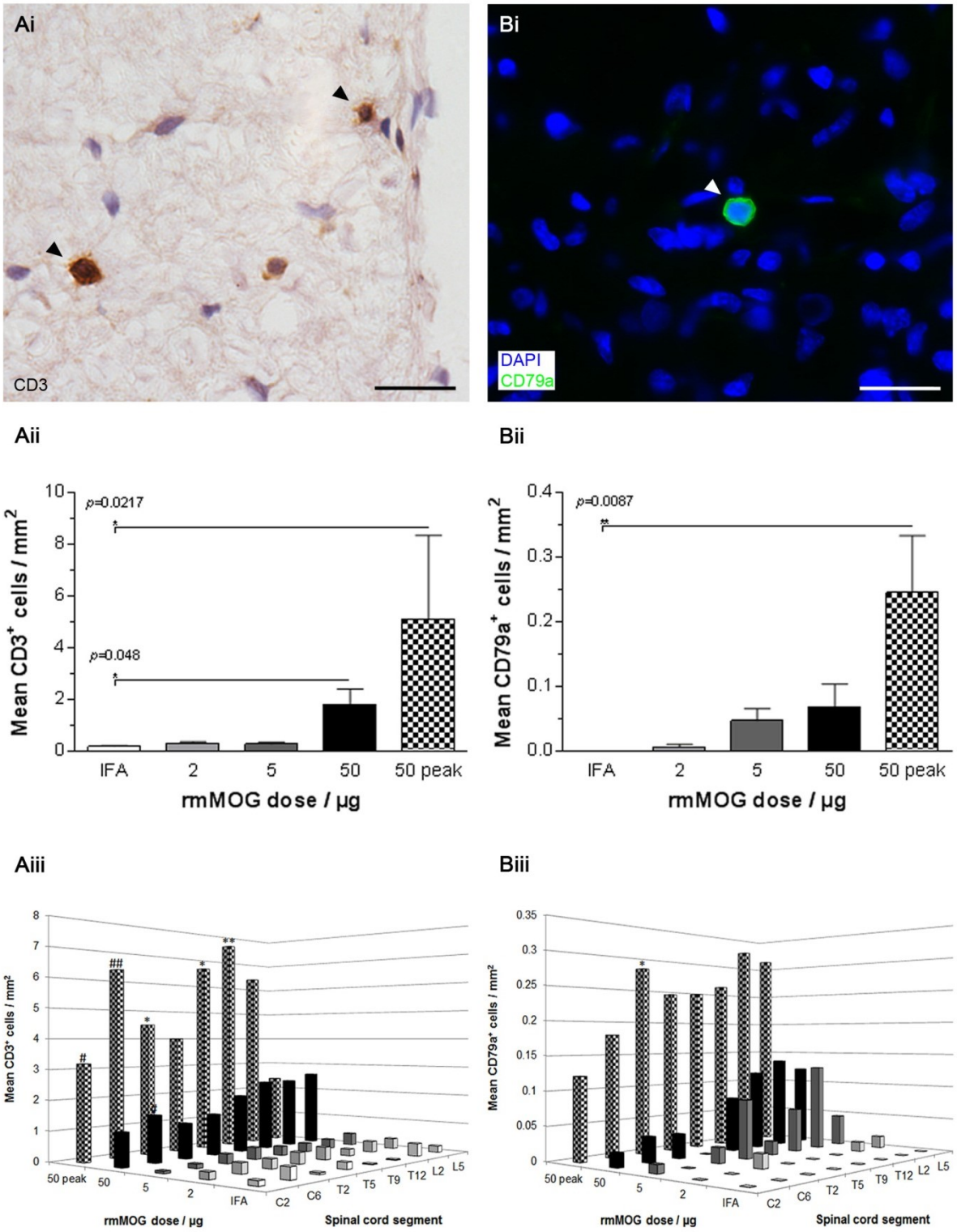

Figure 2.3.5. Quantification of T and B cell infiltration in the spinal cord. IHC for CD3 (Ai) and IF for CD79a (Bi) were performed on spinal cord sections. A significant increase in T cell (Aii) and B cell (Bii) infiltration in animals culled at the peak of neurological deficit was observed (Kruskal-Wallis with Dunn's multiple comparisons test; mean ± SEM; * = $p \leq 0.05$, ** = $p \leq 0.05$; n = 3 for IFA, 4 for remaining groups) throughout the spinal cord (Aiii and Biii; * = $p \leq 0.05$ compared to IFA, ** = $p \leq 0.01$ compared to IFA, # = $p \leq 0.05$ compared to 5, ## = $p \leq 0.01$ compared to 5). T and B cell infiltration in asymptomatic animals was not significantly different to that in animals immunised with IFA only. Scale bar: Ai and Bi = 20µm.

2.3.2.4 Asymptomatic animals had a peripheral anti-MOG antibody response

In order to determine whether the peripheral immune system recognises and responds to subclinical doses of rmMOG, the levels of anti-MOG antibodies (total IgG, IgG1 and IgG2a) in serum obtained from blood collected at 14 and 21 dpi and at termination at 28 dpi were measured using ELISAs.

The levels of total IgG, IgG1 and IgG2a anti-MOG antibodies were significantly increased in animals immunised with 50µg of rmMOG compared to naïve animals and those immunised with IFA only, whereas they were not significantly different to those in asymptomatic animals immunised with 2 or 5µg of rmMOG at termination (Figure 2.3.6 A). The level of anti-MOG IgG1 antibody in asymptomatic animals, although not significantly different, was much lower than that in animals immunised with 50µg of rmMOG (Aii). The levels of total IgG and both subtypes in asymptomatic animals did not change with time from 14 dpi to termination at 28 dpi (B).

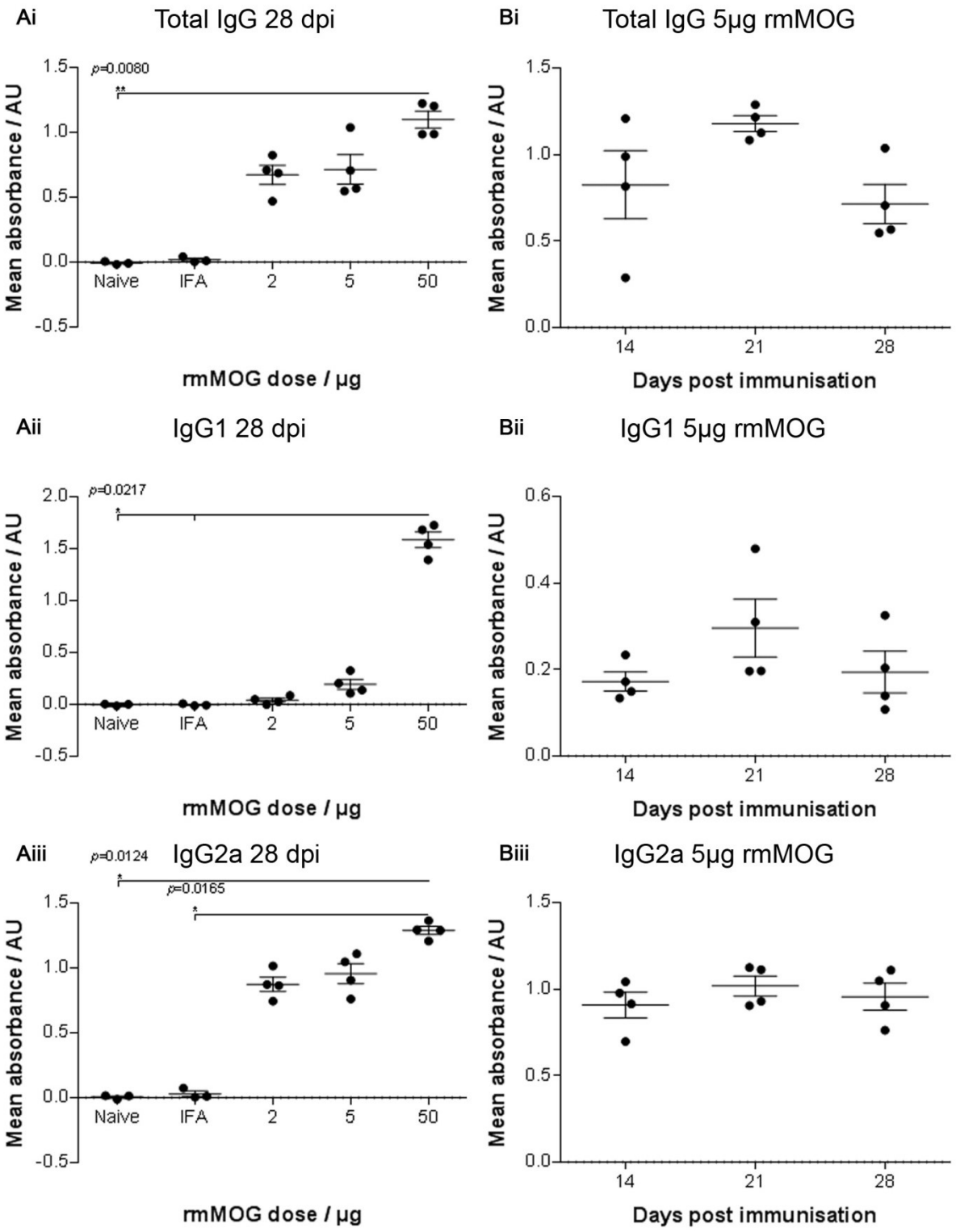

Figure 2.3.6. Measurement of peripheral anti-MOG antibody levels. Blood was collected at 14 and 21 dpi and at termination at 28 dpi and levels of anti-MOG antibodies in serum were measured using ELISAs. Asymptomatic animals immunised with 2 or 5µg of rmMOG had the same levels of total IgG (Ai; Kruskal-Wallis with Dunn's multiple comparisons test; mean ± SEM; ** = $p \leq 0.01$; $n = 3$ for naïve and IFA, 4 for 2, 5 and 50µg), IgG1 (Aii; * = $p \leq 0.05$) and IgG2a (Aiii) anti-MOG antibodies at termination as animals immunised with 50µg of rmMOG, whereas those in naïve animals and animals immunised with IFA only were significantly lower. The levels of all antibodies in asymptomatic animals immunised with 5µg of rmMOG did not increase between 14 dpi and termination (B; $n = 4$ per time point).

2.4 Discussion

2.4.1 Expression and purification of rmMOG

A soluble recombinant protein corresponding to the N-terminal amino acids 1-118 of mouse MOG was successfully expressed and purified from transformed *E. coli* glycerol stocks. western blotting of the separated protein confirmed that the identity of the protein was MOG. Coomassie staining of the separated protein showed bands at approximately 20, 40 and 60kDa. All of these bands consisted of MOG protein, confirming its purity, and corresponded to monomer, dimer and trimer respectively (Reynolds *et al.*, 2002). The monomer:dimer ratio was 8.7:1. High monomer:dimer ratios are thought to be more encephalitogenic (unpublished observations from this laboratory), hence immunisation with this batch of rmMOG was expected to result in a high incidence and severity of EAE. A band underneath that of the monomer, at approximately 14kDa, was observed following both Coomassie staining and western blotting. Although the identity of this MOG peptide is not known, its presence does suggest that some degradation had occurred. This band was, however, also observed for a control batch of rmMOG produced previously and used successfully in MOG-EAE models, hence it was concluded that the rmMOG produced here was also suitable for use in the MOG-EAE model study that follows.

2.4.2 MOG-EAE in the DA rat

The rmMOG produced here was used in subsequent studies in the development of a chronic model of cortical pathology driven by meningeal inflammation. This required a subclinical dose of rmMOG (Kerschensteiner *et al.*, 2004, Merkler *et al.*, 2006, Gardner *et al.*, 2013), which was determined by evaluating the severity of clinical and pathological EAE induced by immunisation of DA rats with a range of doses of the protein. MOG-EAE in the DA rat is characterised by the synergistic actions of auto-antibody and encephalitogenic T cell responses accompanied by macrophage infiltration (Storch *et al.*, 1998b, Weissert *et al.*,

1998), and either a relapsing-remitting or progressive clinical course (Papadopoulos *et al.*, 2006), reproducing the immunopathology and clinical course of MS (Storch *et al.*, 1998a, Lucchinetti *et al.*, 2000, Compston and Coles, 2008).

2.4.2.1 EAE induced by immunisation with 50µg rmMOG

Immunisation with 50µg of rmMOG emulsified in IFA induced relapsing-remitting disease with 100% incidence. Complete weakness of both hind limbs was observed in the majority of animals at first relapse, followed by remission, defined as a clinical score reduction of 2 maintained for 2 days (Weissert *et al.*, 1998). This is in contrast to studies in which immunisation with 200µg of rmMOG induced relapsing-remitting disease whereas immunisation with 50µg of rmMOG favoured the development of progressive disease (Papadopoulos *et al.*, 2006). It is possible that the animals culled at the peak of neurological deficit may have developed progressive disease if they had been left longer. It is likely that this difference in clinical course is due to the different batch of rmMOG used. For example, differences in the monomer:dimer ratio of batches of rmMOG have been shown to affect the incidence, clinical course and severity of EAE (unpublished observations from this laboratory). Although monomer:dimer ratios are not usually documented in the literature, that of the batch used here was high in comparison to batches produced previously in this laboratory. This was despite the same protocol, using dialysis buffer containing 1M arginine that is thought to produce mainly monomer (unpublished observations from this laboratory), being used. However, another study using the same immunisation protocol as that used in the current study, described a variable clinical course, with animals developing chronic, relapsing-remitting or acute disease, or no disease (Zeis *et al.*, 2008).

Clinical disease was associated with demyelination in spinal cord WM of the majority of animals culled at the peak of neurological deficit. The animal in which pathology in the spinal cord was not observed had developed atypical symptoms, characterised by disturbances in balance and coordination. This suggested a change in the site of pathology from spinal cord

to cerebellum and brainstem (Muller *et al.*, 2000), hence it was not surprising that demyelination in the spinal cord was not observed in this animal. Demyelination was most extensive in the lower thoracic and lumbar cord, consistent with ascending paralysis in a distal to rostral direction (Miller *et al.*, 2010). Its presence in the dorsal and lateral funiculi has been observed previously in MOG-induced EAE in the DA rat (Steinbrecher *et al.*, 2005) and is consistent with the neurological deficit these animals developed given the WM tracts affected. For example, damage to the corticospinal tract has been shown to be correlated with clinical score, grid walk score and open field locomotion score in a targeted EAE model (Kerschensteiner *et al.*, 2004), hence this site of pathology in the current study is consistent with the paresis of these animals. Demyelination was not present in spinal cord GM, which is the case for the majority of rodent EAE models (Storch *et al.*, 1998b). Pathology in the spinal cord was also not observed in diseased animals immunised with 50µg of rmMOG not culled at the peak of neurological deficit but at 28 dpi. It is possible that remyelination had occurred in these animals between the peak of neurological deficit at approximately 16-18 dpi and termination at 28 dpi, when animals had weakness of the tail only. Remyelination has been observed in rats with relapsing-remitting MOG-induced EAE 10 days after the onset of clinical disease (Papadopoulos *et al.*, 2006), which would be consistent with the timescale here. Alternatively, although the spinal cord was harvested as completely as possible and lumbar sections were obtained, sacral sections were not. Given that immune cell infiltration of the CNS begins in the lower spinal cord (Miller *et al.*, 2010), it is possible that demyelination would have been observed in sacral sections.

Areas of demyelination in the spinal cord were associated with the presence of a high number of activated macrophages/microglia. T cell infiltration was also observed throughout the spinal cord in the parenchyma as well as in the perivascular and meningeal compartments. As well as reproducing the pathology of WMLs in MS (Lucchinetti *et al.*, 2000), this immunopathology is similar to that observed in previous studies investigating MOG-EAE in the DA rat (Storch *et al.*, 1998b, Papadopoulos *et al.*, 2006,

Schreiner *et al.*, 2009), which showed inflammatory infiltrates consisting of macrophages and T cells around vessels and in the meninges, with spread into the parenchyma adjacent to the pia mater.

2.4.3 Subclinical MOG-EAE in the DA rat

This study has allowed the identification of a suitable subclinical dose of rmMOG batch pXVII, for subsequent use in the development of the chronic model of cortical pathology driven by meningeal inflammation. As specified in the study that first developed a targeted EAE model, this dose should not result in clinical symptoms, but should result in a peripheral anti-MOG antibody response that is the same as that in animals with clinical symptoms. Additionally, little inflammation and no demyelination should be observed in the CNS. The dose will depend on the strain used and its susceptibility to MOG-induced EAE (Kerschensteiner *et al.*, 2004, Merkler *et al.*, 2006, Gardner *et al.*, 2013). Although cortical GMLs have been observed with low incidence in studies of MOG-induced EAE in the DA rat, high doses of rmMOG of 65-75μg were used, resulting in severe clinical EAE (Steinbrecher *et al.*, 2005, Prins *et al.*, 2013), in contrast to the subclinical dose identified in the current study. The absence of cortical pathology following immunisation with this subclinical dose of rmMOG would suggest that any cortical pathology observed following the subsequent injection of pro-inflammatory cytokines was the result of this injection rather than the immunisation only, and that any other cortical changes were the result of this cortical pathology rather than spinal cord pathology. For example, changes in the expression of genes for glutamate receptors and mitochondrial proteins in normal appearing cerebral cortex of female DA rats immunised with 50μg of rmMOG, in which inflammatory demyelination was observed only in the spinal cord, have been shown. These were suggested to be the result of retrograde degeneration following axonal damage induced in spinal cord lesions (Zeis *et al.*, 2008). Therefore, animals with clinical disease may not be used in the development of the chronic model.

2.4.3.1 Clinical EAE not induced by immunisation with 5μg rmMOG

Animals immunised with 5μg (as well as 2μg) of rmMOG were asymptomatic and had no spinal cord demyelination or macrophage/microglia activation, suggesting that this dose was too low to induce an anti-myelin immune response in the CNS and that it may represent a suitable subclinical dose.

Previous studies in DA rats have also used 5μg as a subclinical dose (Gardner *et al.*, 2013), although studies in Lewis rats have used 25-50μg (Kerschensteiner *et al.*, 2004, Merkler *et al.*, 2006). The susceptibility of rats to MOG-induced EAE is strain-dependent (Storch *et al.*, 1998b), with Lewis rats known to be relatively resistant and DA rats susceptible (Weissert *et al.*, 1998, Stefferl *et al.*, 1999b). This difference is thought to be due in part to the MHC haplotype $RT1^{av1}$ present in DA rats, which appears to render this strain susceptible, in contrast to the haplotype $RT1^{1}$ present in Lewis rats (Weissert *et al.*, 1998).

However, there is also a role for genetic factors other than the MHC haplotype. ACI, Lewis and PVG rats, all with the same RT^{av1} MHC haplotype as DA rats, are relatively resistant. Lower incidence in these animals is associated with less demyelination and inflammation in the spinal cord than in DA rats following the same immunisation method, which is suggested to be due to differences in the efficiency of B and T cell responses following immunisation with MOG conferred by non-MHC genes (Lorentzen *et al.*, 1997, Weissert *et al.*, 1998). For example, the expression of the receptors for IL2, IL7 and IL18 is increased in lymph node T cells from naïve DA compared to PVG rats, resulting in increased differentiation to Th1 and Th17 cells following immunisation with MOG and consequent increased expression of the Th1 and Th17 cytokines IFN-γ, IL17 and IL22 (Thessen Hedreul *et al.*, 2009). Th1 and Th17 cells have been shown to induce EAE following adoptive transfer (Jäger *et al.*, 2009), and these T cells appear to be resistant to apoptosis in DA rats (Lukic *et al.*, 2001). Additionally,

macrophages isolated from DA rats produced more TNF following stimulation *in vitro* than those isolated from PVG rats (Gillett *et al.*, 2010).

The high efficiency of B and T cell responses in the DA rat compared to that in resistant strains described above are consistent with the observations that 50μg of rmMOG induces EAE in the DA but not Lewis rat and that a low dose of rmMOG is required for it to be subclinical in the DA rat.

2.4.3.2 Increased lymphocyte infiltration not observed following immunisation with 5μg rmMOG

The presence of T cell infiltration has been observed following the adoptive transfer of myelin-specific T cells in the absence of clinical disease and demyelination, which was shown to be due to the low level of activation of the T cells (Kawakami *et al.*, 2004). However, as well as being asymptomatic and having no spinal cord demyelination or macrophage/microglia activation, little or no spinal cord B or T cell infiltration was observed in animals immunised with 5μg (and 2μg) of rmMOG, with the numbers of these cells not significantly different to those in animals immunised with IFA only. This is consistent with the hypothesis that this dose was too low to induce significant myelin-reactive T cell infiltration in the CNS.

As described in 1.2.1.3, myelin-reactive T cells are activated in the periphery, expand and traffic to the CNS (Hafler and Weiner, 1987), which they enter prior to the onset of clinical symptoms (Brown and Sawchenko, 2007). A recent study has shown that this infiltration occurs in two stages. The first stage is dependent on the expression of the chemokine (C-C motif) receptor 6 (CCR6) on T cells, which allows them to enter the CNS across the blood-CSF barrier (meninges and choroid plexus) that expresses the CCR6 ligand chemokine (C-C motif) ligand 20 (CCL20). In the CSF/meningeal compartment they become reactivated on encountering their specific myelin epitope presented by APCs and infiltrate the spinal cord

parenchyma (Bartholomäus *et al.*, 2009, Kivisäkk *et al.*, 2009). The second stage is dependent on the first stage and on the production of pro-inflammatory cytokines including TNF, IFN-γ and IL17 by the T cells rather than their expression of CCR6 (Brown and Sawchenko, 2007, Reboldi *et al.*, 2009). The pro-inflammatory cytokines result in disruption of the BBB, mediated by alteration of components of adherens and tight junctions, and activation, mediated by increased expression of cell adhesion molecules (Alvarez *et al.*, 2011), facilitating further entry of T cells.

Given that animals immunised with 5μg of rmMOG had no significant spinal cord T cell infiltration, it appears that this dose of rmMOG is too low to induce sufficient activation of T cells to allow both stages of infiltration to occur. However, low doses of antigen have also been shown to favour the anti-inflammatory Th2 response and high doses the pathogenic Th1 response (Hosken *et al.*, 1995, Grakoui *et al.*, 1999), hence it is possible that 5μg of rmMOG constitutes a low dose and favours the Th2 response. In the study of Grakoui *et al.* (1999), the change from Th2 response to Th1 response occurred over the same ten-fold range as that observed in the current study for the change from subclinical to clinical dose. Further studies could investigate the phenotype of spinal cord T cell infiltrates in asymptomatic and diseased animals.

2.4.3.3 Antibody response induced by immunisation with 5μg rmMOG

It was necessary to determine whether this dose of rmMOG was too low to induce a peripheral anti-MOG antibody response as well as significant spinal cord T cell infiltration.

The levels of total IgG, IgG1 and IgG2a anti-MOG antibodies in serum as measured using ELISAs were not significantly different in asymptomatic animals immunised with 5μg of rmMOG than in diseased animals immunised with 50μg of rmMOG, and did not change with time from 14 dpi to 28 dpi. This is in agreement with a study using Lewis rats that showed that the level of total IgG did not change with time (Kerschensteiner *et al.*, 2004) but in

contrast to a study using DA rats that showed that it was maximal at 21 dpi (Gardner *et al.*, 2013). This finding indicates that the maximal peripheral anti-MOG antibody response will have been reached by 21 dpi, when the injection of pro-inflammatory cytokines in the model of cortical pathology driven by meningeal inflammation will be performed. Although the level of IgG1 in animals immunised with 5μg of rmMOG was not significantly different to that in animals immunised with 50μg of rmMOG, it was much lower. However, a previous study showed that it was not significantly increased in animals immunised with 5μg of rmMOG until 32 dpi (Gardner *et al.*, 2013), which may explain why it was low in the current study using blood collected at termination at 28 dpi.

The induction of IgG2a, IgG2b and IgG3 antibodies is characteristic of a Th1 response, whereas that of IgG1 antibodies is characteristic of a Th2 response (Germann *et al.*, 1995). The treatment of Lewis rats with anti-MOG IgG2a antibodies following the adoptive transfer of MBP-specific T cells has been shown to result in extensive demyelination and severe or lethal disease, in contrast to the moderate effects of treatment with anti-MOG IgG1 antibodies. The pathogenicity of the antibodies was shown to be dependent on their ability to fix complement (Piddlesden *et al.*, 1993).

Hence the peripheral immune system is able to induce the adaptive immune response to MOG protein, necessary for the development of targeted EAE models (Kerschensteiner *et al.*, 2004, Merkler *et al.*, 2006), in animals immunised with 5μg of rmMOG. Additionally, although the level of IgG1 induced by the anti-inflammatory Th2 response was low, that of IgG2a induced by the pathogenic Th1 response was the same as that in animals immunised with 50μg of rmMOG. This indicated that the low dose did not result in a change from pathogenic to anti-inflammatory response, in contrast to what has been found in studies using, for example, ovalbumin as antigen (Hashiguchi *et al.*, 2000).

The intravenous injection of anti-MOG antibodies has been shown to result in more severe clinical and pathological EAE induced by the transfer of MBP-specific T cells (Lassmann *et al.*, 1988, Linington *et al.*, 1988). However, despite the pathogenic peripheral anti-MOG IgG2a antibody response in animals immunised with 5µg of rmMOG in the current study, they did not develop clinical or pathological EAE. This is consistent with the finding that high levels of anti-MOG antibodies alone are not sufficient to induce disease, with disruption of the BBB, mediated by encephalitogenic T cells, required (Litzenburger *et al.*, 1998). We suggest that the number of MOG-specific T cells reactivated in the CSF/meningeal compartment is insufficient to cause disruption and activation of the BBB in animals immunised with 5µg of rmMOG, preventing the second stage of immune cell infiltration. In animals immunised with 50µg of rmMOG, the number of T cells, or their secretion of pro-inflammatory cytokines, is sufficient to cause disruption and activation of the BBB and subsequent infiltration of myelin-specific lymphocytes, macrophages and anti-MOG antibodies in the CNS. The synergistic action of cellular and humoral mechanisms then results in clinical and pathological EAE. Hence, we propose that a detailed investigation of the role of T cells in the CSF/meningeal compartment of animals immunised with 5 and 50µg of rmMOG will be required to determine why the former dose is subclinical despite the peripheral anti-MOG antibody response.

2.4.4 Conclusions

Batch pXVII of rmMOG was successfully expressed and purified and 5µg was identified as a suitable subclinical dose as it did not induce spinal cord demyelination or significant lymphocyte infiltration and clinical disease despite inducing a peripheral anti-MOG antibody response. This batch and dose of rmMOG was suitable for use in the development of the chronic model of cortical pathology driven by meningeal inflammation.

Chapter 3

Model of subpial demyelination driven by meningeal inflammation in the DA rat

3.1 Introduction

3.1.1 Cortical GM pathology in MS

Immunohistochemical studies using autopsy samples have shown that cortical GML burden may be greater than that of WMLs, with a mean demyelinated area of 25.0-28.8% compared to 5.0-15.6% (Bø *et al.*, 2003b, Gilmore *et al.*, 2009). It is now widely accepted that cortical GM pathology is involved in clinical progression (Calabrese *et al.*, 2010a) and studies, mainly using clinical MRI, have correlated it with both cognitive (Calabrese *et al.*, 2009a) and motor (Calabrese *et al.*, 2007) disability as well as with the cognitive and motor decline observed during the progressive stages of MS (Calabrese *et al.*, 2009c, Calabrese *et al.*, 2010b, Jacobsen *et al.*, 2014). Studies support a major role for cortical GM pathology in driving this progression, and associated worsening of cognitive and motor symptoms, in MS (Reynolds *et al.*, 2011).

Cortical GM pathology is characterised by demyelination, and the current classification of GMLs is based on their location within the layers of the cortex as described in 1.2.2.2 (Peterson *et al.*, 2001, Bø *et al.*, 2003b). Subpial lesions extend from the pial surface into GM layers without entering WM and may involve multiple gyri. They account for up to 50-70% of all GMLs (Peterson *et al.*, 2001, Bø *et al.*, 2003a, Magliozzi *et al.*, 2007), although 93% of subpial lesions detected using immunohistochemical stains are not detected even using double inversion recovery MRI (Seewann *et al.*, 2012).

Studies have shown that there is no significant correlation between the extent of cortical GM and WM demyelination, suggesting that cortical GMLs develop independently from WMLs (Bø *et al.*, 2003b, Kutzelnigg *et al.*, 2005, Vercellino *et al.*, 2005, Bö *et al.*, 2007). However, there is a significant correlation between the extent of cortical GM demyelination in the cerebellum and that in the forebrain (Kutzelnigg *et al.*, 2005, Kutzelnigg *et al.*, 2007, Gilmore

et al., 2009). The authors suggest that this indicates a common mechanism of demyelination mediated by soluble factors produced in the CSF/meningeal compartment diffusing into the underlying cortical GM. The CSF has long been implicated in MS. Oligoclonal bands are present in the CSF of 87.7% of MS patients (Dobson *et al.*, 2013) and the finding of at least two oligoclonal bands may be used to support diagnoses (Polman *et al.*, 2011). This hypothesis is also supported by the high prevalence of subpial GMLs as well as the lack of significant peripheral immune cell infiltration previously observed in cortical GMLs.

3.1.2 Inflammation associated with cortical GMLs

Inflammation in cortical GMLs is characterised by extensive microglial activation with characteristically only mild peripheral immune cell infiltration in perivascular cuffs, in contrast to WMLs (Peterson *et al.*, 2001, Kutzelnigg *et al.*, 2005, Magliozzi *et al.*, 2010). MHC class II-positive and CD68-positive macrophages/microglia with activated morphology are distributed throughout cortical GMLs as well as in NAGM (Peterson *et al.*, 2001, Bø *et al.*, 2003a, Magliozzi *et al.*, 2007, Magliozzi *et al.*, 2010). Recent studies have, however, also shown the presence of T cell infiltrates as well as perivascular cuffs in subpial cortical GMLs (Lucchinetti *et al.*, 2011, Magliozzi *et al.*, 2013).

3.1.2.1 Meningeal inflammation

Diffuse inflammatory infiltrates

Further support for the hypothesis that demyelination is mediated by soluble factors produced in the CSF/meningeal compartment diffusing into the underlying cortical GM comes from studies investigating meningeal inflammation. Diffuse inflammatory infiltrates, consisting of B and T cells and macrophages, are frequently observed in the cerebral leptomeninges in studies using autopsy samples from PPMS and SPMS cases (Guseo and Jellinger, 1975, Kutzelnigg *et al.*, 2005, Kooi *et al.*, 2009, Howell *et al.*, 2011, Choi *et al.*, 2012) and are particularly frequent in cases with extensive subpial cortical GM

demyelination. There is a significant positive correlation between the total length of meningeal infiltration and the extent of cortical GM demyelination in the forebrain as well as the density of CD68-positive microglia in the underlying cortical GM (Howell *et al.*, 2011). Similar correlations between meningeal T cell infiltration and microglial expression of MHC class II, CD68, inducible NOS and allograft inflammatory factor 1 in cortical GM have been observed (Dal Bianco *et al.*, 2008), leading the authors to suggest that microglial activation may be partly driven by meningeal inflammation.

Lymphoid-like structures

As well as these diffuse inflammatory infiltrates, ectopic lymphoid follicle-like structures have also been observed in the meninges, particularly those of the sulci, in approximately 40% of SPMS cases in studies using autopsy samples (Serafini *et al.*, 2004, Magliozzi *et al.*, 2007, Magliozzi *et al.*, 2010, Howell *et al.*, 2011). They consist of aggregates of CD20+ B cells, some of which are Ki67+ indicating proliferation, together with CD35+ follicular dendritic cells, IgA, -G or -M+ plasmablasts/plasma cells and CD3+ T cells. The cases in which these structures are found have been defined as F+ SPMS. It has been suggested that the decreased flow of CSF in the sulci results in a protected environment that allows the homing and retention of immune cells and development of lymphoid-like structures, which in turn results in an inflammatory milieu in the CSF (Reynolds *et al.*, 2011). The number of cells expressing the pro-inflammatory cytokines TNF and IFN-γ and the gene expression of these cytokines are increased in the inflamed meninges of F+ SPMS patients. TNF is expressed by cells with monocyte/macrophage morphology in meninges as well as some microglia in superficial GM, whereas IFN-γ is expressed by a proportion of cells, mainly CD8+ T cells, in meninges (Serafini *et al.*, 2007, Magliozzi *et al.*, 2010, Gardner *et al.*, 2013). The levels of these cytokines in post-mortem CSF of F+ SPMS cases are also increased, although this increase did not reach significance for IFN-γ (Gardner *et al.*, 2013).

The cases in which lymphoid-like structures are found have more severe cortical GM pathology and clinical course than those in which they are not. The extent of subpial cortical GM demyelination is also greater in F+ SPMS cases. Gradients of microglial activation and neuronal loss in cortical GM layers, with the greatest activation or loss in cortical layer I closest to the pia mater, have also been observed, as well as a gradient of astrocyte loss that resulted in a thinning, or loss, of the glia limitans (Magliozzi *et al.*, 2010). Finally, the presence of lymphoid-like structures has been associated with a younger age at onset, age at wheelchair dependence and age at death (Magliozzi *et al.*, 2007). Diffuse inflammatory infiltrates in the meninges have similarly been associated with a younger age at onset, time to disease progression, time to wheelchair dependence and age at death (Howell *et al.*, 2011).

However, another study using autopsy samples from progressive MS cases failed to show a correlation between the extent of meningeal inflammation and subpial demyelination and also failed to show the presence of lymphoid-like structures (Kooi *et al.*, 2009). It is suggested that this failure was due to limited sampling of the whole brain and poor preservation of meninges as a result of suboptimal retrieval, processing and handling protocols (Aloisi *et al.*, 2010).

It is suggested that meningeal inflammation, consisting of diffuse inflammatory infiltrates and/or lymphoid-like structures, results in increased concentrations of pro-inflammatory cytokines in the CSF. These diffuse from the pial surface into the cortex resulting in GM pathology, directly or indirectly through the activation of microglia, and a more severe clinical course (Peterson *et al.*, 2001, Reynolds *et al.*, 2011). However, there is currently no animal model of chronic cortical GM pathology driven by meningeal inflammation with which to test this hypothesis.

3.1.3 Targeted EAE models

Pathology in the majority of current EAE models is focused on spinal cord WM (Sriram and Steiner, 2005), whereas MS affects the brain with prominent involvement of cerebral and cerebellar cortical GM as described in 3.1.1. In order to target pathology to specific anatomical locations within the rodent CNS, targeted EAE models have recently been developed. These involve the immunisation of animals with a subclinical dose of recombinant MOG to prime the immune system followed by the injection of pro-inflammatory cytokines at the desired location to attract the primed auto-reactive T cells and antibodies and induce demyelination (Kerschensteiner *et al.*, 2004, Merkler *et al.*, 2006, Sasaki *et al.*, 2010). The immunisation of female Lewis rats with 50μg of rrMOG emulsified in IFA, which was a subclinical dose in this strain, followed 18-22 dpi by the injection of 250ng of rrTNF and 150U of rrIFN-γ into the motor cortex, for example, resulted in all types of GML in the injected cortex. These were associated with activated microglia, infiltration of T cells and axonal damage. No cortical GM pathology was observed in the contralateral cortex (Merkler *et al.*, 2006). However, the value of this model is limited by the physical injury and BBB damage induced by the direct injection of cytokines into the motor cortex.

3.1.3.1 Model of cortical GM pathology driven by meningeal inflammation

This laboratory has recently developed a targeted EAE model to test the hypothesis that TNF and IFN-γ produced in the meninges can diffuse into the underlying cortical GM and result in subpial lesions, and that avoids the damage induced by direct injection (Gardner *et al.*, 2013). The injection of cytokines was into the SAS, the space filled with CSF between the pia and arachnoid mater. It is continuous around the brain but varies in thickness and may be absent where the pia and arachnoid mater are in direct contact and where blood vessels and nerves leave the brain (Adeeb *et al.*, 2013). It is separated from the cortical GM by the single, interrupted layer of cells of the pia mater, a narrow (6nm) space containing collagen fibres, and the basal lamina and astrocyte end-feet that comprise the glia limitans

(Lopes and Mair, 1974). The cells of the pia mater are joined by gap junctions rather than tight junctions and form a permeable barrier (Alcolado *et al.*, 1988). There are layers (5-12) (Lopes and Mair, 1974) of astrocytic elements, also joined by gap junctions, which comprise the glia limitans, resulting in a less permeable barrier (Johanson *et al.*, 2005).

The immunisation of female DA rats with a subclinical dose of 5μg of rmMOG emulsified in IFA followed 20-23 dpi by the injection of 1.25μg of rrTNF and 75ng of rrIFN-γ into the SAS of the sagittal sulcus resulted in subpial lesions similar to those described in SPMS (Peterson *et al.*, 2001, Bø *et al.*, 2003a, Kutzelnigg *et al.*, 2005). Microglia with activated morphology were associated with myelin sheaths, particularly at the edge of the lesion, and a gradient of microglial activation was observed, again similar to that described in SPMS (Magliozzi *et al.*, 2010). Lesions were associated with B cell, CD4+ and CD8+ T cell and macrophage accumulation in the meninges. No demyelination was observed in control animals immunised with IFA and injected with cytokines or in animals immunised with rmMOG and injected with PBS. This model appears to be highly reproducible but, as in the motor cortex model (Merkler *et al.*, 2006), its value is limited by the lack of chronic pathology due to the acute nature of the cytokine delivery. Demyelination was maximal at 7 days after injection and remyelination was complete at 14 days after injection (Gardner *et al.*, 2013).

3.1.4 Aims

We aimed to further develop the acute model of cortical pathology driven by meningeal inflammation (Gardner *et al.*, 2013), involving the immunisation of DA rats with a subclinical dose of rmMOG followed by the injection of TNF and IFN-γ into the SAS of the sagittal sulcus. We aimed to determine the effect of the dose of TNF and IFN-γ on the duration and extent of pathology.

To fulfil this aim, the following were performed:

- Reproduction of the acute model using the same doses of TNF and IFN-γ used by Gardner *et al.* (2013) and determination of the extent of subpial demyelination and inflammation (activated macrophages/microglia and Tc, Th and B cells) at 1 week and 2 weeks after injection.
- Repeat using two- and four-fold higher doses of TNF and IFN-γ.

3.2 Methods

3.2.1 Induction of subclinical EAE

3.2.1.1 Animals

Female DA rats (Charles River, Germany) aged 8 to 12 weeks and weighing approximately 160g were housed as described in 2.2.2.1. Animal work was carried out in compliance with Home Office regulations (project licence 70/7213).

3.2.1.2 Immunisation

Animals received an intradermal injection into the dorsal aspect of the base of the tail of 10µg of rmMOG (a batch expressed and purified previously in this laboratory, batch pXIIIa; *n* = 36) diluted in PBS emulsified in an equal volume of IFA as described in 2.2.2.2. The total injection volume was 100µl. This dose and batch of rmMOG were used as they were shown to result in reproducible subpial demyelination in pilot studies performed in this laboratory of the acute model of cortical pathology driven by meningeal inflammation (unpublished observations).

3.2.1.3 Clinical scoring

Following immunisation animals were weighed and scored daily as described in 2.2.2.3. Animals were removed from the experiment if they reached the humane endpoints of a loss of 25% of their body mass (from the day prior to the development of deficit) for 48 hours or complete weakness of both hind limbs for more than 48 hours without weight gain, in compliance with Home Office regulations. These animals received an i.p. injection of an overdose of 200mg/ml Euthatal.

3.2.2 Injection of TNF and IFN-γ

The immunisation of animals was followed 19-22 dpi by the injection of TNF and IFN-γ into the SAS of the sagittal sulcus. The coordinates from Bregma were obtained from a rat brain atlas (Paxinos and Watson, 1998) and were 0.9mm caudal to Bregma to target the motor cortex, at midline and to a depth of 2.3mm from the dura mater as shown in Figure 3.2.1 A. A previous study using this model made the injection at a depth of 2.5mm from the dura mater (Gardner *et al.*, 2013). However, this was found to result in frequent injection into the underlying corpus callosum rather than the SAS in pilot studies performed in this laboratory, hence the depth was reduced in the current study.

3.2.2.1 Cytokines

The doses of TNF (R&D Systems) (reconstituted and diluted in 0.1% (w/v) BSA in PBS) and IFN-γ (Peprotech, Rocky Hill, New Jersey, USA) (reconstituted in pH8 sodium phosphate (10mM; Sigma-Aldrich) and diluted in 0.1% (w/v) BSA in PBS) are shown in Table 3.2.1. The low dose was that used previously in this laboratory in the development of the acute model of cortical pathology driven by meningeal inflammation (Gardner *et al.*, 2013).The intermediate and high doses were two- and four-fold higher than this low dose respectively, and were used in order to determine whether higher doses increase the duration, as well as extent, of subpial demyelination and inflammation. Control animals received an injection of PBS only. Monastral blue (copper(II) phthalocyanine-tetrasulfonic acid tetrasodium salt; Sigma-Aldrich) was added at 1:1000 as a tracer as in Kerschensteiner *et al.*, 2004, Merkler *et al.*, 2006 and Rodriguez *et al.*, 2014. The time points investigated are shown in Table 3.2.1.

Immunisation	TNF / µg	IFN-γ / ng	Time point / weeks	Number of animals
10µg rmMOG	1.25	75	1	4
10µg rmMOG	2.5	150	1	4
10µg rmMOG	5	300	1	4
10µg rmMOG	1.25	75	2	3
10µg rmMOG	2.5	150	2	4
10µg rmMOG	5	300	2	3

Table 3.2.1. Groups for TNF and IFN-γ dose response study.

3.2.2.2 Stereotactic injection

Animals were placed under general anaesthesia as described in 2.2.2.2 and the top of the head was shaved and Videne applied. Animals were mounted on a stereotactic frame (Stoelting, Rathmines, Dublin, Ireland) and received subcutaneous (s.c.) injections of 0.9% saline (Sigma-Aldrich) and 0.01mg/kg buprenorphine analgesic (Vetergesic; Alstoe Animal Health, Sheriff Hutton, North Yorkshire, UK), a dose that has been shown to have no effect on the immune response (Carrigan *et al.*, 2004). The surface of the skull was exposed, the lateral and anterior coordinates from Bregma were determined and a small hole was drilled using a miniature power drill (RS Components, Corby, Northamptonshire, UK). Animals received a 1µl injection using a very fine glass capillary (Harvard Apparatus, Edenbridge, Kent, UK) mounted on the 26 gauge Hamilton needle of a 10µl Hamilton syringe (Figure 3.2.1 B; Hamilton, Bonaduz, Graubünden, Switzerland) and a syringe pump (KD Scientific, Holliston, Massachusetts, USA) set to 0.2µl/min. The needle was left in place for 5 minutes to allow diffusion away from the injection site. Following retraction of the needle, the incision was closed using simple interrupted silk sutures (Mersilk (Ethicon; Covidien, Dublin, Ireland)), which were removed 7-10 days after surgery. Recovery from surgery was without incident and overt clinical signs in the majority of cases. The experiment was terminated at 1 and 2 weeks after injection.

A

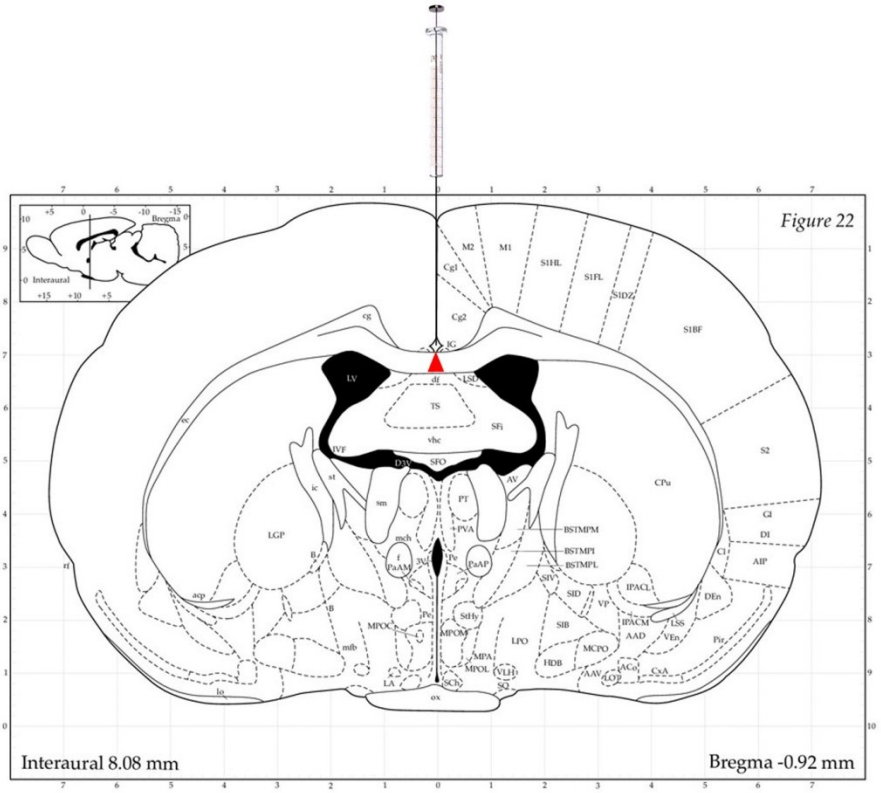

B

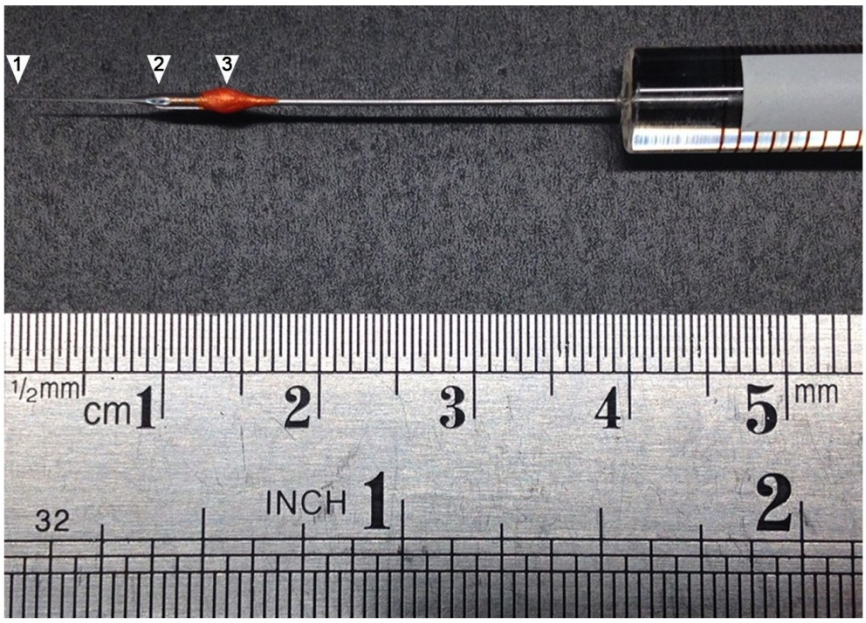

Figure 3.2.1. Stereotactic injection of TNF and IFN-γ. Animals received an injection of TNF and IFN-γ into the SAS of the sagittal sulcus at coordinates from Bregma of anterior -0.9mm, lateral ±0.0mm and ventral -2.3mm (red arrowhead in A; adapted from Paxinos and Watson, 1998). Injections were made using a glass capillary with an internal diameter of approximately 30µm at its tip (arrowhead 1 in B) mounted on the 26 gauge Hamilton needle of a 10µl Hamilton syringe (arrowhead 2) using nail polish (arrowhead 3) to create a seal.

3.2.3 Determination of pathology

3.2.3.1 Tissue harvesting and treatment

Animals received an i.p. injection of an overdose of 200mg/ml Euthatal at the termination of the experiment and were perfused as described in 2.2.3.1. The brain was harvested and post-fixed in 4% PFA for 4 hours at 4°C followed by cryoprotection in 30% (w/v) sucrose in PBS for 48 hours or until equilibrium was reached at 4°C.

Tissue was briefly rinsed in PBS, placed in a mould filled with optimal cutting temperature compound and frozen in isopentane on dry ice. 10µm sections in the coronal plane were cut using a cryostat and stored at -20°C. Monastral blue was used to identify the injection site.

3.2.3.2 Immunofluorescence

Extensive prior optimisation was required for IF protocols. Various methods of tissue post fixation and antigen retrieval were evaluated, including the use of pH6 citrate buffer, methanol and 4% PFA as well as Triton X-100 in antibody diluents. Sections were blocked with a high concentration of normal serum for 60 minutes and incubated with various concentrations of primary antibodies overnight. Amplification using biotinylated secondary antibodies was also evaluated. The protocols described below were found to be most suitable, resulting in clear, specific and strong IF.

In order to identify areas of demyelination and the presence of activated macrophages/microglia, double IF for MOG and Iba1 (see Table 3.2.2 for details of primary antibodies) respectively was performed as described in 2.2.3.2.

Similarly, in order to identify the presence of Th and Tc cells, double IF for CD4 and CD8 respectively was performed. Sections were blocked with 5% (v/v) normal goat serum (NGS;

Sigma-Aldrich) in PBST for 60 minutes and incubated with anti-CD4 primary antibody diluted in 1% (v/v) NGS in PBST overnight at 4°C. Sections were incubated with goat anti-mouse IgG2a biotinylated secondary antibody (Southern Biotech, Birmingham, Alabama, USA) at 1:500 in the same diluent for 60 minutes followed by incubation with Alexa Fluor 488 conjugated streptavidin at 1:1000 for 60 minutes in the dark. Sections were incubated with anti-CD8 primary antibody overnight at 4°C followed by incubation with goat anti-mouse IgG1 Alexa Fluor 546 conjugated secondary antibody (Alexa Fluor Dyes) at 1:1000 for 60 minutes in the dark.

Finally, IF for CD79a (Table 3.2.2) was performed to identify the presence of B cells. The protocol used was the same as that for MOG and Iba1 but omitting methanol. This was replaced with heat mediated pH6 citrate buffer (0.1M citric acid, 0.1M sodium citrate (both Sigma-Aldrich)) retrieval using a vegetable steamer.

Antigen	Cell specificity	Species	Dilution	Source
CD4[1]	CD4+ Th cell	Mouse	1 in 500	AbD Serotec, Kidlington, Oxfordshire, UK
CD8	CD8+ Tc cell	Mouse	1 in 500	AbD Serotec
CD79a[1]	B cell	Mouse	1 in 500	Pierce Antibodies
Iba1	Activated macrophages/ microglia	Rabbit	1 in 1000	Wako
MOG[1]	Myelin and oligodendrocytes	Mouse	1 in 20	Reynolds' group

Table 3.2.2. Primary antibodies used for IF. [1]Antigens requiring a biotinylated secondary antibody.

3.2.3.3 Imaging and analysis

Sections were imaged using a Nikon Eclipse 80i microscope with a QImaging QICAM digital camera and Image-Pro Plus software. This software was able to tile multiple high magnification images to yield high resolution images of complete sections.

Image-Pro Plus 7.0 was used to quantify areas of demyelination (Figure 3.2.2 A) while immune cells in the meninges were quantified manually using the 20x objective lens. While looking down the eyepiece, cells in the meninges were counted by moving along a length of meninges extending from 2mm to the left of the sagittal sulcus to 2mm to the right of it. Quantification was performed blinded to eliminate bias. Only cells with nuclei, identified using DAPI, were quantified, and only in the meninges, as this was where immune cell infiltration was mainly confined. Numbers of cells were normalised to the length of meninges analysed. ImageJ was used to quantify areas of Iba1 IR (B). Briefly, all Iba1 images for a single study were taken at the same exposure as far as was possible. The same threshold was then applied to these images in ImageJ to select the Iba1 IR. Quantification was performed on 3 consecutive sections per animal and a mean calculated.

3.2.4 Statistical analysis

All data are presented as the mean ± the SEM. GraphPad Prism 5 was used to construct graphs and perform statistical analysis. Groups were compared using Kruskal-Wallis one-way ANOVA with Dunn's multiple comparisons post-hoc test unless otherwise stated. A p value of <0.05 was considered to be statistically significant.

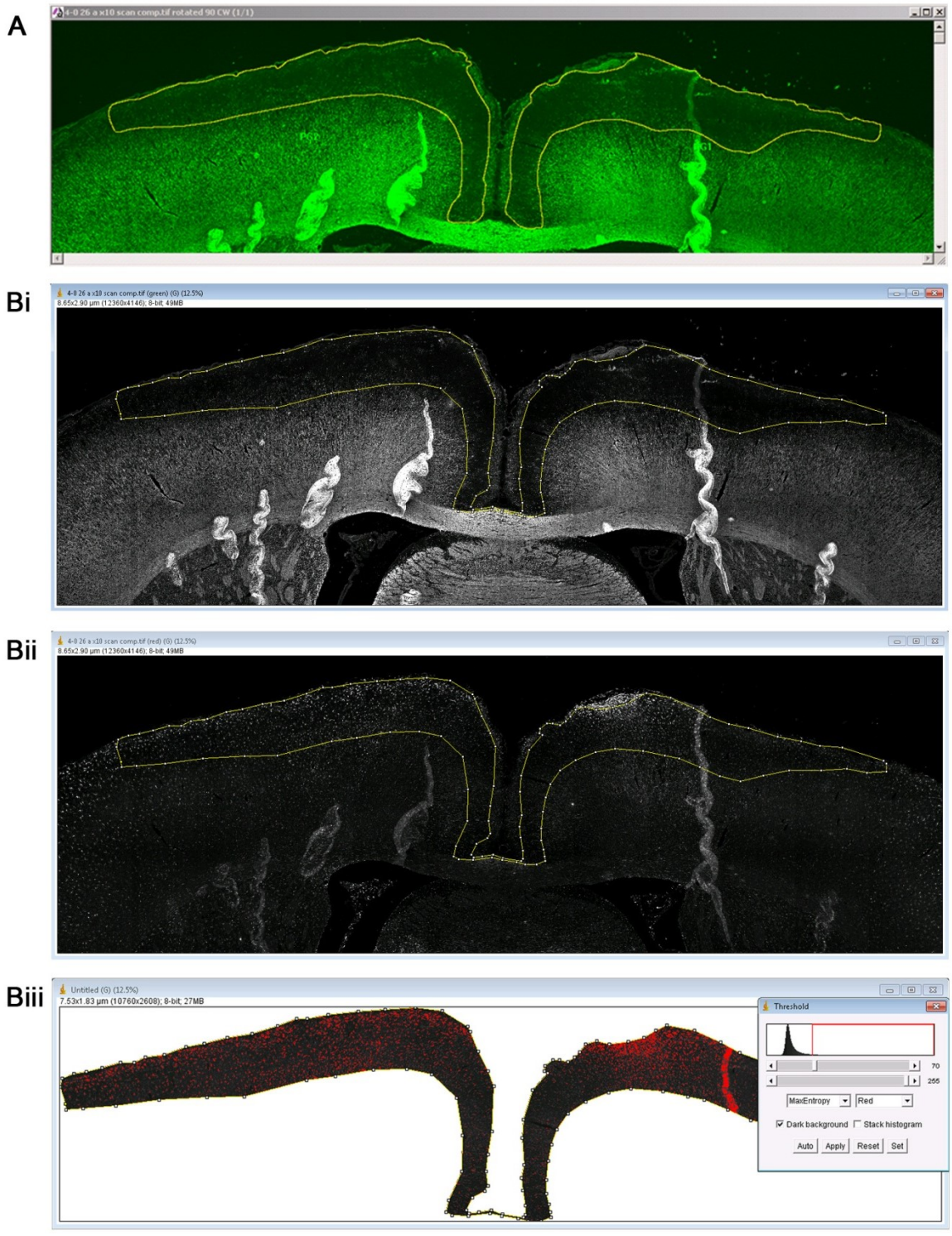

Figure 3.2.2. Quantification of area of demyelination and Iba1 immunoreactivity. The total area of demyelination in each brain section was quantified using tiled images of MOG and Iba1 double IF sections taken using the 10x objective lens and Image-Pro Plus 7.0 software. Iba1 was removed from the composite, individual areas of demyelination were selected (yellow in A) and calculated areas summed. The area of Iba1 immunoreactivity in areas of demyelination was quantified using the same images and ImageJ software. All images were taken at the same exposure as far as was possible. The channels were split and areas of demyelination were selected in the image of the MOG channel (Bi). This selection was copied to the image of the Iba1 channel (Bii). The inverse was cleared and the same threshold was applied to all selections to select the Iba1 immunoreactivity and calculate its area (Biii), which was normalised to the area of demyelination.

3.3 Results

3.3.1 Induction of subclinical EAE

3.3.1.1 Incidence of clinical EAE

Female DA rats were immunised with 10μg of rmMOG. Despite this dose and batch having been shown to be subclinical as well as result in reproducible subpial demyelination in pilot studies performed in this laboratory, a significant proportion of animals developed clinical EAE. Only asymptomatic animals or those with a clinical score less than 2, corresponding to partial weakness of one limb, at the time of injection were used. Of the 36 animals immunised with rmMOG, 10 animals (28%) were culled prior to the injection of TNF and IFN-γ due to the humane endpoint of a clinical score of 3.5, corresponding to complete weakness of both hind limbs preceded by ascending paralysis from the tail, for more than 48 hours being reached. A further 3 animals displayed atypical symptoms, characterised by disturbances in balance and coordination, or complete weakness of both hind limbs at the time of injection although they had not reached humane endpoints, and were not used. The mean day of disease onset in these 13 animals (36%) was 16 dpi.

3.3.2 Injection of TNF and IFN-γ

3.3.2.1 Identification of the injection site

Monastral blue, added to the cytokine solution to enable the identification of the injection site, was confined to the meninges of the sagittal sulcus in 64% of animals (Figure 3.3.1 A). However, it was observed in the cingulate cortex (B) or corpus callosum (C) as well as in the sulcus in 27% of animals and was not observed at all in the remaining 9% of animals. In the case of accurate injections, it was present throughout the sagittal sulcus over approximately 2mm, with a peak at the injection site that decreased progressively with increasing distance along the anteroposterior axis, as well as on the superior surface of the cortex.

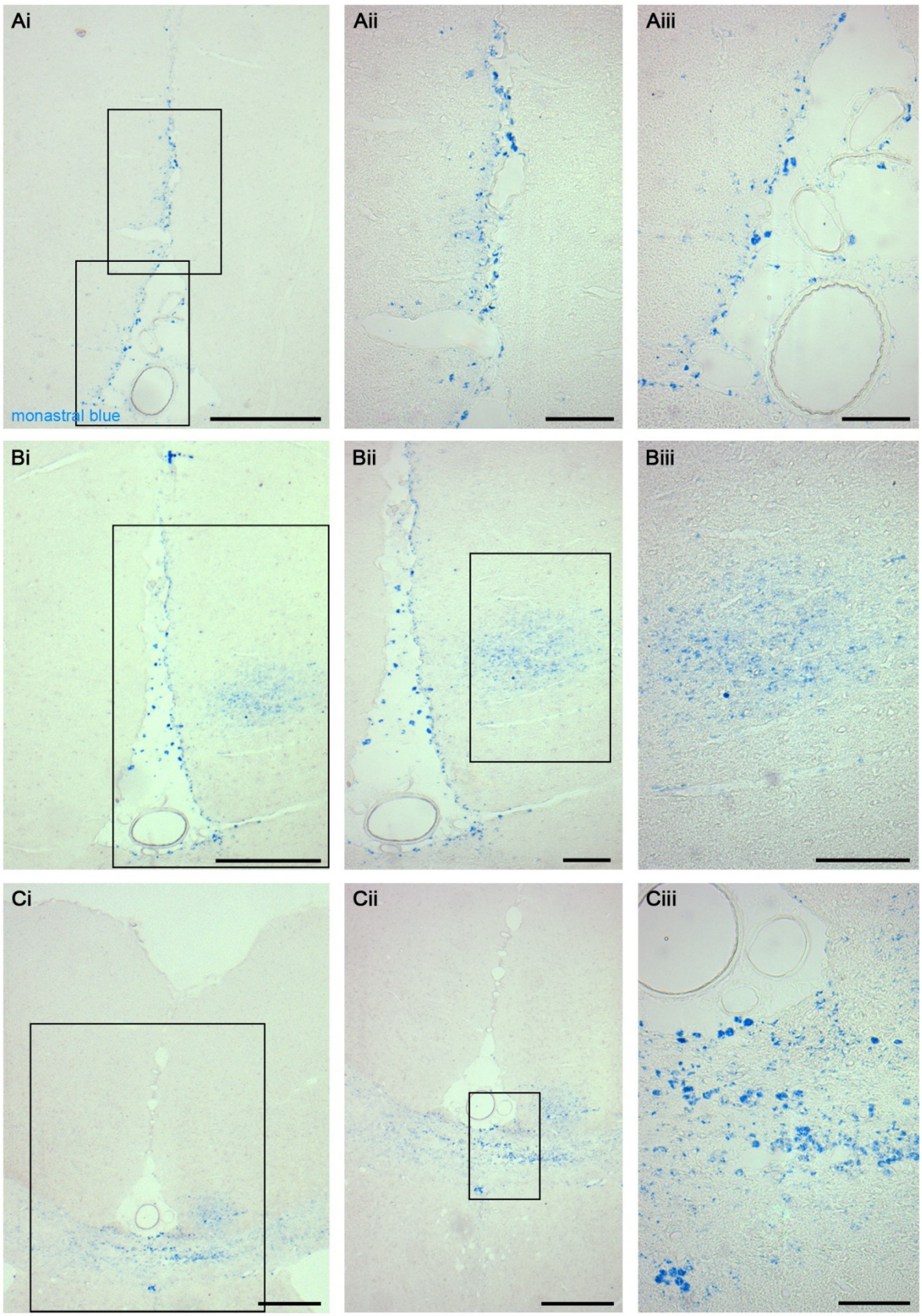

Figure 3.3.1. Monastral blue enabled identification of the injection site. Bright-field microscopy was performed on injection site sections. Monastral blue was observed in the meninges of the sagittal sulcus and walls of the meningeal blood vessels at the base of the sulcus (A), although it was also observed in the cingulate cortex (B) and corpus callosum (C). Images on the right are magnifications of the boxed areas in those on the left. Scale bars: Ai, Bi, Ci and Cii = 200μm, Aii, Aiii, Bii, Biii and Ciii = 50μm.

3.3.2.2 Subpial demyelination

In order to identify areas of demyelination, IF for MOG was performed on sections cut at the injection site, where the monastral blue was most dense. Extensive subpial demyelination, similar to the Type III GMLs observed in MS cortex, was present 1 week after injection of low (Figure 3.3.2 B), intermediate (C) and high (D) doses of TNF and IFN-γ, but was absent in control animals injected with PBS only (A). Demyelination was observed in both hemispheres and affected the cingulate cortex but particularly the primary and secondary motor cortices and primary somatosensory cortex. Cortical GM layers were defined using the DAPI stain; layer I was defined as the layer with a low density of nuclei between the meninges and layers II-III, with a high density of nuclei. Demyelination extended through cortical GM layers I-III. Demyelination in the corpus callosum was observed in one animal injected with 5μg TNF + 300ng IFN-γ, in which monastral blue had also been observed in the corpus callosum.

A similar pattern of demyelination was present 2 weeks after injection of intermediate (Figure 3.3.3 B) and high (C) doses of TNF and IFN-γ, although it appeared to be less extensive than that at 1 week after injection. Very little demyelination was observed after injection of the low dose of TNF and IFN-γ (A). Demyelination in the corpus callosum was observed in one animal injected with 5μg TNF + 300ng IFN-γ, in which monastral blue had again also been observed in the corpus callosum (C).

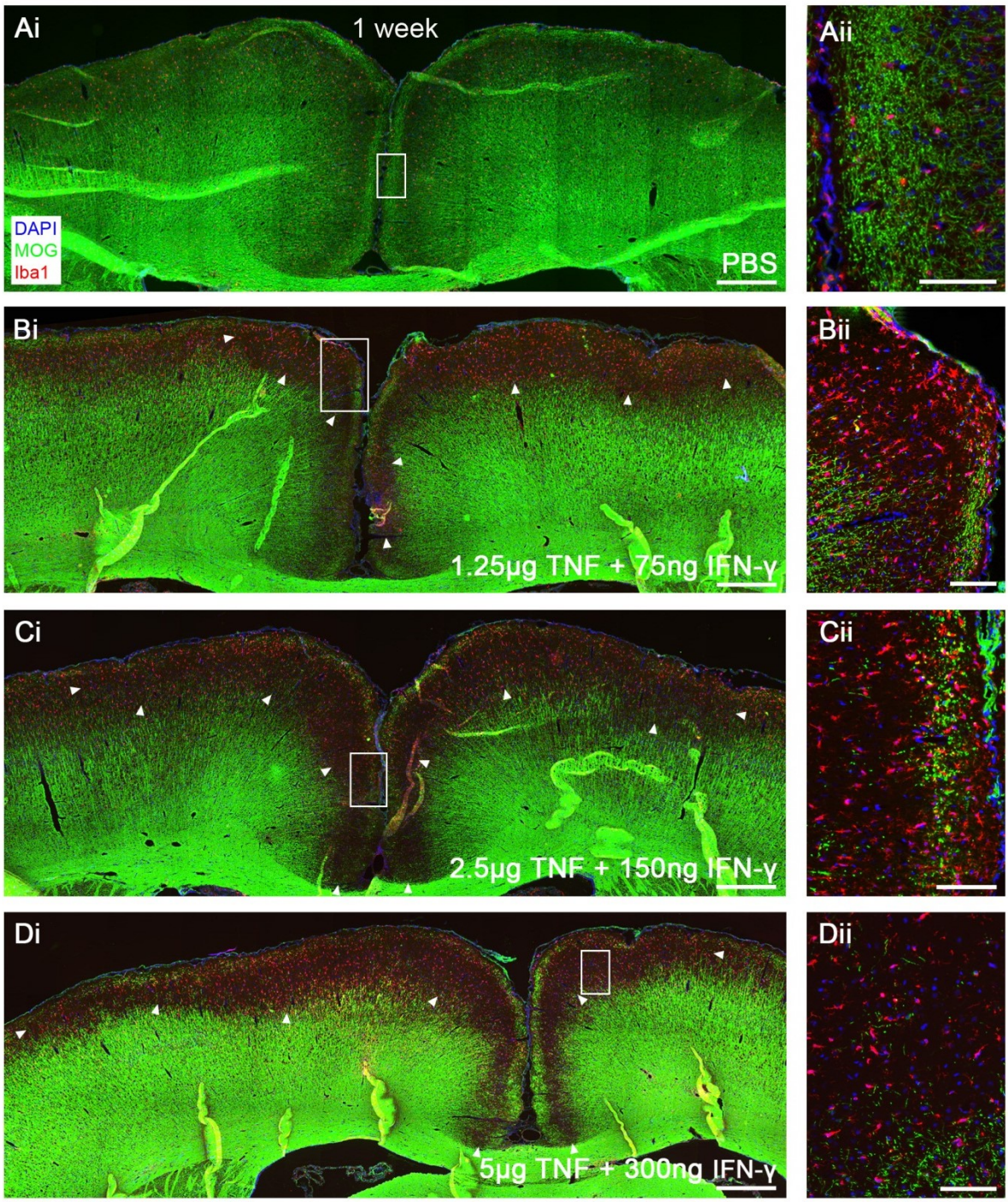

Figure 3.3.2. Extensive subpial demyelination present 1 week after injection of TNF and IFN-γ. IF for MOG and Iba1 was performed on injection site sections and showed demyelination in both hemispheres through cortical layers I-III after injection of low (B; lesion border indicated by arrowheads), intermediate (C) and high (D) doses of TNF and IFN-γ, but not after injection of PBS only (A). Demyelination affected the cingulate cortex adjacent to the sagittal sulcus (particularly evident in C) but was most evident in the primary and secondary motor cortices and primary somatosensory cortex on the superior surface. Images on the right are magnifications of the boxed areas in the images on the left. Scale bar: Ai, Bi, Ci and Di = 500µm, Aii, Bii, Cii and Dii = 100µm.

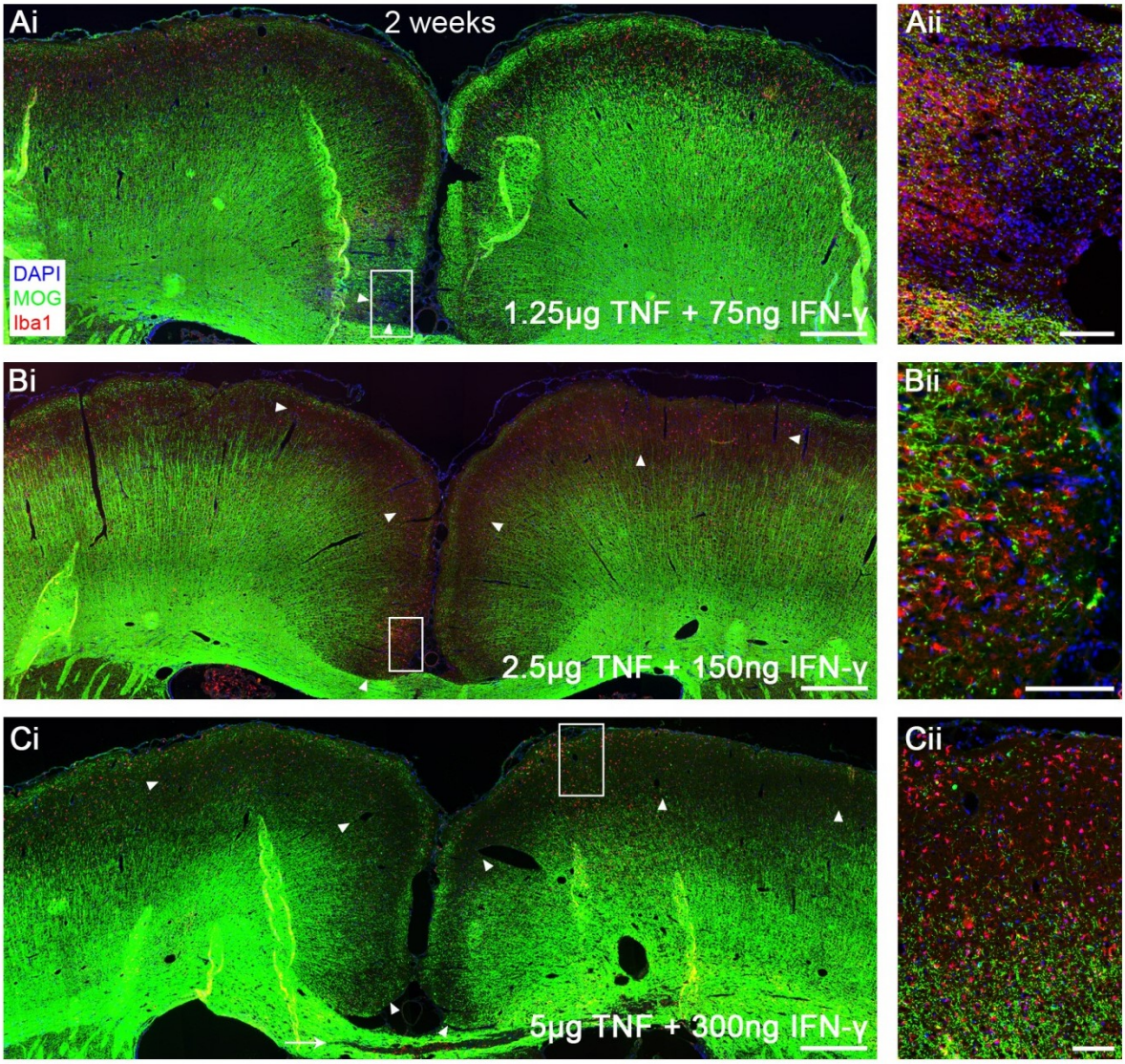

Figure 3.3.3. Subpial demyelination present 2 weeks after injection of TNF and IFN-γ. IF for MOG and Iba1 was performed on injection site sections and showed very little demyelination after injection of the low dose of TNF and IFN-γ (A; lesion border indicated by arrowheads), although demyelination in both hemispheres through cortical layers I-III was observed after injection of intermediate (B) and high (C) doses of TNF and IFN-γ. The pattern of demyelination was similar to that observed 1 week after injection, with the cingulate, motor and somatosensory cortices affected. Demyelination in the corpus callosum was also observed in one animal injected with the high dose of TNF + IFN-γ (arrow in C). Images on the right are magnifications of the boxed areas in the images on the left. Scale bar: Ai, Bi and Ci = 500µm, Aii, Bii and Cii = 100µm.

Areas of demyelination were quantified as described in 3.2.3.3 and the effect of both the dose of TNF and IFN-γ (Figure 3.3.4 A) and time point (B) variables were determined using two-way ANOVA with Tukey's multiple comparisons post-hoc test. The total area of subpial demyelination increased with increasing dose of TNF and IFN-γ at 1 week after injection (A). The area of demyelination was significantly greater in animals injected with the high dose than in those injected with the low dose (factor of 2.93) and was also greater in these animals than in those injected with the intermediate dose (factor of 1.12), although this was not statistically significant. Similarly, the area of demyelination was greater in animals injected with the intermediate dose than in those injected with the low dose (factor of 2.62), although again this was not statistically significant. This TNF and IFN-γ dose-dependent increase in area of demyelination was not observed at 2 weeks after injection (A).

The variation in the area of demyelination with increasing time after injection is more clearly demonstrated in Figure 3.3.4 B. Consistent with observation, the area of demyelination was significantly greater at 1 week after injection than at 2 weeks after injection in animals injected with the intermediate (factor of 3.74) and high (factor of 5.00) doses of TNF and IFN-γ, although there was no significant difference in the area of demyelination at 1 week and 2 weeks after injection in animals injected with the low dose.

IF for MOG was performed on sections cut 500μm anterior to (Figure 3.3.5 A) and 500μm posterior to (C) the injection site as well as those cut at the injection site (B) in order to determine the anterior to posterior extent and pattern of demyelination. Subpial demyelination extended at least 500μm either side of the injection site and the pattern of demyelination appeared to be consistent across the 1mm sampled. Areas of demyelination were quantified and the total area of subpial demyelination did not change across the 1mm at 1 week after injection in animals injected with all doses of TNF and IFN-γ (Figure 3.3.6 A). This was also true at 2 weeks after injection in animals injected with the intermediate and high doses of TNF and IFN-γ, although there appeared to be some variation in animals

injected with the low dose, in which a significantly greater area of demyelination at 500μm posterior to the injection site than at 500μm anterior to the injection site (factor of 2.43) or at the injection site (factor of 2.34) was shown (B).

3.3.2.3 Microglial activation

In order to identify activated macrophages/microglia associated with areas of demyelination, double IF for Iba1 and MOG respectively was performed on sections cut at the injection site. A high density of activated macrophages/microglia was present at 1 week after injection of PBS only (Figure 3.3.7 Ai) as well as low (Bi), intermediate (Ci) and high (Di) doses of TNF and IFN-γ. Microglial activation was observed particularly adjacent to the sagittal sulcus in the absence of demyelination after injection of PBS only (Aii, Aiii) and in demyelinated areas in superficial layers of cingulate and motor cortices (Bii, Biii, Cii, Ciii, Dii, Diii), although it was not confined to these areas but also extended into surrounding myelinated areas. Iba1+ cells were also present in the meninges and were particularly evident in meninges overlying areas of subpial demyelination (as shown in A, for example) and in those lining the sagittal sulcus (several of these cells shown in B). These cells generally had an amoeboid morphology characterised by a large cell soma but the retention of short, thick processes that allowed them to be identified as activated microglia rather than amoeboid macrophages. A similar pattern of microglial activation was present at 2 weeks after injection of the 3 doses of TNF and IFN-γ.

Iba1 immunoreactivity was quantified as described in 3.2.3.3 and the effect of both the dose of TNF and IFN-γ (Figure 3.3.8 A) and time point (B) was determined. The total Iba1 immunoreactivity in areas of subpial demyelination increased with increasing dose of TNF and IFN-γ at 1 week after injection (A). Iba1 immunoreactivity was significantly greater in animals injected with the intermediate dose than in those injected with the low dose (factor of 1.63). However, there was no further increase after injection of the high dose. There was no effect of the dose of TNF and IFN-γ on Iba1 immunoreactivity at 2 weeks after injection (A).

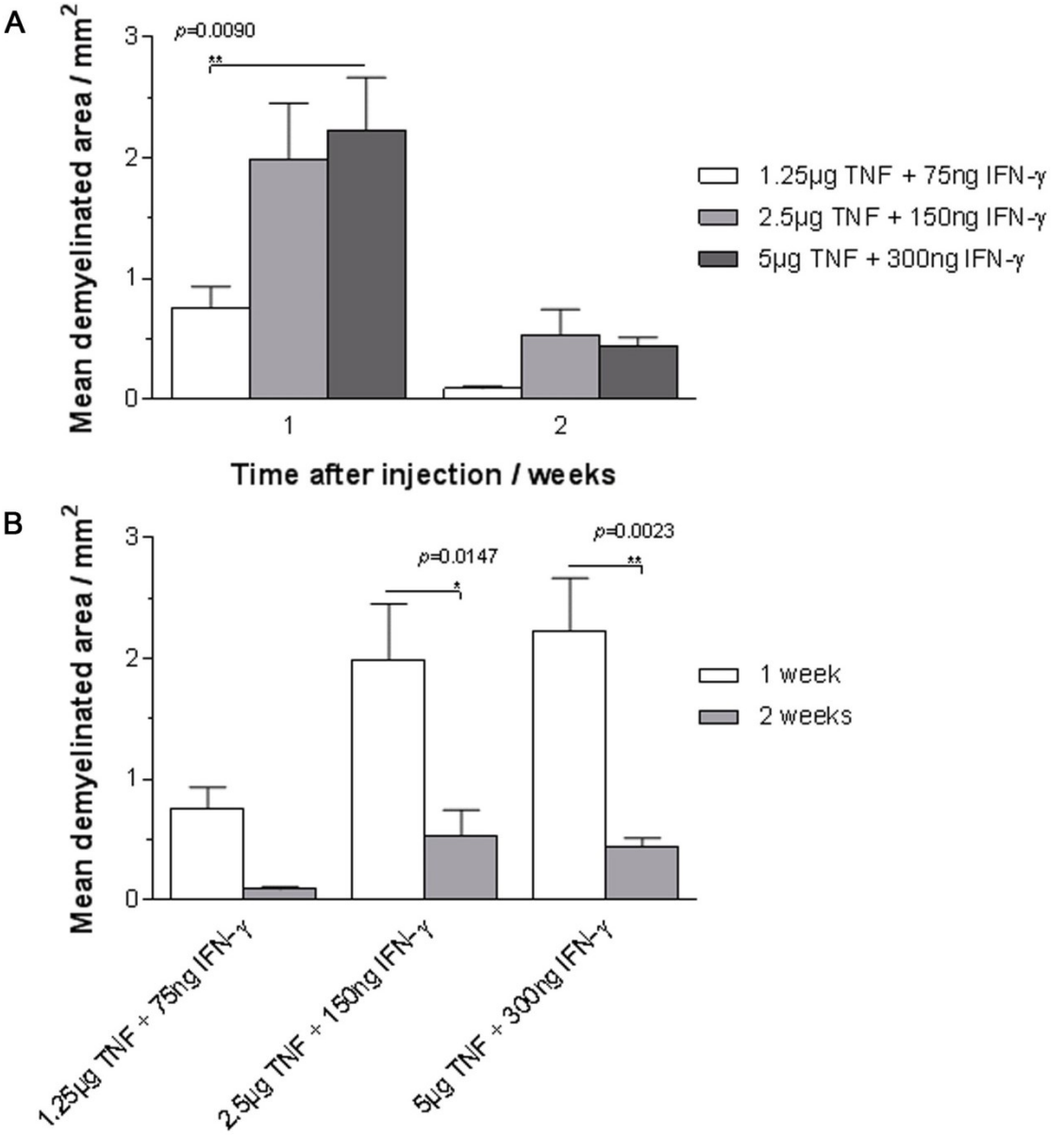

Figure 3.3.4. Effect of dose of TNF and IFN-γ and time point on area of demyelination. The area of demyelination was TNF and IFN-γ dose-dependent at 1 week, but not at 2 weeks, after injection (A). The area of demyelination was also time-dependent. It was greater at 1 week after injection than at 2 weeks after injection (B; two-way ANOVA with Tukey's multiple comparisons test; mean ± SEM; * = $p \leq 0.05$, ** = $p \leq 0.01$, n = 4 for low, intermediate and high doses at 1 week and intermediate dose at 2 weeks, 3 for low and high doses at 2 weeks).

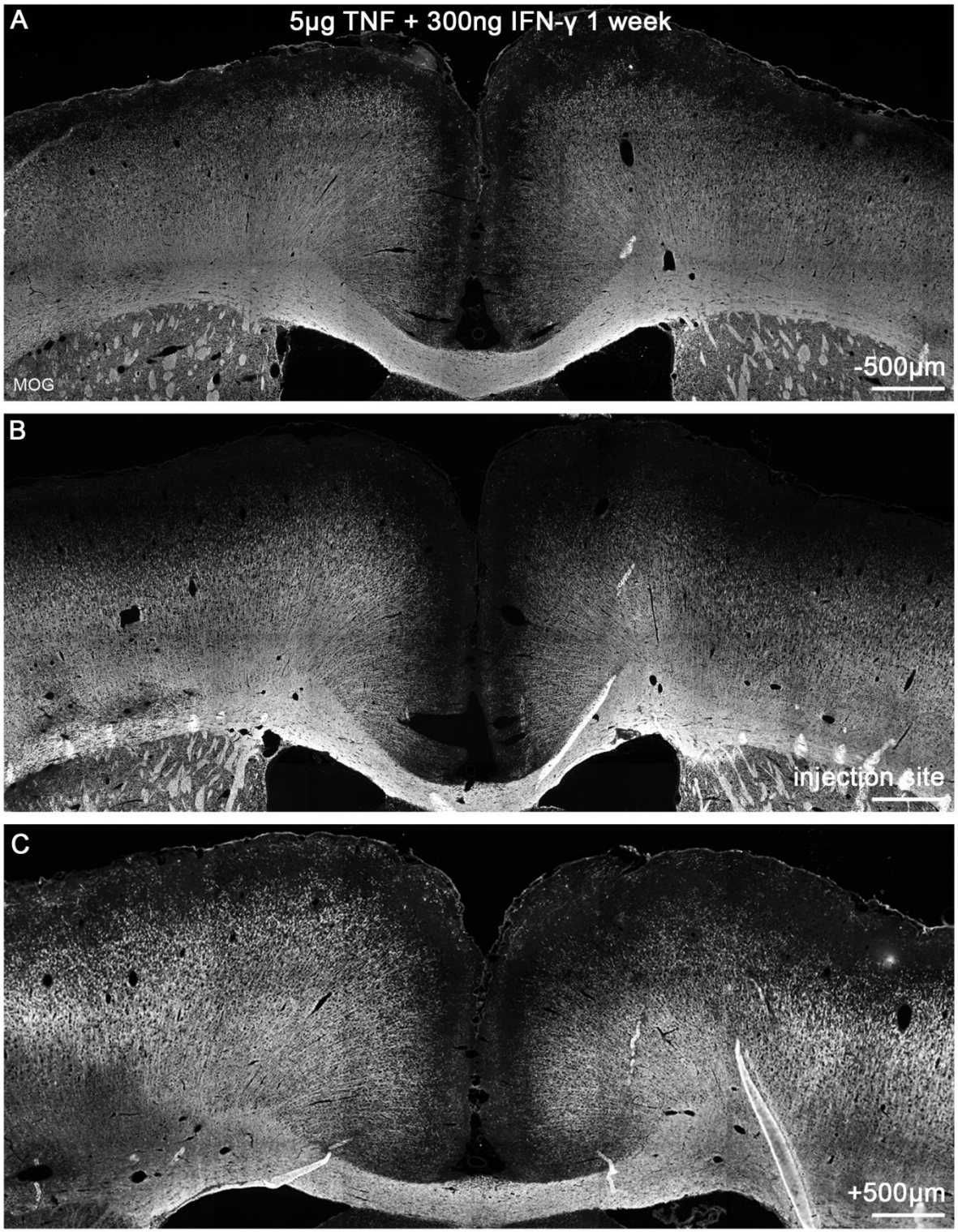

Figure 3.3.5. Subpial demyelination extended at least 500µm either side of the injection site after injection of TNF and IFN-γ. IF for MOG was performed on injection site sections (B) and sections cut 500µm anterior to (A) and 500µm posterior to (C) the injection site. The extent and pattern of demyelination appeared to be consistent in all three sections. The images shown are from one animal 1 week after injection of the high dose of TNF and IFN-γ. Scale bars = 500µm.

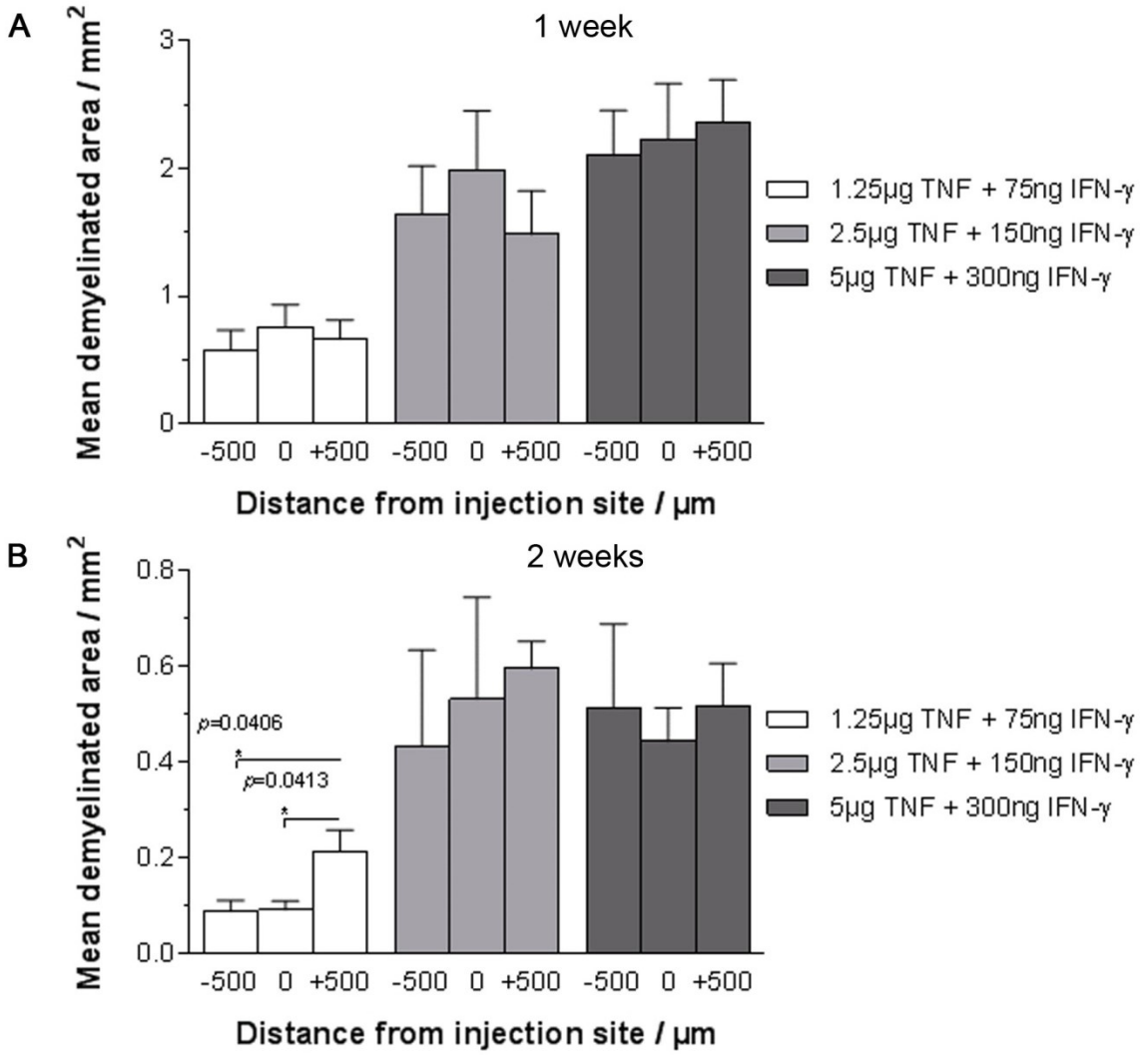

Figure 3.3.6. The area of demyelination did not change across 1mm spanning the injection site after injection of TNF and IFN-γ. The area of demyelination was the same 500µm anterior to (-500) and 500µm posterior to (+500) the injection site as at the injection site (0) at 1 week after injection in animals injected with all doses of TNF and IFN-γ (A). There was some variation in the area of demyelination at 2 weeks after injection in animals injected with the low dose of TNF and IFN-γ, although it was the same at 500µm anterior to and 500µm posterior to the injection site as at the injection site in animals injected with the intermediate and high doses (B; Kruskal-Wallis with Dunn's multiple comparisons test; mean ± SEM; * = $p \leq 0.05$; n = 4 for low, intermediate and high doses at 1 week and intermediate dose at 2 weeks, 3 for low and high doses at 2 weeks).

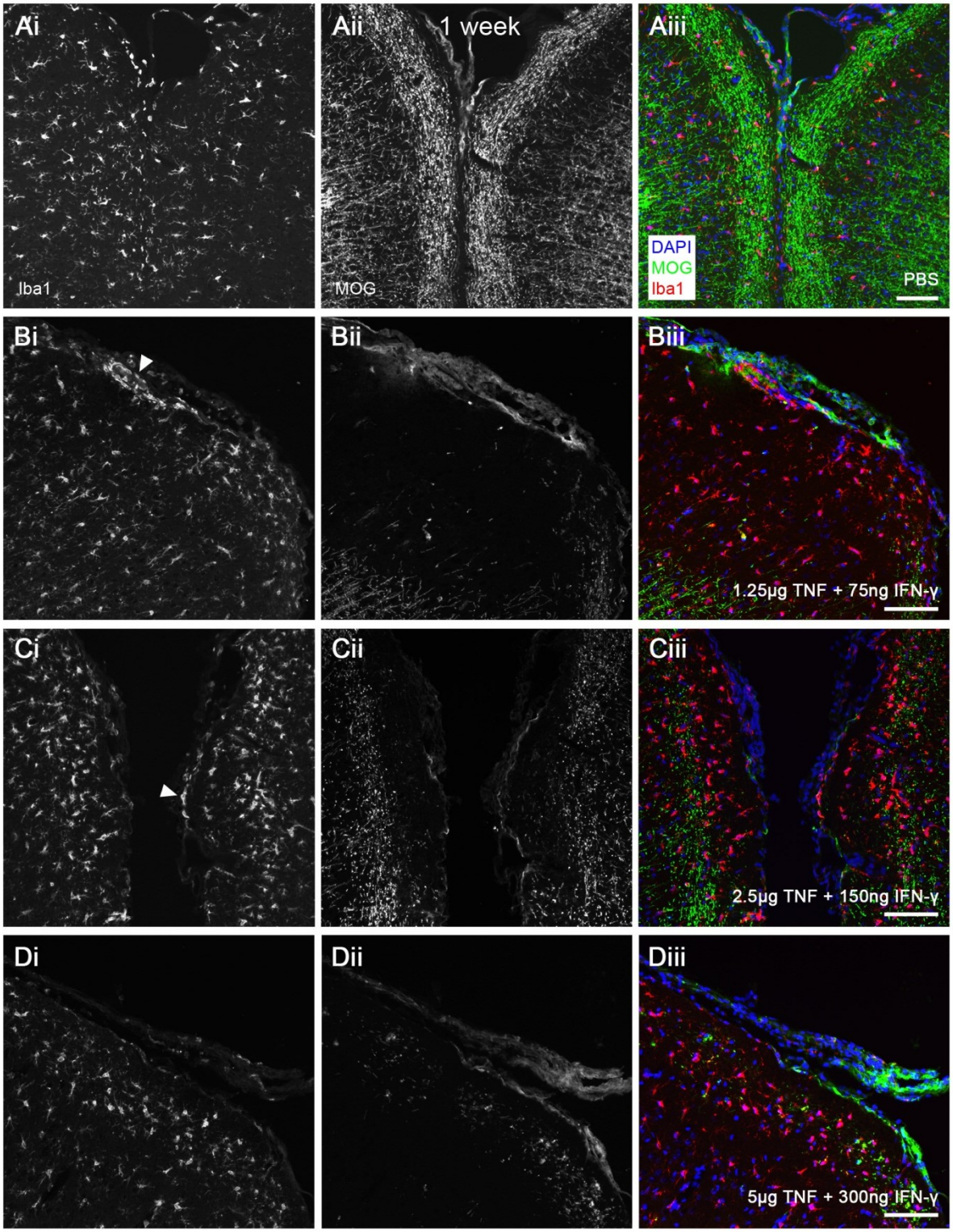

Figure 3.3.7. Microglial activation after injection of TNF and IFN-γ. IF for Iba1 was performed on injection site sections and showed the presence of activated macrophages/microglia (images on the left), particularly close to the pial surface, after injection of PBS only (A) and low (B), intermediate (C) and high (D) doses of TNF and IFN-γ. Activated macrophages/microglia were particularly evident in demyelinated areas (images in the centre, composite images on the right) . Note the presence of activated macrophages/microglia in the meninges overlying subpial demyelination (B) and lining the sagittal sulcus (C; arrowheads). Images are representative and from animals at 1 week after injection. Scale bars = 100µm.

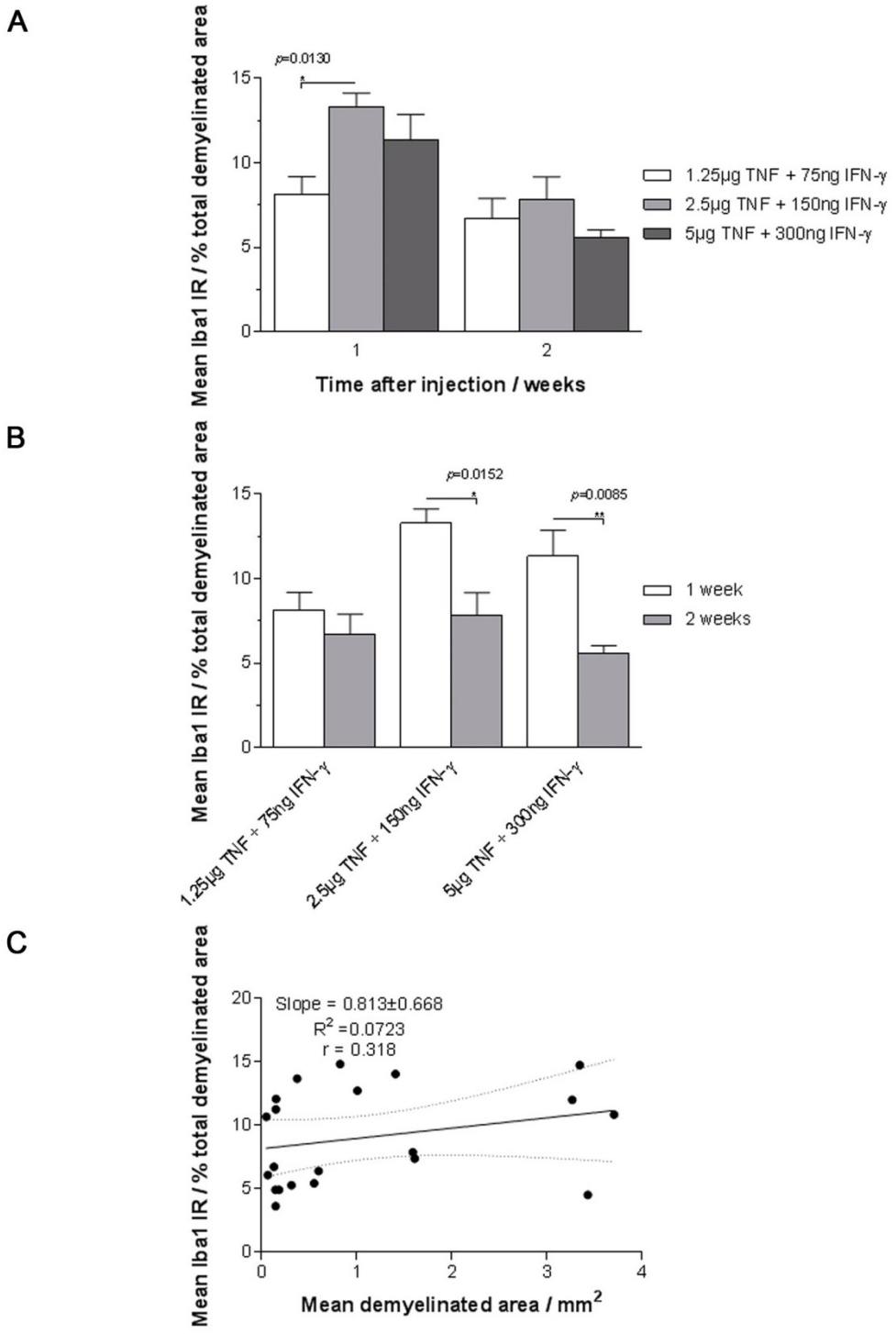

Figure 3.3.8. Effect of dose of TNF and IFN-γ and time point on microglial activation. Iba1 immunoreactivity in demyelinated areas was TNF and IFN-γ dose-dependent at 1 week, although there was no further effect of the high dose, but not at 2 weeks after injection (A). Iba1 immunoreactivity was also time-dependent. It was greater at 1 week after injection than at 2 weeks after injection (B; two-way ANOVA with Tukey's multiple comparisons test; mean ± SEM; * = $p \leq 0.05$, ** = $p \leq 0.01$; n = 4 for low, intermediate and high doses at 1 week and intermediate dose at 2 weeks, 3 for low and high doses at 2 weeks). There was no significant correlation between Iba1 immunoreactivity and area of demyelination (C; Spearman correlation).

The variation in microglial activation with increasing time after injection is shown more clearly in Figure 3.3.8 B. It was significantly greater at 1 week after injection than at 2 weeks after injection in animals injected with the intermediate (factor of 1.69) and high (factor of 2.03) doses of TNF and IFN-γ, although there was no significant difference in Iba1 immunoreactivity at 1 week and 2 weeks after injection in animals injected with the low dose. Although there appeared to be a positive correlation between the total area of subpial demyelination and the total Iba1 immunoreactivity in these areas, it was not significant (C).

3.3.2.4 Immune cell infiltration

In order to identify the presence of CD4+ and CD8+ T cells and B cells, double IF for CD4 and CD8 and IF for CD79a respectively were performed on sections cut at the injection site. These immune cells were observed in the meninges lining the sagittal sulcus and those on the superior surface of the cortex as well as in the sagittal sulcus 1 week after injection of TNF and IFN-γ (Figure 3.3.9 A). They were diffusely distributed and aggregates were not observed. Immune cell infiltration appeared to be mainly confined to the meninges and the sagittal sulcus, with very little present in the cortex and corpus callosum. Very few immune cells were also observed after injection of PBS only. A similar pattern of immune cell infiltration was present two weeks after injection of the 3 doses of TNF and IFN-γ.

Immune cells were quantified manually using the 20x objective lens and the effect of both the dose of TNF and IFN-γ (Bi, Ci, Di) and time after injection (Bii, Cii, Dii) were determined. As for the total area of subpial demyelination and the total Iba1 immunoreactivity in these areas, the total number of immune cells in the meninges increased with the dose of TNF and IFN-γ at 1 week, but not 2 weeks, after injection.

CD4+ T cells

The number of CD4+ T cells was significantly greater in animals injected with the high dose than in those injected with the intermediate (factor of 1.92) and low (factor of 3.62) doses

and those injected with PBS only (factor of 23.8) at 1 week after injection (Figure 3.3.9 Bi). The number of CD4+ T cells was greater in animals injected with the intermediate dose than in those injected with the low dose (factor of 1.89) and those injected with PBS only (factor of 12.4), and in animals injected with the low dose than in those injected with PBS only (factor of 6.56), although these dose-dependent effects were not statistically significant. There were no statistically significant differences at 2 weeks after injection. The effect of time point on the number of CD4+ T cells is demonstrated in Bii. The only statistically significant difference was observed in animals injected with the high dose of TNF and IFN-γ, in which the number of CD4+ T cells was significantly greater at 1 week after injection than at 2 weeks after injection (factor of 1.82).

CD8+ T cells

The number of CD8+ T cells was significantly greater in animals injected with the intermediate dose than in those injected with the low dose (factor of 1.80) and those injected with PBS only (factor of 3.03) at 1 week after injection (Figure 3.3.9 Ci). It was also significantly greater in these animals than in those injected with the high dose (factor of 1.56). At 2 weeks after injection, the number of CD8+ T cells was significantly greater in animals injected with the low dose than in those injected with the high dose (factor of 1.82). The effect of time point is shown in Cii. The number of CD8+ T cells was significantly greater at 1 week after injection than at 2 weeks after injection in animals injected with the intermediate dose of TNF and IFN-γ (factor of 1.66).

CD79a+ B cells

As for the number of CD4+ T cells, the number of CD79a+ B cells was significantly greater in animals injected with the high dose than in those injected with the intermediate (factor of 1.56) and low (factor of 2.32) doses and those injected with PBS only (factor of 4.29) at 1 week after injection (Figure 3.3.9 Di). Again, although the number of B cells was greater in animals injected with the intermediate dose than in those injected with the low dose (factor of

1.48) and those injected with PBS only (factor of 2.74), and in animals injected with the low dose than in those injected with PBS only (factor of 1.85), these dose-dependent effects were not statistically significant. There were no statistically significant differences at 2 weeks after injection. The number of B cells was significantly greater at 1 week after injection than at 2 weeks after injection in animals injected with the high dose of TNF and IFN-γ (factor of 3.70), although there was no significant difference in the number of B cells at 1 week and 2 weeks after injection in animals injected with the low and intermediate doses (Dii).

Immune cell proportions

CD8+ T cells were more abundant than CD4+ T cells and B cells in the meninges (Figure 3.3.10). The number of CD8+ T cells was significantly greater than the number of CD4+ T cells at 1 week after injection in animals injected with PBS only (factor of 14.5) and in those injected with the low (factor of 3.73) and intermediate (factor of 3.55) doses of TNF and IFN-γ (A) as well as at 2 weeks after injection in animals injected with the low (factor of 2.46) and intermediate (factor of 2.43) doses (B). The number of CD8+ T cells also appeared to be greater than the number of B cells at both 1 week and 2 weeks after injection, although this was only statistically significant in animals injected with the intermediate dose of TNF and IFN-γ (factors of 2.01 and 1.98 at 1 and 2 weeks after injection respectively). There were no significant differences in the number of these immune cells at either 1 week or 2 weeks after injection of the high dose.

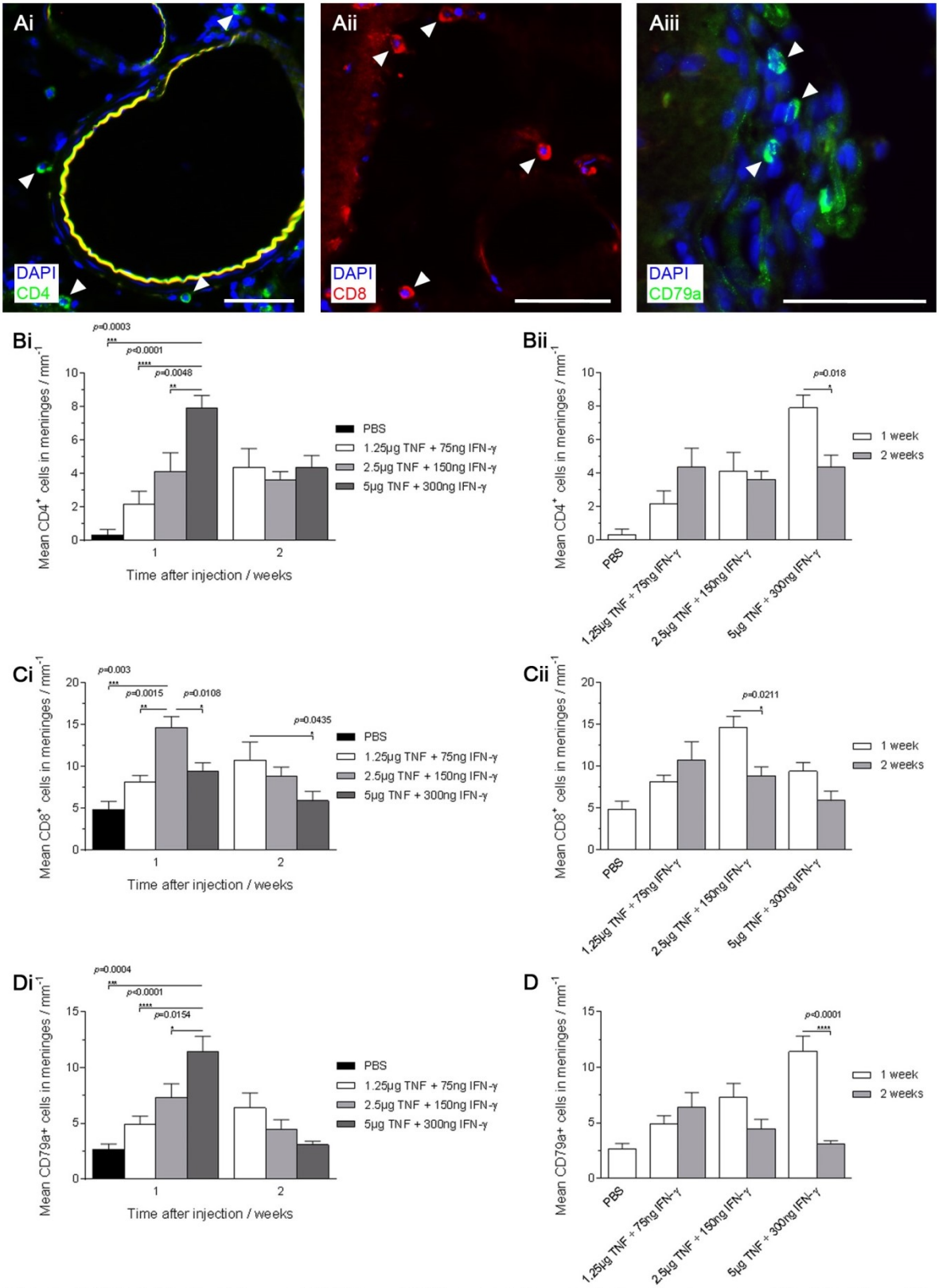

Figure 3.3.9. Effect of dose of TNF and IFN-γ and time point on immune cell infiltration. IF for CD4, CD8 and CD79a was performed on injection site sections and showed the presence of CD4+ (Ai) and CD8+ T cells (Aii) and B cells (Aiii; arrowheads). Images are representative. Scale bars = 50µm. Immune cell infiltration was TNF and IFN-γ dose-dependent at 1 week, but not at 2 weeks, after injection (Bi, Ci, Di). Immune cell infiltration was time-dependent for higher doses (Bii, Cii, Dii; two-way ANOVA with Tukey's multiple comparisons test; mean ± SEM; * = $p \leq 0.05$, ** = $p \leq 0.01$, *** = $p \leq 0.001$, **** = $p \leq 0.0001$; $n = 4$ for all doses at 1 week and intermediate dose at 2 weeks, 3 for low and high doses at 2 weeks).

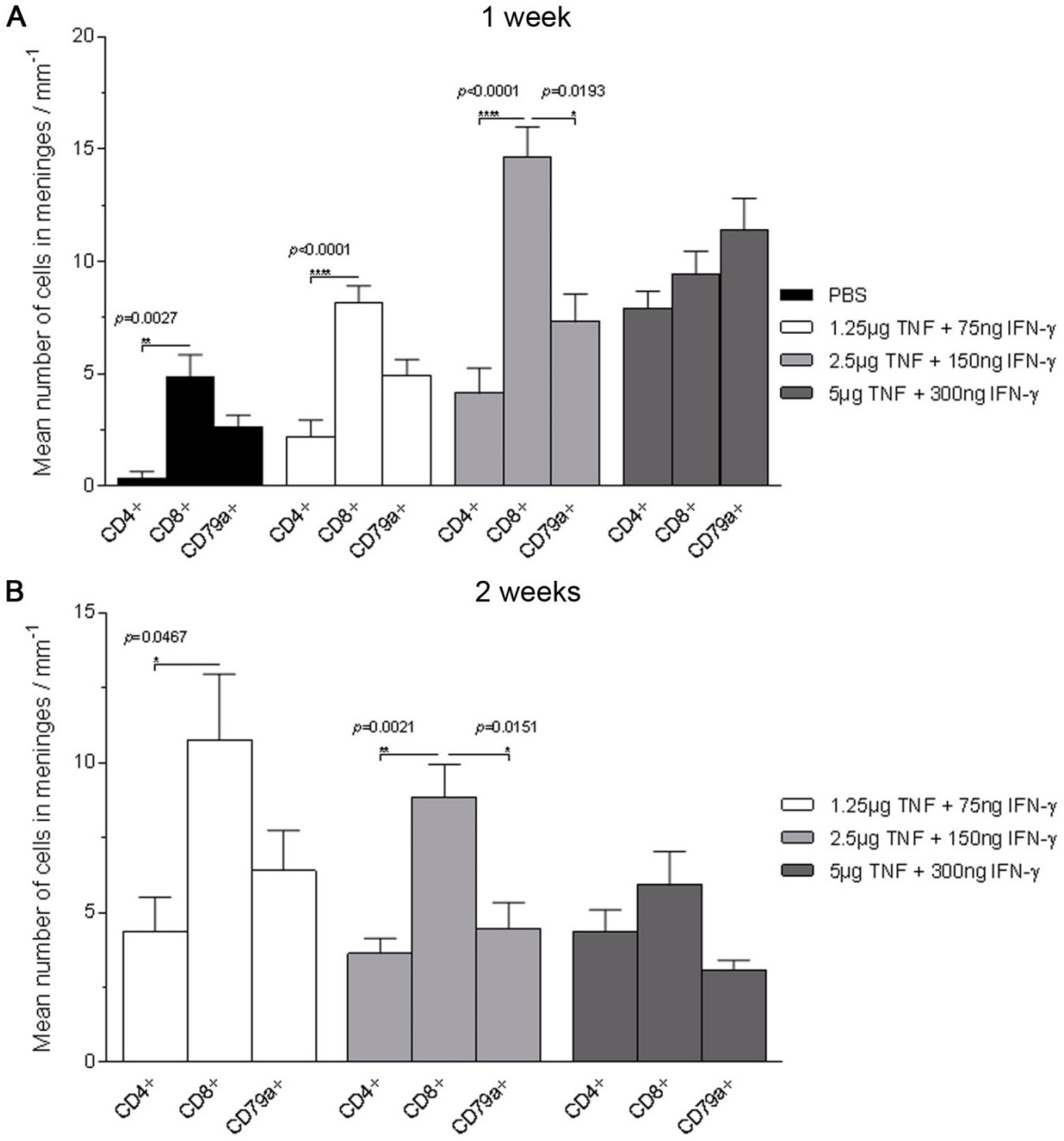

Figure 3.3.10. Immune cell infiltration after injection of TNF and IFN-γ consisted mainly of CD8+ T cells. CD8+ T cells outnumbered CD4+ T cells at 1 week after injection in animals injected with PBS only and in those injected with the low and intermediate doses of TNF and IFN-γ (A). They also outnumbered CD79a+ B cells in animals injected with the intermediate dose. CD8+ T cells outnumbered CD4+ T cells at 2 weeks after injection in animals injected with the low and intermediate doses of TNF and IFN-γ, and B cells in animals injected with the intermediate dose (B; Kruskal-Wallis with Dunn's multiple comparisons test; mean ± SEM; * = $p \leq 0.05$, ** = $p \leq 0.01$, **** = $p \leq 0.0001$; $n = 4$ for all doses at 1 week and intermediate dose at 2 weeks, 3 for low and high doses at 2 weeks).

3.4 Discussion

3.4.1 Stereotactic injection into the SAS of the sagittal sulcus

The targeted EAE model used in the current study was developed to test the hypothesis that an inflammatory milieu in the CSF/meningeal compartment can result in subpial cortical GMLs (Peterson *et al.*, 2001, Reynolds *et al.*, 2011), hence it was important to achieve a high frequency of accurate injections into the SAS of the sagittal sulcus, the space filled with CSF between the pia and arachnoid mater. The resulting cortical GM pathology would then be a result of the inflammatory milieu in the CSF/meningeal compartment after injection of TNF and IFN-γ, and associated release and diffusion of pro-inflammatory cytokines from the pial surface. It was also important to achieve accurate injections into the SAS to avoid the physical injury and BBB damage induced by direct injection into the motor cortex in another targeted EAE model (Merkler *et al.*, 2006). Studies have shown that cortical stab wounds in otherwise naïve rats result in extensive physical injury, characterised by demyelination with a corresponding increase in the number of oligodendrocytes (Xie *et al.*, 1995). They also result in an increase in the number of macrophages and microglia, some of which were replicating and which reached a maximum at 1 week after wounding, as well as astrocytes (Fujita *et al.*, 1998), although these studies used blades to induce the stab wounds rather than the glass capillaries used in the current study. It has also been shown that focal cortical damage in the form of a cryolesion results in exacerbation of pathological EAE, with an increase in the number of T cells and activated microglia in the brain (Phillips *et al.*, 1995, Sun *et al.*, 2000). It also results in BBB damage, which is in contrast to the preservation of BBB integrity in GMLs (van Horssen *et al.*, 2007). Hence any cortical GM pathology observed after injection into the cortex would not be consistent with that in GMLs in MS, and may be due to the injection itself rather than the injection of TNF and IFN-γ. However, achieving accurate injections was technically challenging due to the narrow width of the sagittal sulcus and its base, the diameter of which was approximately 200μm, with the cortical GM adjacent and

corpus callosum WM below. The intersection of the coronal and sagittal sutures at Bregma was also highly variable between animals, hence the lateral as well as the anterior coordinate of injection was difficult to determine. Despite this, accurate injections, determined using monastral blue, were achieved in the majority of animals in the current study.

Tracers such as monastral blue and Indian ink are widely added to injection solutions to enable the identification of the injection site as well as CSF drainage pathways following stereotactic injection, and can persist for several months (Zhang *et al.*, 1992, Kida *et al.*, 1993, Kerschensteiner *et al.*, 2004, Merkler *et al.*, 2006, Gardner *et al.*, 2013, Rodriguez *et al.*, 2014). Monastral blue was confined to the meninges of the sagittal sulcus in 64% of animals in this study, validating the accuracy of injection. In these animals, monastral blue spread along the anteroposterior axis but did not spread into the cortex. In some animals, it was also observed on the superior surface of the cortex. This pattern is consistent with CSF drainage pathways, several of which have been described. Approximately half of the CSF drains from the SAS through arachnoid villi and granulations in the walls of the sagittal sinuses into venous blood (Boulton *et al.*, 1998, Weller *et al.*, 2010), whereas approximately half drains in an anterior direction along channels in the SAS adjacent to the olfactory nerves through the cribriform plate, to connect with the nasal mucosa lymphatics and cervical lymph nodes (Figure 3.4.1; Zhang *et al.*, 1992, Kida *et al.*, 1993, Boulton *et al.*, 1998, Johnston *et al.*, 2004). The rate of CSF flow over the cortex has not been determined, although the rate of CSF bulk flow per whole brain is approximately 2µl per minute, resulting in a turnover rate of approximately 10 times per day (Pardridge, 2011, Chiu *et al.*, 2012). However, we suggest that the rate of CSF flow in the deep sulcus is lower than that of CSF bulk flow, resulting in a protected environment (Reynolds *et al.*, 2011) that allows the retention of monastral blue in the CSF/meningeal compartment. In the case of accurate injections, we conclude that injection into the SAS of the sagittal sulcus is a good route to target the CSF/meningeal compartment.

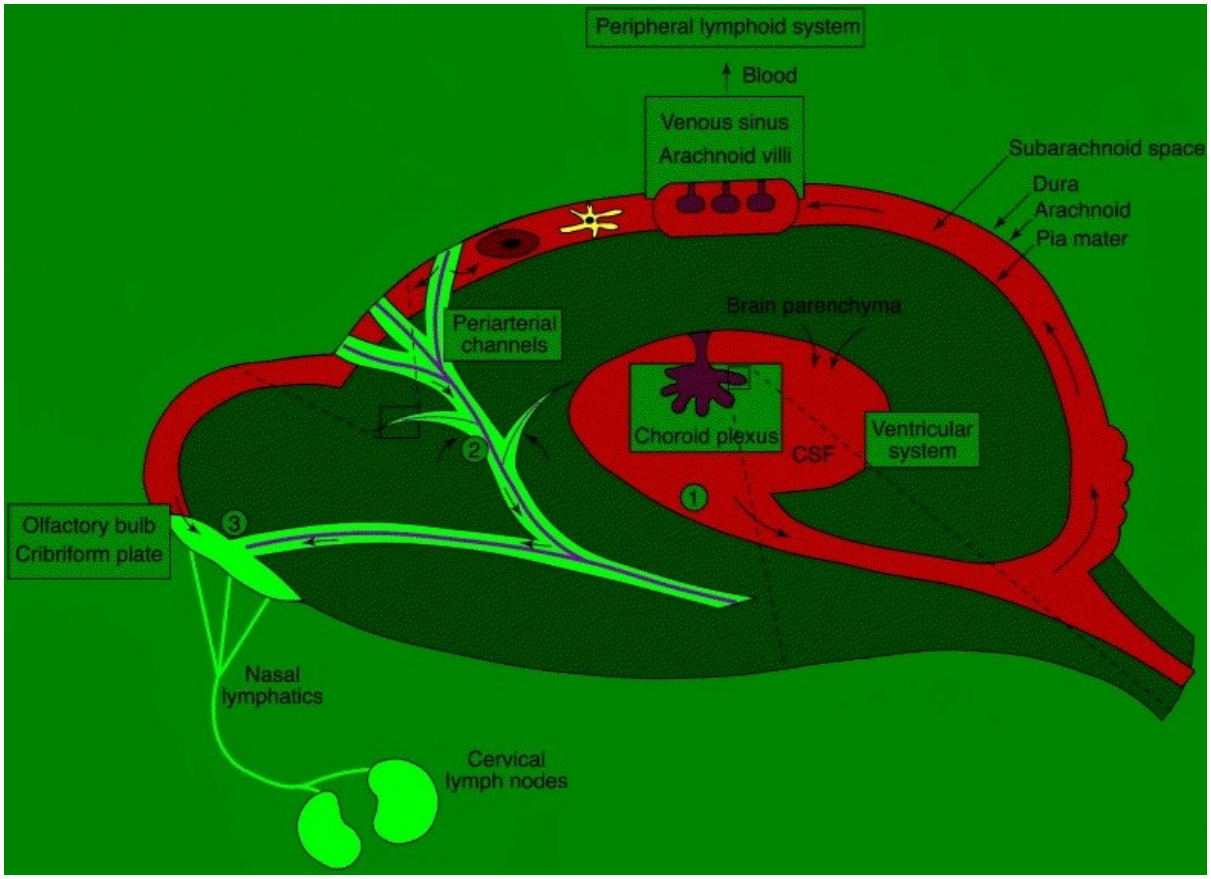

Figure 3.4.1. CSF drainage pathways. CSF drains along the SAS to either the spleen or cervical lymph nodes. Drainage to the spleen is mediated by arachnoid villi that allow entry to the venous sinuses while drainage to the cervical lymph nodes is mediated by the cribriform plate that connects the SAS and the nasal lymphatics in the rat. Adapted from Aloisi *et al.*, 2000.

3.4.2 Subpial demyelination after injection of TNF and IFN-γ

In this study, the injection of TNF and IFN-γ into the SAS of the sagittal sulcus of female DA rats immunised with a subclinical dose of rmMOG successfully induced subpial demyelination, consistent with a previous study using this model (Gardner *et al.*, 2013) and confirming that an inflammatory milieu in the CSF/meningeal compartment can indeed result in subpial cortical GMLs. A previous study suggested that the injection of TNF and IFN-γ into the motor cortex induced subpial demyelination as a result of the drainage of the cytokines into the CSF/meningeal compartment (Merkler *et al.*, 2006), whereas the current study and that of Gardner *et al.*, 2013 suggest that the cytokines may diffuse directly into the cortex from the SAS if produced by the infiltrating immune cells in the meninges. This is consistent with the hypothesis proposed on the basis of studies using autopsy samples from MS cases

that soluble factors, suggested to include TNF and IFN-γ (Sharief and Hentges, 1991, Spuler *et al.*, 1996, Serafini *et al.*, 2007, Magliozzi *et al.*, 2010, Romme Christensen *et al.*, 2012, Gardner *et al.*, 2013), produced in the CSF/meningeal compartment diffuse into the underlying cortical GM.

Neither leukocortical nor intracortical demyelination was observed, suggesting that the pathogenesis of subpial demyelination is distinct. This is supported by the distance from the meninges and the association between intracortical demyelination and blood vessels (Peterson *et al.*, 2001, Bø *et al.*, 2003a). Additionally, it suggests that the injected TNF and IFN-γ do not gain access to the cortex via perivascular pathways in sufficient quantity to cause pathology, supported by the relative lack of monastral blue observed in the cortex. Demyelination of the corpus callosum WM underlying the sagittal sulcus injection site was also absent, except in animals in which monastral blue was present at this location. This suggests that the subpial demyelination can develop independently from WM demyelination, as previously proposed (Bø *et al.*, 2003b, Kutzelnigg *et al.*, 2005, Vercellino *et al.*, 2005, Bö *et al.*, 2007).

The cortical GMLs observed were similar to the Type III GMLs observed in MS cortex, extending from the pial surface into GM layer III and associated with mild peripheral immune cell infiltration (Peterson *et al.*, 2001, Bø *et al.*, 2003b). The finding that activated macrophages/microglia, CD4+ and CD8+ T cells and B cells were present in the meninges is consistent with the diffuse inflammatory infiltrates present in the meninges in approximately 40% of SPMS cases (Serafini *et al.*, 2004, Magliozzi *et al.*, 2007, Magliozzi *et al.*, 2010, Howell *et al.*, 2011). Additionally, the observation that the immune cell infiltration in the meninges in the current study was particularly evident in meninges overlying areas of subpial cortical GM demyelination is in keeping with the correlation between meningeal inflammation and underlying subpial cortical GM demyelination and microglial activation in F+ SPMS cases (Magliozzi *et al.*, 2007, Magliozzi *et al.*, 2010, Howell *et al.*, 2011). The

same extent of microglial activation and immune cell infiltration in the meninges was not observed in control animals immunised with rmMOG and injected with PBS only, in which subpial demyelination was absent. Although it was not feasible to include control animals immunised with IFA and injected with TNF and IFN-γ in this study, a previous study has shown that the same extent of microglial activation and immune cell infiltration was also not observed in these animals, again in the absence of significant subpial demyelination (Gardner *et al.*, 2013). These findings indicate a significant role for the reactivation of myelin-reactive T cells in the CSF/meningeal compartment as well as TNF and IFN-γ in activating meningeal blood vessels resulting in macrophage infiltration (Bartholomäus *et al.*, 2009, Kivisäkk *et al.*, 2009).

The increasing area of subpial demyelination with the increasing levels of TNF and IFN-γ at 1 week after injection further indicates a significant role for these cytokines in mediating this pathology. These demyelinating, inflammatory effects of TNF and IFN-γ have been previously demonstrated. For example, the overexpression of TNF in the CNS of transgenic mice resulted in spontaneous, chronic inflammatory demyelination associated with CD4+ and CD8+ T cell infiltration in the meninges and microgliosis (Probert *et al.*, 1995). Individual treatment of oligodendrocytes with TNF or IFN-γ has been shown to induce dose-dependent apoptosis, with combined treatment resulting in accelerated apoptosis (Buntinx *et al.*, 2004). Combined treatment of microglia induced microglial activation, resulting in NOS expression and NO production (Mir *et al.*, 2008). The treatment of microglia with IFN-γ has also been shown to increase the synthesis and secretion of TNF, which, in an autocrine manner, may induce further microglial activation (Aloisi, 2001, Takeuchi *et al.*, 2006). *In vivo*, the injection of TNF and IFN-γ into the spinal cord resulted in mononuclear cell infiltrates (Simmons and Willenborg, 1990). Taken together, these studies and the current study suggest that TNF and IFN-γ diffuse into the cortex from the SAS, resulting in subpial demyelination, directly or indirectly through the activation of microglia.

3.4.3 Mechanism of subpial demyelination

3.4.3.1 Humoral immune system

As stated, no significant subpial demyelination is observed in control animals immunised with IFA and injected with TNF and IFN-γ (Gardner *et al.*, 2013), indicating that the presence of these cytokines in the SAS alone is not sufficient to induce subpial demyelination but that an existing cellular/humoral anti-myelin immune response is also required.

This suggests that demyelination may be antibody-mediated, which in turn has been shown to depend on the fixation of complement by anti-MOG antibodies (Piddlesden *et al.*, 1993) and its deposition on myelin sheaths (Storch *et al.*, 1998a). Ig and complement deposition on myelin sheaths, although transient, has been observed in targeted EAE models (Merkler *et al.*, 2006, Gardner *et al.*, 2013). However, a study using autopsy samples from MS patients showed a relative lack of deposition in purely cortical GMLs (Brink *et al.*, 2005), although active GMLs have not been studied.

It also suggests a role for B cells in the pathogenesis of subpial demyelination, although they were not the most abundant immune cell in the meninges in the current study. Although the B cell infiltration was confined to the meninges consistent with that in MS cases (Frischer *et al.*, 2009), lymphoid-like structures consisting of aggregates of B cells, some of which are proliferating, together with follicular dendritic cells, plasmablasts/plasma cells and T cells, were not observed. Lymphoid-like structures have been observed in the meninges of mice with MOG-induced EAE, but only in those with progressive relapsing EAE with a high level of inflammation in the CNS, suggesting that a chronic inflammatory milieu is required (Magliozzi *et al.*, 2004). Additionally, it appears that the development of lymphoid-like structures depends on the B cell chemokine CXCL13, B cell activating factor (BAFF) and the cytokine lymphotoxin-$\alpha_1\beta_2$ (Magliozzi *et al.*, 2004, Columba-Cabezas *et al.*, 2006). Hence the absence of lymphoid-like structures in the current study may be due to the acute, rather than

chronic, inflammatory milieu resulting from the injection of TNF and IFN-γ, and/or insufficient production of CXCL13, BAFF and lymphotoxin-$\alpha_1\beta_2$. Chapter 4 aims to evaluate LV vectors as a delivery system to achieve a chronic inflammatory milieu in the CSF/meningeal compartment and studies involving the injection of the molecules involved in the development of lymphoid-like structures into the SAS are ongoing.

Studies in EAE have yielded conflicting results regarding the role of B cells. One study showed that B cell-deficient mice were susceptible to MOG peptide-induced EAE (Hjelmström *et al.*, 1998) whereas another study showed that these mice were resistant to recombinant MOG-induced EAE, but not to encephalitogenic MOG peptide-induced EAE (Lyons *et al.*, 1999). However, later studies have shown that the MOG amino acids 35-55 peptide used in these studies is recognised by T cells (Delarasse *et al.*, 2013), and is partly occluded within the dimer interface of recombinant MOG (Clements *et al.*, 2003), hence these findings may indicate a significant role for T cells rather than B cells in this model. B cells, as well as differentiating into anti-MOG antibody-producing plasma cells, also function as APCs and activate Th cells (Rodríguez-Pinto, 2005) and secrete cytokines, including IFN-γ (Harris *et al.*, 2005), lymphotoxin and TNF (Bar-Or *et al.*, 2010). A recent study has shown that B cells are required for reactivation of myelin-reactive T cells, their cytokine secretion and their subsequent recruitment of further immune cells (Pierson *et al.*, 2014), independent of their production of anti-MOG antibodies (Jagessar *et al.*, 2012, Molnarfi *et al.*, 2013), and we suggest that the B cells observed in the meninges in the current study contribute to the inflammatory milieu in the CSF/meningeal compartment by reactivating T cells and secreting cytokines.

3.4.3.2 Cellular immune system

T cells

The finding of increasing total number of CD4+ and CD8+ T cells in the meninges with the increasing levels of TNF and IFN-γ at 1 week after injection indicates a role for these

cytokines in stimulating T cell infiltration. Consistent with this proposed role, the treatment of cultured endothelial cells, which comprise the BBB, with TNF or IFN-γ has been shown to result in decreased integrity of the barrier they form and increased expression of intercellular adhesion molecule 1 and vascular adhesion molecule 1 (Fabry *et al.*, 1992, Wong and Dorovini-Zis, 1995, Dobbie *et al.*, 1999). Additionally, TNF and IFN-γ induce the expression of chemokines including CCL2, CCL5, CXCL10 and IL8 in astrocytes (Oh *et al.*, 1999), facilitating further entry of T and B cells, plasma cells and macrophages to the CNS (Hellings *et al.*, 2002). Myelin-reactive T cells then become reactivated on encountering their specific myelin epitope presented by APCs in the CSF/meningeal compartment (Bartholomäus *et al.*, 2009, Kivisäkk *et al.*, 2009). These studies suggest that the injection of TNF and IFN-γ stimulated activation of the BBB and subsequent immune cell infiltration.

CD4+ and CD8+ T cells in the meninges have previously been observed in this model (Gardner *et al.*, 2013), and are also observed in EAE models (Brown and Sawchenko, 2007, Bartholomäus *et al.*, 2009) as well as in MS cases, particularly in lymphoid-like structures (Serafini *et al.*, 2007, Frischer *et al.*, 2009, Howell *et al.*, 2011). A recent study has shown that T cells in the meninges of marmosets with MOG-induced EAE are associated with early subpial demyelination, suggesting a role for the local infiltration of these cells in the meninges in the pathogenesis of subpial demyelination in this model (Kramann *et al.*, 2014). The presence of these cells in the meninges suggests that their entry to the CNS is via meningeal blood vessels. Their presence in the meninges on the superior surface of the cortex as well as in those lining the sagittal sulcus is consistent with CSF drainage pathways, with TNF and IFN-γ proposed to drain from the sagittal sulcus to the superior surface (Zhang *et al.*, 1992, Kida *et al.*, 1993) where they facilitate entry of T and B cells as described. Very few T cells were present in areas of subpial demyelination, consistent with a previous study (Gardner *et al.*, 2013) and with cortical GMLs in MS cases, in which characteristically only mild peripheral immune cell infiltration is observed (Peterson *et al.*, 2001, Kutzelnigg *et al.*, 2005, Magliozzi *et al.*, 2010), suggesting that these cells do not have

a direct cytotoxic role in the pathogenesis of cortical GMLs. This is in contrast to the perivascular T cell infiltrates observed in the spinal cord WMLs of EAE (Storch *et al.*, 1998b), in which they are suggested to have an indirect role by secreting cytokines (Lovett-Racke *et al.*, 2011), again indicating that the pathogenesis of GMLs and WMLs is distinct.

Th1 CD4+ cells secrete IFN-γ, IL2, lymphotoxin-α and TNF (Dittel, 2008, Zhu *et al.*, 2010) and Tc CD8+ cells similarly secrete cytokines, including TNF and IFN-γ (Harty and Bevan, 1999), further contributing to the inflammatory milieu in the CSF/meningeal compartment. CD3+ T cells in the meninges of F+ SPMS cases have been shown to express IFN-γ (Gardner *et al.*, 2013). Although MS and EAE have historically been regarded as CD4+ T cell-mediated due to association with MHC class II alleles, with Th1 cells being the main pathogenic cells, the recent studies described in 1.3.3.1 have suggested a role for CD8+ T cells. In the current study, CD8+ T cells were the most abundant immune cell in the meninges. A previous study using this model did not compare the number of CD4+ and CD8+ T cells in the meninges, although it appears that CD4+ T cells were more abundant (Gardner *et al.*, 2013). Tc cells are more common than Th cells in cortical GMLs in progressive MS cases (Bø *et al.*, 2003a, Frischer *et al.*, 2009) and their oligoclonal expansion in blood (Skulina *et al.*, 2004), CSF (Jacobsen *et al.*, 2002) and active lesions (Babbe *et al.*, 2000) has been demonstrated, which is not the case for Th cells. Tc cells from MS patients show greater rolling and arrest in meningeal blood vessels than Th cells when injected in mice, indicating selective entry of these cells to the CNS (Battistini *et al.*, 2003), consistent with CD8+ T cells being the most abundant immune cell in the meninges in the current study. We suggest that these cells contribute to the inflammatory milieu in the CSF/meningeal compartment by promoting BBB permeability and secreting chemokines (Mars *et al.*, 2011), resulting in subsequent recruitment of further immune cells. Their secretion of cytokines may also increase the recruitment and activation of microglia (Harty and Bevan, 1999).

Macrophages/microglia

The injection of TNF and IFN-γ also induced the infiltration or local proliferation of activated microglia, particularly at the leading edge of the subpial cortical GMLs but also in the meninges, with a high density of cells with an amoeboid morphology being observed. This finding is consistent with the extensive microglial activation induced by the injection of these cytokines into the motor cortex as well as the SAS in previous studies, in which they were closely associated with myelin sheaths (Merkler *et al.*, 2006, Gardner *et al.*, 2013), and suggests a role for microglia in the pathogenesis of subpial demyelination. Additionally, the trend for a positive correlation between the extent of subpial demyelination and microglial activation in these areas was similar to that observed previously (Merkler *et al.*, 2006, Gardner *et al.*, 2013). This finding is also consistent with the distribution of MHC class II-positive and CD68-positive macrophages/microglia with amoeboid morphology throughout cortical GMLs and NAGM in MS cases (Peterson *et al.*, 2001, Bø *et al.*, 2003a, Magliozzi *et al.*, 2007, Magliozzi *et al.*, 2010). Meningeal inflammation has been correlated with microglial activation as well as subpial cortical GM demyelination in the underlying cortical GM (Magliozzi *et al.*, 2007, Magliozzi *et al.*, 2010, Howell *et al.*, 2011), again confirming the role of the inflammatory milieu in the CSF/meningeal compartment in cortical GM pathology.

IFN-γ is the best known inducer/potentiator of the antigen presenting and pro-inflammatory functions of macrophages/microglia (Colton *et al.*, 1994, Aloisi *et al.*, 2000, Aloisi, 2001), with IFN-γ receptors constitutively expressed on 'resting' microglia and their activation following intrathecal injection of IFN-γ resulting in MHC class II expression (Vass and Lassmann, 1990). This in turn results in the differentiation of naïve T cells into Th1 cells (Aloisi *et al.*, 1999b), although the lack of T cell infiltration in the cortex indicates that the antigen presenting function of microglia may not be significant. TNF also induces microglial activation, with TNFR1 and TNFR2 expressed (Dopp *et al.*, 1997). Activation results in expression of the pro-inflammatory cytokines IL1β and IL6 and inducible NOS, formation of oxygen radicals as well as prolonged survival of cultured microglia. Additionally, TNFR1

mediates an autocrine positive feedback loop resulting in TNF-induced TNF expression by microglia (Kuno *et al.*, 2005).

Several mechanisms by which microglial activation results in demyelination have been proposed. The NO radicals produced are cytotoxic to oligodendrocytes *in vitro* (Merrill *et al.*, 1993) and the glutamate produced as a result of increased glutaminase expression (Takeuchi *et al.*, 2006) results in excitotoxic oligodendrocyte death. The application of glutamate receptor agonists to the optic nerve *in vivo* results in apoptotic oligodendrocyte death and demyelination (Matute, 1998). IFN-γ and TNF also both stimulate increased phagocytosis of myelin (Smith *et al.*, 1998), which may be opsonised by anti-myelin antibodies or complement protein fragment C3bi (Gitik *et al.*, 2010) and which is mediated by Fc and complement receptors, the expression of which is increased in activated microglia (Mosley and Cuzner, 1996). Although the phenotype of the Iba1+ activated microglia observed in the current study is not known, a previous study using this model showed the presence of Iba1+ activated microglia that were also CD68+, indicative of phagocytosis (Gardner *et al.*, 2013). The TNF and IFN-γ produced by activated microglia also induce oligodendrocyte death directly, with that induced by TNF being mediated by TNFR1 and the death molecule apoptosis-inducing factor rather than caspases (Buntinx *et al.*, 2004, Jurewicz *et al.*, 2005, Horiuchi *et al.*, 2006).

However, a previous study using this model showed that the extent of microglial activation at 1-3 days after injection of TNF and IFN-γ was the same in animals immunised with rmMOG and those immunised with IFA only, and only became more extensive in the animals immunised with rmMOG at 7 days after injection when demyelination was maximal (Gardner *et al.*, 2013). This suggests that acute microglial activation is not sufficient to induce demyelination and that an existing cellular/humoral anti-MOG immune response is also required. Given that immune cell infiltration in the meninges preceded maximal demyelination as well as microglial activation (Gardner *et al.*, 2013), it is possible that the

TNF and IFN-γ secreted by myelin-reactive T cells, once reactivated, is required to activate microglia.

3.4.4 Acute versus chronic presence of TNF and IFN-γ

Although it resulted in increased extent of pathology, increasing the doses of TNF and IFN-γ injected into the SAS in the current study did not result in increased duration of pathology. The acute nature of pathology, with subpial demyelination, microglial activation and T and B cell infiltration in the meninges being significantly greater at 1 week after injection than at 2 weeks after injection of the higher doses of TNF and IFN-γ, was consistent with that observed previously in targeted EAE models (Merkler *et al.*, 2006, Gardner *et al.*, 2013). This is perhaps not surprising, as the small volume of cytokines will have been rapidly catabolised by proteases, diluted or drained in the CSF, resulting in a loss of the pro-inflammatory signalling that results in microglial activation and immune cell infiltration.

3.4.4.1 Acute inflammation

We suggest that the secretion of TNF and IFN-γ by myelin-reactive T cells and activated microglia induced by the injection of TNF and IFN-γ decreases with time, deactivating the BBB and decreasing the entry of additional T cells to the CNS. Additionally, there may also be a role for microglia in the resolution of inflammation. They have been shown to secrete the anti-inflammatory cytokines IL10 and TGF-β *in vitro*, which inhibit further microglial activation by decreasing their secretion of pro-inflammatory cytokines, chemokines and nitrogen and oxygen radicals (Aloisi, 2001, Qian *et al.*, 2006) as well as their expression of MHC class II molecules (O'Keefe *et al.*, 1999). IL10 is thought to be important in the recovery from EAE of DA rats, whereas TGF-β may be important in the resistance to EAE of Albino Oxford rats (Blaževski *et al.*, 2013). Finally, it is likely that both FoxP3+ regulatory T cells and Type 1 regulatory T cells are involved in the resolution of inflammation. The adoptive transfer of the former has been shown to improve, and the depletion worsen, EAE (Kleinewietfeld and Hafler, 2014) and their suppressive capacity is impaired in RRMS

patients (Viglietta *et al.*, 2004), which is also true for IL10-secreting Type 1 regulatory T cells (Astier *et al.*, 2006). Further study will be required to determine the role of anti-inflammatory cytokines and regulatory T cells in the resolution of inflammation in this model. We suggest that chronic meningeal inflammation will be required to achieve chronic microglial activation, and conclude that meningeal inflammation does not become self-sustaining after the injection of higher doses of TNF and IFN-γ.

3.4.4.2 Acute demyelination

The decreased extent of subpial demyelination at 2 weeks after injection than at 1 week after injection indicates that remyelination has taken place. New oligodendrocytes forming myelin sheaths have been identified in subpial GMLs in MS cases, regardless of disease duration or age at death (Chang *et al.*, 2012). Increased g-ratios (ratio of axon diameter to total fibre diameter on electron micrographs) indicative of remyelination have also been observed, at a similar time point, in GMLs following the injection of TNF and IFN-γ into the motor cortex (Merkler *et al.*, 2006). A study using a model of chronic demyelination showed that the induction of acute inflammation by the injection of saline/charcoal or by meningitis, resulting in macrophage and lymphocyte infiltration respectively, stimulates remyelination by transplanted OPCs (Foote and Blakemore, 2005). Studies have shown that macrophages contribute to remyelination both by the phagocytosis of myelin debris, which has been shown to inhibit OPC differentiation (Robinson and Miller, 1999), and by the secretion of growth factors, including insulin-like growth factor 1, which stimulate the differentiation and proliferation of OPCs and oligodendrocytes (Kotter *et al.*, 2005). Additionally, TNF signalling mediated by TNFR2 has been shown to be required for the proliferation of immature oligodendrocytes in a mouse cuprizone model (Arnett *et al.*, 2001), whereas an inhibitory role for IFN-γ has been shown (Lin *et al.*, 2006). These studies suggest that the acute inflammation, consisting of microglial activation and immune cell infiltration, induced by the injection of TNF and IFN-γ in the current study may stimulate remyelination, resulting in the acute demyelination observed. Further study of the dynamics and mechanism of

remyelination in this model could include the quantification of established OPC and oligodendrocyte phenotypic markers as well as the growth factors that stimulate remyelination.

Finally, data have suggested that the clinical presentation and course of MS are dependent on age (Confavreux and Vukusic, 2006). Remyelination efficiency is decreased in models induced by toxic agents (Gilson and Blakemore, 1993, Shields *et al.*, 1999, Shen *et al.*, 2008), associated with decreased recruitment and differentiation of OPCs, in older animals (Sim *et al.*, 2002), while the susceptibility of axons to injury is increased in a targeted EAE model (Hampton *et al.*, 2012). In the current study, animals aged 8 to 12 weeks were followed for 2 weeks, whereas the mean age of death and disease duration of the SPMS cases used in Chapter 5 were 51.1 and 25.5 years respectively, suggesting that chronic cortical GM pathology may be achieved in older animals. However, we conclude that the injection of higher doses of TNF and IFN-γ is not sufficient to induce chronic subpial demyelination in the animals used.

The acute nature of the pathology observed in this model represents a major limitation given the chronic nature of the human disease. A previous study using this model also failed to show neuronal loss (Gardner *et al.*, 2013), in contrast to the substantial neuronal loss in MS GMLs (Wegner *et al.*, 2006, Magliozzi *et al.*, 2010). This suggests that neuronal loss in MS GMLs occurs over many years due to chronic pathology. Chapter 4 aims to evaluate a delivery system to achieve a chronic inflammatory milieu in the CSF/meningeal compartment using this model. It is not known whether this will result in chronic subpial demyelination.

3.4.5 Conclusions

We have shown that the injection of TNF and IFN-γ into the SAS of the sagittal sulcus of female DA rats immunised with a subclinical dose of rmMOG induced acute subpial demyelination. The microglial activation in these areas and immune cell infiltration in the

meninges are similar to that in subpial GMLs, confirming the value of this model of subpial demyelination driven by meningeal inflammation, and supports the hypothesis that an inflammatory milieu in the CSF/meningeal compartment results in subpial demyelination. We have also shown that increasing the doses of TNF and IFN-γ does not increase the duration of pathology, hence an alternative strategy to achieve their chronic presence in the CSF/meningeal compartment will be required to further develop this model.

Chapter 4

Evaluation of LV vectors in the DA rat

4.1 Introduction

4.1.1 Chronic pathology in MS

4.1.1.1 Chronic demyelination

Remyelination in early WMLs in MS can be extensive, with 80.7% showing remyelination (Goldschmidt *et al.*, 2009) by newly formed myelin sheaths surrounding preserved axons, and is correlated with the density of oligodendrocytes (Lucchinetti *et al.*, 1999). Remyelination in chronic WMLs can also be extensive (Patrikios *et al.*, 2006, Patani *et al.*, 2007), although its extent is more variable, with 13.2% being completely remyelinated and 60.4% showing no remyelination (Goldschmidt *et al.*, 2009). Remyelination in cortical GMLs is more extensive than that in chronic WMLs, with 18% showing extensive remyelination and 54% showing remyelination at the edges of the lesions (Albert *et al.*, 2007), including in subpial cortical GMLs (Chang *et al.*, 2012). Despite this cortical GM remyelination, it is now widely accepted that there is a role for accumulating cortical GM pathology in clinical progression (Kutzelnigg *et al.*, 2005, Calabrese *et al.*, 2010a), with GML area correlated with age at death (Gilmore *et al.*, 2009). These studies indicate that remyelination fails at a certain stage, suggested to be due to a decrease in the number of OPCs and their differentiation (Kuhlmann *et al.*, 2008). The densities of OPCs and oligodendrocytes are unchanged in demyelinated cortex in biopsy samples from early MS cases, whereas they are decreased in demyelinated cortex in autopsy samples from progressive MS cases (Rodriguez *et al.*, 2014).

4.1.1.2 Chronic cortical GM pathology in SPMS

Cortical GM demyelination is characteristic of PPMS and SPMS (Kutzelnigg *et al.*, 2005) and can affect 28.8% of the GM (Gilmore *et al.*, 2009), with subpial GMLs, which may involve multiple gyri, accounting for up to 50-70% of all GMLs (Peterson *et al.*, 2001, Bø *et al.*, 2003a, Magliozzi *et al.*, 2007). This extensive subpial demyelination and the associated

inflammatory infiltrates in the meninges, which resemble tertiary lymphoid organs in a significant proportion of SPMS cases (defined as F+ SPMS; 41.4%, 54% and 40% in Magliozzi *et al.*, 2007, Magliozzi *et al.*, 2010 and Howell *et al.*, 2011 respectively), suggests that subpial cortical GM pathology is chronic rather than acute. The associated neuronal loss in outer cortical GM layers (Wegner *et al.*, 2006, Magliozzi *et al.*, 2010) also suggests that it occurs over many years due to chronic pathology, consistent with the accumulation of chronic cognitive, motor and sensory symptoms. Neuronal loss of approximately 50% has been shown in cortical GMLs, associated with the presence of apoptotic neurons, most of which are pyramidal neurons in cortical GM layers III and V (Magliozzi *et al.*, 2010). Synapse loss has also been demonstrated (Wegner *et al.*, 2006, Dutta *et al.*, 2011). Additionally, neuronal loss of approximately 30% has been shown in hippocampal GMLs. These sites of neuronal loss are consistent with the cognitive and motor symptoms seen in MS, with the pathology in hippocampal GM suggested to contribute to memory impairment (Papadopoulos *et al.*, 2009).

4.1.2 Lack of chronic demyelination in targeted EAE models of MS

As described in 1.3.4, targeted EAE models have been developed that allow pathology to be targeted to specific anatomical locations within the rodent CNS. These models involve the immunisation of animals with a subclinical dose of recombinant MOG to prime the immune system followed by the injection of pro-inflammatory cytokines at the desired location to attract the primed auto-reactive T cells and antibodies and induce demyelination (Kerschensteiner *et al.*, 2004, Merkler *et al.*, 2006, Sasaki *et al.*, 2010). However, the value of these models is limited by the lack of chronic cortical GM pathology due to the acute nature of the cytokine delivery and resulting acute cytotoxic/inflammatory episode. Leukocortical, intracortical and subpial demyelination is maximal at 3 days after injection of TNF and IFN-γ into the motor cortex, with remyelination complete at 14 days after injection (Merkler *et al.*, 2006). Similarly, subpial demyelination is maximal at 7 days after injection of these cytokines into the SAS of the sagittal sulcus, with remyelination again complete at 14

days after injection (Gardner *et al.*, 2013). This study also failed to show neuronal loss in the outer cortical layers.

In Chapter 3, we reproduced this acute model, developed to test the hypothesis that TNF and IFN-γ produced in the meninges can diffuse into the underlying cortical GM and result in subpial demyelination, using the same as well as two- and four-fold higher doses of these cytokines to determine the effect of the dose on the duration as well as the extent of pathology. However, as described in 3.4.4, the total area of subpial demyelination and the microglial activation in these areas were significantly greater at 1 week after injection than at 2 weeks after injection in animals injected with the higher doses of TNF and IFN-γ. This also appeared to be the case for the number of CD4+ and CD8+ T cells and B cells in the meninges, indicating that, consistent with previous targeted EAE models, the pathology induced is acute rather than chronic even after injection of a four-fold higher dose of TNF and IFN-γ. Hence the pathogenesis in this acute model may not be the same as that in chronic MS. It is currently not known whether a chronic inflammatory milieu in the CSF/meningeal compartment in the rodent will result in chronic subpial demyelination.

A recent study attempted to induce chronic demyelination using the targeted EAE model developed by Merkler *et al.*, 2006, and investigated the hypothesis that repeated demyelination leads to the failure of remyelination (Rodriguez *et al.*, 2014). Up to 4 consecutive subpial cortical GMLs were induced at 21 day intervals at the same location, with extensive subpial demyelination being observed at 3 days, with almost complete remyelination at 21 days, after the first, second and fourth injections. This was associated with a decreased density of oligodendrocytes, which subsequently increased to those observed in control animals at 21 days after injection. The density of OPCs was unchanged at 3 days after the first injection but was increased at 21 days, whereas it was already increased at 3 days and was unchanged at 21 days after the second and fourth injections. These findings indicate that the differentiation of OPCs to mature oligodendrocytes was not

impaired, in contrast to their findings in MS. The infiltration of macrophages/microglia in this model was also transient, indicating that cortical remyelination is not impaired even after repeated inflammatory demyelination at the same location (Rodriguez *et al.*, 2014). Efficient remyelination, without depletion of OPCs, has similarly been observed after 3 episodes of brainstem WM demyelination in a rat ethidium bromide model (Penderis *et al.*, 2003). The authors suggest that 4 episodes of demyelination may not be sufficient for remyelination to fail in the rodent CNS, in which remyelination is known to be a robust process (Münzel and Williams, 2013), and that repeated cortical demyelination may not lead to the failure of remyelination in MS.

Given that neither the injection of higher doses of TNF and IFN-γ in the current study nor the repeated injection of these cytokines in a previous study (Rodriguez *et al.*, 2014) resulted in chronic subpial demyelination in targeted EAE models, we aimed to develop a system that would enable their chronic delivery using lentiviral vectors.

4.1.3 Lentiviral vectors

4.1.3.1 Introducing lentiviral vectors

Lentiviral (LV) vectors are currently the most widely used for the delivery of genes of interest due to their greater efficacy as well as safety compared to both other viral vectors and non-viral vectors (Seidlits *et al.*, 2013). LV vectors result in long-term stable integration of the gene of interest into the chromosomes of non-dividing as well as dividing cells. The LV consists of a homodimer of 7-12 kb single stranded RNA molecules packaged in lipid (Cockrell and Kafri, 2007) containing 9 open reading frames that encode at least 15 proteins (Tiscornia *et al.*, 2006), including core proteins (*gag* gene), replication enzymes (*pol* gene) and surface glycoprotein gp160 (*env* gene) as well as regulatory and accessory proteins. Receptor-mediated entry to host cells is facilitated by the surface subunit of gp160 (gp120) binding to human CD4, which induces a conformational change of the transmembrane

subunit of gp160 (gp41), facilitating LV and host cell membrane fusion. Following capsid protein uncoating, the LV reverse transcriptase and integrase enzymes mediate integration of the LV genome into the chromatin of the host cells (Cockrell and Kafri, 2007, Sakuma *et al.*, 2012). The LV tropism may be altered by replacing gp160 with, for example, the glycoprotein of the vesicular stomatitis virus (VSV-G). This, as well as being more stable than gp160, allowing concentration by ultracentrifugation of the pseudotyped LV, also interacts with the ubiquitous membrane component phosphatidylserine, mediating entry to various tissue and cell types of various species *in vitro* and *in vivo* (Akkina *et al.*, 1996). Studies have shown that LV proteins do not induce adaptive or innate immune responses (Abordo-Adesida *et al.*, 2005).

Replication-deficient LV vectors are produced by removing all dispensable genes from the human immunodeficiency virus type 1 (HIV-1) genome and separating the *cis*- and *trans*-acting elements. Third generation LV vectors consist of four plasmids, with one containing the transgene and the remaining three containing the *trans*-acting elements required for packaging, namely Gag-Pol, Rev (regulatory protein) and VSV-G. These four plasmids are transfected into 293T human embryonic kidney (HEK) cells and LV accumulates in the supernatant, from which a high titre LV preparation may be obtained by ultracentrifugation (Figure 4.1.1; Tiscornia *et al.*, 2006, Kutner *et al.*, 2009).

4.1.3.2 LV vectors in the CNS

To date, there are no reports of LV vector injection into the SAS, although spinal intrathecal injection of LV vector in neonatal mice has been shown to result in transduction of pial and leptomeningeal cells 4 weeks after injection (Fedorova *et al.*, 2006). Additionally, the spinal intrathecal injection of naked DNA in rats resulted in the detection of transgene products in the CSF 4 months after injection (Hughes *et al.*, 2009). A similar if not increased transduction efficiency when using an LV vector rather than naked DNA would be expected. The intracerebroventricular injection of choroid plexus-specific LV vector in mice, for

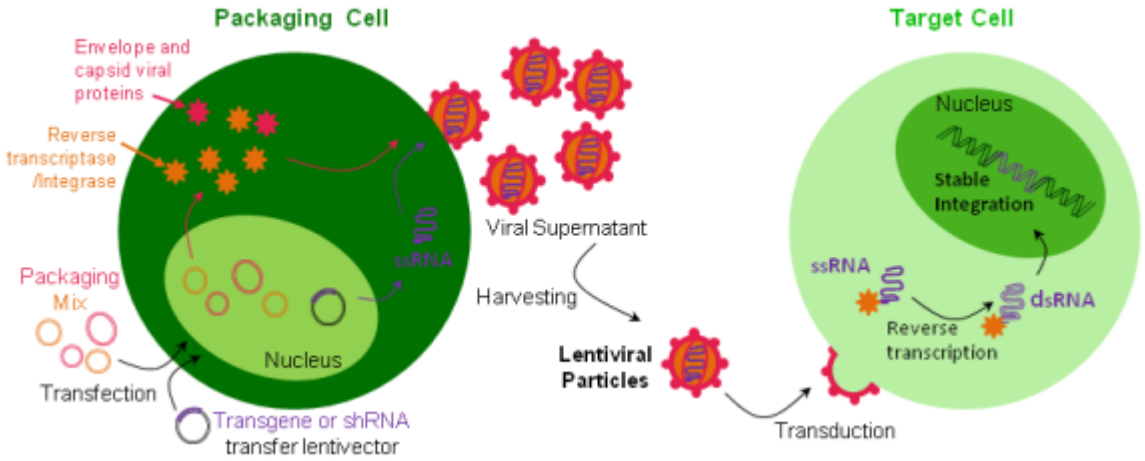

Figure 4.1.1. Production of LV vectors and stable transgene integration into host cell chromatin. Transfection of 293T HEK packaging cells with transfer vector containing the transgene and packaging plasmids containing core protein, replication enzyme and VSV-G genes results in production of LV vectors and their release into the supernatant, from which it is harvested. Following receptor-mediated entry to target cells, the single stranded RNA is reverse transcribed and the resulting double stranded DNA is stably integrated into host cell chromatin (Amsbio, 2013).

example, also resulted in transduction 4 months after injection (Regev *et al.*, 2010). A study in which LV vector was injected into the neural scar formed following a T8 lesion of the dorsal column in rats showed that astrocytes, neurons, microglia, OPCs and macrophages are transduced, as well as meningeal cells *in vitro* (Hendriks *et al.*, 2007).

One study used an adenoviral vector rather than an LV vector, which does not result in integration of the gene of interest into the chromatin of the host cells, to achieve the chronic expression of high levels of TNF in the substantia nigra of mice in which nigrostriatal neurodegeneration had been induced by the injection of 6-hydroxydopamine into the striatum. This resulted in gliosis and inflammatory infiltrates composed of monocytes/macrophages as well as neuronal loss at up to 100 days after injection, although the chronic expression of low levels of TNF resulted in decreased neurodegeneration (Chertoff *et al.*, 2011).

4.1.3.3 Hydrogels

LV vectors may be delivered from hydrogels, which allow localised and sustained expression of transgenes at or near the injection site. They are formed by the cross-linking of hydrophilic

polymers, which may be natural, such as collagen or fibrin, or synthetic, such as polyethylene glycol. LV vectors are released from hydrogels by diffusion, the rate of which depends on the porosity, hydrophilicity or hydrophobicity and kinetics and mechanism of degradation of the hydrogels and the interaction between the hydrogel polymer and LV vector. Subject to the application, LV vectors are either retained in hydrogels to allow transduction of infiltrating cells, or released, over days to weeks, to allow increasing transduction of nearby cells with time (Seidlits *et al.*, 2013). The injection of LV vectors has been shown to rapidly but transiently induce an innate immune response, characterised by IL6, IFN-α and IFN-β, resulting in decreased transduction (Brown *et al.*, 2007, Vandendriessche *et al.*, 2007), as well as an adaptive immune response. It has been suggested that LV vector delivery from hydrogels shields them from the immune system (Mok *et al.*, 2007).

Fibrin hydrogels have been used to achieve the sustained release of incorporated adenoviral vector containing the β-galactosidase gene *in vitro* (Breen *et al.*, 2006) and hyaluronan/methyl cellulose hydrogels for the local release of incorporated erythropoietin to induce endogenous neural stem and progenitor cells *in vivo* in the subventricular zone in a mouse model of stroke (Wang *et al.*, 2012). Collagen hydrogels, which will be investigated in the current study, have been used to deliver LV vector immobilised to hydroxyapatite nanoparticles, which have been shown to increase the activity of LV vectors. Following s.c. implantation, the activity of the LV vector was better maintained with than without the hydrogel, with localised and sustained expression of luciferase for at least 4 weeks after implantation (Shin and Shea, 2010).

4.1.4 Aims

We aimed to evaluate LV vectors as a delivery system to achieve the chronic presence of TNF and IFN-γ in the SAS of the DA rat that would enable the further development of the acute model of cortical pathology driven by meningeal inflammation (Gardner *et al.*, 2013).

These studies involved the injection of a high titre LV vector, pseudotyped with VSV-G and containing the gene for enhanced green fluorescent protein (eGFP) under the transcriptional control of the cytomegalovirus (CMV) promoter, into the SAS of the sagittal sulcus.

To fulfil this aim, the following were performed:

- Evaluation of the transduction efficiency using the eGFP fluorescence and determination of the time course and the anterior to posterior distribution of eGFP expression, as well as the identification of the cell types in which eGFP is expressed, 1, 4 and 12 weeks after injection into naïve rats.
- Repeat in animals immunised with a subclinical dose of rmMOG, which was identified in Chapter 2, to determine whether the LV vector results in non-specific demyelination and inflammation in this model at 1 week after injection.
- Repeat 1, 2 and 4 weeks after injection of the LV vector together with a collagen hydrogel, to achieve localised and sustained transduction.

4.2 Methods

4.2.1 Induction of subclinical EAE

4.2.1.1 Animals

Female DA rats (Charles River, Germany) aged 8 to 12 weeks and weighing approximately 160g were housed as described in 2.2.2.1. Animal work was carried out in compliance with Home Office regulations (project licence 70/7213).

4.2.1.2 Immunisation

Animals received an intradermal injection into the dorsal aspect of the base of the tail of 5µg of rmMOG (the batch expressed and purified in the current study, batch pXVII) diluted in PBS emulsified in an equal volume of IFA as described in 2.2.2.2. This dose of rmMOG batch pXVII was identified as a suitable subclinical dose in Chapter 2. Control animals received an injection of PBS emulsified in an equal volume of IFA. The total injection volume was 100µl.

4.2.1.3 Clinical scoring

Following immunisation, animals were weighed and scored daily as described in 2.2.2.3. Animals were removed from the experiment if they reached the humane endpoints of a loss of 25% of their body mass (from the day prior to the development of deficit) for 48 hours or complete weakness of both hind limbs for more than 48 hours without weight gain, in compliance with Home Office regulations. These animals received an i.p. injection of an overdose of 200mg/ml Euthatal.

4.2.2 Injection of LV vector

The immunisation of animals was followed 19-22 dpi by the injection of LV vector into the SAS of the sagittal sulcus. The coordinates from Bregma were obtained from a rat brain

atlas (Paxinos and Watson, 1998) and were 0.9mm caudal to Bregma to target the motor cortex, at midline and to a depth of 2.3mm from the dura mater as shown in Figure 3.2.1 A.

Production of the LV vector was carried out by Dr Stuart M. Ellison and Professor Nicholas D. Mazarakis (Gene Therapy, Division of Brain Sciences, Imperial College London). Briefly, 293T HEK cells (ATCC CRL-11268) were grown in Dulbecco's modified Eagle's medium supplemented with penicillin/streptomycin, 4mM L-glutamine and 10% (v/v) fetal calf serum (all Sigma-Aldrich). HIV-1-based LV vectors were produced using a modified transient calcium phosphate transfection protocol (Ellison *et al.*, 2013). Twelve 150mm tissue culture dishes were seeded with 1.2 x 10^7 293T HEK cells per dish and incubated overnight (37°C, 5% CO_2). Cells were transfected with 45µg of transfer vector plasmid expressing eGFP (pRRLsincppt-CMV-eGFP-WPRE), 45µg of plasmid expressing HIV-1 Gag-Pol (pRSV-Rev), 9µg of plasmid expressing HIV-1 Rev (pMD2-LgpRRE) and 15.3µg of the VSV-G envelope plasmid (all Addgene, Cambridge, Massachusetts, USA). Sixteen hours post transfection, media was replaced with fresh media supplemented with 10mM sodium butyrate (Sigma-Aldrich). Thirty-six hours post induction, media containing LV vector was harvested and filtered through a 45µm filter. LV vector was purified and concentrated by ultracentrifugation overnight at 6000*g* (F500 rotor, Beckman Coulter, High Wycombe, Buckinghamshire, UK). The pellet was resuspended in PBS, repelleted by ultracentrifugation for 90 minutes at 68,500*g* (SW-32 Ti rotor) and resuspended over several hours in TSSM dilution buffer (20mM Tromethamine, 100mM sodium chloride, 10mg/ml sucrose and 10mg/ml mannitol; all Sigma-Aldrich). LV vector preparations were stored at -80°C.

Functional titres were determined by flow cytometry as described previously (Ellison *et al.*, 2013). Briefly, 12-well tissue culture plates were seeded with 5 x 10^5 293T HEK cells per well. At 16-24 hours post seeding, cells in a single well were quantified using a haemocytometer. Cells in the remaining wells were transduced with a serial dilution of the LV vector with 8mM polybrene (Sigma-Aldrich) for 6 hours. Seventy-two hours post

transduction, the percentage of eGFP+ cells was determined by flow cytometry and the titre calculated (number of cells on day of transduction x fraction of eGFP+ cells x dilution factor).

4.2.2.1 Stereotactic injection

Animals received a 1µl injection as described in 3.2.2.2. Recovery from surgery was without incident and overt clinical signs in all cases. The experiment was terminated at 1, 2, 4 or 12 weeks after injection as detailed below.

4.2.2.2 Injection of LV vector in naïve animals

Naïve animals received an injection of the LV vector preparation VSVg.cmv_eGFP. This vector was pseudotyped with VSV-G and carried the eGFP gene driven by the CMV promoter. Its titre was 9.75 x 10^9 transducing units (TU) /ml, resulting in 9.75 x 10^6 TU in the 1µl injection volume. The pH7.3 dilution buffer TSSM was used as the vehicle control. The time points investigated are shown in Table 4.2.1.

4.2.2.3 Injection of LV vector in rmMOG-immunised animals

In order to determine whether the injection of LV vector results in non-specific demyelination and inflammation in this model, that is, not induced by the injection of pro-inflammatory cytokines, the immunisation of animals with 5µg of rmMOG batch pXVII as described in 4.2.1.2 was followed 22 dpi by the injection of VSVg.cmv_eGFP. This LV vector preparation had a titre of 2.63 x 10^{10} TU/ml, resulting in 2.63 x 10^7 TU in the 1µl injection volume. Control animals had been immunised with PBS emulsified in an equal volume of IFA as shown in Table 4.2.2. Monastral blue was added at 1:1000 as a tracer.

4.2.2.4 Injection of LV vector and collagen hydrogel

This collagen hydrogel experiment was performed in collaboration with Dr Ben Newland and Professor Abhay Pandit (Network of Excellence for Functional Biomaterials, National University of Ireland, Galway, Ireland). Naïve animals received an injection of LV vector with

a collagen hydrogel in order to identify whether the inclusion of the collagen hydrogel resulted in changes in the distribution and time course of eGFP expression.

Collagen hydrogel was prepared *in situ* prior to each surgery as previously described (Hoban *et al.*, 2013). All components were kept on ice throughout to prevent premature gelation. Briefly, 50µl of bovine collagen type I prepared from Achilles tendon (3mg/ml; Ben Newland) was neutralised with sodium hydroxide (1M; Sigma-Aldrich) and added to 5µl of PBS (10x). The cross-linker consisted of 0.4mg of poly(ethylene glycol) ether tetrasuccinimidyl glutarate (4S-StarPEG) dissolved in 5µl of PBS (10x) and was added to the collagen solution. For the injection solution, 2.4µl of collagen hydrogel solution was carefully mixed with 1.6µl of VSVg.cmv_eGFP (approximately 1:1 volume:volume ratio). The glass capillary used for injection in this experiment had an internal diameter of approximately 100µm at its tip rather than approximately 30µm due to the high viscosity of the collagen hydrogel. This LV vector preparation had a titre of 5.18×10^{10} TU/ml, resulting in 2.07×10^{7} TU in the 1µl injection volume. Control animals received an injection of VSVg.cmv_eGFP diluted 2:5 in PBS (10x). The time points investigated are shown in Table 4.2.3.

Prior to using the collagen hydrogel *in vivo*, the relative concentrations of collagen and 4S-StarPEG had been optimised to result in gelation at 37°C in approximately 15 minutes, which would be the approximate length of time required until retraction of the needle following injection. The expected *in vivo* gelation time was determined by placing 4µl of the collagen hydrogel onto the hydrophobic surface polytetrafluoroethylene (Teflon tape; DuPont, Wilmington, Delaware, USA) and incubating at 37°C until gelation had occurred. Monastral blue was not used in this experiment as its 8 tertiary amine groups (compared to the 4 of 4S-StarPEG) were found to cause cross-linking of the collagen resulting in instant gelation.

Immunisation	Injection	Time point / weeks	Number of animals
Naïve	TSSM	1	4
Naïve	VSVg.cmv_eGFP	1	4
Naïve	VSVg.cmv_eGFP	4	4
Naïve	VSVg.cmv_eGFP	12	4

Table 4.2.1. Groups for VSVg.cmv_eGFP time course study.

Immunisation	Injection	Time point / weeks	Number of animals
PBS in IFA	VSVg.cmv_eGFP	1	4
5µg rmMOG in IFA	VSVg.cmv_eGFP	1	4

Table 4.2.2. Groups for rmMOG and VSVg.cmv_eGFP study.

Immunisation	VSVg.cmv_eGFP with collagen hydrogel or PBS	Time point / weeks	Number of animals
Naïve	PBS	1	4
Naïve	collagen hydrogel	1	4
Naïve	PBS	2	4
Naïve	collagen hydrogel	2	4
Naïve	PBS	4	4
Naïve	collagen hydrogel	4	4

Table 4.2.3. Groups for VSVg.cmv_eGFP and collagen hydrogel study.

4.2.3 Determination of the effects of injection in the brain

4.2.3.1 Tissue harvesting and treatment

Animals received an i.p. injection of an overdose of 200mg/ml Euthatal at the termination of the experiment and were perfused as described in 2.2.3.1. The brain was harvested and post-fixed in 4% PFA for 4 hours at 4°C followed by cryoprotection in 30% (w/v) sucrose in PBS for 48 hours or until equilibrium was reached at 4°C.

Tissue was briefly rinsed in PBS, placed in a mould filled with optimal cutting temperature compound and frozen in isopentane on dry ice. 10µm sections in the coronal plane were cut

using a cryostat and stored at -20°C. Monastral blue was used to identify the injection site, where applicable.

4.2.3.2 Immunofluorescence

The antigens shown in Table 4.2.4 were detected using the same IF protocol as that for MOG and Iba1 described in 2.2.3.2 but omitting methanol retrieval for antigens other than MOG. For CD79a, this was replaced with heat mediated pH6 citrate buffer retrieval using a vegetable steamer. Some antigens required a biotinylated secondary antibody prior to a fluorophore-conjugated secondary antibody as indicated in the Table and as was described for MOG in 2.2.3.2.

Antigen	Cell specificity	Species	Dilution	Source
CD3[1]	T cell	Mouse	1 in 500	BD Pharmingen
CD79a[1]	B cell	Mouse	1 in 500	Pierce Antibodies
Collagen 1[1]	Meninges	Rabbit	1 in 500	Abcam, Cambridge, Cambridgeshire, UK
ED1	Phagocytic macrophages/ microglia	Mouse	1 in 50	Reynolds' group
GFAP[1]	Astrocytes	Rabbit	1 in 1000	Dako
Iba1	Activated macrophages/ microglia	Rabbit	1 in 1000	Wako
Laminin	Meninges	Rabbit	1 in 5000	Sigma-Aldrich
MOG[1]	Myelin and oligodendrocytes	Mouse	1 in 20	Reynolds' group

Table 4.2.4. Primary antibodies used for IF. [1]Antigens requiring a biotinylated secondary antibody.

4.2.3.3 Imaging and analysis

Sections were imaged using a Nikon Eclipse 80i microscope with a QImaging QICAM digital camera and Image-Pro Plus software. This software was able to tile multiple high magnification images to yield high resolution images of complete sections.

ImageJ was used to quantify areas of eGFP fluorescence (Figure 4.2.1) and Iba1 IR. Briefly, all eGFP and Iba1 images for a single study were taken at the same exposure as far as was possible. The same threshold was then applied to these images in ImageJ to select the eGFP fluorescence or Iba1 IR. The area of eGFP fluorescence was normalised to the area of the section whereas the area of Iba1 IR was normalised to the area analysed, which extended from the corpus callosum to the superior surface of the cortex and from 1mm to the left of the sagittal sulcus to 1mm to the right of it. Quantification was performed on 3 consecutive sections per animal and a mean calculated.

4.2.4 Statistical analysis

All data are presented as the mean ± the SEM. GraphPad Prism 5 was used to construct graphs and perform statistical analysis. Two and three groups were compared using Mann-Whitney *U* test and Kruskal-Wallis one-way ANOVA with Dunn's multiple comparisons post-hoc test respectively as stated. A p value of <0.05 was considered to be statistically significant.

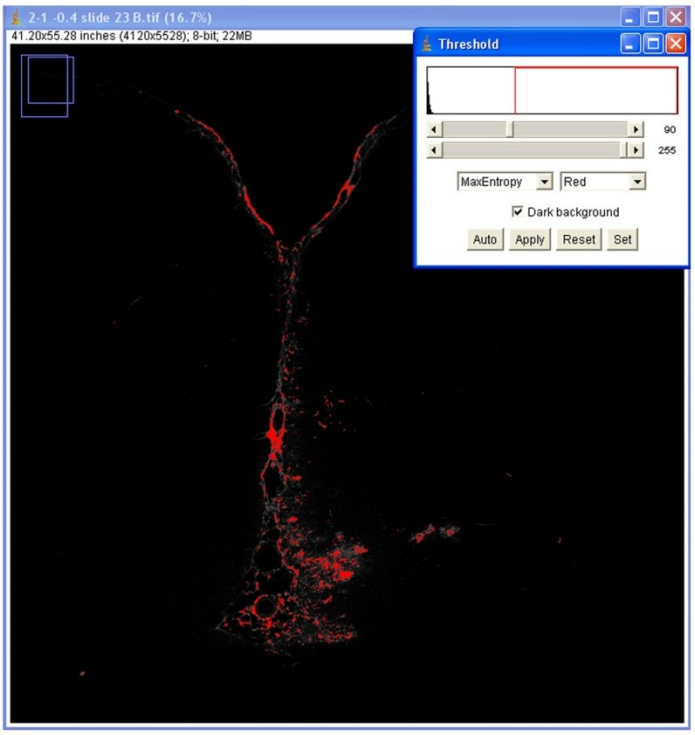

Figure 4.2.1. Quantification of area of eGFP fluorescence. The total area of eGFP fluorescence in each brain section was quantified using tiled images of sections taken using the 10x objective lens and ImageJ software. All images were taken at the same exposure as far as was possible. The same threshold was applied to select the eGFP fluorescence (red) and calculate its area, which was normalised to the area of the section.

4.3 Results

4.3.1 Injection of LV vector in naïve animals

4.3.1.1 eGFP expression was maintained for 12 weeks

Following the injection of VSVg.cmv_eGFP into the SAS of the sagittal sulcus of naïve female DA rats, sections were cut from approximately 2mm anterior, to approximately 2mm posterior, to the injection site and DAPI staining was performed on selected sections. eGFP expression was present in 3 of 4 animals at 1 (Figure 4.3.1) and 12 weeks after injection (Figure 4.3.2) and in 1 of 4 animals at 4 weeks after injection. No GFP primary antibody was required to detect eGFP expression. It was observed anterior (Figure 4.3.1 A, Figure 4.3.2 Ai) and posterior to the injection site (Figure 4.3.1 C, Figure 4.3.2 Aiii, Bi, Bii) in these animals and was present in the sagittal sulcus (Figure 4.3.1 Di, Diii) and walls of the meningeal blood vessels at the base of the sulcus (Div) as well as on the superior surface of the cortex (particularly evident in C) and in the remains of the inferior sagittal fissure (A). This is an example of an animal in which the injection was accurate. However, it appears that the injections were inaccurate in the animals shown in Figure 4.3.2. It is likely that the injection in the animal shown in A was too deep, resulting in extensive eGFP expression in the medial septal nucleus and nucleus of the horizontal/vertical limb of the diagonal band (Ai), dorsal fornix (Aii) and corpus callosum (Aii and Aiii), whereas it may not have been at midline in the animal shown in B, resulting in eGFP expression in the cingulate cortex (Bi). No eGFP expression was observed in animals 1 week after injection of the vehicle control, TSSM.

Areas of eGFP fluorescence were quantified as described in 4.2.3.3 and plotted against distance from the injection site (Figure 4.3.3 Ai), which was taken to be at the peak area of eGFP fluorescence. These curves showed that eGFP is expressed in a gradient around the injection site over approximately 4mm, with a peak area of eGFP fluorescence at the

injection site that decreased progressively with increasing distance from the injection site along the anteroposterior axis. The total eGFP fluorescence was determined by calculating the area under these curves (Aii). Although Kruskal-Wallis one-way ANOVA could not be performed as eGFP was only expressed in one animal at 4 weeks after injection, a Mann-Whitney *U* test showed that there was no significant difference in total eGFP fluorescence at 1 and 12 weeks after injection of VSVg.cmv_eGFP. Similarly, there was no significant difference in the length along the anteroposterior axis over which eGFP expression was observed at 1 and 12 weeks after injection (B).

In order to determine the cell types in which eGFP was expressed, confocal imaging and IF were performed on sections cut at the injection site (Figure 4.3.4). Confocal imaging showed that eGFP expression was present in cells with the morphology of astrocytes (Ai) and double IF showed that it was colocalised with glial fibrillary acidic protein (GFAP), an intermediate filament protein expressed by astrocytes (Aii). eGFP expression was present in astrocyte cell bodies as well as end-feet and processes. Several layers of astrocytic elements, together with the basal lamina, comprise the glia limitans (Lopes and Mair, 1974). In this animal, colocalisation of eGFP with laminin, a major protein of the basal lamina (Sixt *et al.*, 2001), was also observed (Biii). Additionally, eGFP expression was present outside the glia limitans in meningeal tissue (Bi) in cells with the morphology of the mesothelial cells and layers of flattened fibroblasts that comprise the pia mater (Bii, also evident in Figure 4.3.1). Double IF to show colocalisation with E-cadherin, a cell adhesion molecule expressed in mesothelial cells of the pia and arachnoid mater, was unsuccessful due to the non-specific IF observed using the E-cadherin antibody, consistent with previous findings (Lewis-Tuffin *et al.*, 2010). Confocal imaging showed that eGFP expression was present in a small number of cells with the morphology of pyramidal neurons (C). However, despite extensive attempts at optimisation, double IF to show colocalisation with GluR2/3, subunits of the AMPA glutamate receptor expressed in pyramidal cells in cortical layers II/III, V and VI (Kondo *et al.*, 1997), could not be achieved.

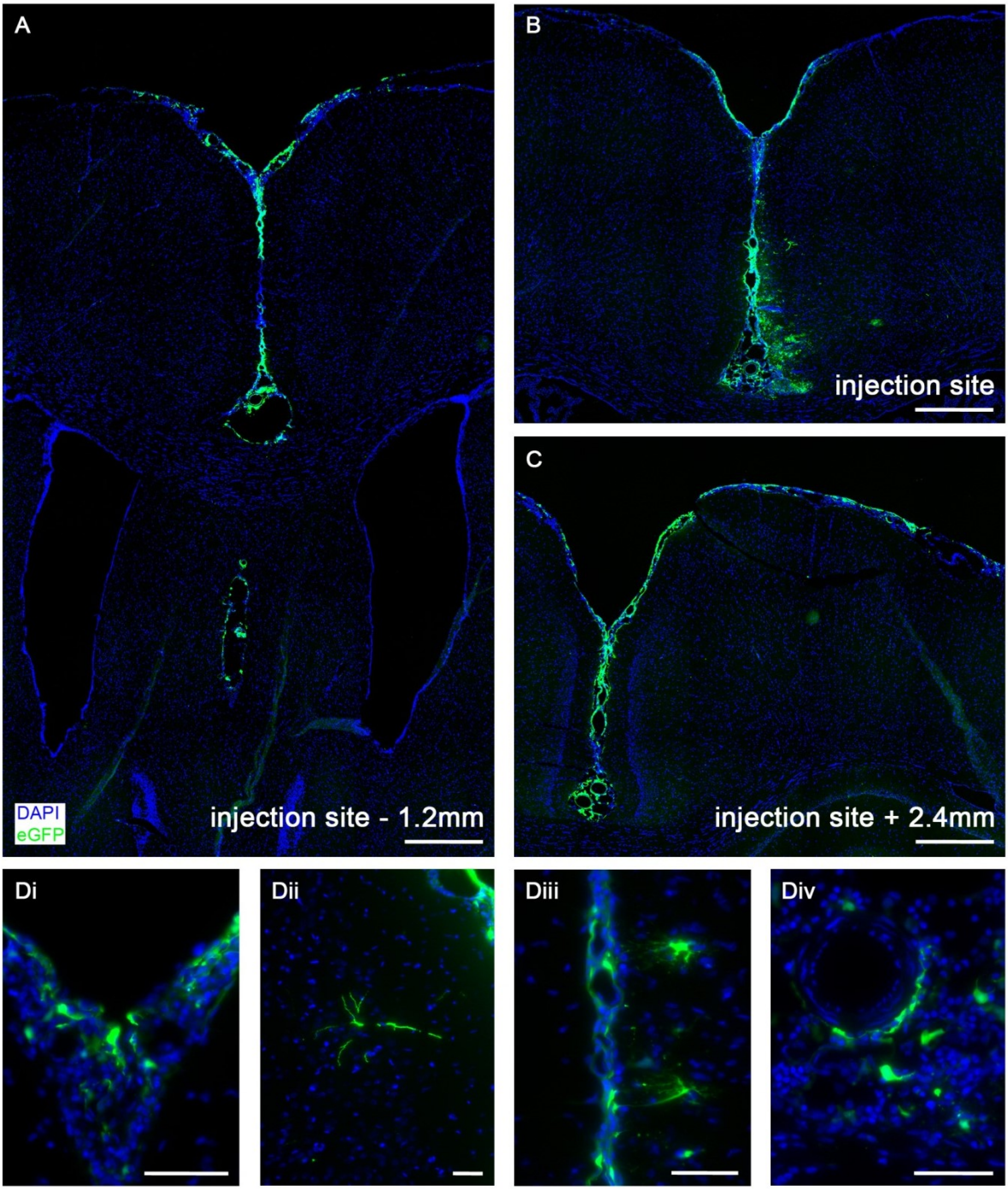

Figure 4.3.1. eGFP expression present 1 week after injection of VSVg.cmv_eGFP. DAPI staining was performed on injection site sections (B) and sections cut anterior (A) and posterior (C) to the injection site and showed eGFP expression in the sagittal sulcus and walls of meningeal blood vessels as well as on the superior surface of the cortex (particularly evident in C) and in the remains of the inferior sagittal fissure (A). The extent and pattern of eGFP expression appeared to be consistent in all three sections. The images shown are from one animal 1 week after injection of VSVg.cmv_eGFP. Images in Di-Div are magnifications of the top of the sagittal sulcus (Di), areas adjacent to the sagittal sulcus (Dii and Diii) and a meningeal blood vessel at the base of the sulcus (Div). Scale bar: A, B and C = 200µm, Di, Dii, Diii and Div = 50µm.

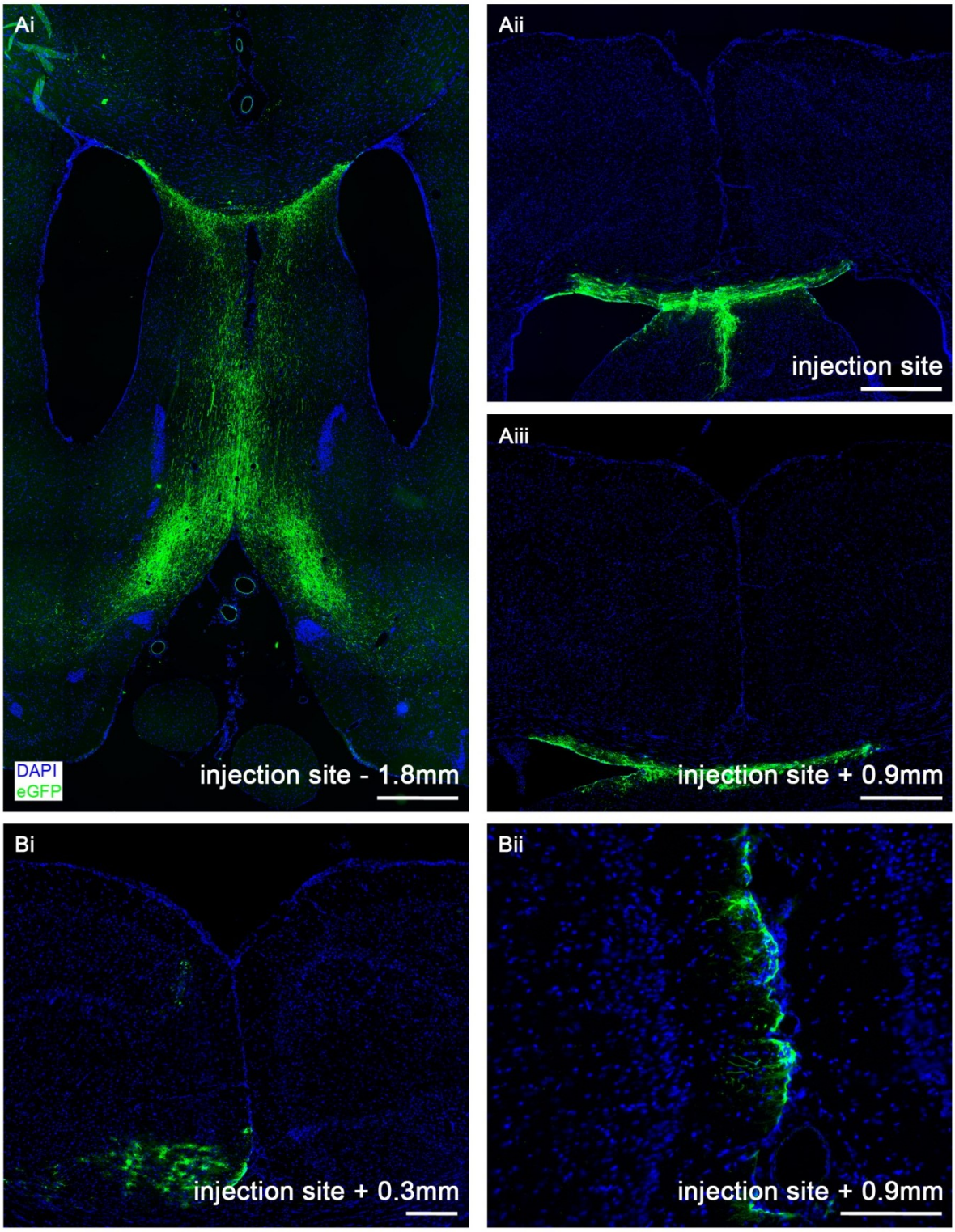

Figure 4.3.2. eGFP expression present 12 weeks after injection of VSVg.cmv_eGFP. DAPI staining was performed on injection site sections (Aii) and sections cut anterior (Ai) and posterior (Aiii, Bi and Bii) to the injection site and showed extensive eGFP expression in the medial septal nucleus, nucleus of the horizontal/vertical limb of the diagonal band (Ai), dorsal fornix (Aii), corpus callosum (Aii and Aiii) and cingulate cortex (Bi) as well as in the sagittal sulcus (Bii). The images shown are from two animals 12 weeks after injection of VSVg.cmv_eGFP. Scale bars = 200µm.

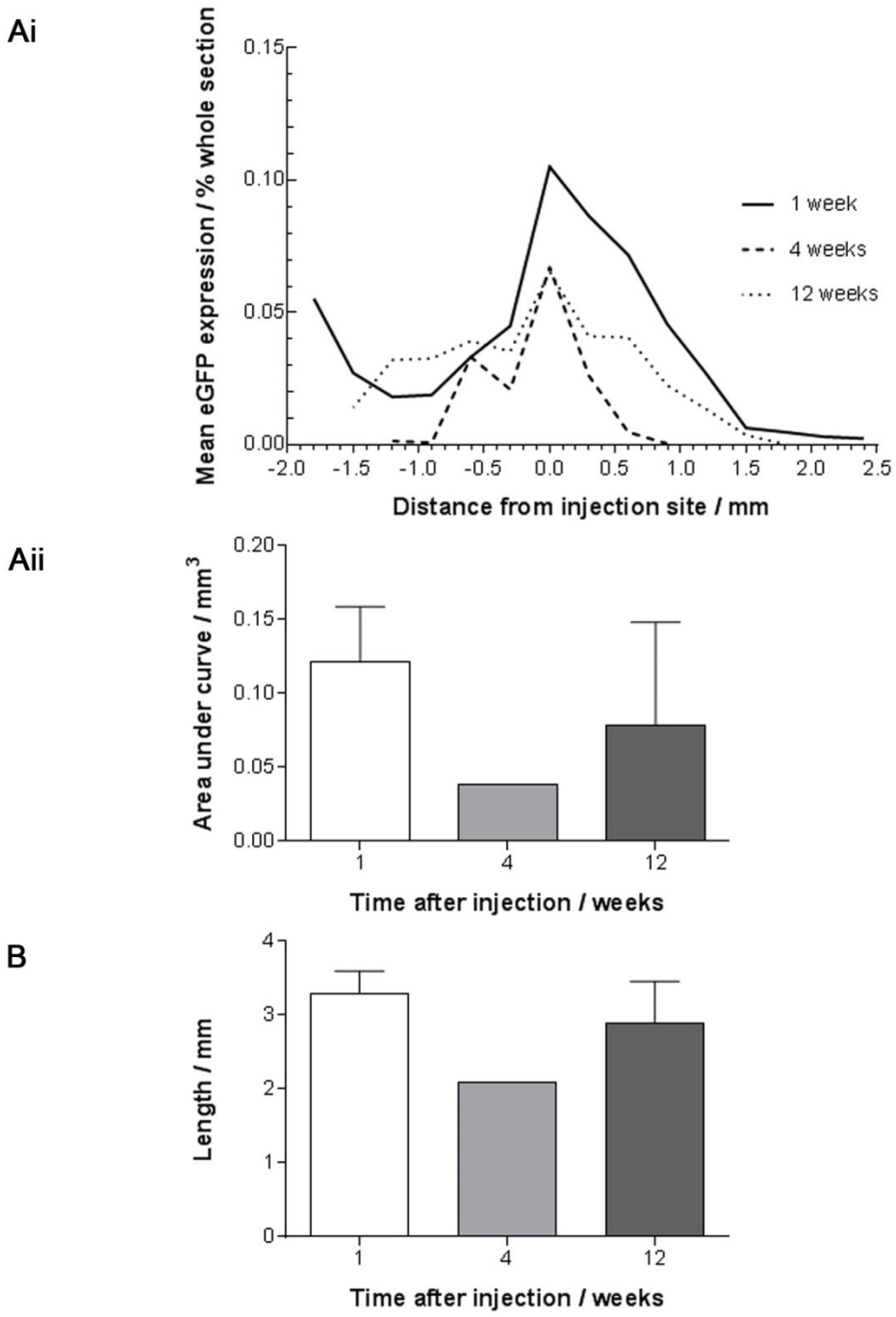

Figure 4.3.3. eGFP expression was maintained for 12 weeks after injection of VSVg.cmv_eGFP. eGFP was expressed in a gradient around the injection site from anterior to posterior (Ai). The total eGFP expression, determined by calculating the area under the curve of eGFP expression against distance from injection site, was the same at 1, 4 and 12 weeks after injection (Aii). The anterior to posterior spread of eGFP expression was also the same at 1, 4 and 12 weeks after injection (B; mean ± SEM; *n* = 3 for 1 and 12 weeks, 1 for 4 weeks).

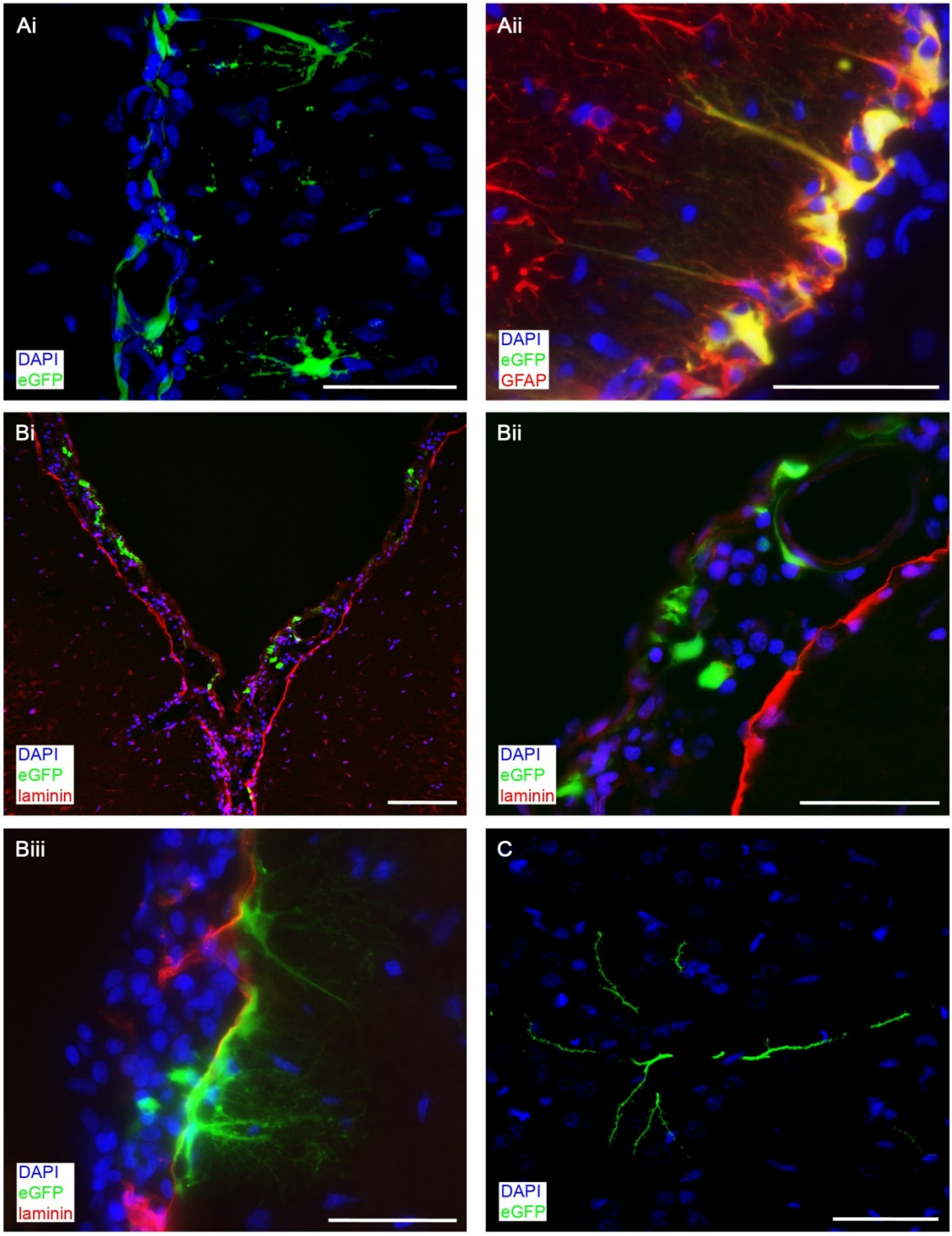

Figure 4.3.4. Localisation of eGFP expression. Confocal imaging and double IF were performed on injection site sections to determine the cellular localisation of eGFP expression after injection of VSVg.cmv_eGFP. Confocal imaging showed eGFP expression in cells with the morphology of astrocytes (Ai) and double IF showed that it colocalised with GFAP (Aii). Colocalisation with laminin varied. eGFP expression could be observed on the pial side of the glia limitans expressing laminin (Bi, Bii) as well as in the glia limitans (Biii). Confocal imaging showed eGFP expression in cells with the morphology of pyramidal neurons (C). Scale bar: Ai, Aii, Bii, Biii and C = 50μm, Bi = 100μm.

4.3.1.2 Microglial activation

In order to identify the presence of activated macrophages/microglia following injection of VSVg.cmv_eGFP, IF for Iba1 was performed on sections cut at the injection site. A high density of activated macrophages/microglia was present at 1 week after injection (Figure 4.3.5 Ai). Microglial activation was particularly evident adjacent to the sagittal sulcus towards the superior surface of the cortex and was not associated with the eGFP expression. Iba1+ cells generally had an amoeboid morphology characterised by a large cell soma but the retention of short, thick processes (Aii). No colocalisation of eGFP with Iba1 was observed. Activated macrophages/microglia were also present at 2 weeks after injection (B). It is likely that the injection in the animal shown was too deep, resulting in extensive eGFP expression in the corpus callosum. In this animal, microglial activation was particularly evident at the base of the sagittal sulcus. Microglial activation was less evident at 1 week after injection of TSSM (C).

Iba1 immunoreactivity was quantified as described in 4.2.3.3. Although there were trends for increased Iba1 immunoreactivity at 1 week after injection of VSVg.cmv_eGFP compared to TSSM control and decreased Iba1 immunoreactivity at 4 weeks compared to 1 week after injection of VSVg.cmv_eGFP, these were not statistically significant (D).

4.3.2 Injection of LV vector in rmMOG-immunised animals

The experiment described in 4.3.1 was repeated in rats immunised with the 5μg subclinical dose of rmMOG identified in Chapter 2, with immunisation followed 22 dpi by the injection of VSVg.cmv_eGFP with monastral blue into the SAS of the sagittal sulcus. The aim of this experiment was to determine whether the injection of VSVg.cmv_eGFP results in non-specific, that is, not caused by the injection of TNF and IFN-γ, demyelination and inflammation.

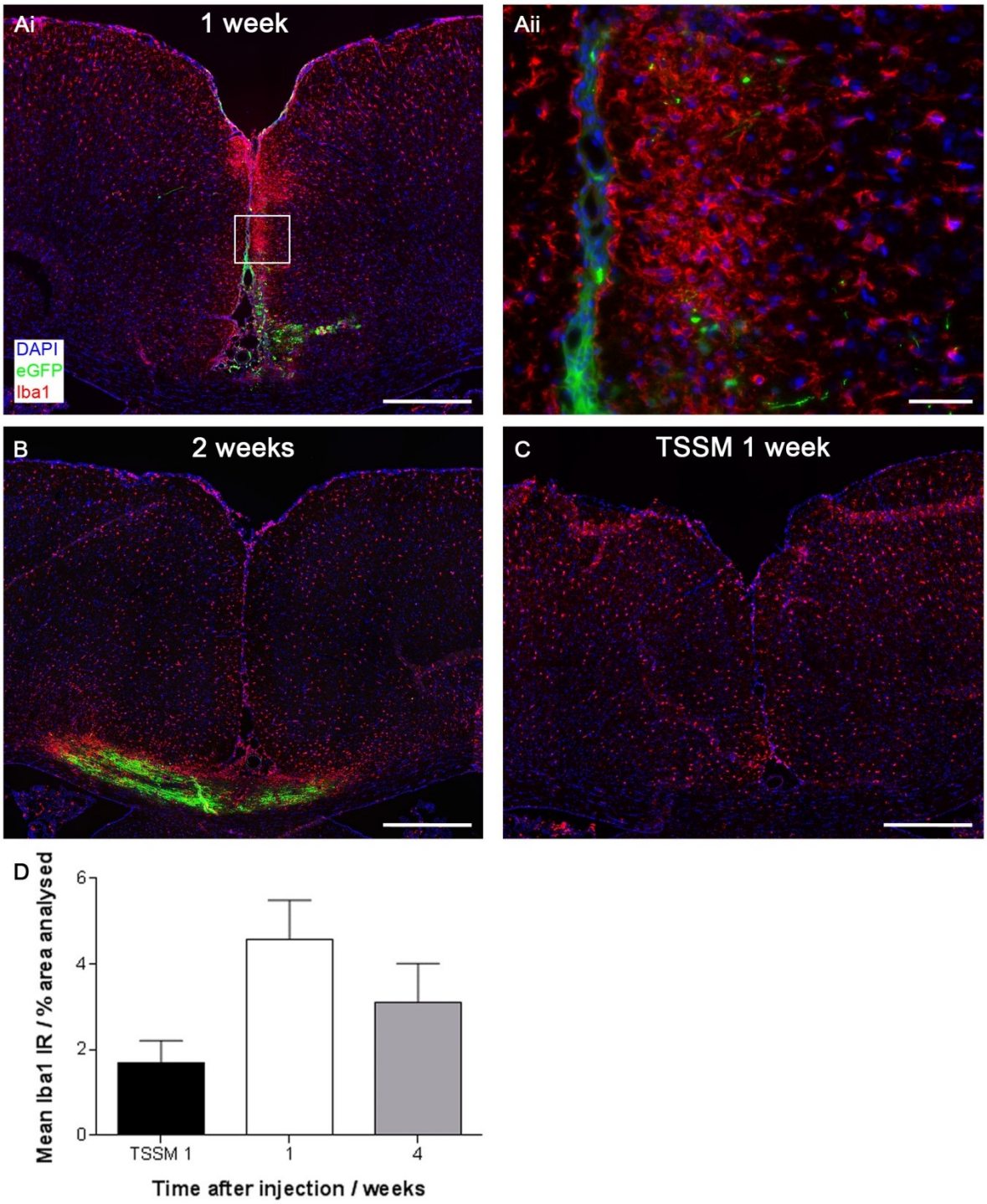

Figure 4.3.5. Microglial activation after injection of VSVg.cmv_eGFP. IF for Iba1 was performed on injection site sections and showed the presence of activated macrophages/microglia, particularly at 1 week after injection and adjacent to the sagittal sulcus (A; image in Aii is a magnification of the boxed area in Ai). Note that no colocalisation of eGFP and Iba1 was observed. Activated macrophages/microglia were also observed at 2 weeks after injection of VSVg.cmv_eGFP (B) but were less evident at 1 week after injection of TSSM (C). Scale bar: Ai, B and C = 500µm, Aii = 50µm. Iba1 immunoreactivity appeared to be increased at 1 week after injection of VSVg.cmv_eGFP compared to TSSM control, and appeared to be decreased at 4 weeks after injection compared to at 1 week after injection (E; Kruskal-Wallis with Dunn's multiple comparisons test; mean ± SEM; *n* = 5 per group).

4.3.2.1 eGFP expression was unchanged in rmMOG-immunised animals

Monastral blue, which was visible by eye during sectioning, enabled identification of the injection site as well as determination of the injection accuracy (Figure 4.3.6 A). eGFP expression in these sections cut at the injection site, on which DAPI staining had been performed, was again visualised (B). Monastral blue was observed in the sagittal sulcus and appeared to be localised in cells with monocyte/macrophage morphology. Although eGFP expression was again localised in cells with the morphology of astrocytes, particularly evident in their end-feet (Bii), rather than macrophages, a similar pattern in the sulcus was observed. This finding indicates that monastral blue was effective as a tracer, with no apparent interaction with VSVg.cmv_eGFP and no effect on its expression of eGFP.

In this experiment, eGFP expression was present in 4 of 4 IFA-immunised and 4 of 4 rmMOG-immunised animals. This indicates that the experimental modifications made following the experiment described in 4.3.1 were effective. These included measures to prevent both blocking of the glass capillary mounted on the Hamilton needle and warming of the LV vector preparation in surgery. Additionally, injections were described as accurate in all animals. This is likely to be due to new Hamilton syringes, with fixed rather than removable needles, being used. These needles were completely straight, in contrast to the removable needles for which this was not the case, and which additionally did not always screw onto the Hamilton needle completely parallel to it, introducing errors in the lateral injection coordinate.

The total eGFP fluorescence was again determined (Figure 4.3.7 A). A Mann-Whitney *U* test showed that there was no significant difference at 1 week after injection of VSVg.cmv_eGFP in animals immunised with IFA only and in those immunised with 5μg of rmMOG. Similarly, there was no significant difference in the length along the anteroposterior axis over which eGFP expression was observed in these two groups (B).

4.3.2.2 Absence of demyelination in rmMOG-immunised animals

In order to determine whether the injection of VSVg.cmv_eGFP in animals immunised with 5μg of rmMOG resulted in demyelination, IF for MOG was performed on sections cut at the injection site. Normal myelination was observed in animals immunised with IFA only (Figure 4.3.8 Bi), with uninterrupted MOG IF from the superior surface of the cortex to the base of the sulcus that extends from the pial surface into underlying cortical GM (Bii, Biii), similar to that observed in naïve control animals 1 week after injection of TSSM (A). Normal myelination was also observed in animals immunised with 5μg of rmMOG (Ci). However, one small area of potential demyelination was observed in 1 of 4 animals. This was characterised by a partial loss of MOG IF adjacent to the sagittal sulcus, in which eGFP expression was present (Cii, Ciii), and measured 0.0235mm^2. Also note the extensive eGFP expression present in perivascular spaces in the animal shown in Bi, which will be discussed in 4.4.1.2.

4.3.2.3 Microglial activation was unchanged in rmMOG-immunised animals

IF for Iba1 was again performed on sections cut at the injection site in order to identify the presence of activated macrophages/microglia. Iba1+ cells were present in both animals immunised with IFA only (Figure 4.3.9 Ai) and in those immunised with 5μg of rmMOG (Aii). Microglial activation was particularly evident adjacent to the sagittal sulcus and at its base (pictured) although it did not appear to be associated with the expression of eGFP and no colocalisation of eGFP with Iba1 was observed.

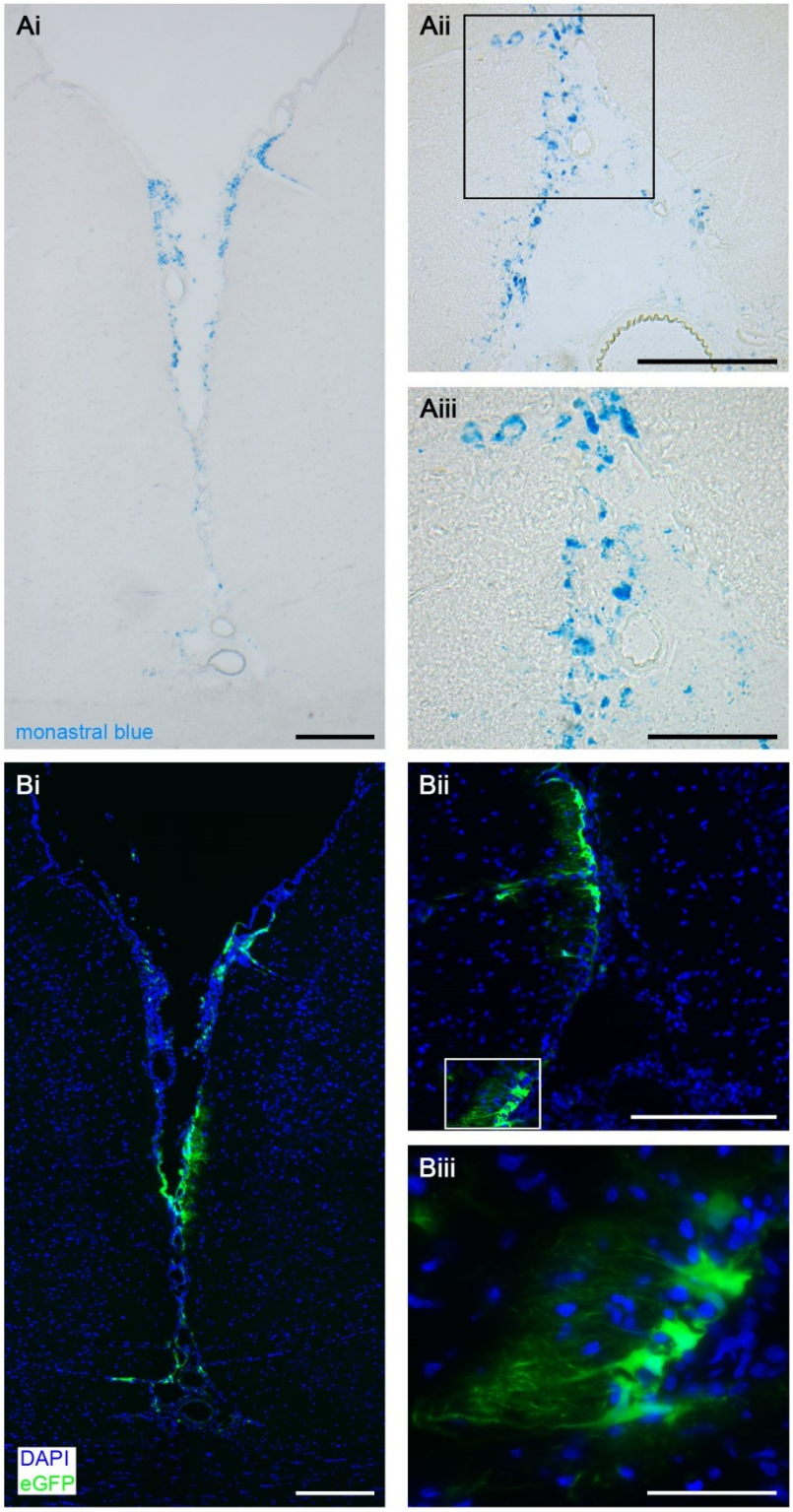

Figure 4.3.6. Monastral blue and eGFP expression after injection of VSVg.cmv_eGFP.
Bright-field (A) and fluorescence microscopy (B) were performed on DAPI-stained injection site sections. The pattern of monastral blue in the sagittal sulcus (A) was similar to that of eGFP expression (B). The images shown are from two animals (represented in images i and ii/iii) 1 week after injection of VSVg.cmv_eGFP. Images in Aiii and Biii are magnifications of the boxed areas in Aii and Bii. Scale bars: Ai, Aii, Bi and Bii = 200µm, Aiii and Biii = 50µm.

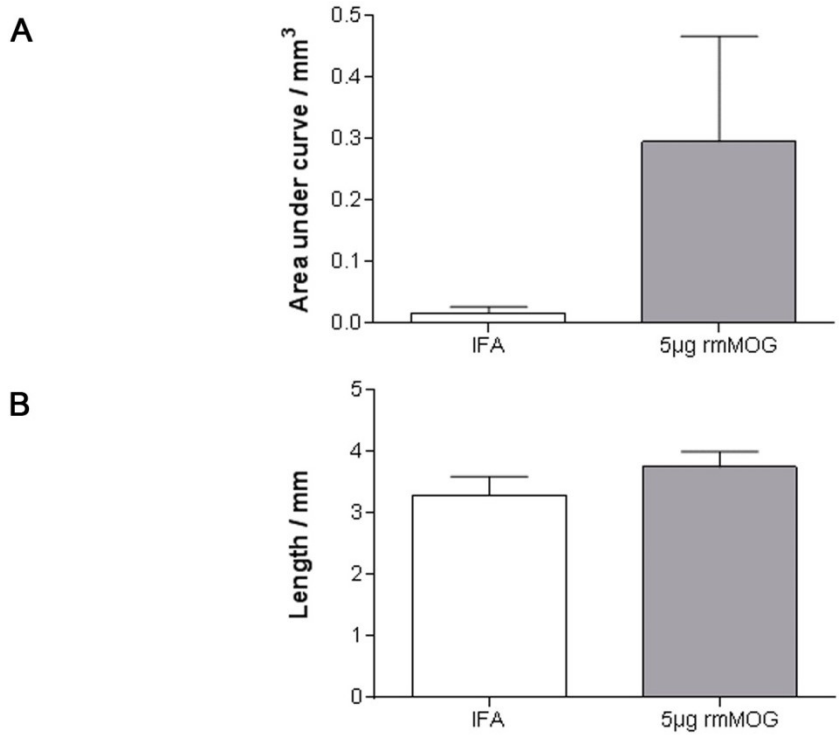

Figure 4.3.7. No change in eGFP expression after injection of VSVg.cmv_eGFP in rmMOG-immunised animals. The total eGFP expression, determined by calculating the area under the curve of eGFP expression against distance from injection site, was the same in IFA-immunised and rmMOG-immunised animals (A). The anterior to posterior spread of eGFP expression was also the same (B; Mann-Whitney *U*; mean ± SEM; *n* = 4 per group).

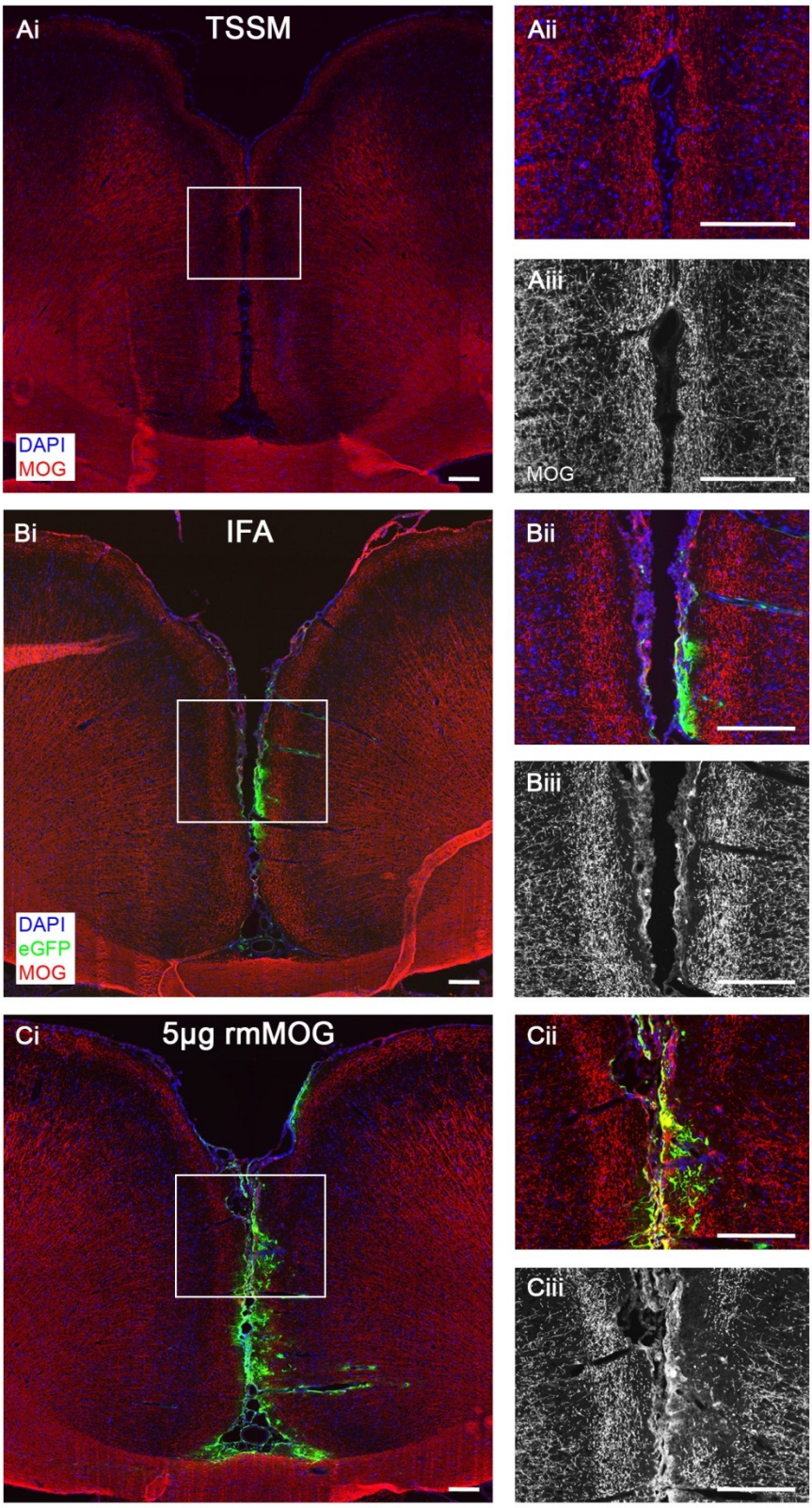

Figure 4.3.8. Absence of demyelination after injection of VSVg.cmv_eGFP in rmMOG-immunised animals. IF for MOG was performed on injection site sections and showed normal myelination similar to that in naïve control animals 1 week after injection of TSSM (A) in IFA-immunised animals 1 week after injection of VSVg.cmv_eGFP (B) as well as in all rmMOG-immunised animals (Ci), although one small area without MOG was observed in one animal adjacent to the sagittal sulcus (Cii and Ciii). Images in i/ii are composite and those in iii are single MOG IF, note the presence of crosstalk resulting from the emission of eGFP being detected through the filter for Alexa Fluor 546; images in ii/iii are magnifications of the boxed areas in i. Scale bars = 200µm.

Similarly, qualitatively similar densities of ED1+ cells were present in animals immunised with IFA only (Bi) and in those immunised with 5µg of rmMOG (Bii). ED1 has been shown to be expressed on the membranes of cytoplasmic granules and its expression to be correlated with phagocytic activity (Damoiseaux *et al.*, 1994). ED1+ phagocytic cells were also particularly evident at the base of the sagittal sulcus but as for Iba1, no colocalisation of eGFP with ED1 was observed.

Iba1 immunoreactivity was quantified and showed a trend for increased Iba1 immunoreactivity 1 week after injection of VSVg.cmv_eGFP in animals immunised with 5µg of rmMOG compared to those immunised with IFA only, although this was not statistically significant (C).

Finally, IF for CD3 and CD79a was performed on sections cut at the injection site in order to determine the presence of T and B cells respectively. Again, qualitatively similar, low densities of CD3+ T cells and CD79a+ B cells were present at the base of the sagittal sulcus in animals immunised with IFA only (Figure 4.3.10 Ai, Bi) and in those immunised with 5µg of rmMOG (Aii, Bii). No colocalisation of eGFP with CD3 or CD79a was observed.

4.3.3 Injection of LV vector and collagen hydrogel

Finally, in order to achieve localised, sustained expression of eGFP at the injection site, collagen hydrogel was injected as part of the LV vector preparation into the SAS of the sagittal sulcus of naïve rats as described in 4.2.2.4. Although this experiment was technically challenging due to the small volumes involved and the variability of the collagen type 1 hydrogel, VSVg.cmv_eGFP with collagen hydrogel was successfully injected into the SAS.

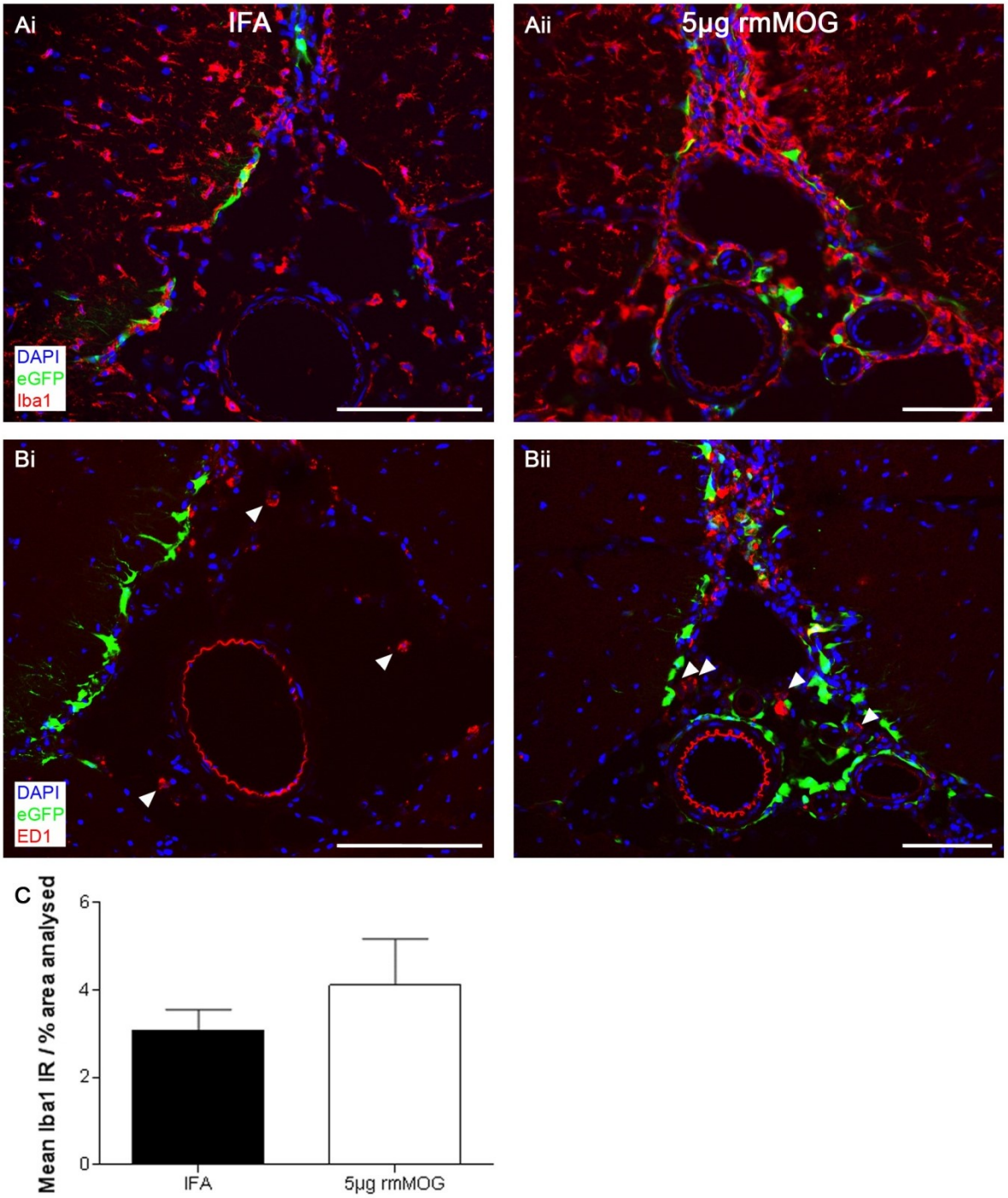

Figure 4.3.9. No increase in microglial activation after injection of VSVg.cmv_eGFP in rmMOG-immunised animals. IF for Iba1 (A) and ED1 (B) was performed on injection site sections and showed qualitatively similar densities of Iba1+ and ED1+ cells in IFA-immunised (i) and rmMOG-immunised (ii) animals 1 week after injection of VSVg.cmv_eGFP. Note that no colocalisation of eGFP and Iba1/ED1 was observed. Scale bars = 200µm. Iba1 immunoreactivity was the same in IFA-immunised and rmMOG-immunised animals (C; Mann-Whitney *U*; mean ± SEM; *n* = 4 per group).

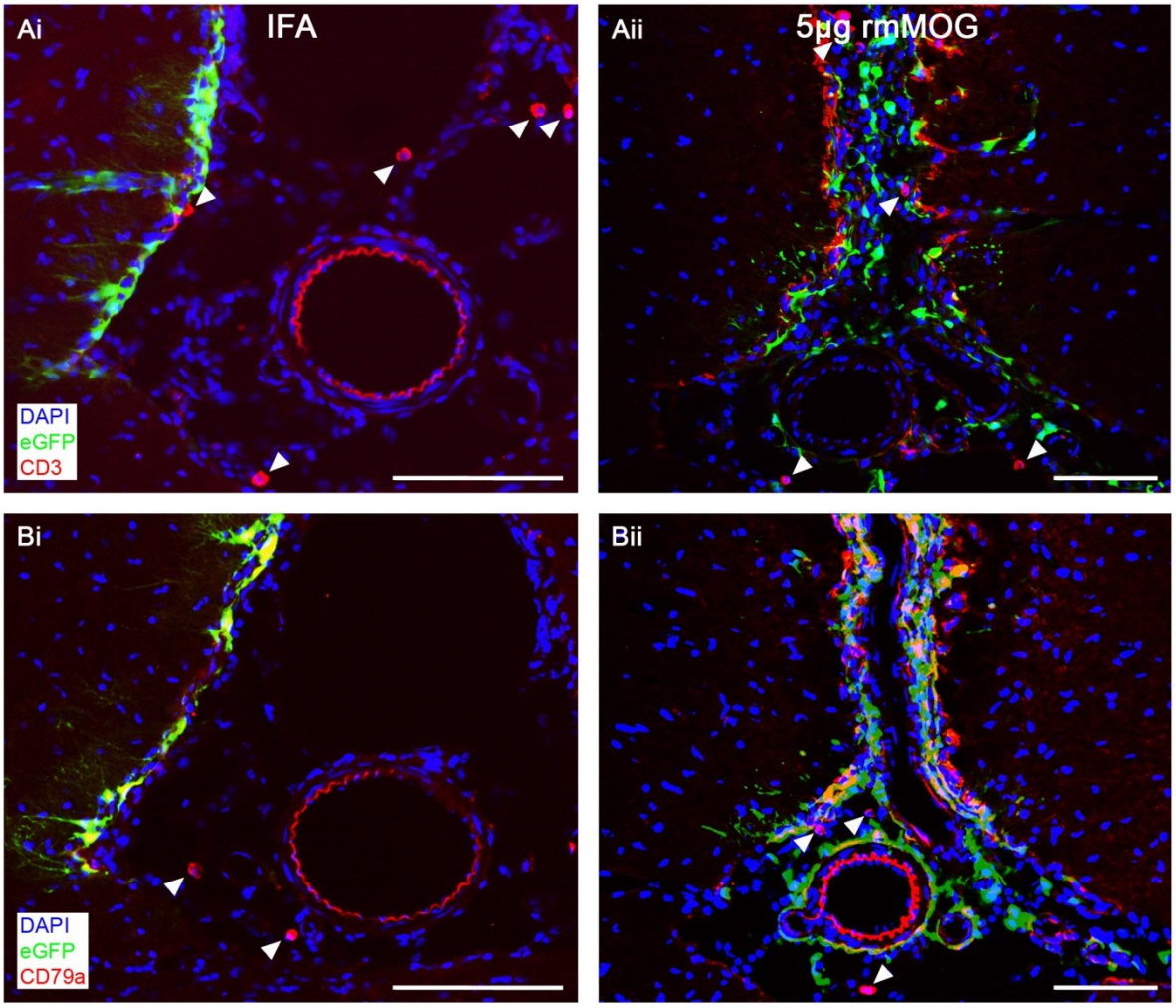

Figure 4.3.10. No increase in immune cell infiltration after injection of VSVg.cmv_eGFP in rmMOG-immunised animals. IF for CD3 (A) and CD79a (B) was performed on injection site sections and showed qualitatively similar densities of CD3+ T cells and CD79a+ B cells in IFA-immunised (i) and rmMOG-immunised (ii) animals 1 week after injection of VSVg.cmv_eGFP. Note that no colocalisation of eGFP and CD3/CD79a was observed. Scale bars = 200µm.

4.3.3.1 Increased spread of eGFP expression with collagen hydrogel

eGFP expression was present in DAPI-stained sections cut at the injection site after injection of VSVg.cmv_eGFP with both PBS (Figure 4.3.11 A) and collagen hydrogel (B). The pattern of eGFP expression was similar to that observed previously and was present mainly in the sagittal sulcus (pictured), in cells with the morphology of astrocytes.

eGFP expression was present in 4 of 4, 2 of 4 and 3 of 4 animals at 1, 2 and 4 weeks respectively after injection of VSVg.cmv_eGFP with PBS. However, it was only present in 3 of 4 animals at 2 weeks after injection with collagen hydrogel and was not present in these animals at 1 and 4 weeks after injection. As a result, total eGFP fluorescence and length along the anteroposterior axis over which eGFP expression was observed could only be compared between the two groups at 2 weeks after injection. Curves of area of eGFP fluorescence against distance from the injection site at 2 weeks after injection showed that eGFP was expressed in a gradient around the injection site (Figure 4.3.12 Ai). The peak area of eGFP fluorescence appeared greater in the PBS group, although the anterior to posterior spread was greater in the collagen hydrogel group. Quantification of total eGFP fluorescence from these curves showed that it was not significantly different in the two groups (Aii), although quantification of length along the anteroposterior axis over which eGFP expression was observed confirmed that it was significantly greater (factor of 1.89) following injection with collagen hydrogel than with PBS (Bi).

Although eGFP expression was not present following injection of VSVg.cmv_eGFP with collagen hydrogel at 1 and 4 weeks after injection, it was present at these time points following injection with PBS, allowing the time course and anterior to posterior spread of eGFP fluorescence to be investigated as in the first experiment in this Chapter. This showed a significantly greater (factor of 15.2) total area of eGFP fluorescence at 4 weeks after injection than at 2 weeks after injection (Aiii) with no significant difference in its spread (Bii).

4.3.3.2 Collagen hydrogel could not be detected

In order to determine whether the collagen hydrogel could be detected, which would enable its distribution and time course of degradation to be investigated, IF for collagen type 1 was performed on sections cut at the injection site. A similar extent and pattern of collagen type 1 expression was observed after injection of VSVg.cmv_eGFP with PBS (Figure 4.3.13 A) and collagen hydrogel (B). This suggests that the collagen type 1 detected was endogenous. Collagen fibres are present in the narrow space that, together with the glia limitans and pia mater, separates the SAS from the cortical GM (Lopes and Mair, 1974). This is consistent with the presence of collagen type 1 expression in what appear to be the meninges in the sagittal sulcus (Aii, Bii). No colocalisation of eGFP with collagen type 1 was observed.

4.3.3.3 Microglial activation was unchanged with collagen hydrogel

Finally, IF for Iba1 was performed on sections cut at the injection site and showed the presence of activated macrophages/microglia after injection of VSVg.cmv_eGFP with both PBS (Figure 4.3.14 A) and collagen hydrogel (B), which was particularly evident adjacent to the sagittal sulcus. Again, colocalisation of eGFP with Iba1 was not observed and microglial activation did not appear to be associated with eGFP expression. For example, eGFP expression was present towards the superior surface of the cortex in the animal shown in B, whereas microglial activation was mainly observed towards the base of the sagittal sulcus.

As for eGFP fluorescence, comparisons between the Iba1 immunoreactivity in the PBS and collagen hydrogel groups could only be performed at 2 weeks after injection. Quantification showed a trend for greater Iba1 immunoreactivity 2 weeks after injection of VSVg.cmv_eGFP with PBS than after its injection with collagen hydrogel, although this was not significant (Ci). There was no significant difference in Iba1 immunoreactivity at 1, 2 and 4 weeks after injection of VSVg.cmv_eGFP with PBS (Cii).

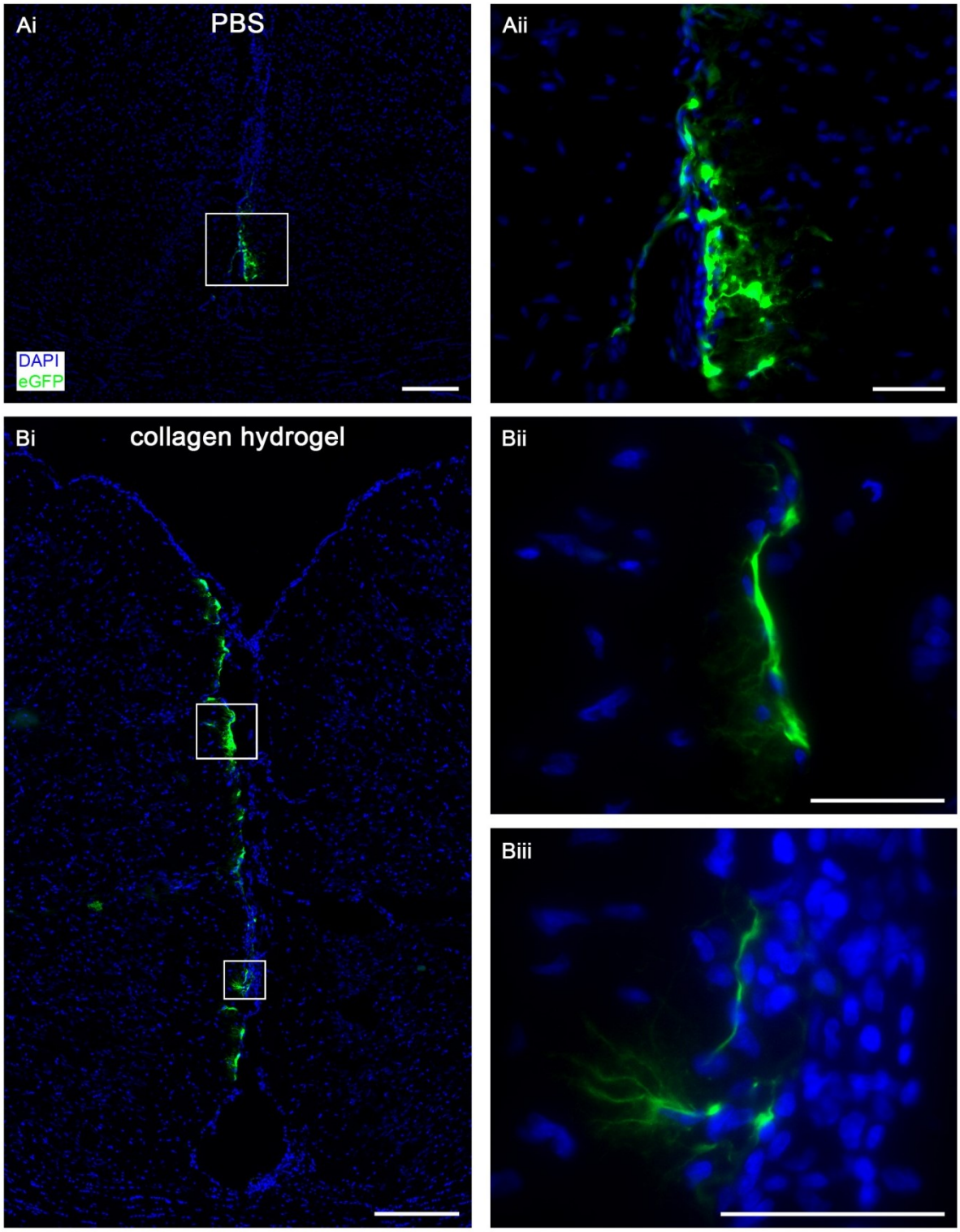

Figure 4.3.11. eGFP expression present after injection of VSVg.cmv_eGFP with collagen hydrogel. DAPI staining was performed on injection site sections and showed eGFP expression in the sagittal sulcus after injection of VSVg.cmv_eGFP with both PBS (A) and with collagen hydrogel (B). Images in Aii and Bii-Biii are magnifications of the boxed areas in Ai and Bi. Scale bar: Ai and Bi = 200μm, Aii, Bii and Biii = 50μm.

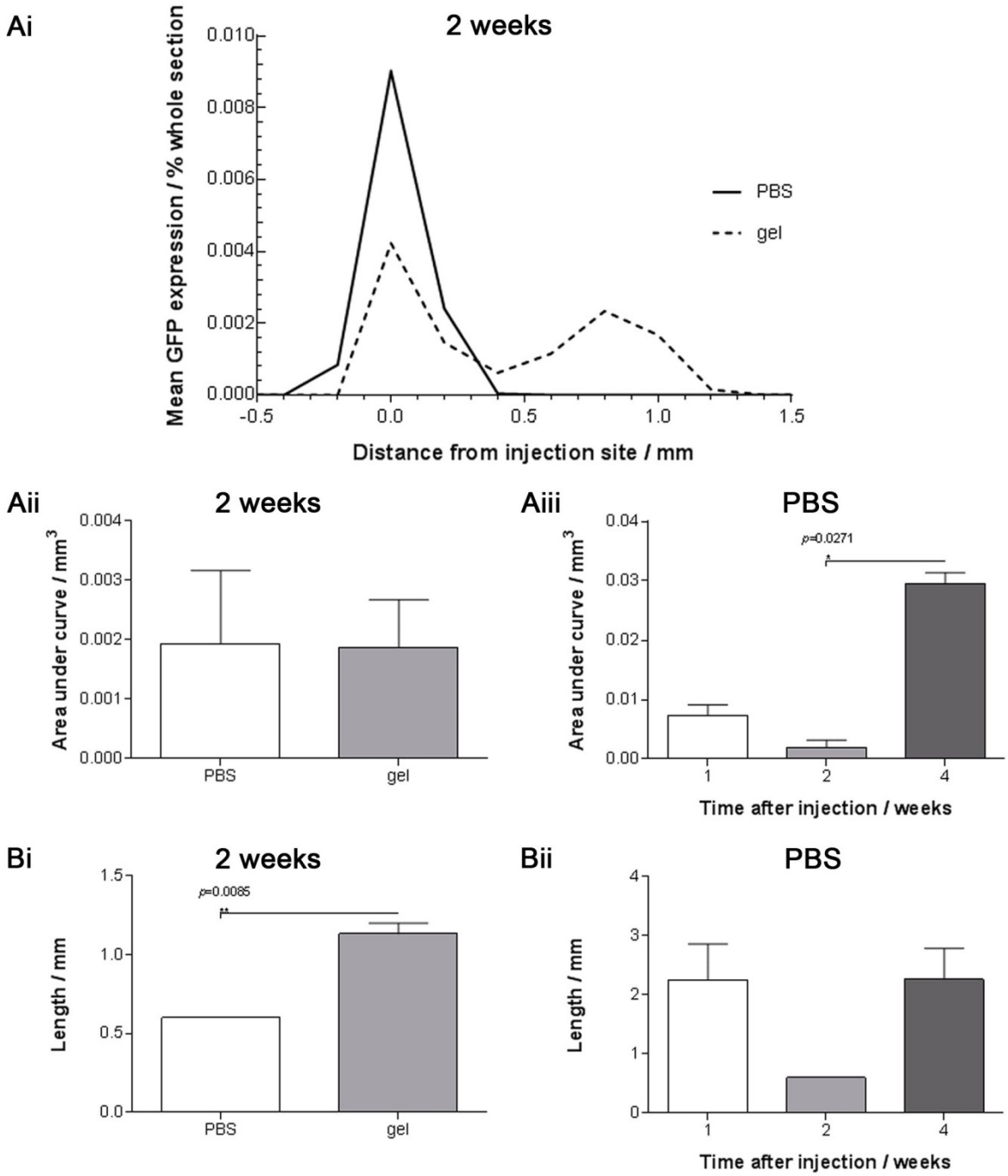

Figure 4.3.12. eGFP expression after injection of VSVg.cmv_eGFP with collagen hydrogel. eGFP was expressed in a gradient around the injection site from anterior to posterior 2 weeks after injection of VSVg.cmv_eGFP with both PBS and collagen hydrogel (Ai). The total eGFP expression, determined by calculating the area under the curve of eGFP expression against distance from injection site, was the same 2 weeks after injection with PBS and collagen hydrogel (Aii). The total eGFP expression was increased at 4 weeks after injection with PBS compared to after 2 weeks (Aiii; Kruskal-Wallis with Dunn's multiple comparisons test; mean ± SEM; * = $p \leq 0.05$; n = 4 for 1 week, 2 for 2 weeks, 3 for 4 weeks). The anterior to posterior spread of eGFP expression was increased 2 weeks after injection with collagen hydrogel (Bi; Mann-Whitney U; mean ± SEM; ** = $p \leq 0.01$; n = 2 for PBS, 3 for gel) and was the same at 1, 2 and 4 weeks after injection with PBS (Bii).

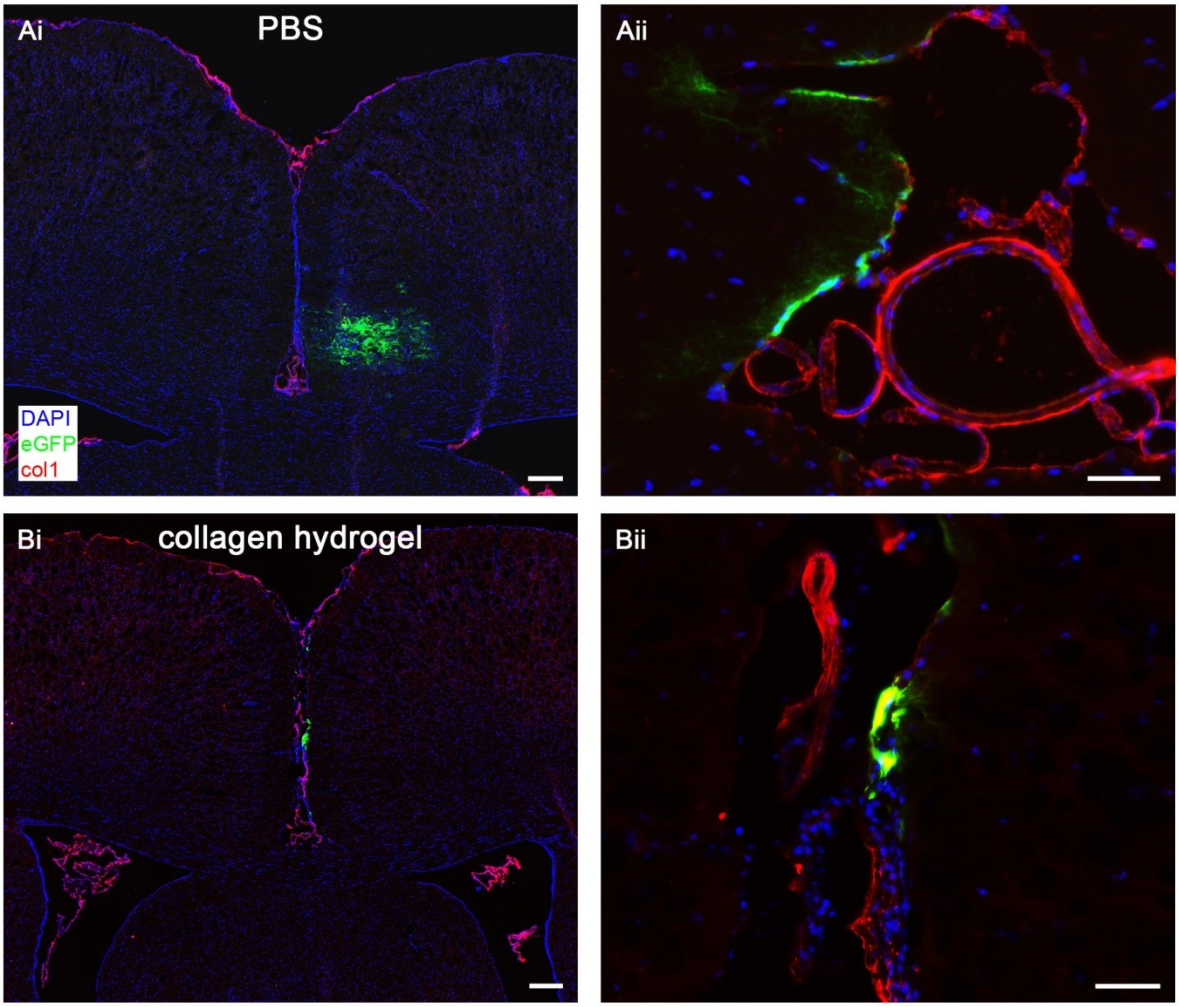

Figure 4.3.13. Collagen detection after injection of VSVg.cmv_eGFP with collagen hydrogel. IF for collagen type 1 was performed on injection site sections and showed similar extents and patterns of collagen type 1 expression after injection of VSVg.cmv_eGFP with both PBS (A) and collagen hydrogel (B). Note that no colocalisation of eGFP and collagen type 1 was observed. Scale bar: Ai and Bi = 200μm, Aii and Bii = 50μm.

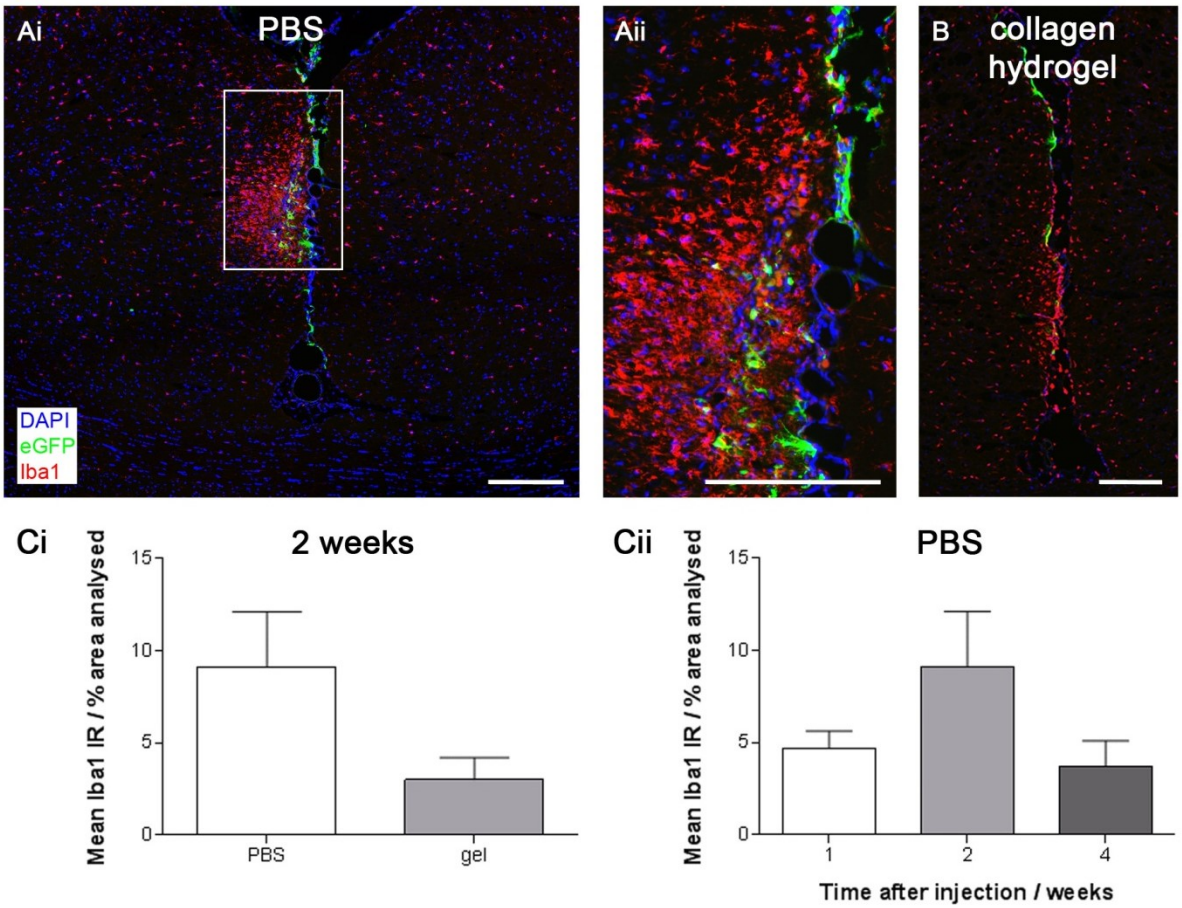

Figure 4.3.14. No increase in microglial activation after injection of VSVg.cmv_eGFP with collagen hydrogel. IF for Iba1 was performed on injection site sections and showed the presence of activated macrophages/microglia adjacent to the sagittal sulcus after injection of VSVg.cmv_eGFP with both PBS (A; the image in Aii is a magnification of the boxed area in Ai) and collagen hydrogel (B). Note that no colocalisation of eGFP and Iba1 was observed. Scale bars = 200μm. Iba1 immunoreactivity was the same 2 weeks after injection of VSVg.cmv_eGFP with PBS and collagen hydrogel (Ci; Mann-Whitney *U*; mean ± SEM; *n* = 2 for PBS, 3 for gel) and was the same 1, 2 and 4 weeks after injection with PBS (Cii; Kruskal-Wallis with Dunn's multiple comparisons test; mean ± SEM; *n* = 4 for 1 week, 2 for 2 weeks, 3 for 4 weeks).

4.4 Discussion

4.4.1 LV vector-mediated eGFP expression

LV vectors have been shown to transduce most cell types present in the CNS *in vivo*, including astrocytes, neurons and oligodendrocytes (Jakobsson and Lundberg, 2006). LV vectors based on HIV-1 such as that used in the current study are the most widely used for gene transfer to the CNS and are typically pseudotyped with VSV-G, resulting in long-term stable expression of the gene of interest. Initial studies suggested that LV vectors pseudotyped with this glycoprotein preferentially transduced neurons, with one study showing that 88.7% of transduced cells following injection into the striatum were neurons (Blömer *et al.*, 1997). However, later studies suggested that this preference was a result of the ubiquitous internal promoter rather than the VSV-G, which had low activity in glial cells (Jakobsson *et al.*, 2003). It is thought that LV vectors pseudotyped with VSV-G are able to enter all cell types present in the CNS with similar efficiency, but that the resulting transduction depends on the internal promoter activity in these cell types (Jakobsson and Lundberg, 2006).

4.4.1.1 Long-term eGFP expression

The results of the current study, using an LV vector based on HIV-1 pseudotyped with VSV-G and containing the gene for eGFP under the transcriptional control of the ubiquitous internal CMV promoter, are consistent with these previous findings. Long-term, up to 12 weeks, eGFP expression was observed, the total fluorescence and anterior to posterior spread of which was not significantly different at this long-term time point than at 1 week after injection, suggesting constant, stable expression. Although there are no reports of LV vector injection into the SAS to date, the intracerebroventricular injection of choroid plexus-specific LV vector in mice has been shown to result in transduction 4 months after injection (Regev *et al.*, 2010), consistent with the stable expression observed here. This finding

suggests that the LV vector would also mediate long-term stable expression of TNF and IFN-γ in the model of cortical pathology driven by meningeal inflammation, which we suggest will result in a long-term cytotoxic/inflammatory episode.

Although eGFP expression was present in 3 of 4 animals at 1 and 12 weeks after injection of VSVg.cmv_eGFP in naïve animals, it was present in only 1 of 4 animals at 4 weeks after injection. Studies have shown downregulation of the CMV promoter following transduction of human embryonic stem cells with LV vector after 50 days in culture (Norrman *et al.*, 2010), shown to be mediated by DNA methylation and histone deacetylation (Grassi *et al.*, 2003). This downregulation of the CMV promoter may explain the relative absence of eGFP expression in animals at 4 weeks after injection. However, given the presence of eGFP expression in animals at 12 weeks after injection, it is unlikely that this was the case. It has also been shown that LV vectors pseudotyped with VSV-G can be cytotoxic at high concentrations (Sakuma *et al.*, 2012), which would result in the death of transduced cells. Given that animals received the same number of transducing viral particles, it is again unlikely that this was the case, although future experiments could investigate the expression of markers of cell death. However, given the variable nature of *in vivo* studies, it is not possible to rule out either CMV promoter downregulation or VSV-G pseudotype cytotoxicity in the current study. We suggest that the relative absence of eGFP expression in animals at 4 weeks after injection may be due to experimental complications, including blocking of the glass capillary mounted on the Hamilton needle. This became apparent on retraction of the needle, when blood clots could be observed at the bottom of the glass capillary, with or without the appearance of liquid around the nail polish seal. Experimental modifications were made to prevent blocking of the glass capillary prior to subsequent experiments in this Chapter. These included the expulsion of a drop of the LV vector preparation prior to lowering of the needle to prevent blood from entering it, and strengthening of the nail polish seal.

4.4.1.2 eGFP expression in relevant cell types

The cell types in which eGFP expression was observed in the current study are also consistent with previous findings. It was present in the astrocyte end-feet of the glia limitans and appeared to be present in cells with the morphology of the mesothelial cells and fibroblasts of the pia mater as well as in cells with the morphology of pyramidal neurons, although colocalisation of eGFP with established phenotypic markers of these cells could not be achieved. Transduction of astrocytes and neurons has been shown *in vivo* 2 weeks after intraspinal injection (Hendriks *et al.*, 2007) while transduction of pial and leptomeningeal cells has been shown *in vivo* 4 weeks after spinal intrathecal injection (Fedorova *et al.*, 2006) of LV vector pseudotyped with VSV-G and containing the transgene under the transcriptional control of the CMV promoter. The former study also showed transduction of meningeal cells *in vitro* as well as macrophages/microglia *in vivo*. This latter finding is in contrast to the current study, in which colocalisation of eGFP with Iba1 or ED1 was not observed, although another study did show only weak activity of the CMV promoter in mononuclear cells (Liu *et al.*, 2006). However, the cellular localisation of eGFP expression in the current study is different to that of TNF and IFN-γ in MS, in which they are expressed in monocytes/macrophages and T cells in inflamed meninges (Serafini *et al.*, 2007, Magliozzi *et al.*, 2010, Gardner *et al.*, 2013) and some microglia in superficial GM in F+ SPMS cases (Gardner *et al.*, 2013). Despite this, we suggest that its long-term presence in the sagittal sulcus and in the walls of the meningeal blood vessels at the base of the sulcus would be optimal for achieving a chronic inflammatory milieu in the CSF/meningeal compartment. The injection of a viral vector based on herpes simplex virus type 1 or an adenoviral vector containing the IFNG gene into the cisterna magna resulted in expression in choroidal, ependymal and leptomeningeal cells and increased levels of IFN-γ in the CSF (Furlan *et al.*, 2001, Millward *et al.*, 2007), which have also been found in MS (Romme Christensen *et al.*, 2012, Gardner *et al.*, 2013). Although there are no reports of the injection of viral vectors containing the TNF gene into the SAS to date, this study suggests that the injection of an LV

vector containing the genes for TNF and IFN-γ would result in increased levels of these cytokines in the CSF, as required in the model of subpial demyelination.

The eGFP expression in astrocytes, cells of the meninges in the sagittal sulcus and walls of the blood vessels in the meninges suggests that VSVg.cmv_eGFP transduced the cells that the LV vector preparation contacted following injection into the SAS of the sagittal sulcus. The SAS is separated from the cortical GM by the mesothelial cells and layers of flattened fibroblasts that comprise the pia mater, a narrow space containing collagen fibres and the basal lamina and layers of astrocytic elements that comprise the glia limitans (Lopes and Mair, 1974). The finding of eGFP expression on the superior surface of the cortex is consistent with CSF drainage pathways, with the LV vector preparation proposed to diffuse from the sagittal sulcus to the superior surface (Zhang *et al.*, 1992, Kida *et al.*, 1993). The eGFP expression adjacent to the sagittal sulcus in the cingulate cortex, as well as in the corpus callosum, is likely to be the result of diffusion of the LV vector preparation from the CSF to the brain interstitial fluid across the barrier formed by the pia mater and glia limitans, the cells of which are joined by gap junctions rather than tight junctions rendering this barrier permeable (Alcolado *et al.*, 1988, Johanson *et al.*, 2005). The pia mater also allows the formation of perivascular spaces, which function as the lymphatic system of the brain. Blood vessels enter and exit the parenchyma across the pia mater, which adheres to the vessels resulting in a space between it and the vessels. Tracer studies have suggested that perivascular spaces may mediate exchange between the vessels and the CSF (Rennels *et al.*, 1985). A recent study using *in vivo* two-photon imaging showed that subarachnoid CSF rapidly enters the parenchyma and contacts the basal lamina of brain capillaries along perivascular spaces and exchanges with the brain interstitial fluid, which is also removed from the parenchyma along these spaces (Iliff *et al.*, 2012). We suggest that the eGFP expression in perivascular spaces and brain parenchyma is likely to be the result of entry of the LV vector preparation along these perivascular spaces, which has been observed previously following the injection of a viral vector based on herpes simplex virus type 1 into

the cisterna magna (Furlan *et al.*, 2001). These data show that the injection of LV vector into the SAS of the sagittal sulcus is a successful strategy to achieve widespread gene expression at the surface of the cerebral cortex.

4.4.1.3 Absence of long-term microglial activation

In order for this to be a useful strategy, it is important that LV vector-mediated transduction does not induce inflammatory changes in cortical GM. The finding that Iba1 immunoreactivity was not significantly different after injection of VSVg.cmv_eGFP and the vehicle control suggests that the LV vector did not induce inflammatory changes. The trend for increased Iba1 immunoreactivity at 1 week compared to 4 weeks after injection, together with the observation that microglial activation was most apparent adjacent to the sagittal sulcus towards the superior surface of the cortex and was not associated with eGFP expression, suggests that the microglial activation was a result of an initial, acute innate immune response to the midline injection.

This is consistent with a previous study that showed the presence of ED1+ cells along the needle tract at 30 days after intrastriatal injection of saline as well as LV vector pseudotyped with VSV-G and containing the gene for eGFP under the transcriptional control of the CMV promoter (Abordo-Adesida *et al.*, 2005). The authors suggest that these phagocytic cells remain from the immune response to the injection. This study also showed that LV proteins do not induce cellular or innate immune responses, with the immune system recognising only the transgene product and not the capsid or virion. Consequently, transduced cells are only recognised if an immune response is raised against the transgene, which is not the case for eGFP.

4.4.2 Absence of non-specific demyelination and inflammation

Results from the experiment involving the injection of VSVg.cmv_eGFP into animals immunised with rmMOG or IFA only indicate that the transduction efficiency of the LV vector

preparation, evaluated using total eGFP fluorescence and its spread, was unchanged by a peripheral anti-MOG antibody response. This is comparable to a previous study that showed unchanged transduction following intrastriatal injection of LV vector containing the gene for eGFP in animals immunised with LV vector, regardless of the transgene this LV vector contained, or saline only (Abordo-Adesida *et al.*, 2005).

This experiment has also allowed us to conclude that the injection of the LV vector did not result in non-specific demyelination and inflammation in animals immunised with rmMOG, that is, not induced by the injection of TNF and IFN-γ, and suggests that LV vectors are suitable for the delivery of genes of interest in this model.

A previous study investigated transduction by an LV vector, pseudotyped with VSV-G and containing the lacZ reporter gene under the transcriptional control of the phosphoglycerate kinase (PGK) promoter, following injection into the dorsal funiculus of naïve rats (Zhao *et al.*, 2003). Injection was associated with tissue damage at 5 days after injection, which was variable but could be extensive. It was characterised by a focal area of necrosis and primary demyelination at the injection site, associated with an inflammatory infiltrate consisting of activated macrophages/microglia but few CD8+ T cells and no CD4+ T cells. Although a small area of potential demyelination was present adjacent to the needle tract at 1 week after injection in the current study, macrophage infiltration in the parenchyma was not observed, suggesting a different pathogenetic mechanism. This previous study also showed tissue damage 5 days after injection of PBS alone, although it was less extensive than after injection of the LV vector. The authors suggest that tissue damage was largely the result of toxicity associated with high concentrations of the LV vector, with a further contribution of the injection itself, which would result in the activation of microglia and subsequent demyelination by the mechanisms described in 3.4.3.2. Hence, it is not possible to determine whether the small area of potential demyelination observed here is the result of toxicity, the injection itself or the peripheral anti-MOG antibody response. If it was the result of toxicity or

the injection itself, demyelination would also have been expected in animals immunised with IFA only. However, if it was the result of the peripheral anti-MOG antibody response, demyelination would have been expected in more than 1 of the 4 animals immunised with rmMOG.

4.4.3 Effect of collagen hydrogel

In the final experiment of this Chapter, naïve animals received an injection of VSVg.cmv_eGFP with a collagen hydrogel in order to prevent extensive diffusion of the LV vector so that a higher concentration of TNF and IFN-γ may be achieved in a more localised area in future experiments. LV vectors may be delivered from hydrogels to provide sustained release, over days to weeks, and increased concentrations of the LV vectors locally, increasing their cellular internalisation and consequently the expression of the transgenes they contain (Seidlits *et al.*, 2013). This sustained release may also result in persistent expression and increasing expression with time. For example, the delivery of adenovirus from silk-elastin-like protein polymer hydrogels resulted in increased duration of expression compared to a bolus injection of adenovirus (Cresce *et al.*, 2008). Hence increased duration and extent of eGFP expression at the injection site was expected after injection of VSVg.cmv_eGFP with collagen hydrogel in the current study.

4.4.3.1 Delayed eGFP expression

eGFP expression was only present at 2 weeks after injection of VSVg.cmv_eGFP with collagen hydrogel and was not present at 1 and 4 weeks after injection. This was in contrast to the eGFP expression present at all time points after injection of VSVg.cmv_eGFP with PBS. This suggests that the collagen hydrogel delayed expression, which is consistent with a previous study. Although a small amount of LV vector was released from a collagen hydrogel at 1 day *in vitro*, maximal transgene expression was observed at 2 weeks after s.c. implantation *in vivo*, with decreased and absent expression at 4 and 6 weeks respectively (Shin and Shea, 2010). This is comparable with the eGFP expression observed at 2 weeks,

with absent expression at 1 and 4 weeks, observed in the current study. The authors suggest that the LV vector is initially retained in the collagen hydrogel, with its degradation rate by collagenases and its pore size limiting the infiltration of local cells, as LV vectors have been shown not to bind directly to collagen (Shin *et al.*, 2010). We suggest that degradation rate and pore size hence also limit the release of VSVg.cmv_eGFP, resulting in delayed eGFP expression. The authors of the previous study also propose that the decreased transgene expression at later time points was the result of clearance of transduced cells by the immune system or a turnover of the transduced cells. However, given that the Iba1 immunoreactivity was not significantly different in the collagen hydrogel and PBS groups at 2 weeks after injection, and that eGFP expression was present at 4 weeks after injection in the PBS group and was actually greater than that at 2 weeks after injection, it is unlikely that the absence of eGFP expression at 4 weeks after injection in the collagen hydrogel group is the result of these mechanisms. Additionally, a study using a collagen hydrogel to deliver an adenoviral vector containing the gene for human platelet-derived growth factor subunit B to a dermal wound showed a lack of an anti-collagen IgG response (Gu *et al.*, 2004), indicating that the collagen hydrogel induces neither an adaptive nor innate immune response.

4.4.3.2 Increased spread of eGFP expression

In contrast to the increased eGFP expression at the injection site and decreased spread of eGFP expression expected from the previous studies using hydrogels to deliver viral vectors described above, there was no significant difference in the peak area of eGFP fluorescence, but an increased anterior to posterior spread in the collagen hydrogel group. We suggest that although the properties of the collagen hydrogel may limit the release of VSVg.cmv_eGFP at early time points, resulting in delayed eGFP expression, the collagen hydrogel is not optimised for sustained release in this model but rather allows rapid release and subsequent spread at later time points. Although we aimed to investigate the distribution and time course of degradation of the collagen hydrogel in the current study, only what

appeared to be endogenous collagen type 1 in the meninges could be identified. This may be the result of degradation of the collagen hydrogel and its subsequent drainage in the CSF, or a collagen type 1 IF protocol that lacked the sensitivity required to detect the injected collagen.

Given that the rationale for using the collagen hydrogel in the current study was to prevent extensive spread of the LV vector, it is clear that the collagen hydrogel used here is not suitable for the delivery of LV vectors in this model. However, the increased retention and stability of LV vectors delivered from collagen hydrogels promoted efficient, localised transgene expression (Shin and Shea, 2010) and hence further experiments would be worthwhile. We propose that these could use a collagen hydrogel with a higher collagen content, which has been shown to slow release (Premaraj *et al.*, 2006). Although the relative concentrations of collagen and the cross-linker 4S-StarPEG had been optimised to result in gelation at 37°C in approximately 15 minutes in the current study, the extent of cross-linking also determines the degradation rate (Shin and Shea, 2010), and hence an increase in the relative concentration of the cross-linker may slow degradation and subsequent release. Finally, the immobilisation of LV vector to hydroxyapatite nanoparticles has been shown to further increase the retention and stability of LV vectors delivered from collagen hydrogels (Shin and Shea, 2010), indicating that the use of additional nanoparticles may also be considered.

4.4.4 Conclusions

We conclude that the extensive and long-term eGFP expression and its localisation in the sagittal sulcus, in the absence of long-term microglial activation, observed here would be optimal for achieving the chronic bathing in pro-inflammatory cytokines of the surface of the brain required to develop the model of cortical pathology driven by meningeal inflammation. Additionally, we suggest that LV vectors are suitable for the delivery of genes of interest in this model given the absence of non-specific demyelination following injection in animals

immunised with rmMOG. Future experiments will involve the production of a bicistronic LV vector containing the genes for TNF and IFN-γ. This technology has been used previously in, for example, a macaque model of Parkinson's disease. A tricistronic LV vector containing the genes required for dopamine synthesis resulted in restoration of dopamine levels and motor function for 12 months following intrastriatal injection (Jarraya *et al.*, 2009). These future experiments may also involve the use of a collagen hydrogel, following optimisation, to prevent extensive diffusion of the LV vector so that a higher concentration of TNF and IFN-γ may be achieved at the injection site.

Chapter 5

Expression of inflammatory cytokines and receptors in meninges in F+ SPMS

5.1 Introduction

5.1.1 GMLs in MS

Cortical GMLs have been observed in neuropathological studies since 1892 (Taylor, 1892; reviewed in Kutzelnigg and Lassmann, 2005), but it is only in the last decade that the extent of cortical GM pathology in progressive MS has been made clear (Peterson *et al.*, 2001, Bø *et al.*, 2003b, Kutzelnigg *et al.*, 2005). Findings obtained from these studies, combined with those obtained from longitudinal clinical MRI studies (Calabrese *et al.*, 2012), support a major role for cortical GM pathology in driving progression, and associated worsening of motor and cognitive symptoms, in MS (Reynolds *et al.*, 2011).

Cortical GM pathology is characterised by demyelination, which may be leukocortical, intracortical or subpial (Peterson *et al.*, 2001, Bø *et al.*, 2003b) as described in 1.2.2.2. Subpial lesions are the most common type and may involve multiple gyri, accounting for up to 50-70% of all GMLs, followed by leukocortical lesions, which account for 25-34% (Peterson *et al.*, 2001, Bø *et al.*, 2003a, Magliozzi *et al.*, 2007).

5.1.2 Inflammation associated with subpial GMLs

Inflammation in subpial GMLs is characterised by extensive microglial activation with characteristically only mild peripheral immune cell infiltration in perivascular cuffs, in contrast to WMLs (Peterson *et al.*, 2001, Kutzelnigg *et al.*, 2005, Magliozzi *et al.*, 2010). However, a study using biopsy samples from early MS patients found T cell infiltrates in the majority of subpial GMLs (Lucchinetti *et al.*, 2011) and a subsequent study using autopsy samples from SPMS patients found perivascular cuffs in 42% of subpial GMLs (Magliozzi *et al.*, 2013), suggesting that immune cell infiltration does have a role in GMLs. The lack of significant peripheral immune cell infiltration previously observed and the high prevalence of subpial

GMLs suggest a role for the CSF and immune cell infiltration in the overlying meninges in pathology of the underlying subpial cortical GM (Gardner *et al.*, 2013).

5.1.2.1 Meningeal inflammation

Diffuse inflammatory infiltrates have frequently been observed in the cerebral leptomeninges in studies using autopsy samples from PPMS and SPMS cases (Guseo and Jellinger, 1975, Kutzelnigg *et al.*, 2005, Kooi *et al.*, 2009, Howell *et al.*, 2011, Choi *et al.*, 2012) and were particularly frequent in cases with extensive subpial cortical GM demyelination, although one study showed no spatial correlation between the infiltrates and demyelination (Kooi *et al.*, 2009). They have also been observed in a study using cortical biopsy samples from early MS patients (Lucchinetti *et al.*, 2011), indicating that meningeal inflammation is not restricted to progressive stages.

As well as these diffuse inflammatory infiltrates, ectopic lymphoid follicle-like structures have also been observed in the meninges, particularly those of the sulci, in a significant proportion of SPMS cases in studies using autopsy samples (41.4%, 54% and 40% in Magliozzi *et al.*, 2007, Magliozzi *et al.*, 2010 and Howell *et al.*, 2011 respectively). They consist of aggregates of CD20+ B cells together with CD35+ follicular dendritic cells, Ki67+ proliferating CD20+ B cells, IgA, -G or -M+ plasmablasts/plasma cells and CD3+ T cells. The cases in which they are found have been defined as F+ SPMS and those in which they are not found as F- SPMS.

The presence of these lymphoid-like structures has been associated with subpial GM demyelination and gradients of microglial activation and neuronal loss in cortical GM layers, with the greatest activation or loss in cortical layer I closest to the pia mater. A similar gradient of astrocyte loss that resulted in a thinning, or loss, of the glia limitans has also been described (Magliozzi *et al.*, 2010). Additionally, their presence has been associated with a younger age at onset, age at wheelchair dependence and age at death

(Magliozzi *et al.*, 2007). Diffuse inflammatory infiltrates in the meninges have similarly been associated with subpial GM demyelination and a younger age at onset, time to disease progression, time to wheelchair dependence and age at death (Howell *et al.*, 2011).

The occurrence of diffuse inflammatory infiltrates and lymphoid-like structures in the SAS of the cerebral leptomeninges, particularly those of the deep sulci, has led to the hypothesis that the decreased flow of CSF in the sulci results in a protected environment that allows the homing and retention, and subsequent lymphoid organisation, of immune cells, which in turn results in an inflammatory milieu in the CSF (Reynolds *et al.*, 2011).

5.1.2.2 Inflammatory milieu

It has been suggested that inflammatory infiltrates and lymphoid-like structures may be sites of immune cell activation and expansion in chronic disease (Serafini *et al.*, 2004, Serafini *et al.*, 2007, Magliozzi *et al.*, 2007, Magliozzi *et al.*, 2010) and become sources of pro-inflammatory cytokines, auto-antibodies and self-reactive T cells (Aloisi and Pujol-Borrell, 2006, Serafini *et al.*, 2007, Carragher *et al.*, 2008). Studies have shown the presence of B cell subsets found exclusively in lymphoid organs in CSF from MS patients (Corcione *et al.*, 2004) and the presence of related B cell clones in lesions as well as meninges and CSF (Owens *et al.*, 2003, Lovato *et al.*, 2011). Additionally, myelin-reactive T cell activation in the SAS is thought to be a key event in the initiation of EAE, as proliferating T cells have been detected initially in the SAS and subsequently in the spinal cord parenchyma, and before clinical symptoms (Kivisäkk *et al.*, 2009). These findings indicate a role for the activation and expansion of B and T cells, in the meninges, in the pathogenesis of MS.

The immune cells in the meninges are separated from the underlying subpial cortical GM by only a single, interrupted layer of cells of the pia mater, and the basal lamina and astrocyte end-feet, components of the glia limitans (Lopes and Mair, 1974). Given the structure of the pia mater and the thinning or loss of the glia limitans observed in F+ SPMS cases

(Magliozzi *et al.*, 2010), the pia mater and the glia limitans do not appear to represent a significant barrier to the diffusion of pro-inflammatory cytokines, auto-antibodies, lytic enzymes, nitrogen and oxygen radicals and metalloproteinases (MMPs) released by the immune cells (Brown and Sawchenko, 2007, Ransohoff, 2009).

Support for the inflammatory milieu in the CSF/meningeal compartment comes from studies such as that of Gardner *et al.* (2013), which showed that the number of cells expressing the pro-inflammatory cytokines TNF and IFN-γ and the gene expression of these cytokines are increased in the meninges of F+ SPMS cases. The same study showed increased levels of these cytokines in post-mortem CSF from these cases (Gardner *et al.*, 2013). These findings were in agreement with previous studies that showed the presence of TNF- and IFN-γ-expressing cells in inflamed meninges (Magliozzi *et al.*, 2010, Serafini *et al.*, 2007) and increased levels of TNF and IFN-γ in CSF (Obradović *et al.*, 2012, Romme Christensen *et al.*, 2012). TNF has also been detected on the other side of the barrier formed by the pia mater and glia limitans in active subpial GMLs in F+ SPMS cases (Magliozzi *et al.*, 2010). The levels of other inflammatory mediators, including MMP9 and osteopontin, are also increased in CSF from MS patients (Romme Christensen *et al.*, 2013), but it is the lymphoid chemokine CXCL13 that has received particular attention. Its levels in CSF have been shown to predict conversion from CIS to MS (Brettschneider *et al.*, 2010) and have been correlated with MRI activity in RRMS patients (Kuenz *et al.*, 2008) and with axonal damage in SPMS patients (Romme Christensen *et al.*, 2013).

5.1.3 Aims

Both the human tissue studies described above and the *in vivo* model studies described in 1.3.4 and in Chapter 3 have suggested that cytotoxic and/or pro-inflammatory molecules diffusing from the chronically inflamed CSF/meningeal compartment into the underlying cortical GM may result in subpial GMLs in MS (Gardner *et al.*, 2013). However, to date, a

complete study has not been performed and we aimed to determine the identity of these molecules.

To fulfil these aims, the following were performed:

- Selection of post-mortem F+ SPMS and F- SPMS cases and NNCs.
- Characterisation of cases and identification of potential lymphoid-like structures using haematoxylin and eosin (H&E) staining and CD20 and MOG IHC.
- Dissection of meninges and RT^2 Profiler PCR Array real-time PCR followed by validation PrimeTime qPCR Assays.
- Further investigation into the role of CXCL9.

5.2 Methods

The methods described in 5.2.1 to 5.2.2.3 were performed with equal contribution by Miss Eleanor Browne, who also required RNA from F+ and F- SPMS cases and NNCs for her PhD studies. Case selection was performed together whereas Miss Browne and the author each performed half of the block screening, meningeal dissection and RNA extraction. Subsequent experiments using RNA were performed solely by the author.

5.2.1 Characterisation of cases for meningeal PCR

5.2.1.1 Case selection

Tissue blocks were obtained from the UK Multiple Sclerosis Tissue Bank (Imperial College London, London, UK). The Tissue Bank operates a prospective donor scheme, collecting tissues with fully informed consent, approved by the National Research Ethics Committee (reference 08/MRE09/31).

Cases had previously been characterised (Howell *et al.*, 2011) as F+ SPMS (median age at death 45.5 years, range 40-59 years) or F- SPMS (median age at death 58.5 years, range 45-62 years). NNCs (median age at death 67 years, range 35-77 years) were also included (*n*=10 per group). Individual case details, including the age at which a patient received disease modifying treatment and its duration (if known) are presented in Table 5.2.1.

5.2.1.2 Block selection

Tissue blocks, measuring 2cm x 2cm x 1cm, were taken from whole coronal slices taken at the time of dissection of fresh tissue, frozen in isopentane on dry ice and stored at -80°C. Approximately 10 cortical blocks were selected per case from a range of brain areas based on the presence of well demarcated sulci (Figure 5.2.1 A). 10µm sections were cut using a cryostat and stored at -20°C.

Case	Sex	Age of death	Disease duration	Cause of death	Immunotherapy	PMD
NNC						
C14	M	64	NA	Cardiac failure	NA	18
C25	M	35	NA	Carcinoma of the tongue	NA	22
C28	F	60	NA	Ovarian cancer	NA	13
C45	M	77	NA	Cardiopulmonary degeneration, prostate cancer, old age, Alzheimer's disease	NA	22
C48	M	68	NA	Metastatic colon cancer	NA	10
C51	M	68	NA	Ischaemic heart disease	NA	24
C54	M	66	NA	Pancreatic cancer	NA	16
PDC8	F	71	NA	Myocardial infarction	NA	17
PDC22	M	75	NA	Squamous cell carcinoma of the lung	NA	12
PDC36	F	57	NA	Metastatic carcinoma of the breast	NA	22
F-SPMS						
MS296	M	59	40	MS	NA	22
MS301	F	62	19	Septicaemia, recurrent urinary tract infection, hypokalaemia, MS	NA	16
MS304	M	52	23	Pulmonary embolism, metastatic carcinoma colon primary, MS	NA	13
MS311	F	45	16	Pneumonia	NA	22
MS318	F	59	34	MS	NA	13
MS326	M	62	32	MS, prostate cancer	NA	24
MS335	M	62	37	Recurrent aspiration pneumonia, MS, renal failure	NA	22
MS347	M	49	28	Metastatic pancreatic carcinoma	NA	13
MS364	F	56	34	Bronchopneumonia, MS	NA	14
MS376	F	48	20	MS	NA	19

F+ SPMS						
MS289	M	45	18	MS	NA	9
MS317	F	48	29	Aspiration pneumonia due to MS	NA	21
MS330	F	59	39	Pneumonia, MS	NA	21
MS352	M	43	18	Bronchopneumonia, MS	Campath-1H age 33	26
MS356	F	45	16	MS	NA	10
MS371	M	40	16	Bronchopneumonia	Avonex age 33, 35 months	27
MS377	F	50	23	Aspiration pneumonia	NA	22
MS402	M	46	20	MS, bronchopneumonia	NA	12
MS407	F	44	19	Septicaemia, pneumonia	Rebif age 42	22
MS426	F	48	29	MS	NA	21

Table 5.2.1. Details of cases used for meningeal analyses. Age of death and disease duration in years; PMD, post-mortem delay in hours; M, male; F, female.

5.2.1.3 Block screening

Each block was examined for the presence of meningeal infiltrates. H&E staining was initially performed. Sections were immersed in haematoxylin for 2 minutes followed by destaining in warm running tap water for 5 minutes. Sections were immersed in eosin 1% (Raymond A Lamb Ltd from Thermo Scientific) for 2 minutes followed again by destaining. Sections were dehydrated using ethanol gradients and cleared using xylene followed by mounting in DPX.

Blocks were assigned an index of inflammation based on the maximum density of meningeal infiltrates observed (Howell *et al.*, 2011; Figure 5.2.1 B). Sections with no meningeal infiltrates, sections with at least one moderate meningeal infiltrate and sections with substantial meningeal infiltrates were assigned indices of 0, + and ++ respectively. Substantial meningeal infiltrates were defined as dense clusters of small, round lymphocytic cells resembling potential lymphoid-like structures.

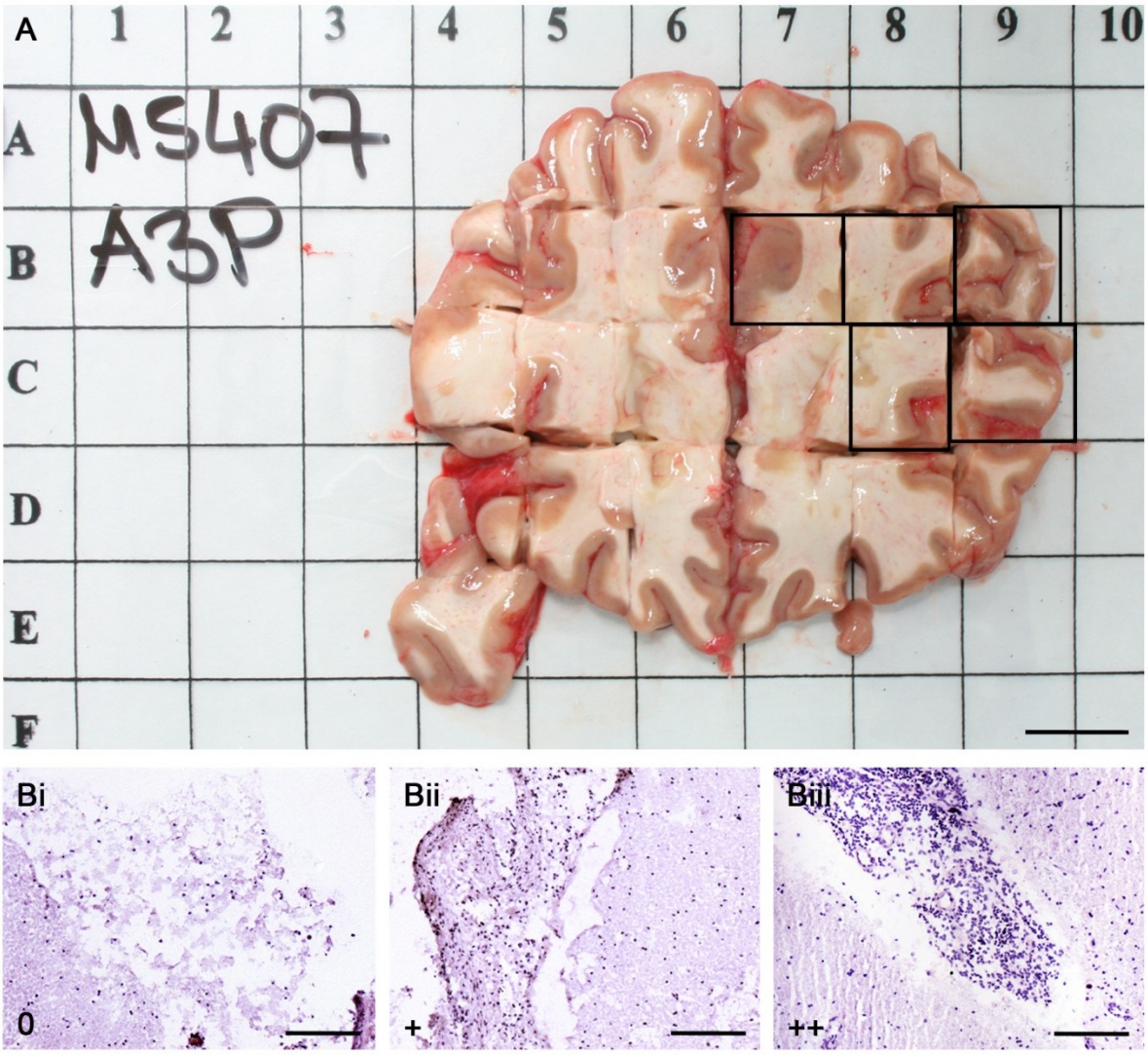

Figure 5.2.1. Block selection and screening. Cortical tissue blocks were taken from whole coronal slices taken at the time of dissection of fresh tissue (A). Blocks were selected based on the presence of well demarcated sulci, including the cingulate, inferior frontal, lateral, insular and superior temporal sulci contained in the boxed blocks. Scale bar = 2cm. Sections cut from each block were stained with H&E and assigned an index of inflammation based on the maximum density of meningeal infiltrates observed (0, mild (Bi); +, moderate (Bii); ++, severe (Biii)). Scale bar = 200μm.

5.2.1.4 Identification of B cells in meningeal infiltrates and demyelination

In order to identify B cells, the main component of lymphoid-like structures, IHC for CD20 was performed on sections from blocks assigned an index of inflammation of ++. Sections were immersed in 0.3% (v/v) hydrogen peroxide in methanol for 10 minutes to simultaneously fix the tissue and destroy its endogenous peroxidase activity. Sections were blocked with 5% (v/v) NHS in PBST for 60 minutes and incubated with anti-CD20 primary antibody (ScyTek Laboratories Inc, Logan, Utah, USA) overnight at 4°C. Sections were incubated with horse anti-mouse biotinylated secondary antibody at 1:500 in 3% (v/v) NHS in PBST for 60 minutes followed by ABC for 60 minutes. Sections were developed with DAB and counterstained with haematoxylin as described in 5.2.1.3. PBST washes were performed between incubations, which were performed at room temperature unless otherwise stated.

In order to identify areas of demyelination, IHC for MOG was performed on sections in which dense aggregates of CD20+ B cells had been identified in the meninges, using the same protocol as that for CD20, but using MOG primary antibody at 1:20.

5.2.1.5 Correlations

GraphPad Prism 5 was used to construct graphs and perform statistical analysis to determine associations between the presence of lymphoid-like structures in F+ SPMS cases and clinical variables. These included age of onset, age at progression to SPMS, age at which the patient required the use of a wheelchair and age of death as well as the number of years between these disease milestones. A Mantel-Cox test was performed to determine whether Kaplan-Meier survival curves of these clinical variables were significantly different for F+ SPMS cases compared to F- SPMS cases. A Mann-Whitney *U* test was also performed on the corresponding column data, which is presented as mean ± SEM. A p value of <0.05 was considered to be statistically significant.

5.2.2 Meningeal PCR

5.2.2.1 Meningeal dissection

Meninges were dissected from tissue blocks in a cryostat at -20°C. A sterile scalpel was used to dissect 100-250mg of meninges, avoiding GM, from varying numbers of blocks per case, which were placed in RNase-free microfuge tubes (Ambion from Life Technologies) on dry ice and stored at -80°C. All equipment was cleaned with RNaseZap (Ambion) and ethanol prior to use.

5.2.2.2 RNA extraction

RNA was extracted from dissected meninges using an RNeasy Lipid Tissue Mini Kit (Qiagen) according to manufacturer's instructions. Samples were removed from storage, placed on dry ice and homogenised with QIAzol Lysis Reagent (Qiagen; 1ml per 100mg sample) for 30 seconds using a rotor stator homogeniser (IKA, Staufen, Baden-Württemberg, Germany), followed by incubation for 5 minutes at room temperature to allow dissociation. Cell debris was removed by centrifugation (12,000*g*, 5 minutes, 4°C) and a volume of chloroform (Sigma-Aldrich) equal to 20% of the volume of supernatant recovered was added. Samples were shaken vigorously for 15 seconds followed by incubation for 3 minutes at room temperature. The upper aqueous layer containing RNA was removed following centrifugation (12,000*g*, 15 minutes, 4°C). A volume of ethanol equal to the volume recovered was added and the sample vortexed prior to being transferred to an RNeasy Mini spin column. Centrifugation (≥8,000*g*, 15 seconds, room temperature) was repeated, discarding the flow-through, until the whole sample had been transferred to the column. The membrane was washed by the addition of a buffer supplied by the manufacturer followed by centrifugation (≥8,000*g*, 15 seconds, room temperature). Contaminating genomic deoxyribonucleic acid (gDNA) was removed using the RNase-Free DNase Set (Qiagen). Briefly, DNase I incubation mix was added to the membrane and incubated for 15 minutes at room temperature followed by washing of the membrane as described above. RNA was

eluted from the membrane by the incubation of RNase-free water (Sigma-Aldrich) on the membrane for 1 minute followed by centrifugation (≥8,000*g*, 1 minute). In order to increase the concentration of RNA, the above step was repeated using the flow-through. Eluted RNA was stored at -80°C.

5.2.2.3 Concentration and integrity of RNA

The concentration of eluted RNA was determined by measuring the absorbance at 260nm using a spectrophotometer (ND-1000; NanoDrop).

The integrity of eluted RNA was determined using an RNA 6000 Nano Kit (Agilent Technologies, Santa Clara, California, USA) with a 2100 Bioanalyser (Agilent) according to manufacturer's instructions. The 2100 Expert Software algorithm uses a trained, artificial neural network to calculate an RNA integrity number (RIN) based on the integration of informative features extracted from the electropherogram. These features may include the total RNA ratio (area of ribosomal bands:area of electropherogram), the height of the peak corresponding to 18S ribosomal RNA, the fast area ratio (area of fast region:area of electropherogram) and the height of the lower marker (Imbeaud *et al.*, 2005).

5.2.2.4 Reverse transcription

Complementary DNA (cDNA) was reverse transcribed from the eluted RNA using an RT^2 First Strand Kit (SABiosciences from Qiagen) according to manufacturer's instructions. One µg of RNA was reverse transcribed for each sample. Briefly, gDNA elimination mix was incubated for 5 minutes at 42°C and immediately placed on ice. Reverse-transcription (RT) mix was added to the gDNA elimination mix and incubated at 42°C for 15 minutes and then at 95°C for 5 minutes to stop the reaction. RNase-free water was added and the cDNA was stored at -20°C.

5.2.2.5 RT^2 Profiler PCR Array real-time PCR

PCR components mix was prepared by the addition of RT^2 SYBR Green Mastermix (SABiosciences) and RNase-free water to cDNA according to manufacturer's instructions. The PCR components mix was added to the Human Inflammatory Cytokines and Receptors RT^2 Profiler PCR Array (Format A; SABiosciences; 25µl per well). This 96-well array includes SYBR Green-optimised primer assays for the genes and RT controls shown in Table 5.2.2. The array was sealed, centrifuged (1000*g*, 1 minute, room temperature) and placed in the real-time cycler (Stratagene Mx3000P; Agilent). The cycling conditions used are described in Table 5.2.3. One array was run per case.

5.2.2.6 Real-time PCR data analysis

At the end of the run, the threshold cycle (C_T) for each well was calculated using the cycler software (MxPro; Agilent). The baseline was defined by using the automated baseline option and the threshold was defined manually by using the log view of the amplification plots, ensuring that it was above the baseline but within the lower one-third to one-half of the linear phase of the amplification plot and that it was constant across all arrays.

Selection of housekeeping genes (HKGs)

The optimal HKG(s) of the five included in the PCR array; ACTB (β-actin), B2M (β2 microglobulin), GAPDH (glyceraldehyde 3-phosphate dehydrogenase), HPRT1 (hypoxanthine phosphoribosyltransferase 1) and RPLP0 (ribosomal protein, large, P0); was determined using BestKeeper. This is a Microsoft Excel-based tool that uses repeated pairwise correlation analysis (Pfaffl *et al.*, 2004). Highly correlated HKGs are then combined by taking the geometric mean (validated by Vandesompele *et al.*, 2002) to give the BestKeeper. Further pairwise correlation analysis is performed between each HKG and the BestKeeper to give an estimate of the 'power' of the HKG.

Well	Gene	Description
A01	AIMP1	Aminoacyl tRNA synthetase complex-interacting multifunctional protein 1
A02	BMP2	Bone morphogenetic protein 2
A03	C5	Complement component 5
A04	CCL1	Chemokine (C-C motif) ligand 1
A05	CCL11	Chemokine (C-C motif) ligand 11
A06	CCL13	Chemokine (C-C motif) ligand 13
A07	CCL15	Chemokine (C-C motif) ligand 15
A08	CCL16	Chemokine (C-C motif) ligand 16
A09	CCL17	Chemokine (C-C motif) ligand 17
A10	CCL2	Chemokine (C-C motif) ligand 2
A11	CCL20	Chemokine (C-C motif) ligand 20
A12	CCL22	Chemokine (C-C motif) ligand 22
B01	CCL23	Chemokine (C-C motif) ligand 23
B02	CCL24	Chemokine (C-C motif) ligand 24
B03	CCL26	Chemokine (C-C motif) ligand 26
B04	CCL3	Chemokine (C-C motif) ligand 3
B05	CCL4	Chemokine (C-C motif) ligand 4
B06	CCL5	Chemokine (C-C motif) ligand 5
B07	CCL7	Chemokine (C-C motif) ligand 7
B08	CCL8	Chemokine (C-C motif) ligand 8
B09	CCR1	Chemokine (C-C motif) receptor 1
B10	CCR2	Chemokine (C-C motif) receptor 2
B11	CCR3	Chemokine (C-C motif) receptor 3
B12	CCR4	Chemokine (C-C motif) receptor 4
C01	CCR5	Chemokine (C-C motif) receptor 5
C02	CCR6	Chemokine (C-C motif) receptor 6
C03	CCR8	Chemokine (C-C motif) receptor 8
C04	CD40LG	CD40 ligand
C05	CSF1	Colony stimulating factor 1 (macrophage)
C06	CSF2	Colony stimulating factor 2 (granulocyte-macrophage)
C07	CSF3	Colony stimulating factor 3 (granulocyte)
C08	CX3CL1	Chemokine (C-X3-C motif) ligand 1
C09	CX3CR1	Chemokine (C-X3-C motif) receptor 1

C10	CXCL1	Chemokine (C-X-C motif) ligand 1 (melanoma growth stimulating activity, alpha)
C11	CXCL10	Chemokine (C-X-C motif) ligand 10
C12	CXCL11	Chemokine (C-X-C motif) ligand 11
D01	CXCL12	Chemokine (C-X-C motif) ligand 12
D02	CXCL13	Chemokine (C-X-C motif) ligand 13
D03	CXCL2	Chemokine (C-X-C motif) ligand 2
D04	CXCL3	Chemokine (C-X-C motif) ligand 3
D05	CXCL5	Chemokine (C-X-C motif) ligand 5
D06	CXCL6	Chemokine (C-X-C motif) ligand 6 (granulocyte chemotactic protein 2)
D07	CXCL9	Chemokine (C-X-C motif) ligand 9
D08	CXCR1	Chemokine (C-X-C motif) receptor 1
D09	CXCR2	Chemokine (C-X-C motif) receptor 2
D10	FASLG	Fas ligand (TNF superfamily, member 6)
D11	IFNA2	Interferon, alpha 2
D12	IFNG	Interferon, gamma
E01	IL10RA	Interleukin 10 receptor, alpha
E02	IL10RB	Interleukin 10 receptor, beta
E03	IL13	Interleukin 13
E04	IL15	Interleukin 15
E05	IL16	Interleukin 16
E06	IL17A	Interleukin 17A
E07	IL17C	Interleukin 17C
E08	IL17F	Interleukin 17F
E09	IL1A	Interleukin 1, alpha
E10	IL1B	Interleukin 1, beta
E11	IL1R1	Interleukin 1 receptor, type I
E12	IL1RN	Interleukin 1 receptor antagonist
F01	IL21	Interleukin 21
F02	IL27	Interleukin 27
F03	IL3	Interleukin 3 (colony-stimulating factor, multiple)
F04	IL33	Interleukin 33
F05	IL5	Interleukin 5 (colony-stimulating factor, eosinophil)
F06	IL5RA	Interleukin 5 receptor, alpha
F07	IL7	Interleukin 7

F08	IL8	Interleukin 8
F09	IL9	Interleukin 9
F10	IL9R	Interleukin 9 receptor
F11	LTA	Lymphotoxin alpha (TNF superfamily, member 1)
F12	LTB	Lymphotoxin beta (TNF superfamily, member 3)
G01	MIF	Macrophage migration inhibitory factor (glycosylation-inhibiting factor)
G02	NAMPT	Nicotinamide phosphoribosyltransferase
G03	OSM	Oncostatin M
G04	SPP1	Secreted phosphoprotein 1
G05	TNF	Tumour necrosis factor
G06	TNFRSF11B	Tumour necrosis factor receptor superfamily, member 11b
G07	TNFSF10	Tumour necrosis factor (ligand) superfamily, member 10
G08	TNFSF11	Tumour necrosis factor (ligand) superfamily, member 11
G09	TNFSF13	Tumour necrosis factor (ligand) superfamily, member 13
G10	TNFSF13B	Tumour necrosis factor (ligand) superfamily, member 13b
G11	TNFSF4	Tumour necrosis factor (ligand) superfamily, member 4
G12	VEGFA	Vascular endothelial growth factor A
H01	ACTB	Actin, beta
H02	B2M	Beta-2-microglobulin
H03	GAPDH	Glyceraldehyde-3-phosphate dehydrogenase
H04	HPRT1	Hypoxanthine phosphoribosyltransferase 1
H05	RPLP0	Ribosomal protein, large, P0
H06	HGDC	Human Genomic DNA Contamination
H07	RTC	Reverse Transcription Control
H08	RTC	Reverse Transcription Control
H09	RTC	Reverse Transcription Control
H10	PPC	Positive PCR Control
H11	PPC	Positive PCR Control
H12	PPC	Positive PCR Control

Table 5.2.2. RT^2 Profiler PCR Array Human Inflammatory Cytokines and Receptors gene table.

Cycles	Duration	Temperature / °C
1	10 minutes	95
40	15 seconds	95
	1 minute	60

Table 5.2.3. Cycling conditions for RT^2 Profiler PCR Array using Stratagene Mx3000P.

The results of the BestKeeper analysis are shown in Table 5.2.4. Primary estimates of HKG stability were obtained based on standard deviation and coefficient of variance. These values were low for all HKGs, indicating that the stability of these genes was high between cases. Similarly, the Pearson's correlation coefficient was high, and associated with low *p* values, for all HKGs, indicating that the expression of each of these genes correlated well with the expression of the other genes and with that of the BestKeeper.

Studies have shown that the conventional use of a single HKG for normalisation may lead to large errors (Vandesompele *et al.*, 2002) and that multiple HKGs should be used. Given the BestKeeper analysis results, the five HKGs were used in combination for normalisation.

HKG	ACTB	B2M	GAPDH	HPRT1	RPLP0	BestKeeper
n	30	30	30	30	30	30
GM (C_T)	20.04	19.27	21.37	25.93	19.93	21.19
AM (C_T)	20.06	19.28	21.39	25.95	19.95	21.20
Min (C_T)	18.79	18.29	19.93	24.92	18.62	20.16
Max (C_T)	22.19	21.10	23.21	28.28	22.90	23.41
SD (± C_T)	0.62	0.53	0.62	0.63	0.63	0.53
CV (% C_T)	3.11	2.76	2.92	2.41	3.15	2.52
R	0.916	0.857	0.883	0.882	0.864	
p	0.001	0.001	0.001	0.001	0.001	

Table 5.2.4. BestKeeper determination of stable HKGs. *n,* number of samples; GM, geometric mean; AM, arithmetic mean; SD, standard deviation; CV, coefficient of variance; R, Pearson's correlation coefficient between HKG and BestKeeper.

SABiosciences software analysis

Initially, PCR data were analysed using an integrated web-based software package provided by SABiosciences, which automatically performs fold change calculations based on the $\Delta\Delta C_T$ method (Livak and Schmittgen, 2001) from uploaded raw C_T data. It also allows two groups to be compared using a *t*-test and the human gDNA contamination, RT and positive PCR control wells to be interpreted. It excludes wells for which the C_T is above 35.

REST software analysis

Subsequently, PCR data were analysed using REST 2009 (relative expression software tool; Pfaffl *et al.*, 2002), which allows two groups to be compared using a randomisation test. This test does not make distributional assumptions about the data, such as their normality; it only assumes that the treatment was randomly allocated. It randomly and repeatedly reallocates C_T values, of genes of interest and HKGs jointly, to the two groups and determines the apparent fold change based on the $\Delta\Delta C_T$ method each time. The *p* value is determined by the proportion of the apparent fold changes that are as great as those observed. Amplification efficiencies of 100% were assumed, as the manufacturer quotes a mean amplification efficiency of 99%, and 2000 randomisations were performed.

Manual analysis

Finally, PCR data were analysed manually using Microsoft Excel (Microsoft Corporation, Redmond, Washington, USA) and the $\Delta\Delta C_T$ method described in the equations below. GOI refers to gene of interest, GEOMEAN to geometric mean, HKG to housekeeping gene and FC to fold change.

$$\Delta C_T = C_{T\,GOI} - \text{GEOMEAN}(C_{T\,HKG})$$

$$\Delta\Delta C_T = \Delta C_T - \text{MEAN}(\Delta C_{T\,NNC})$$

$$FC = \frac{2^{-\Delta\Delta C_T}}{\text{MEAN}(2^{-\Delta\Delta C_T}{}_{NNC})}$$

All fold change data are presented as mean ± the SEM. GraphPad Prism 5 was used to construct graphs and perform statistical analysis. Three groups were compared using Kruskal-Wallis one-way ANOVA with Dunn's multiple comparisons test. A *p* value of <0.05 was considered to be statistically significant.

5.2.2.7 Validation quantitative PCR

In order to confirm selected results of the PCR array, PrimeTime qPCR Assays (Integrated DNA Technologies, Leuven, Belgium) were used to detect TNF, IFNG and CXCL9 in cDNA samples reverse transcribed in 5.2.2.4. GAPDH and XPNPEP1 were used as HKGs. The latter has recently been identified as a novel stable HKG in post-mortem human CNS tissue, with no known neurodegenerative or neuroinflammatory associations (Durrenberger *et al.*, 2012). Master mix (18µl) consisting of Brilliant II QPCR Low ROX Master Mix (10µl; Agilent), RNase-free water (6µl) and PrimeTime qPCR Assay probe and primers (2µl; details in Table 5.2.5) was added to each well of a 96-well microplate (Applied Biosystems from Life Technologies). cDNA (2µl per well) was added in triplicate. Pooled NNC cDNA with GAPDH assays was used as interplate calibrator and RNase-free water as blank. The plate was sealed, centrifuged (1000*g*, 1 minute, room temperature) and placed in the cycler. The cycling conditions used are described in Table 5.2.6.

Prior to running cDNA samples, 'no RT' reactions were performed using pooled F+ SPMS, pooled F- SPMS and pooled NNC RNA samples, which were run as described for all assays to confirm the absence of contaminating gDNA.

At the end of the run, the C_T for each well was calculated using the cycler software as described in 5.2.2.6.

PCR amplification efficiency and validation of $\Delta\Delta C_T$ method

The PCR amplification efficiency is the rate at which a PCR amplicon is generated. If the amount of a particular PCR amplicon doubles with each cycle, the efficiency is 100% or 2. For the $\Delta\Delta C_T$ method to be valid, the efficiency of the GOI amplification and those of the HKGs must be approximately equal. Hence a validation experiment was performed as described above using cDNA amounts spanning approximately 5 logs for each of the five

Gene	Assay name	Probe sequence 5'-3'	Primer 1 sequence 5'-3'	Primer 2 sequence 5'-3'
TNF	Hs.PT.56a.41006330	56-FAM/AGAAGATGA/ZEN/TCTGACTGCCTGGGC/3IABkFQ	TCAGCTTGAGGGTTTGCTAC	TGCACTTTGGAGTGATCGG
IFNG	Hs.PT.56a.3781960	56-FAM/TCGGTAACT/ZEN/GACTTGAATGTCCAACGC/3IABkFQ	CGACAGTTCAGCCATCACTT	GCAACAAAAAGAAACGAGATGAC
CXCL9	Hs.PT.56a.27316119	56-FAM/TCTTGCTGG/ZEN/TTCTGATTGGAGTGCA/3IABkFQ	AACAGCGACCCTTTCTCAC	AATACAGGAGTGACTTGGAACT
GAPDH	Hs.PT.53a.26759668	5HEX/CGACCAAAT/ZEN/CCGTTGACTCCGACC/3IABkFQ	GCAACAATATCCACTTTACCAGAG	CACATCGCTCAGACACCAT
XPNPEP1	Hs.PT.53a.24812694	5HEX/TGCTCTTCT/ZEN/GTGATGATGGCTGTGC/3IABkFQ	CAGTTGCTGTCCATTTGCTTG	TTGTCTCTGGATTCGATGGC

Table 5.2.5 Details of PrimeTime qPCR Assays and Primers used for validation quantitative PCR.

Cycles	Duration	Temperature / °C
1	10 minutes	95
45	15 seconds	95
	1 minute	60

Table 5.2.6. Cycling conditions for validation quantitative PCR using Stratagene Mx3000P.

assays. Pooled cDNA samples from all cases were used throughout. The efficiency, E, was calculated using the gradient of the standard curve generated by plotting C_T against log of input cDNA amount (Figure 5.2.2 A-E) and the following equation.

$$E = (10^{-1/\text{gradient}} - 1)$$

With the exception of TNF, for which amplification could only be observed at high input cDNA amounts (A), the amplification efficiencies of the other GOIs and the HKGs were good, approximately 100% (B-E). Additionally, ΔC_T as defined in 5.2.2.6 was also plotted against log of input cDNA amount and the gradient calculated, the absolute value of which

was <0.1 in a validation experiment that passed (F; Applied Biosystems, 2008). Again, with the exception of TNF, the gradient was less than 0.1 for the other GOIs and hence these validation experiments passed. The amplification efficiencies of IFNG and CXCL9 and those of GAPDH and XPNPEP1 were approximately equal and the $\Delta\Delta C_T$ method could be used for analysis in addition to the REST software, as described in 5.2.2.6.

Correlations

GraphPad Prism 5 was used to construct graphs and perform linear regression analysis to determine correlations between fold changes of IFNG and CXCL9 and the clinical variables described in 5.2.1.5. Significant correlation was said to be present if the linear regression slope was significantly non-zero with a *p* value of <0.05.

PCR specificity

In order to confirm the specificity of each of the five assays, agarose gel electrophoresis was performed. Briefly, 4µl of loading buffer was added to each 20µl PCR reaction remaining after PCR of pooled cDNA samples from all cases. Samples were run in Tris-acetate-EDTA (all Sigma-Aldrich; 1x) buffer on a 3% agarose gel with ethidium bromide for approximately 60 minutes at 90V until the bands of the ladder (10 bp DNA Ladder; Life Technologies) were well separated. Bands were visualised under ultraviolet illumination.

A single band was expected for each assay if specific. The sizes of the expected PCR amplicons were determined by finding forward and reverse primer sequences in the gene sequences obtained from NCBI databases and are shown in Table 5.2.7.

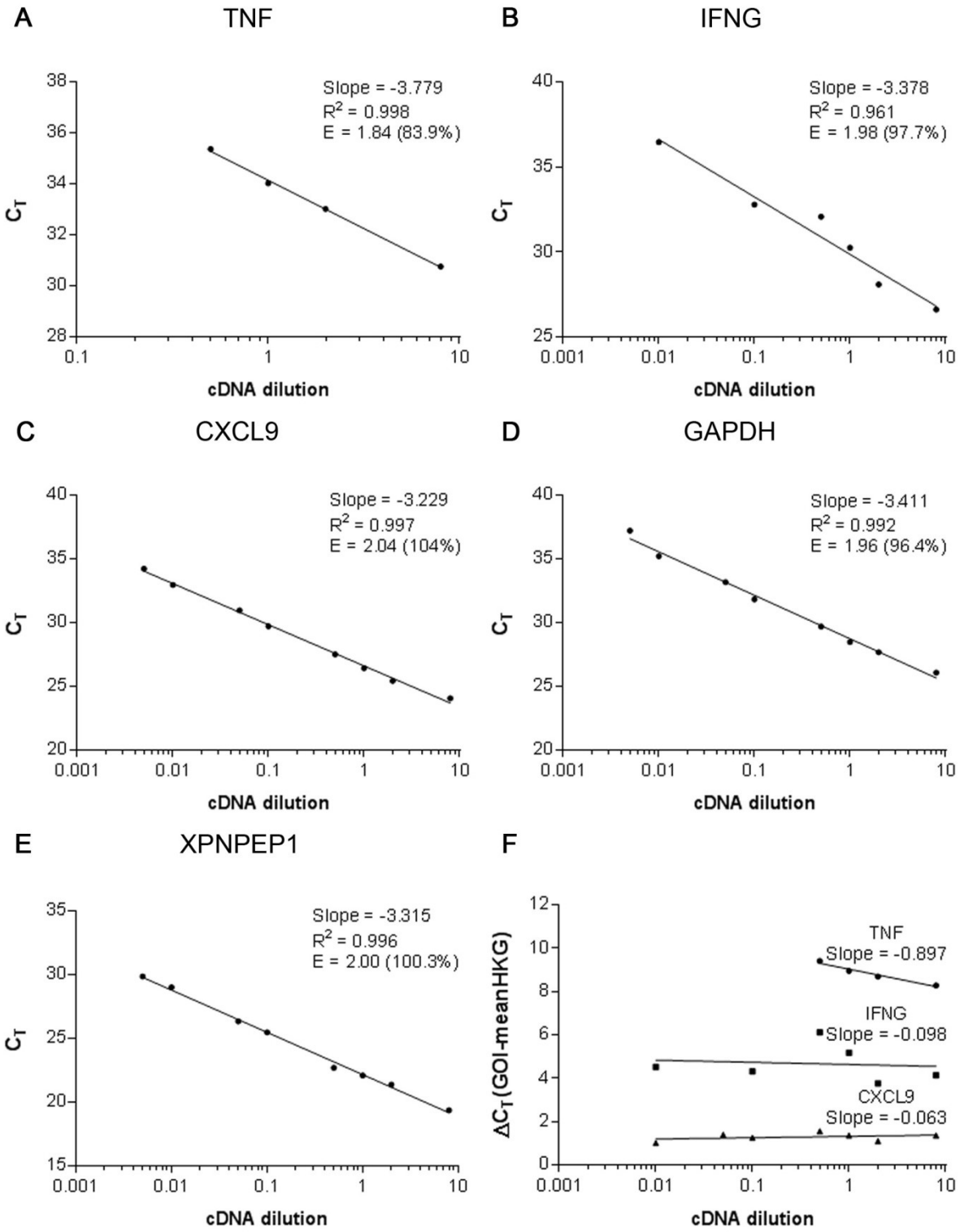

Figure 5.2.2. Determination of PCR amplification efficiency and validation of ΔΔCT method. A validation experiment was performed using input cDNA amounts spanning approximately 5 logs. Amplification efficiencies were calculated using the gradients of the standard curves generated by plotting the threshold cycle against log of input cDNA amount (A-E). The amplification efficiency of TNF was lower than that of the other GOIs and the HKGs, with amplification only observed at high input cDNA amounts (A). The amplification efficiencies of the other GOIs IFNG (B), CXCL9 (C) and the HKGs GAPDH (D) and XPNPEP1 (E) were good, approximately 100%. The difference in threshold cycle between that of the GOI and that of the geometric mean of the HKGs was also plotted against log of input cDNA amount (F). The absolute value of the gradients was less than 0.1 for IFNG and CXCL9, indicating that the ΔΔCT method could be used for analysis for these GOIs.

Gene	Expected PCR amplicon size / bp
TNF	49
IFNG	38
CXCL9	44
GAPDH	38
XPNPEP1	39

Table 5.2.7. Sizes of expected PCR amplicons for each assay.

5.2.3 CSF CXCL9 ELISA

5.2.3.1 Case selection

Aliquots of CSF, frozen in isopentane on dry ice at the time of dissection of fresh tissue and stored at -80°C, were obtained from the UK Multiple Sclerosis Tissue Bank. Cases were selected based on the availability of clear or slightly pink, rather than bloody, CSF aliquots and subsequently on post-mortem delay (PMD). Cases had previously been characterised (Howell *et al.*, 2011) as F+ SPMS (median age at death 44.5 years, range 34-59 years) or F- SPMS (median age at death 71 years, range 52-83 years). NNCs (median age at death 83.5 years, range 32-95 years) were also included (*n*=8 per group). Individual case details, including the age at which a patient received disease modifying treatment and its duration (if known) are presented in Table 5.2.8. Centrifugation (100*g*, 10 minutes, 4°C) was performed and the supernatant used in the CXCL9 ELISA.

5.2.3.2 CXCL9 ELISA

An ELISA was performed to determine the concentrations of CXCL9 in F+ and F- SPMS and NNC CSF using a Quantikine Human CXCL9/MIG kit (R&D Systems) according to manufacturer's instructions. Briefly, plates (coated with a mouse monoclonal antibody against CXCL9) were incubated with 100µl per well of CXCL9 Standards (recombinant human CXCL9; high standard 2000pg/ml, low standard 31.25pg/ml, zero standard Calibrator Diluent RD5P (2.5X)) or CSF samples in triplicate with 100µl per well of Assay Diluent RD1W for two hours. Plates were incubated with 200µl per well of Human CXCL9 Conjugate

Case	Sex	Age of death	Disease duration	Cause of death	Immunotherapy	PMD
NNC						
C5	F	95	NA	Bronchopneumonia	NA	10
C7	F	85	NA	Cancer of the oesophagus	NA	9
C8	F	93	NA	Bronchopneumonia, cerebrovascular accident	NA	9
C15	M	82	NA	Not reported	NA	21
C30	M	75	NA	Cerebrovascular accident, aspiration pneumonia	NA	17
C50	M	32	NA	Haemangiopericytoma cancer metastasised to bones	NA	6
C54	M	66	NA	Pancreatic cancer	NA	16
PDC32	F	91	NA	Not reported	NA	19
F-SPMS						
MS71	F	78	42	Metastatic carcinoma of bronchus	NA	5
MS74	F	64	36	Gastrointestinal bleed/ obstruction, aspiration pneumonia	NA	7
MS139	F	62	22	Bronchopneumonia, MS	NA	9
MS155	F	80	37	Small bowel obstruction, pleurisy, heart problems, MS	NA	13
MS158	F	78	18	Bronchopneumonia, MS	NA	5
MS288	F	83	27	Bronchopneumonia, immobility, MS	NA	12
MS304	M	52	23	Pulmonary embolism, metastatic carcinoma colon primary, MS	NA	13
MS361	F	60	34	Advanced sigmoid colon cancer, MS	NA	10
F+ SPMS						
MS46	M	40	23	Dehydration, MS	NA	18
MS79	F	49	21	Bronchopneumonia, MS	NA	7

MS154	F	34	12	Pneumonia	NA	12
MS160	F	44	16	Aspiration pneumonia, MS	NA	18
MS176	M	37	27	Intestinal obstruction, chronic MS	NA	12
MS286	M	45	16	MS	Methotrexate age 35, 24 months	7
MS402	M	46	20	MS, bronchopneumonia	NA	12
MS426	F	48	29	MS	NA	21

Table 5.2.8. Details of cases used for CSF CXCL9 ELISA. Age of death and disease duration in years; PMD, post-mortem delay in hours; M, male; F, female.

(polyclonal antibody against CXCL9 conjugated to horseradish peroxidase) for 2 hours followed by 200µl per well of Substrate Solution (tetramethylbenzidine with hydrogen peroxide) for 30 minutes in the dark and subsequent addition of 50µl per well of Stop Solution (2N sulphuric acid). Optical density was measured at 450nm and at 540nm using a VersaMax ELISA Microplate Reader and SoftMax Pro software. Washes with Wash Buffer were performed between incubations, which were performed at room temperature.

5.2.3.3 ELISA data analysis

The optical density at 540nm was subtracted from that at 450nm to correct for optical imperfections in the plate. These data were analysed using a web-based software package (elisaanalysis.com; Elisakit.com Pty Ltd, Scoresby, Victoria, Australia), which automatically calculates the mean of triplicates, subtracts the mean zero standard and performs four parameter logistic regression to fit a standard curve and subsequently calculate concentrations of CXCL9 in CSF samples. The background is defined as 3 standard deviations greater than the mean zero standard. Concentrations of CXCL9 are presented as mean ± the SEM. GraphPad Prism 5 was used to construct graphs and perform statistical analysis. Three groups were compared using Kruskal-Wallis with Dunn's multiple comparisons test.

5.2.4 CXCL9 immunofluorescence

In order to identify the presence of CXCL9, IF was performed on sections from selected blocks with substantial meningeal infiltrates resembling potential lymphoid-like structures. Human spleen sections (UK Multiple Sclerosis Tissue Bank) were used as a positive control.

Sections were immersed in -20°C acetone (Sigma-Aldrich) for 6 minutes for fixation of the tissue. Sections were blocked with 5% (v/v) NGS in PBS for 60 minutes and incubated with anti-CXCL9 primary antibody (Table 5.2.9) diluted in 1% (v/v) NGS in PBS overnight at 4°C. Sections were incubated with goat anti-rabbit biotinylated secondary antibody (Vector Laboratories) at 1:500 in the same diluent for 60 minutes followed by incubation with Alexa Fluor 546 conjugated streptavidin (Alexa Fluor Dyes) at 1:1000 for 60 minutes in the dark. Following incubation with DAPI for 5 minutes to identify cell nuclei, sections were incubated with Sudan Black B (0.5%; Molekula, Shaftesbury, Dorset, UK) for 10 minutes and mounted in Vectashield mounting medium. PBS washes were performed between incubations, which were performed at room temperature unless otherwise stated.

In order to identify the presence of T cells for which CXCL9 is a chemokine (Müller *et al.*, 2010), IF for CD4 and CD8 (Table 5.2.9) was performed using the same protocol as that for CXCL9 but replacing acetone with 4% PFA for 20 minutes and using appropriate sera and secondary antibodies.

Antigen	Cell specificity	Species	Dilution	Source
CD20	B cell	Mouse	1 in 2	ScyTek Laboratories Inc
CD4[1]	CD4+ T cell	Mouse	1 in 500	BD Pharmingen
CD8[1]	CD8+ T cell	Mouse	1 in 1000	BD Pharmingen
CXCL9[1]		Rabbit	1 in 100	Santa Cruz Biotechnology, Dallas, Texas, USA

Table 5.2.9. Primary antibodies used for IF. [1]Antigens requiring a biotinylated secondary antibody.

5.3 Results

5.3.1 Characterisation of cases for meningeal PCR

5.3.1.1 Block screening

Meningeal preservation varied between blocks but was generally good in the deep sulci, and as blocks had been selected based on the presence of deep sulci, it was concluded that sufficient meninges of good preservation could be dissected for use with RT^2 Profiler PCR Arrays and PrimeTime qPCR Assays. Blocks from F+ and F- SPMS cases and NNCs were assigned an index of inflammation based on the maximum density of meningeal infiltrates observed following H&E staining of 10μm sections (as described in Howell *et al.*, 2011). Representative images of each index are shown in Figure 5.2.1. No meningeal inflammation was observed in meninges overlying the gyri (Figure 5.3.1 Ai) or in meninges lining the sulci (Aii) in NNCs. Mild meningeal inflammation was observed at higher frequency in F+ than F- SPMS cases (Bi and Bii) and severe meningeal inflammation was observed only in F+ SPMS cases, particularly in meninges lining the sulci (Ci and Cii).

5.3.1.2 Identification of B cells in meningeal infiltrates and demyelination

In order to identify B cells, IHC for CD20 was performed on sections from blocks assigned an index of inflammation of ++ and sections from selected blocks from NNCs and F- SPMS cases. No B cells were observed in meninges in NNCs (Figure 5.3.2 A). Lymphoid-like structures identified following H&E staining (Bi) in blocks from the case with the most substantial meningeal infiltrates, MS402, contained large, dense aggregates of B cells (Bii and Biii). Lymphoid-like structures from cases with less substantial meningeal infiltrates also contained dense aggregates of B cells (Ci and Cii).

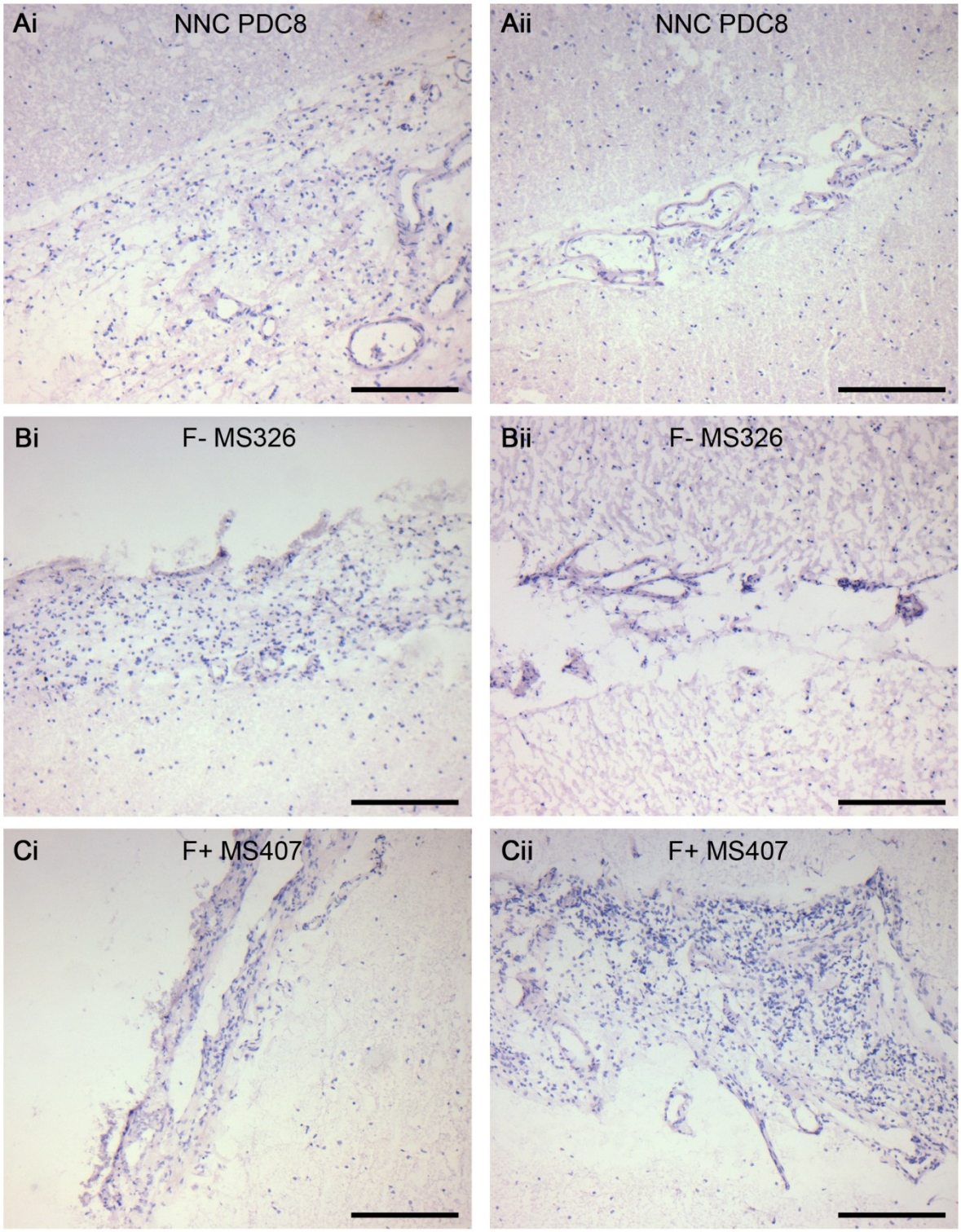

Figure 5.3.1. Severe meningeal inflammation was observed only in F+ SPMS cases. Sections were stained with H&E and blocks assigned an index of inflammation based on the maximum density of meningeal infiltrates observed. Representative images of meninges overlying the gyri (left) and meninges lining the sulci (right) are shown for one case from each group. No moderate meningeal infiltrates were observed in meninges overlying the gyri (Ai) or lining the sulci (Aii) in NNCs. Moderate infiltrates consisting of 5-50 loosely packed cells were observed at higher frequency in F+ than F- SPMS cases (Bi and Bii). Substantial infiltrates consisting of >50 densely packed cells were observed only in F+ SPMS cases, particularly in meninges lining the sulci (Ci and Cii). Scale bar: 200μm.

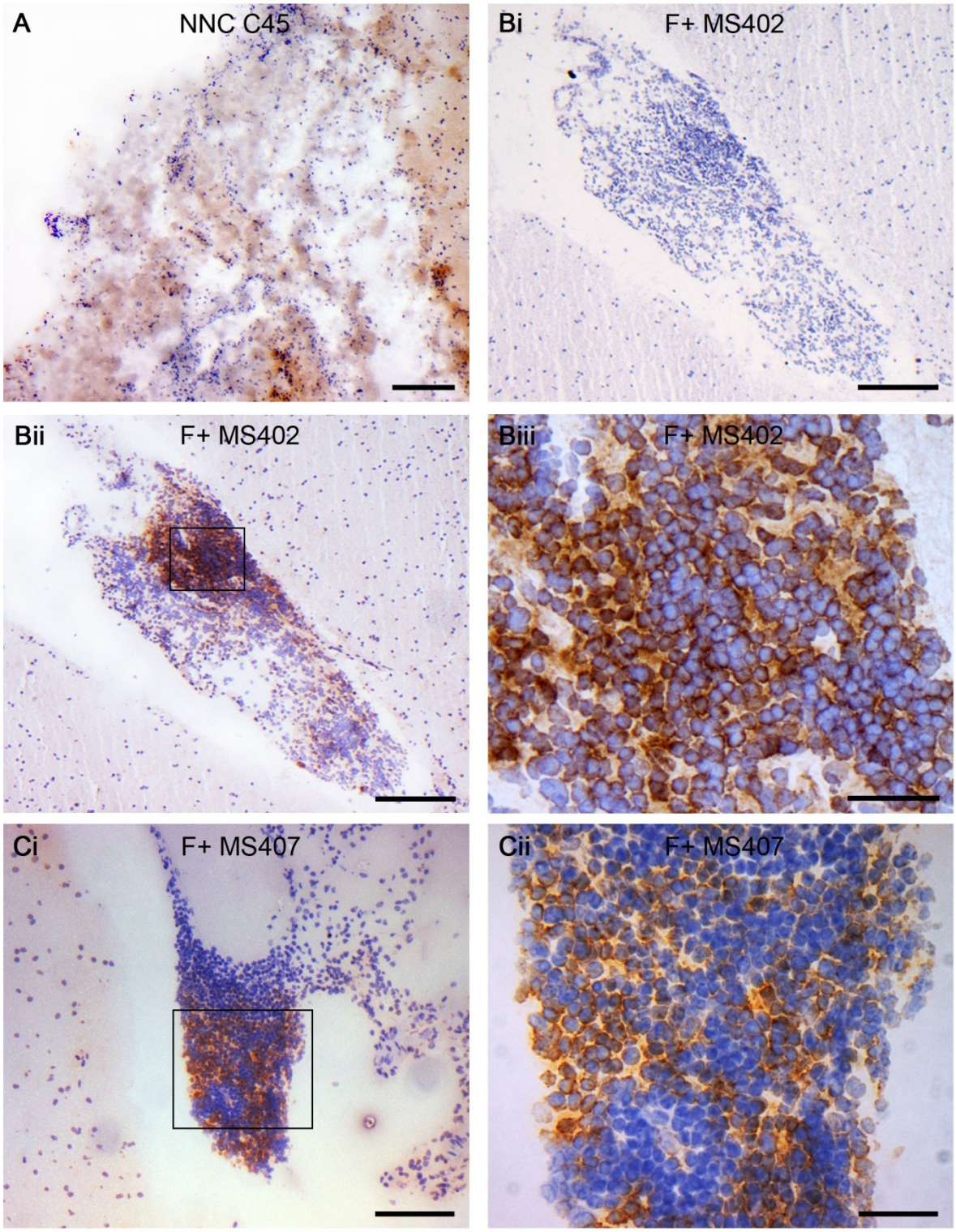

Figure 5.3.2. B cells were present in substantial meningeal infiltrates in F+ SPMS cases. IHC for CD20 was performed to identify B cells. No B cells were observed in meninges in NNCs (A), with only background staining observed following extended DAB development. A lymphoid-like structure identified following H&E staining (Bi) in a block from the case with the most severe meningeal inflammation, MS402, contained a dense aggregate of B cells within the densely packed cells of the lymphoid-like structure (Bii and Biii). A lymphoid-like structure from a case with less severe meningeal inflammation also contained densely packed B cells (Ci and Cii). Images in Biii and Cii are magnifications of the boxed areas in Bii and Ci. Scale bar: A, Bi, Bii and Ci = 200µm; Biii and Cii = 50µm.

In order to identify areas of demyelination, IHC for MOG was performed on sections in which lymphoid-like structures containing dense aggregates of CD20+ B cells had been identified and sections from selected blocks from NNCs and F- SPMS cases. No demyelination was observed in NNCs (Figure 5.3.3 A) and F- SPMS cases (B). Extensive subpial demyelination was present adjacent to lymphoid-like structures identified using the haematoxylin counterstain, which contained dense aggregates of B cells in the adjacent section, in F+ SPMS cases (C). Demyelination could affect all cortical GM layers as well as some of the underlying WM, and could extend along the entire length of the sulcus.

5.3.1.3 Association of follicle status with clinical course

Kaplan-Meier survival analysis was performed to determine the association between the presence of lymphoid-like structures in F+ SPMS cases with clinical variables. The presence of lymphoid-like structures was significantly associated with a younger age at progression to SPMS (Figure 5.3.4 Bi; mean 32 years for F+ SPMS, 40 for F- SPMS), age at which the patient required the use of a wheelchair (Ci; mean 34 years for F+ SPMS, 44 for F- SPMS) and age at death (Di; mean 47 years for F+ SPMS, 55 for F- SPMS). There appeared to be trends toward younger age of onset (Ai) and shorter disease duration (Ei) as well as fewer numbers of years between all other disease milestones (data not shown) in F+ SPMS cases, although no significant associations were observed. This accelerated disease course and earlier death were also demonstrated by the corresponding Kaplan-Meier survival curves (Aii, Bii, Cii, Dii and Eii).

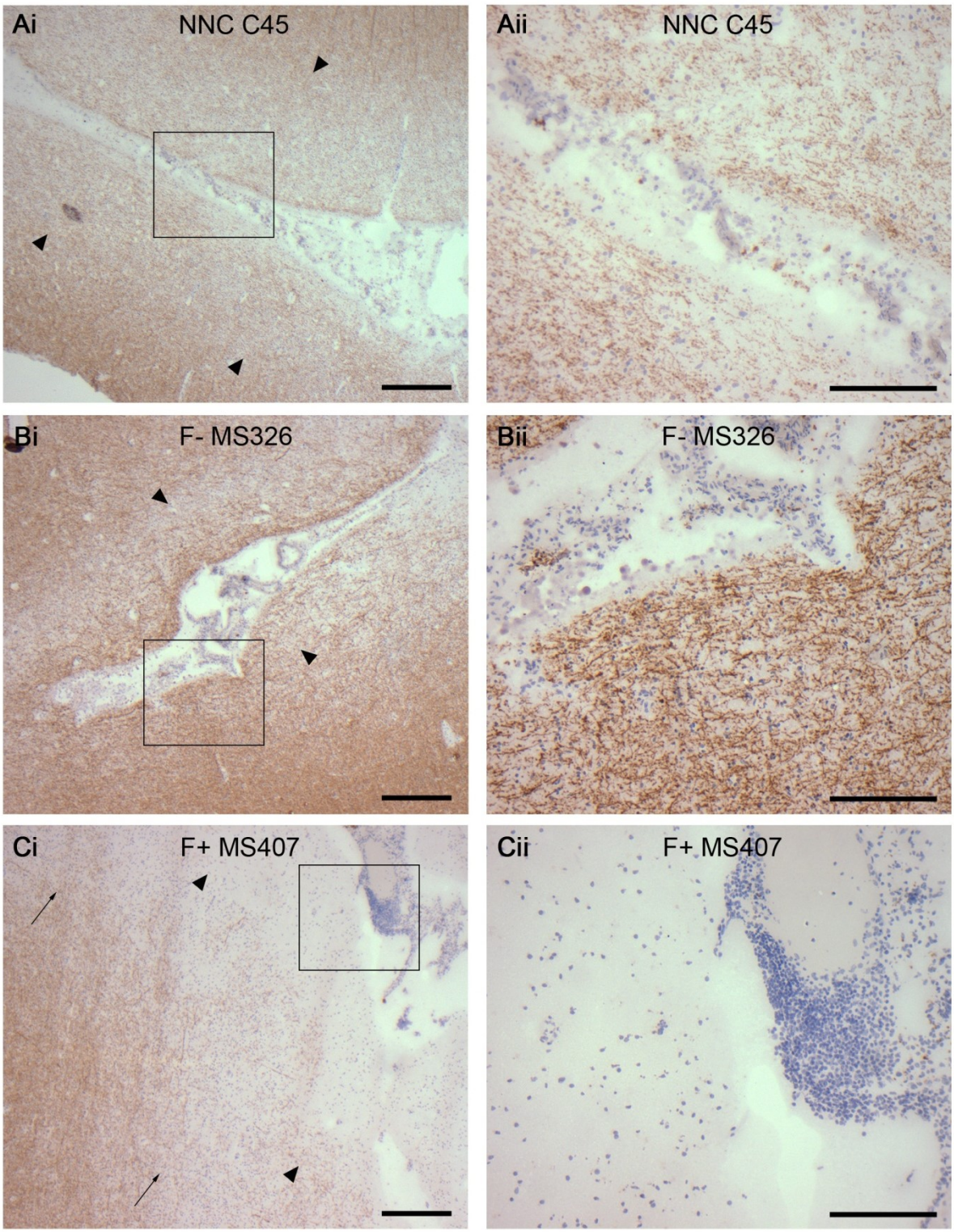

Figure 5.3.3. Lymphoid-like structures are associated with subpial demyelination in F+ SPMS cases. IHC for MOG was performed to identify areas of demyelination. No demyelination was observed in NNCs (Ai and Aii) and F- SPMS cases (Bi and Bii), with a reduced density of myelin in GM compared to WM. Subpial demyelination was present adjacent to lymphoid-like structures in F+ SPMS cases (Ci and Cii; lesion border indicated by arrows). Demyelination is present along the length of the sulcus pictured and affects all of the GM as well as some of the WM, in which the density of myelin is reduced. GM border with WM is indicated by arrowheads. Images on the right are magnifications of the boxed areas in those on the left. Scale bar: Ai, Bi and Ci = 500μm; Aii, Bii and Cii = 200μm.

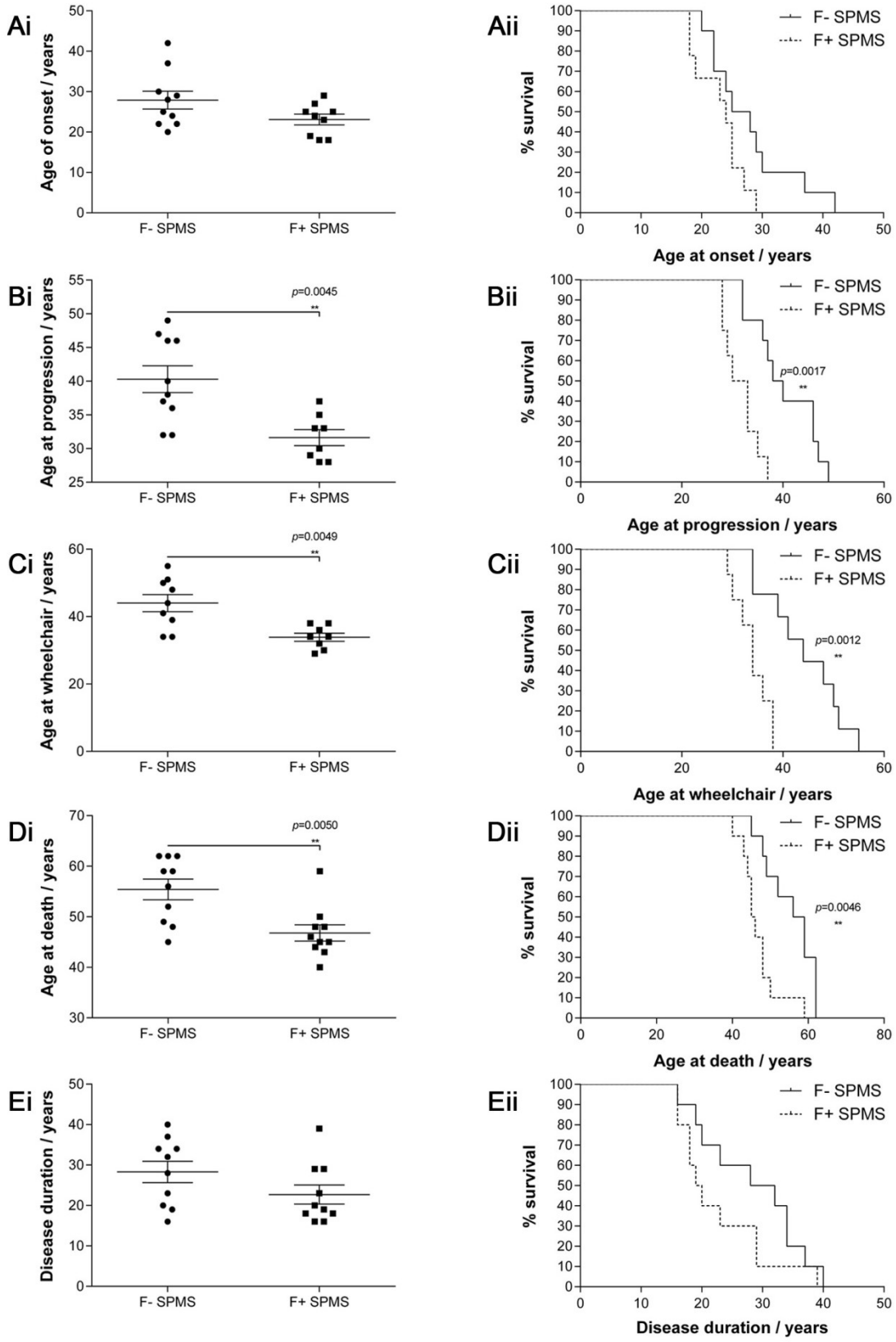

Figure 5.3.4. The presence of lymphoid-like structures is associated with a more severe clinical course. The age at progression (Bi), age at wheelchair use (Ci) and age at death (Di) were all lower in the F+ SPMS group compared to the F- SPMS group (Mann-Whitney *U*; mean ± SEM; ** = $p \leq 0.01$; n = 9-10 for F- SPMS, 8-10 for F+ SPMS). Trends toward younger age of onset (Ai) and shorter disease duration (Ei) as well as younger ages at all disease milestones and fewer numbers of years between all disease milestones (not shown) were also observed, although these did not reach significance. Data were also plotted as Kaplan-Meier survival curves (Aii, Bii, Cii, Dii and Eii; Mantel-Cox).

5.3.2 Meningeal PCR

5.3.2.1 Concentration and integrity of RNA

A total mass of 100-250mg of meninges per case was dissected from tissue blocks and RNA was extracted. The concentration of eluted RNA was determined by measuring the absorbance at 260nm using a spectrophotometer and ranged from approximately 100ng/µl for NNCs to approximately 400ng/µl for SPMS cases (Figure 5.3.5 A). All spectra displayed a single peak at 260nm corresponding to nucleic acid. Additionally, they had ratios of absorbance at 260nm to that at 280nm of 2.0 or above, indicative of RNA without protein contamination (Wilfinger *et al.*, 1997), where ratios of 1.8 or above are considered acceptable (Fleige and Pfaffl, 2006). Most samples also had ratios of absorbance at 260nm to that at 230nm also of approximately 2.0 or above, indicative of RNA without phenol/guanidine contamination from the QIAzol Lysis Reagent used during RNA extraction (Krebs *et al.*, 2009).

The integrity of eluted RNA was determined using an RNA 6000 Nano Kit with a 2100 Bioanalyser to obtain an RIN from the electrophoretic measurements recorded and automated algorithm (Schroeder *et al.*, 2006; Figure 5.3.5 B). The integrity varied between cases but was generally good, approximately 5 or above (mean 5.2 ± 0.17). Electropherograms displayed two peaks corresponding to 18S and 28S ribosomal RNA, although peaks corresponding to degradation products were also observed, which appeared earlier. Linear regression analysis showed that there was no correlation between RIN and PMD (Ci) or age at death (Cii). Additionally, no significant effect of gender (Ciii) or group (Civ) on RIN was observed.

It was concluded that sufficient eluted RNA of acceptable integrity and purity was obtained for use with RT^2 Profiler PCR Arrays and PrimeTime qPCR Assays. Complementary DNA was reverse transcribed from 1µg of RNA per case.

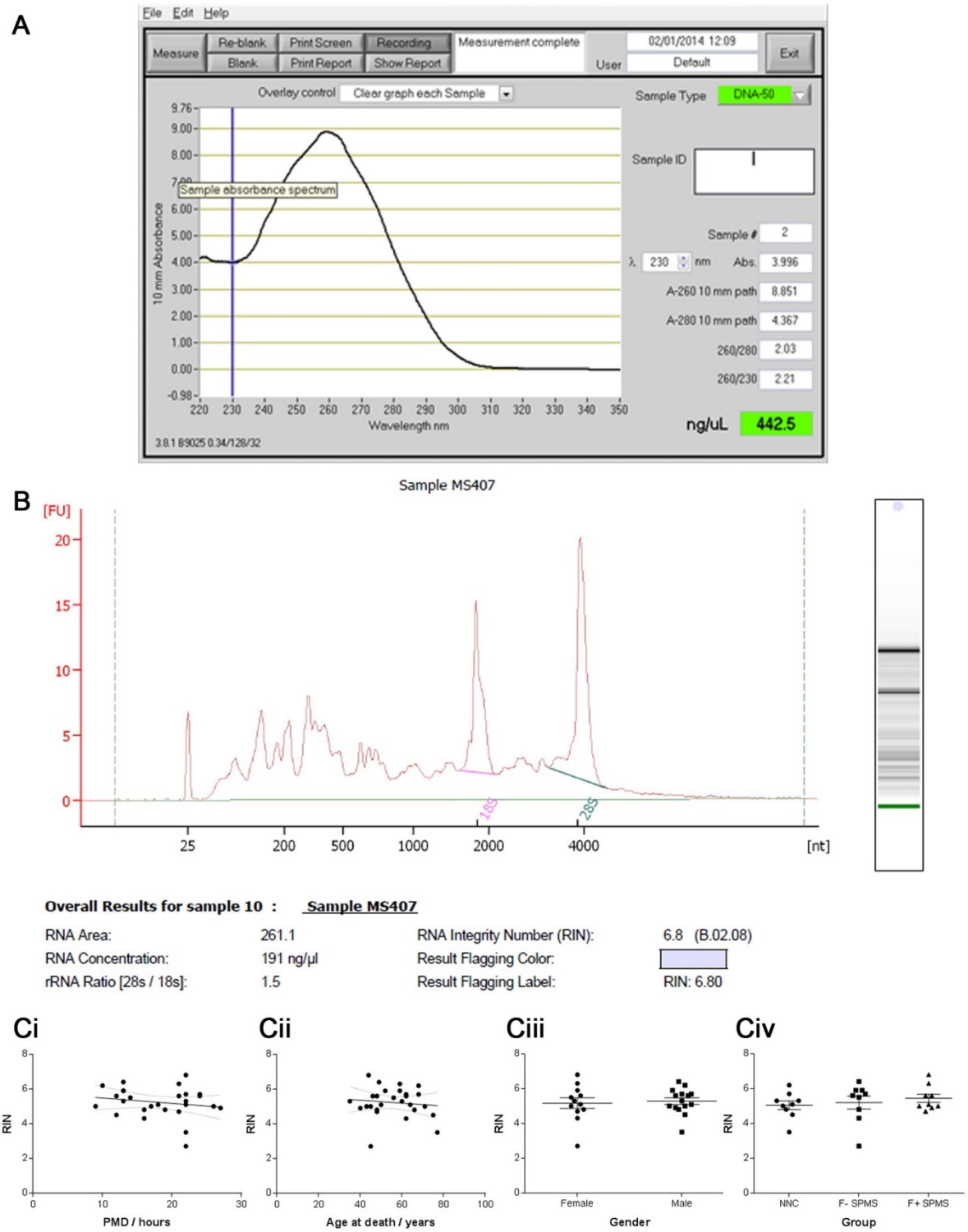

Figure 5.3.5. Determination of concentration and integrity of RNA used for meningeal PCR. The concentration of eluted RNA was determined by measuring the absorbance at 260nm using a NanoDrop spectrophotometer (A). Spectra displayed a single nucleic acid peak at 260nm. Absorbance ratios at 260nm to 280nm and 260nm to 230nm of 2.0 or above, indicative of RNA without protein and phenol/guanidine contamination respectively, were obtained. The integrity of eluted RNA was determined by obtaining an RIN (B). Electropherograms displayed 18S and 28S RNA peaks, although degradation product peaks were also observed earlier in electropherograms. The spectrum (A) and electropherogram (B) are representative. There was no effect on RIN of PMD (Ci), age at death (Cii; linear regression slopes not significantly non-zero), gender (Ciii; Mann-Whitney *U*) or group (Civ; Kruskal-Wallis with Dunn's multiple comparisons test; mean ± SEM).

5.3.2.2 Case exclusion

The neuropathology report for PDC36 became available only after the RT^2 Profiler PCR Arrays and PrimeTime qPCR Assays had been performed. A neuropathological diagnosis of 'multiple deposits of metastatic carcinoma consistent with primary breast cancer' was made. Exclusion criteria for meningeal PCR included metastatic carcinoma, as concentrations of both pro- and anti-inflammatory cytokines and angiogenic factors have been shown to be dysregulated, for example in serum from glioblastoma patients (Albulescu *et al.*, 2013). Hence data obtained using RNA from PDC36 were excluded from the analysis and are not included in the results presented below.

5.3.2.3 RT^2 Profiler PCR Array

One Human Inflammatory Cytokines and Receptors array was run per case. At the end of the run, the C_T for each well was calculated using the cycler software. The threshold was defined manually and was constant at 1000 fluorescence units for all arrays (Figure 5.3.6).

SABiosciences software analysis

Initially, PCR data were analysed using an integrated web-based software package provided by SABiosciences, which automatically performed fold change calculations based on the $\Delta\Delta C_T$ method from uploaded raw C_T data. It also allowed comparison of two groups using *t*-tests and interpretation of human gDNA contamination, RT and positive PCR control wells.

All human gDNA contamination control wells had C_T values greater than or equal to 35, indicating the absence of gDNA contamination in cDNA from all cases. The ΔC_T (GEOMEAN($C_{T\ \text{RT CONTROL}}$) – GEOMEAN($C_{T\ \text{POSITIVE PCR CONTROL}}$)) was less than or equal to 5 for all cases, indicating efficient RT reactions. Finally, the mean positive PCR control well C_T was 20±2 for all cases and no two arrays differed in this value by more than 2, indicating good array reproducibility.

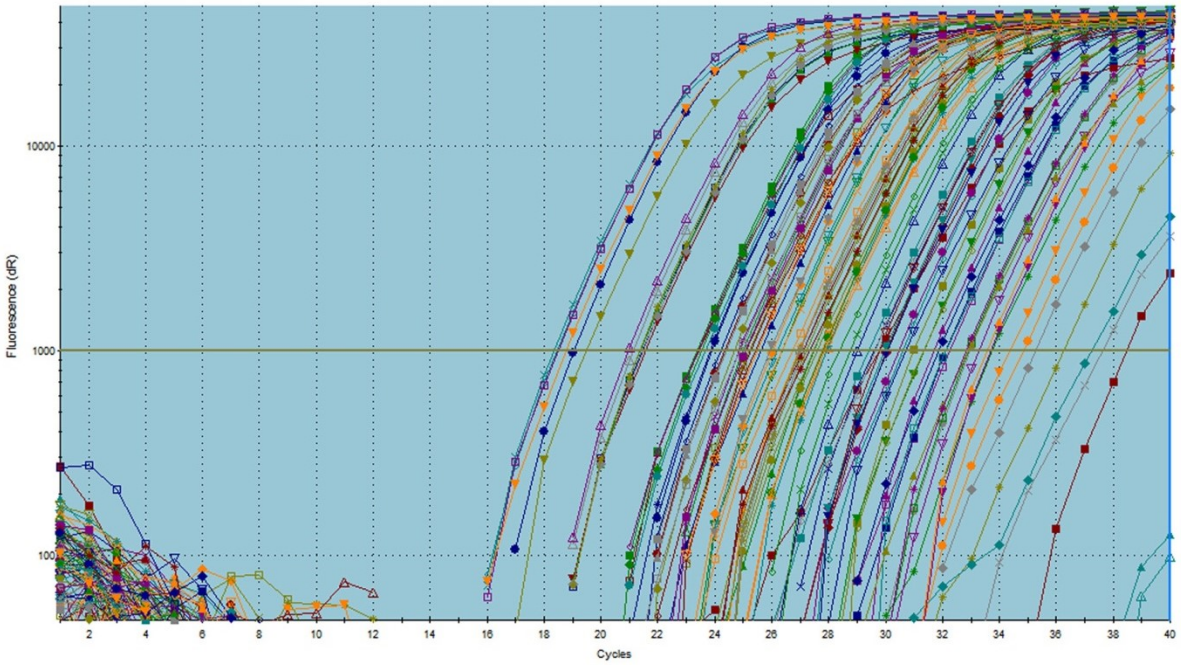

Figure 5.3.6. Representative PCR array amplification plot. The threshold cycle for each well was calculated using the cycler software MxPro. The threshold was defined manually by using the log view of the amplification plot, ensuring that it was above the baseline but within the lower one-third to one-half of the linear phase and constant at 1000 fluorescence units across all arrays.

Both F+ and F- SPMS groups were compared to the NNC group and the F+ SPMS group was also compared to the F- SPMS group using *t*-tests. The statistically significant fold changes are summarised in Table 5.3.1 and are expressed as fold regulations. Fold change values greater than one indicate upregulation, in which case fold regulation is equal to fold change (red in the Table). Fold change values less than one indicate downregulation, in which case fold regulation is equal to the negative inverse of fold change (green in the Table). Seven genes were upregulated and 4 downregulated in the F+ SPMS group compared to the NNC group, 1 gene was downregulated in the F- SPMS group compared to the NNC group and 4 genes were upregulated and 1 downregulated in the F+ SPMS group compared to the F- SPMS group.

REST software analysis

Subsequently, PCR data were analysed using REST 2009, which allowed two groups to be compared using a randomisation test. Amplification efficiencies of 100% were assumed, as the manufacturer quotes a mean amplification efficiency of 99%, and 2000 randomisations were performed.

As for the analysis using the SABiosciences software package, both F+ and F- SPMS groups were compared to the NNC group and the F+ SPMS group was also compared to the F- SPMS group. The statistically significant fold changes are summarised in Table 5.3.2 and Figure 5.3.7 and are again expressed as fold regulations. Eight genes were upregulated and 2 downregulated in the F+ SPMS group compared to the NNC group and 4 genes were upregulated and 1 downregulated in the F+ SPMS group compared to the F- SPMS group. No significant fold changes were obtained when the F- SPMS group was compared to the NNC group.

	F+ SPMS v NNC		F- SPMS v NNC		F+ SPMS v F- SPMS	
Gene	Fold regulation	*p* value	Fold regulation	*p* value	Fold regulation	*p* value
CCR2	2.4750	0.011672				
CCR3	2.2664	0.034785				
CCR4	3.3862	0.024342				
CCR5	1.9160	0.013963				
CXCL13	6.3967	0.060859			5.4369	0.031729
CXCL9	7.7596	0.036981			8.8139	0.035405
IFNG	2.4941	0.029480			2.6478	0.026260
IL10RA					1.5155	0.037191
IL5RA	5.2230	0.000317				
CCL15	-2.6464	0.044652			-2.4086	0.027460
CXCL1	-2.6549	0.012672	-1.7129	0.046490		
CXCL2	-2.0121	0.048616				
CXCL3	-1.9174	0.042616				

Table 5.3.1. Results of analysis using the SABiosciences software package. The statistically significant fold regulations and associated *p* values of F+ SPMS v NNC, F- SPMS v NNC and F+ SPMS v F- SPMS comparisons calculated using *t*-tests are shown. Fold regulations in red indicate upregulation and those in green downregulation.

	F+ SPMS v NNC		F+ SPMS v F- SPMS	
Gene	Fold regulation	*p* value	Fold regulation	*p* value
CCR3	2.416	0.032		
CCR4	4.643	0.002	2.255	0.032
CCR5	1.933	0.028		
CXCL13	6.438	0.026	5.803	0.016
CXCL9	7.828	0.011	8.895	0.003
IL5RA	4.896	0.000	2.242	0.043
LTA	2.310	0.050		
LTB	2.012	0.043		
CCL15	-3.257	0.047	-2.959	0.025
CXCL1	-2.632	0.011		

Table 5.3.2. Results of analysis using REST. The statistically significant fold regulations and associated *p* values of F+ SPMS v NNC and F+ SPMS v F- SPMS comparisons calculated using randomisation tests are shown. Fold regulations in red indicate upregulation and those in green downregulation.

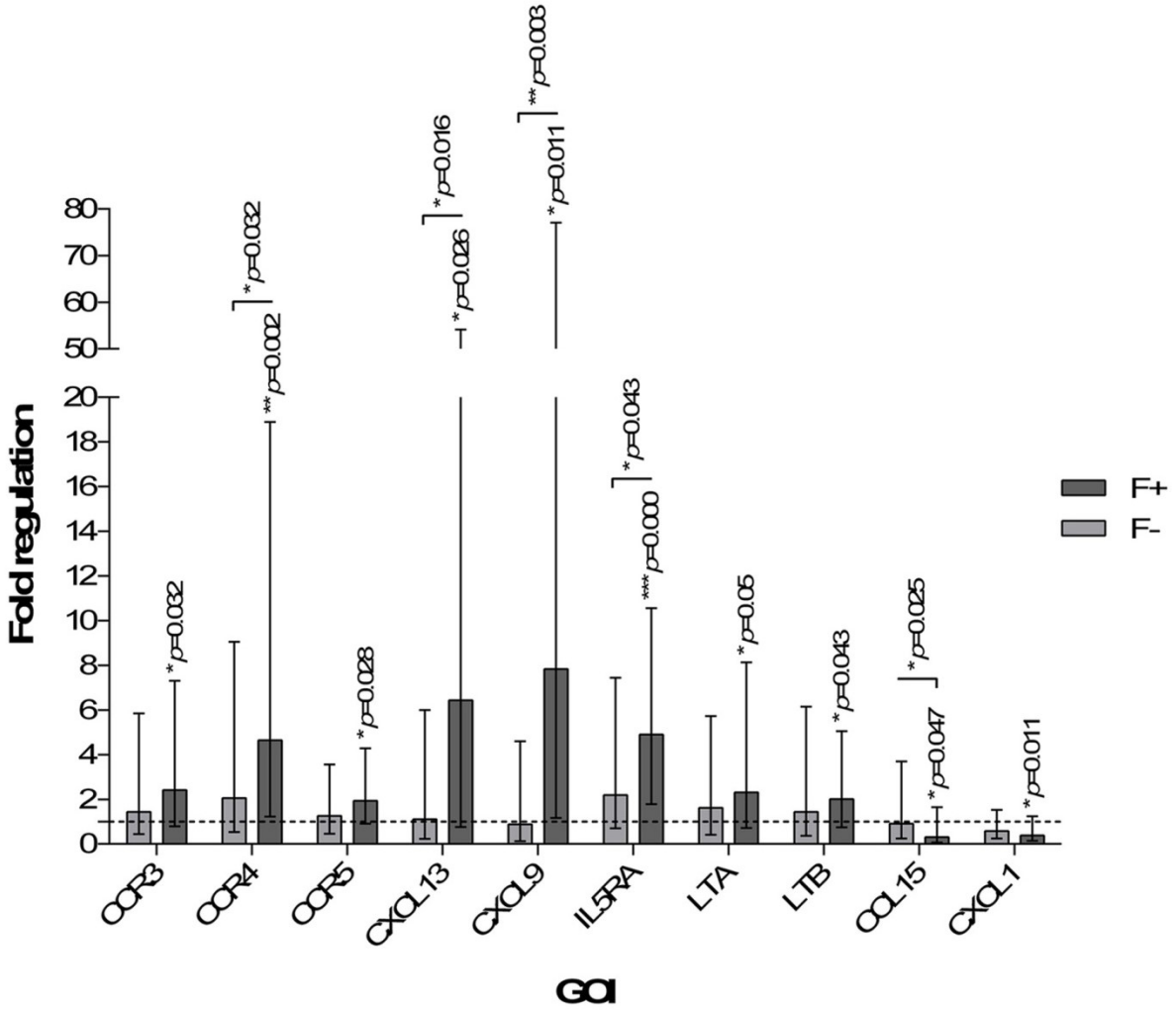

Figure 5.3.7. Results of analysis using REST 2009 software. Statistically significant fold regulations are shown. The horizontal dotted line at a fold regulation of 1 indicates the NNC group. *p* values above the F+ SPMS group indicate the significance of the F+ SPMS v NNC fold regulation. No significant fold regulations were obtained when the F- SPMS group was compared to the NNC group (randomisation test; mean ± SE range; * = $p \leq 0.05$, ** = $p \leq 0.01$, *** = $p \leq 0.001$; $n = 9$ for NNC, 10 for F- and F+ SPMS).

Manual analysis

Finally, PCR data were analysed manually using Microsoft Excel and the $\Delta\Delta C_T$ method. Mean C_T values and fold changes are shown in Table 5.3.3. GraphPad Prism was used to construct graphs and perform statistical analysis of fold changes that had been found to be statistically significant by analysis using the SABiosciences software package or REST. Three groups were compared using Kruskal-Wallis with Dunn's multiple comparisons test. The statistically significant fold changes are summarised in Figure 5.3.8. Fold change values indicating upregulation are shown in A and those indicating downregulation are shown in B. Three genes were upregulated (CXCL13, fold change 5.26; CXCL9, fold change 6.03; IL5RA, fold change 5.63) and 1 downregulated (CXCL1, fold change 0.33) in the F+ SPMS group compared to the NNC group and 1 gene was upregulated (CXCL9, fold change 5.74) in the F+ SPMS group compared to the F- SPMS group. TNF and IFNG, which are used in the model of cortical pathology driven by meningeal inflammation (Gardner *et al.*, 2013), were not regulated in either SPMS group compared to the NNC group (C).

Gene	Mean C_T NNC	Mean C_T F- SPMS	Mean C_T F+ SPMS	Mean FC F- SPMS	Mean FC F+ SPMS
AIMP1	24.41	24.64	24.48	0.917	0.989
BMP2	30.51	30.68	30.85	0.871	0.745
C5	27.70	27.60	28.08	1.045	0.789
CCL1	34.42	34.05	34.15	3.177	1.132
CCL11	34.97	34.93	34.90	1.576	2.045
CCL13	33.42	33.23	32.98	1.001	1.702
CCL15	31.53	31.70	32.96	0.694	0.265
CCL16	34.47	34.32	34.70	0.918	0.548
CCL17	34.24	33.65	33.19	1.368	2.666
CCL2	26.30	26.58	26.19	0.864	0.935
CCL20	28.44	28.68	27.91	1.087	1.140
CCL22	33.89	34.65	33.50	0.231	2.285
CCL23	32.23	32.17	32.08	1.057	0.952
CCL24	34.88	34.69	34.72	1.137	1.096
CCL26	29.86	29.51	30.10	1.143	0.730
CCL3	28.13	28.38	27.61	1.033	0.787
CCL4	25.66	25.90	24.95	1.024	1.532
CCL5	25.47	25.33	24.65	1.169	1.666
CCL7	34.74	34.36	33.98	1.805	3.578
CCL8	34.97	34.89	35.00	2.185	1.514
CCR1	28.46	28.34	28.52	1.358	0.893
CCR2	29.77	28.69	28.44	2.981	2.656
CCR3	33.59	32.85	32.37	2.238	2.529
CCR4	32.16	30.85	30.12	1.616	2.913
CCR5	28.27	27.87	27.25	1.639	1.999
CCR6	32.04	32.16	31.56	0.740	1.169
CCR8	34.60	34.41	34.55	1.106	0.758
CD40LG	31.61	31.78	31.21	0.870	1.276
CSF1	25.47	25.67	26.19	0.789	0.521
CSF2	30.27	30.18	30.39	1.269	0.964
CSF3	26.02	27.00	27.52	0.319	0.264
CX3CL1	27.56	28.11	28.22	0.858	0.636
CX3CR1	31.41	31.72	31.30	0.862	1.177
CXCL1	23.54	24.31	24.93	0.486	0.333

CXCL10	28.61	28.76	26.62	1.194	0.936
CXCL11	28.45	28.55	27.23	2.174	1.007
CXCL12	25.10	25.23	25.03	1.054	1.103
CXCL13	33.88	33.56	31.11	0.723	5.263
CXCL2	22.48	23.36	23.46	0.489	0.446
CXCL3	26.09	27.03	27.00	0.504	0.438
CXCL5	30.59	30.28	30.57	1.372	0.967
CXCL6	27.73	27.92	27.60	1.031	1.177
CXCL9	30.62	30.83	27.68	1.049	6.026
CXCR1	27.52	27.00	27.71	6.055	0.718
CXCR2	28.54	28.09	28.71	4.915	0.786
FASLG	31.40	31.46	31.11	0.945	1.326
IFNA2	32.13	33.30	33.05	0.390	0.483
IFNG	29.67	29.95	28.53	1.074	3.051
IL10RA	25.74	25.74	25.13	0.959	1.411
IL10RB	26.14	25.84	26.22	1.293	0.948
IL13	33.12	33.05	33.23	1.131	0.919
IL15	27.35	27.44	27.09	0.957	1.302
IL16	28.90	28.23	28.49	1.452	1.360
IL17A	34.94	35.00	32.02	0.170	1.262
IL17C	34.28	34.41	34.34	0.984	0.897
IL17F	34.67	34.45	34.34	1.126	1.485
IL1A	31.59	31.91	31.99	0.646	0.631
IL1B	28.05	27.94	28.11	1.014	0.663
IL1R1	24.05	23.99	24.46	0.985	0.743
IL1RN	27.56	26.48	27.12	2.525	1.499
IL21	34.73	34.53	32.75	0.833	9.321
IL27	33.89	33.96	33.78	1.094	0.927
IL3	35.00	34.74	34.87	3.857	2.342
IL33	26.38	26.98	26.50	0.685	0.969
IL5	29.58	30.27	29.96	0.676	0.689
IL5RA	33.84	32.60	31.44	3.463	5.627
IL7	29.70	30.44	30.20	0.834	0.916
IL8	23.37	23.10	24.01	0.905	0.534
IL9	33.79	34.19	33.48	0.360	0.949
IL9R	35.00	35.00	34.96	0.559	1.809

LTA	34.64	34.19	33.94	1.323	1.534
LTB	30.13	29.58	29.10	2.020	1.685
MIF	21.99	21.99	21.88	1.031	1.081
NAMPT	22.25	21.79	22.28	1.765	0.917
OSM	28.92	28.50	28.95	2.337	1.028
SPP1	22.26	22.36	21.64	1.221	1.915
TNF	30.98	31.05	30.60	1.158	1.728
TNFRSF11B	24.55	24.40	24.53	0.985	0.801
TNFSF10	25.21	24.91	25.35	1.160	0.801
TNFSF11	33.85	33.74	34.12	1.144	0.756
TNFSF13	31.89	31.44	32.04	1.214	0.811
TNFSF13B	28.35	27.84	28.21	3.252	0.989
TNFSF4	29.41	28.98	29.26	1.522	1.043
VEGFA	24.25	24.38	24.51	0.811	0.882

Table 5.3.3. C_T values and fold changes obtained following manual analysis using the $\Delta\Delta C_T$ method of all genes for which primer assays were included in the RT^2 Profiler PCR Array. Genes were described in Table 5.2.2. Mean C_T values of *n*=9-10 per group and mean fold changes (FC) of the F- and F+ SPMS groups compared to the NNC group are shown. Fold changes in red and green indicate statistically significant upregulation and downregulation respectively.

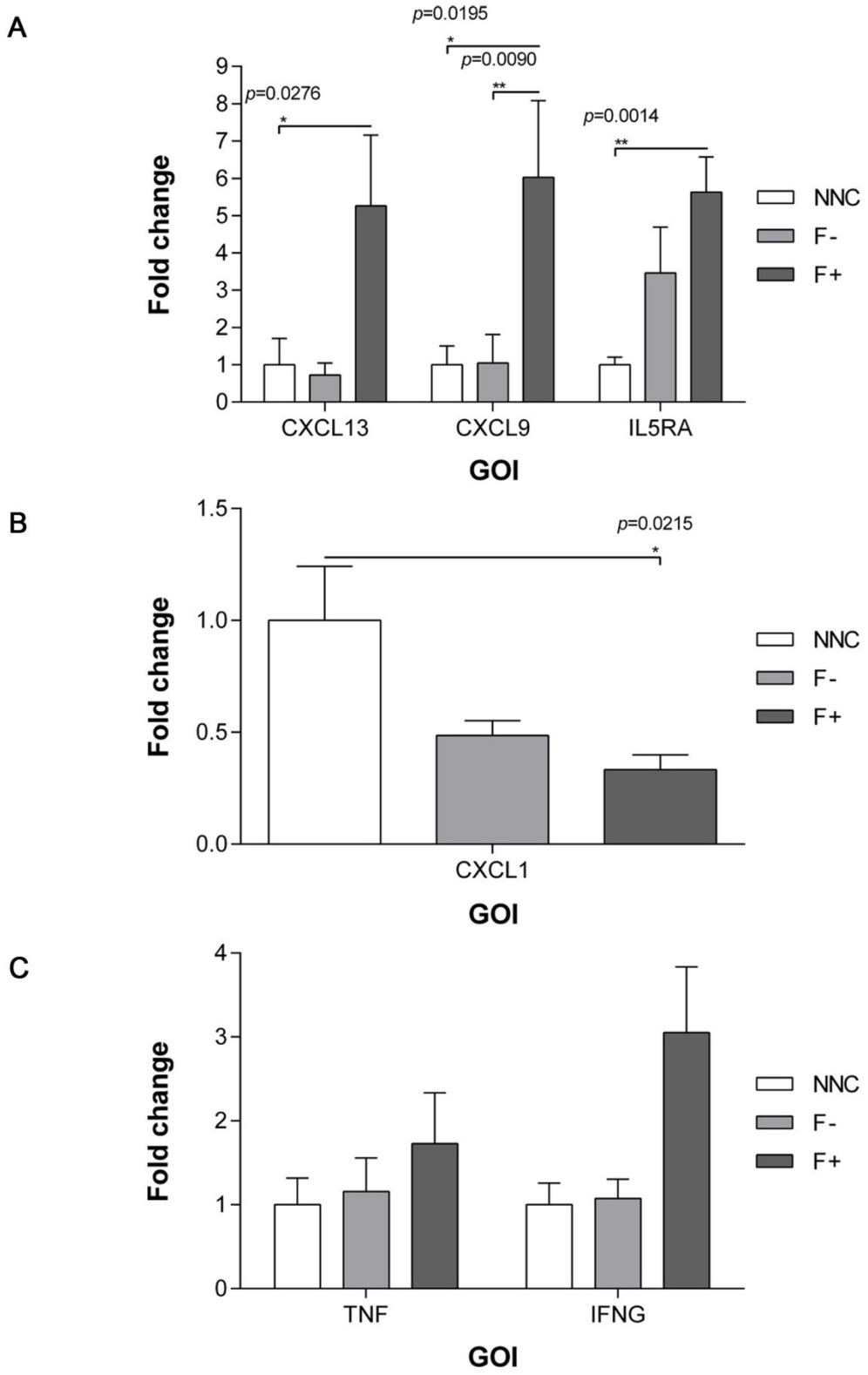

Figure 5.3.8. Results of manual analysis using Microsoft Excel and the ΔΔCT method. Statistically significant fold changes indicating upregulation (A) and downregulation (B) were calculated. Fold changes of TNF and IFNG were not statistically significant (C; Kruskal-Wallis with Dunn's multiple comparisons test; mean ± SEM; * = $p \leq 0.05$, ** = $p \leq 0.01$; n = 9 for NNC, 10 for F- and F+ SPMS).

5.3.2.4 Validation quantitative PCR

In order to confirm results obtained previously in this laboratory and establish further confidence in using TNF and IFN-γ in the model of cortical pathology driven by meningeal inflammation, as well as to confirm the CXCL9 result of the PCR arrays, PrimeTime qPCR Assays were used to detect TNF, IFNG and CXCL9 in cDNA samples. At the end of the run, the C_T for each well was calculated using the cycler software. The threshold was defined manually and was constant at 500 fluorescence units.

Prior to running cDNA samples, 'no RT' reactions were performed using pooled F+ SPMS, pooled F- SPMS and pooled NNC RNA samples, which were run for all assays. No amplification was observed, indicating the absence of gDNA contamination in cDNA. Pooled NNC cDNA with GAPDH assays was used as interplate calibrator. The standard deviation of the interplate calibrator C_T values across all 96-well microplates used was less than 0.1 cycles (0.0882), indicating good reproducibility. Finally, RNase-free water was used as a blank and no amplification was observed.

PCR specificity

In order to confirm the specificity of each of the five assays, agarose gel electrophoresis was performed (Figure 5.3.9). A single band was obtained for each assay and the sizes of the obtained PCR amplicons were equal to those expected, indicating that they were specific.

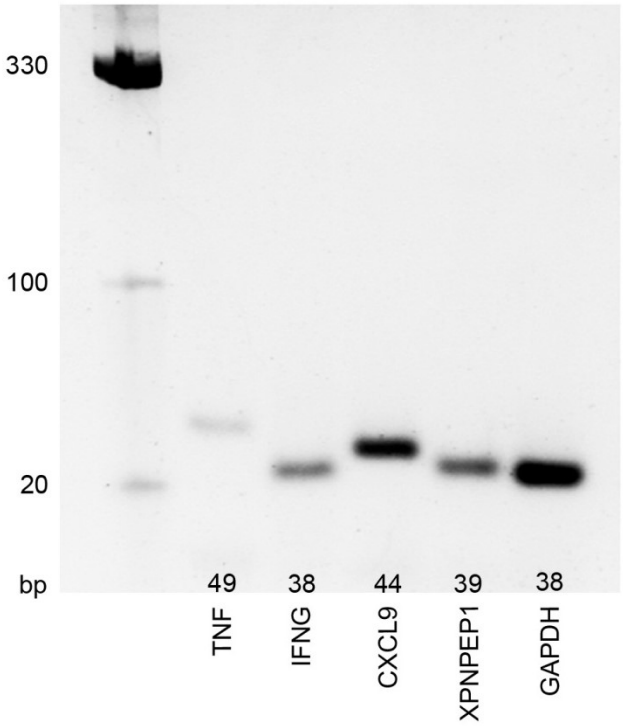

Figure 5.3.9. Confirmation of PrimeTime qPCR Assay specificity. Agarose gel electrophoresis was performed and a single band was obtained for each assay. The sizes of the PCR amplicons obtained were equal to the sizes of the PCR amplicons expected, shown in numbers of base pairs underneath the band for each assay. The ladder is shown on the left.

PCR data analysis

Initially, PCR data were analysed using REST 2009. The amplification efficiencies calculated in 5.2.2.7 were used and 2000 randomisations were performed.

F+ and F- SPMS groups were compared to the NNC group and the F+ SPMS group was also compared to the F- SPMS group. The statistically significant fold changes are summarised in Table 5.3.4. Both IFNG and CXCL9 were upregulated in the F+ SPMS group compared to both the F- SPMS group and the NNC group. No significant fold changes were obtained when the F- SPMS group was compared to the NNC group, nor when TNF was compared between groups.

Data were also analysed manually using the $\Delta\Delta C_T$ method. Fold changes of TNF (Figure 5.3.10 A; included for completeness although the validation experiment did not pass), IFNG (B) and CXCL9 (C) were calculated for each F+ and F- SPMS case and NNC. IFNG was upregulated in the F+ SPMS group compared to the F- SPMS (fold change 4.73) and NNC groups (fold change 5.70) and CXCL9 was also upregulated in the F+ SPMS group compared to both the F- SPMS (fold change 7.43) and NNC groups (D; fold change 8.80).

	F+ SPMS v NNC		F+ SPMS v F- SPMS	
Gene	Fold change	*p* value	Fold change	*p* value
IFNG	4.323	0.005	3.983	0.007
CXCL9	9.297	0.008	10.673	0.003

Table 5.3.4. Results of analysis using REST. The statistically significant fold changes and associated *p* values of F+ SPMS v NNC and F+ SPMS v F- SPMS comparisons calculated using randomisation tests are shown.

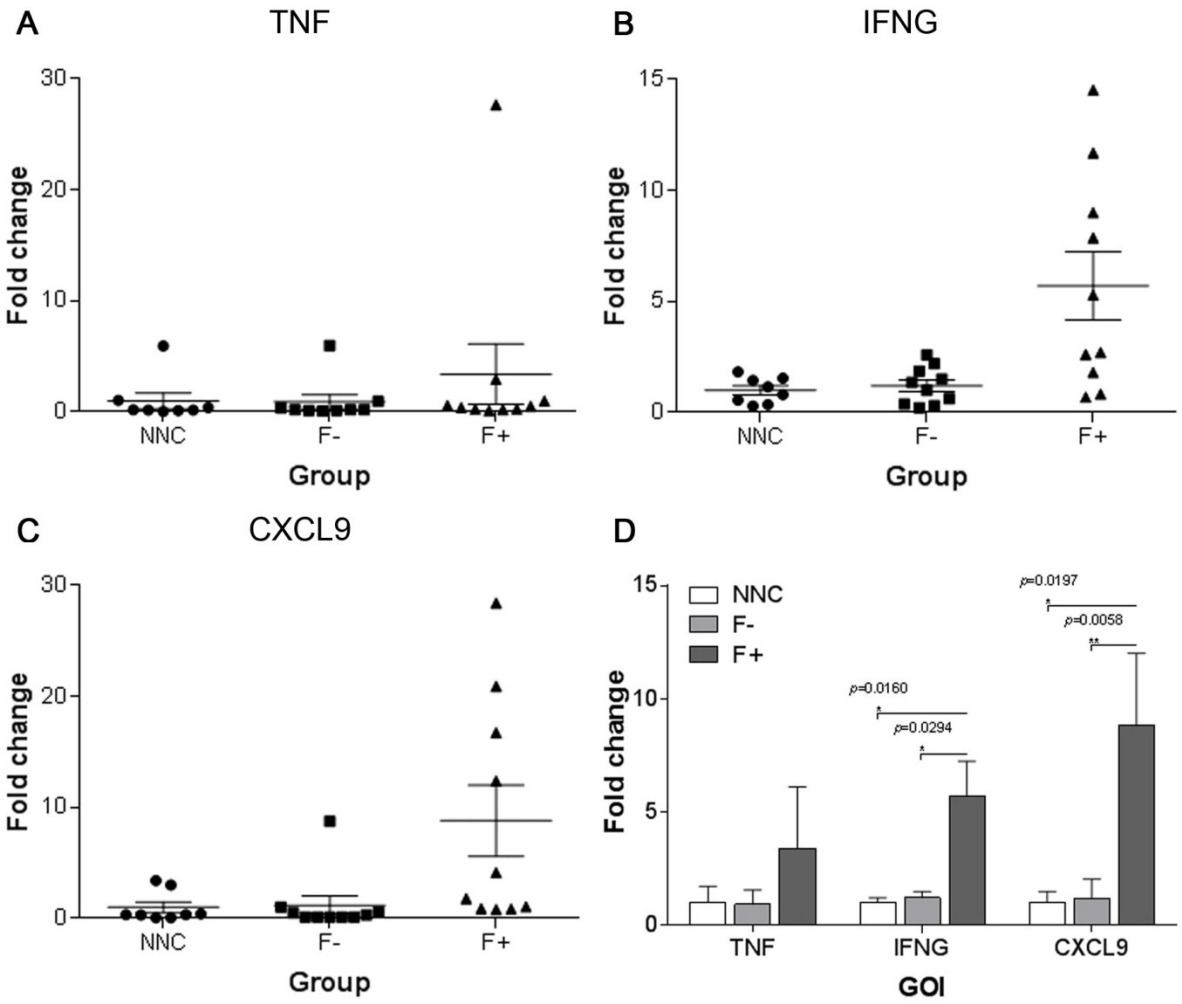

Figure 5.3.10. Results of validation PCR manual analysis using Microsoft Excel and the ΔΔCT method. Fold changes of TNF (A), IFNG (B) and CXCL9 (C) were calculated for each F+ and F- SPMS case and NNC (*n* = 8-10 per group). IFNG and CXCL9 were upregulated in the F+ SPMS group compared to both the F- SPMS and NNC groups (D; Kruskal-Wallis with Dunn's multiple comparisons test; mean ± SEM; * = $p \leq 0.05$, ** = $p \leq 0.01$; n = 8 for NNC, 10 for F- and F+ SPMS).

Clinical correlations

Linear regression analysis was performed to determine correlations between fold changes of IFNG and CXCL9 and the clinical variables described in 5.3.1.3. Although there appeared to be trends toward younger ages at disease milestones and fewer numbers of years between milestones with increasing fold changes of IFNG and CXCL9 (Figure 5.3.11 A), no significant correlations were obtained.

Given that CXCL9 belongs to a subfamily of chemokines that is highly inducible by IFN-γ (Sallusto *et al.*, 1998), the expected significant positive correlation between the fold change of IFNG and that of CXCL9 was shown across all SPMS cases (Bi). This correlation was only present in F+ SPMS cases (Biii) and not in F- SPMS cases (Bii).

5.3.3 CSF CXCL9 ELISA

An ELISA was performed to determine the concentrations of CXCL9 in F+ and F- SPMS and NNC CSF. Data were analysed using a web-based software package, which performs four parameter logistic regression to fit a standard curve (Figure 5.3.12 A) and subsequently calculate concentrations of CXCL9 in CSF samples (B). CXCL9 could only be detected in 6 samples; 2 NNCs, 3 F- SPMS cases and 1 F+ SPMS case. The optical density of the remaining 18 samples was below the defined background, or the calculated concentration of CXCL9 was below that of the low standard of 31.25pg/ml. No significant differences between groups were observed.

5.3.4 CXCL9 immunofluorescence

In order to identify the presence of CXCL9, IF was performed on sections from selected blocks with substantial meningeal infiltrates resembling potential lymphoid-like structures. Human spleen sections were used as control.

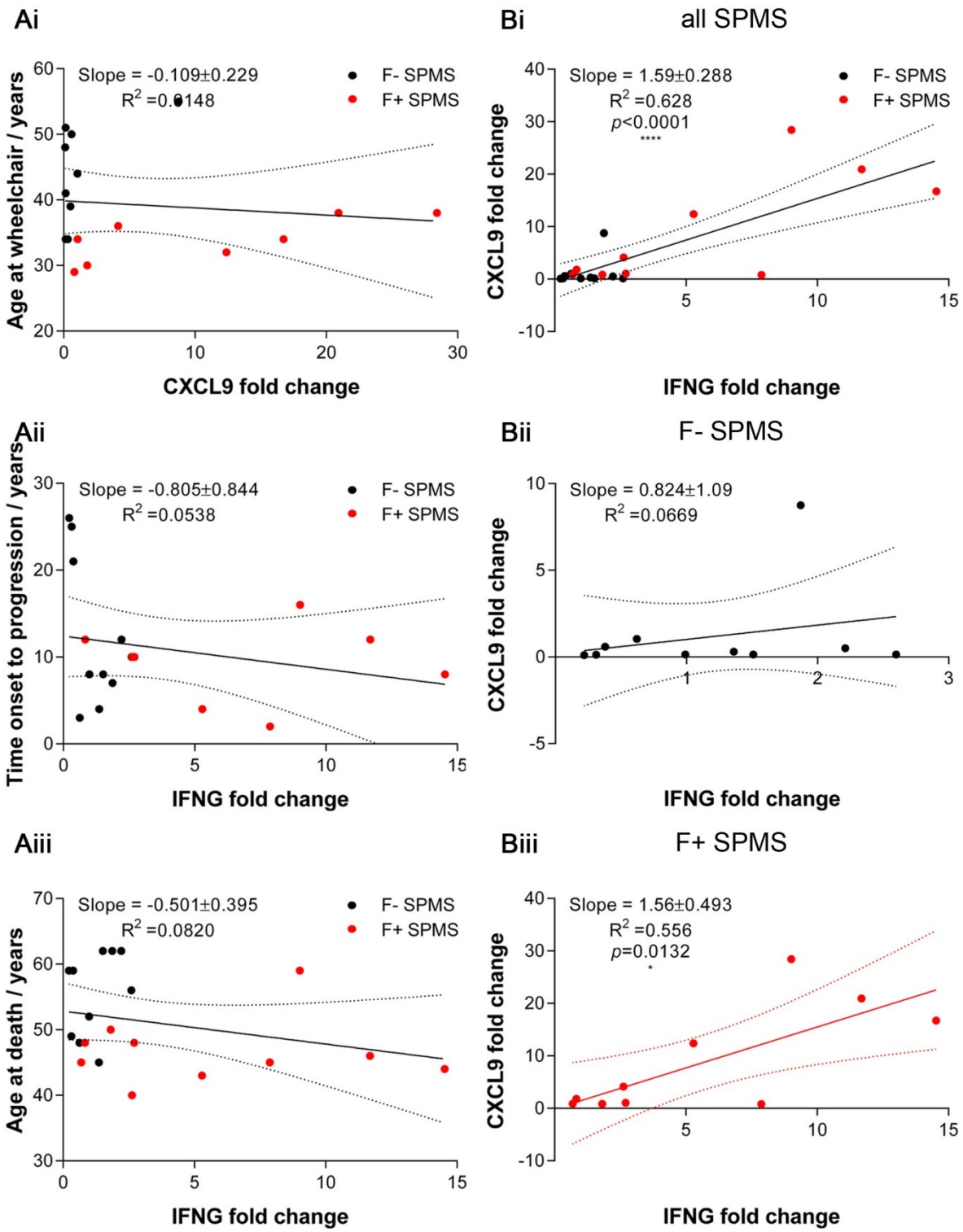

Figure 5.3.11. Correlations between clinical variables, fold changes of IFNG and fold changes of CXCL9. There appeared to be trends toward younger ages at all disease milestones and fewer numbers of years between all milestones with increasing fold changes of both CXCL9 and IFNG, although these did not reach significance (linear regression slopes not significantly non-zero). Selected correlations are shown (A). There was a trend toward younger age at which the patient required the use of a wheelchair with increasing fold change of CXCL9 (Ai) and fewer number of years between onset and progression (Aii) and younger age at death (Aiii) with increasing fold change of IFNG. There was a significant positive correlation between the fold change of IFNG and that of CXCL9 across all SPMS cases (Bi; linear regression slope significantly non-zero; **** = $p \leq 0.0001$). This correlation was only present in F+ SPMS cases (Biii; * = $p \leq 0.05$) and not in F- SPMS cases (Bii).

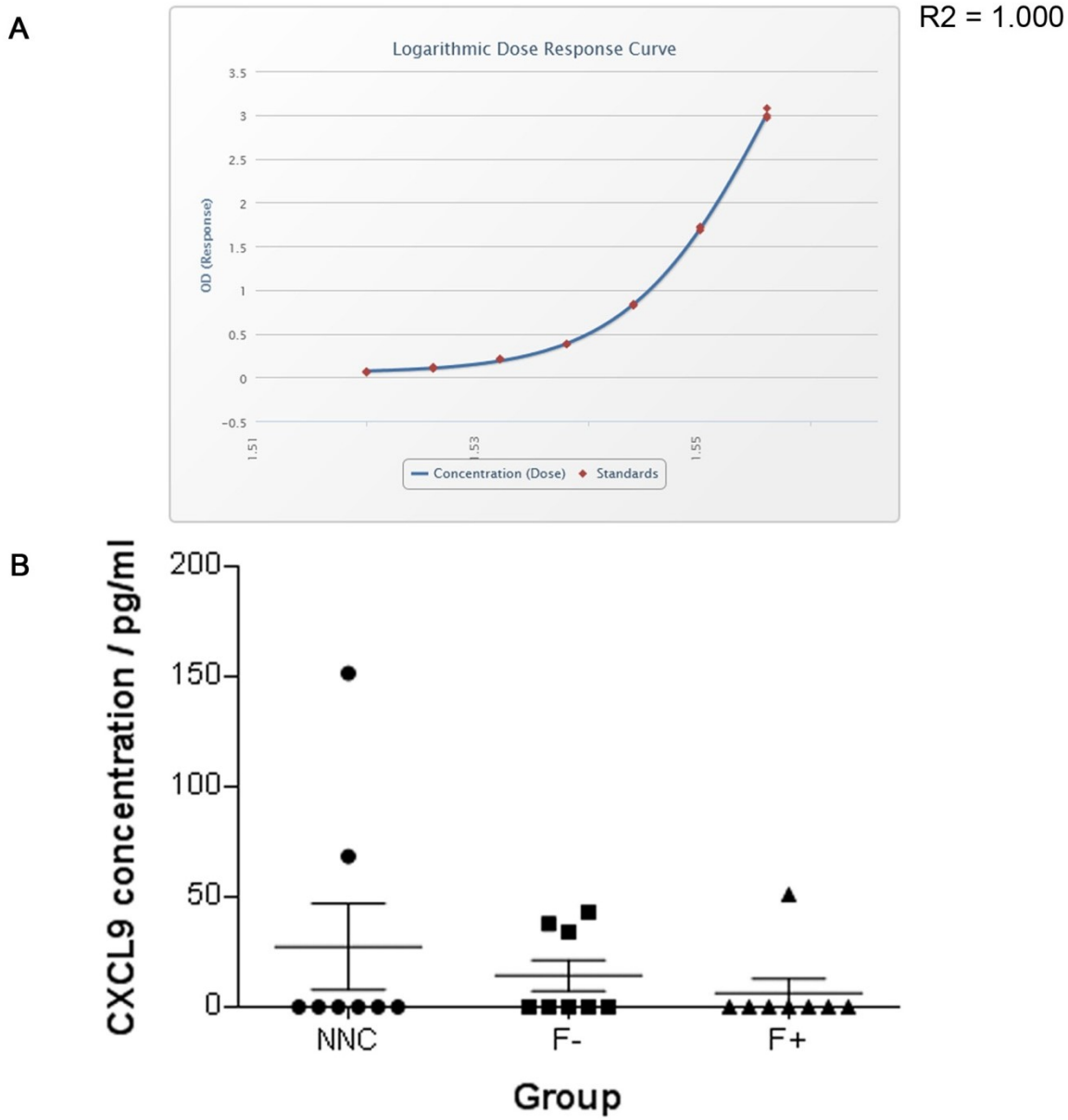

Figure 5.3.12. Low concentrations of CXCL9 in human CSF. An ELISA was performed to determine the concentrations of CXCL9 in F+ and F- SPMS and NNC CSF. Four parameter logistic regression was performed using the web-based software package elisaanalysis.com to fit a standard curve (A). The equation of the curve was subsequently used to calculate concentrations of CXCL9 in CSF samples (B). CXCL9 could only be detected in 6 samples, the optical density was below the defined background for the remaining 18 samples. There were no significant differences between groups (Kruskal-Wallis with Dunn's multiple comparisons test; mean ± SEM; *n* = 8 per group).

CXCL9 appeared to be present in a substantial proportion of cells around B cell-rich zones in spleen sections, but no IF was observed in negative control sections (Figure 5.3.13 A, Bi and Bii). It also appeared to be present in very few cells in the meninges of a block with a potential lymphoid-like structure from MS402, the case with the most substantial meningeal infiltrates (Ci). However, the IF in this case was also present not associated with DAPI and in a punctate pattern (Cii and Ciii), suggesting that it may not be specific for CXCL9.

Attempts to further optimise the CXCL9 IF protocol were not successful. Various methods of tissue fixation and antigen retrieval by membrane permeabilisation were evaluated, including the use of acetone, methanol and 4% PFA as well as Triton X-100 in antibody diluents. Sections were blocked with a high concentration of normal serum for 60 minutes and incubated with various concentrations of primary antibody overnight. Amplification using a biotinylated secondary antibody was evaluated as well as the use of Sudan Black B, which has been shown to reduce autofluorescence resulting from lipofuscin granules present in adult human brain (Romijn *et al.*, 1999, Schnell *et al.*, 1999). The protocol described in 5.2.4 appeared most suitable.

As CXCL9 belongs to a subfamily of chemokines that induce chemotaxis by binding to the CXCR3 receptor expressed by activated CD4+ and CD8+ T cells, memory T cells, NK cells, microglia and dendritic cells (Müller *et al.*, 2007, Müller *et al.*, 2010), IF for CD4 and CD8 was performed on sections from selected blocks with potential lymphoid-like structures and sections from selected blocks from NNCs and F- SPMS cases. As described in 5.3.1.2, very few B cells were observed in meninges in NNCs (Figure 5.3.14 Ai). Very few CD4+ (Aii) and CD8+ (Aiii) T cells were also observed. A qualitative assessment showed that more B cells (Bi) and CD4+ (Bii) and CD8+ (Biii) T cells were present in meninges of F- SPMS cases. Lymphoid-like structures in blocks from the case with the most substantial meningeal infiltrates, MS402, contained, in addition to B cells as described in 5.3.1.2 (Figure 5.3.15 Ai and Aii), large, dense aggregates of CD4+ (Bi and Bii) and CD8+ (Ci and Cii) T cells.

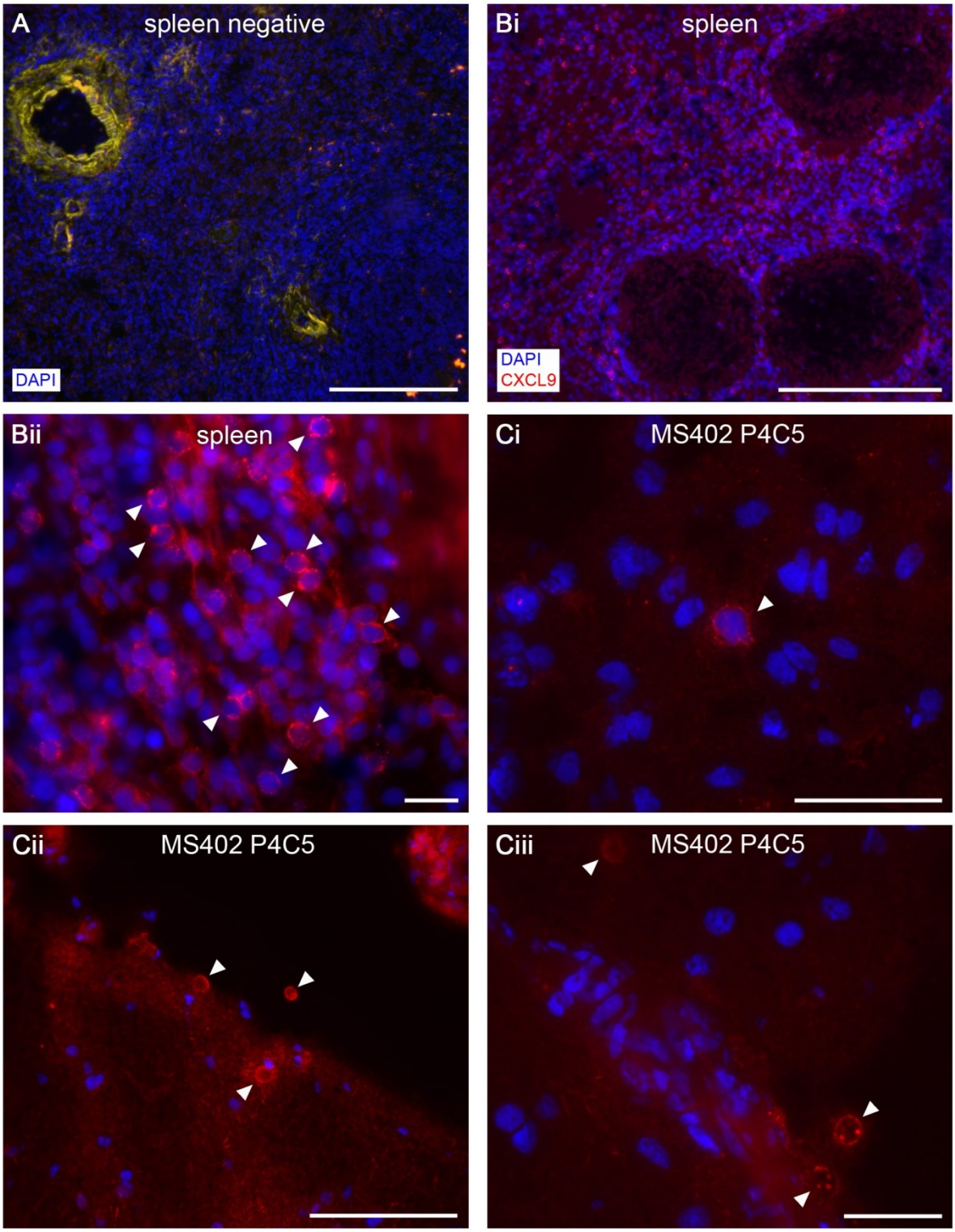

Figure 5.3.13. CXCL9 was not detected in meninges of F+ SPMS. IF for CXCL9 was performed on spleen sections used as positive control. No positive cells were present in negative control sections from which primary antibody had been omitted. Only autofluorescence, which was present in both green and red fluorescence channels and hence appeared orange, was observed (A). CXCL9 appeared to be present in a substantial proportion of cells around B cell-rich zones (Bi and Bii). IF for CXCL9 was also performed on selected blocks with substantial meningeal infiltrates resembling potential lymphoid-like structures. CXCL9 appeared to be present in very few cells in the meninges (Ci). However, fluorescence was also present not associated with DAPI (Cii and Ciii), hence may not be specific. Images are of sections from MS402. Arrowheads indicate positive cells. Scale bars: A and Bi = 200μm; Bii, Ci, Cii and Ciii = 50μm.

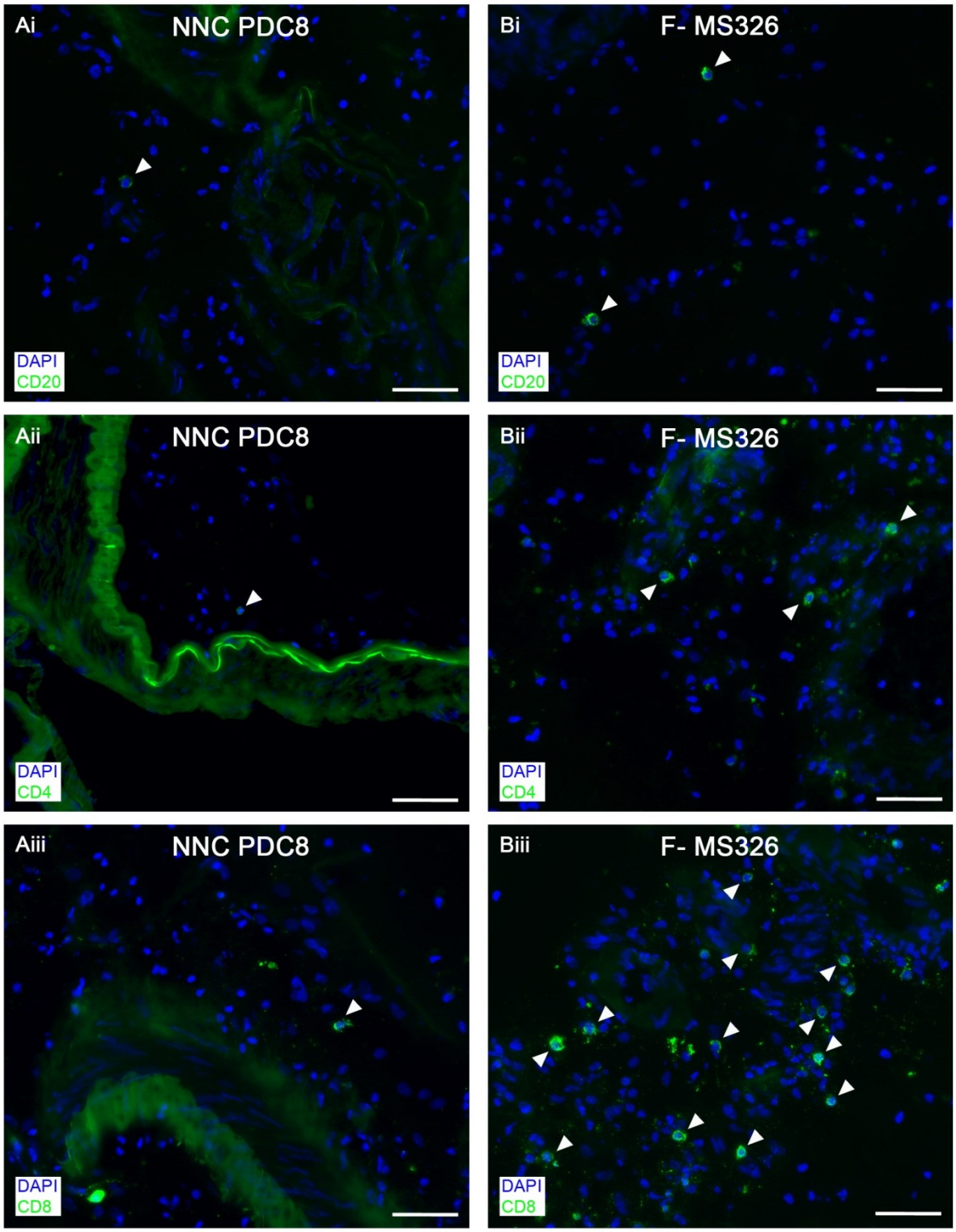

Figure 5.3.14. Lack of T cells in meninges of NNCs and F- SPMS cases. IF for CD20, CD4 and CD8 was performed on consecutive sections from selected blocks from NNCs and F- SPMS cases in order to identify B cells and CD4+ and CD8+ T cells respectively. Very few B cells (Ai) and CD4+ (Aii) and CD8+ (Aiii) T cells were present in meninges of NNCs. A qualitative assessment showed that more B cells (Bi), CD4+ (Bii) and CD8+ (Biii) T cells were present in meninges of F- SPMS cases. Positive cells are indicated by arrowheads. Scale bars: 50µm.

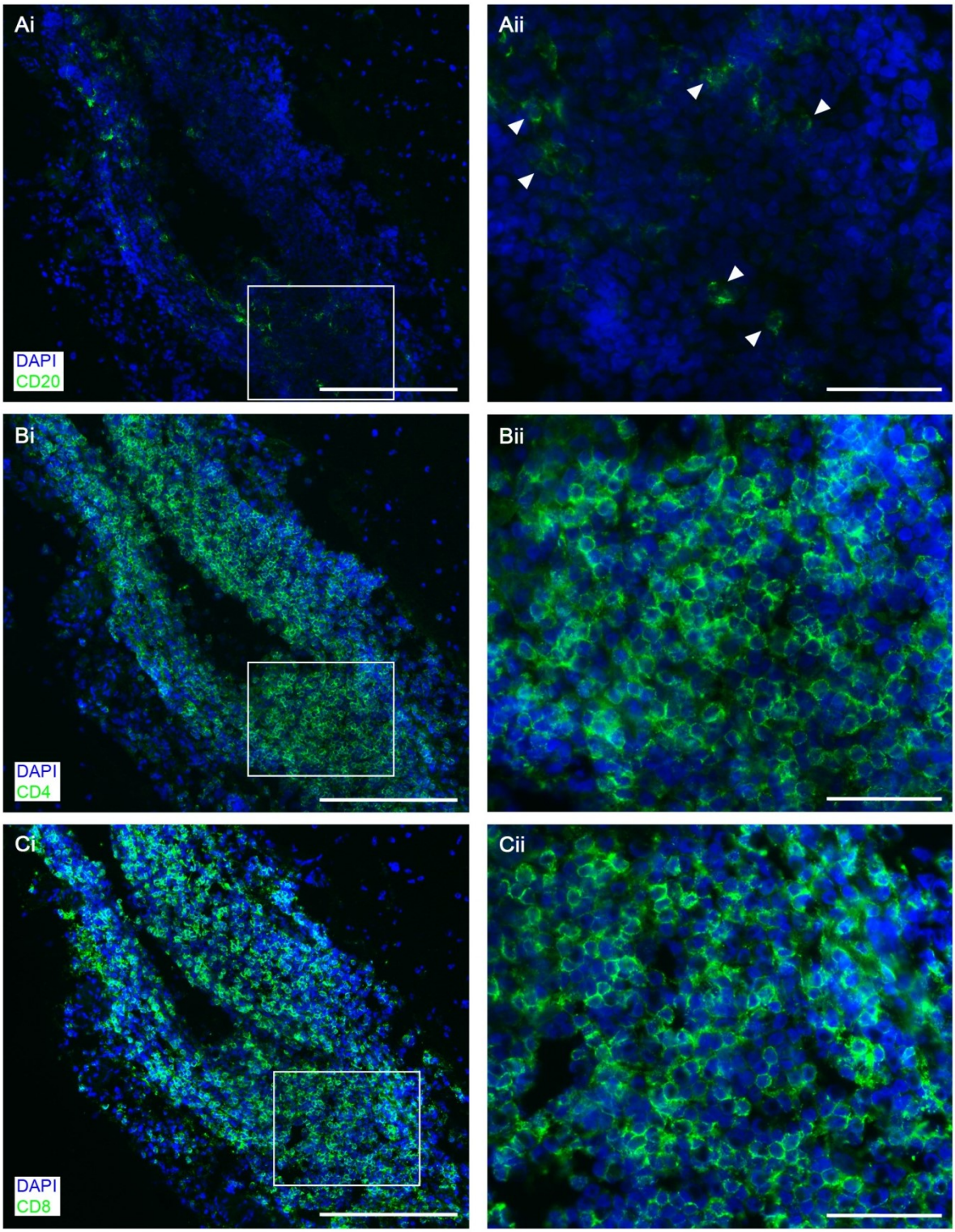

Figure 5.3.15. T cells in potential lymphoid-like structures. IF for CD20, CD4 and CD8 was performed on consecutive sections from selected blocks with substantial meningeal infiltrates resembling potential lymphoid-like structures in order to identify B cells and CD4+ and CD8+ T cells respectively. Potential lymphoid-like structures contained B cells (Ai and Aii) and large, dense aggregates of CD4+ (Bi and Bii) and CD8+ (Ci and Cii) T cells. Images are of sections from block P2B7 from F+ SPMS case MS402. Positive cells are indicated by arrowheads. Images on the right are magnifications of the boxed areas in those on the left. Scale bar: Ai, Bi and Ci = 200μm; Aii, Bii and Cii = 50μm.

5.4 Discussion

We found that CXCL13, IL5RA and IFNG mRNA levels are significantly increased in the meninges of F+ SPMS cases compared to NNCs, whereas CXCL1 mRNA levels are significantly decreased. Amplification could only be observed at high input cDNA amounts for TNF, hence it was not possible to compare TNF mRNA levels between groups. CXCL9 mRNA levels are significantly increased in the meninges of F+ SPMS cases compared to both F- SPMS cases and NNCs, although we could not detect CXCL9 protein in the meninges or post-mortem CSF, nor could we demonstrate significant correlations between CXCL9 mRNA levels and clinical variables.

5.4.1 Characterisation of cases

Cases had previously been characterised as F+ SPMS, if at least one aggregate of CD20+ B cells with CD35+ follicular dendritic cells, proliferating Ki67+ CD20+ B cells and IgA, -G or -M+ plasmablasts/plasma cells was identified, or F- SPMS (Howell *et al.*, 2011). We found that blocks from F+ SPMS cases had severe meningeal inflammation, which was not observed in F- SPMS cases and NNCs. Each case was assigned a majority index based on the index of inflammation of the majority of blocks. Although this was 0 for 2 F+ SPMS cases, it was at least 1 for the remainder. All but 1 F- SPMS case were assigned a majority index of 0, as were all NNCs. Potential lymphoid-like structures could be identified in meninges lining the sulci in 5 blocks from 2 F+ SPMS cases, which contained large, dense aggregates of B cells, the main components of lymphoid-like structures, and were associated with extensive subpial demyelination. We suggest that we did not identify potential lymphoid-like structures in all F+ SPMS cases because of their variable incidence and small size combined with screening of a limited number of blocks. Approximately 10 blocks were screened per case in the current study, whereas up to 30 blocks were screened per case in previous studies (Howell *et al.*, 2011). One study identified lymphoid-like structures in 48 out of 96 blocks from F+ SPMS cases (Magliozzi *et al.*, 2007), which were

present in all brain areas sampled but particularly in the deep sulci. They could consist of only 50-75 B cells per section (Howell *et al.*, 2011). Although blocks were selected from a range of brain areas based on the presence of well demarcated sulci in the current study, these studies suggest that more extensive sampling, particularly of the deep sulci, may be required to identify potential lymphoid-like structures in F+ SPMS cases.

These findings are consistent with previous studies using autopsy samples from progressive MS cases that observed diffuse inflammatory infiltrates as well as lymphoid-like structures in the cerebral leptomeninges associated with increased cortical GM pathology (Guseo and Jellinger, 1975, Kutzelnigg *et al.*, 2005, Magliozzi *et al.*, 2007, Kooi *et al.*, 2009, Magliozzi *et al.*, 2010, Howell *et al.*, 2011, Choi *et al.*, 2012). However, another study failed to show a correlation between the extent of meningeal inflammation and subpial demyelination and also failed to show the presence of lymphoid-like structures (Kooi *et al.*, 2009). Limited sampling of the whole brain and poor preservation of meninges as a result of suboptimal retrieval, processing and handling protocols have been suggested as reasons for this failure (Aloisi *et al.*, 2010). Meningeal inflammation was observed more frequently in meninges lining the sulci rather than in meninges overlying the gyri, again consistent with previous studies that observed lymphoid-like structures in deep sulci (Magliozzi *et al.*, 2007, Magliozzi *et al.*, 2010, Howell *et al.*, 2011), where the decreased flow of CSF is suggested to result in a protected environment that allows the homing and retention of immune cells (Reynolds *et al.*, 2011). The association between meningeal inflammation and subpial demyelination observed in this and previous studies supports the hypothesis that meningeal inflammation results in increased concentrations of pro-inflammatory cytokines in the CSF, which diffuse from the pial surface into the cortex resulting in GM pathology (Peterson *et al.*, 2001, Reynolds *et al.*, 2011).

The presence of lymphoid-like structures in F+ SPMS cases was significantly associated with younger ages at disease milestones. Trends toward fewer numbers of years between

disease milestones were also observed in F+ SPMS cases. These findings are consistent with previous studies that showed younger ages at onset, wheelchair use and death as well as a shorter disease duration and fewer numbers of years between onset and progression and progression and death (Magliozzi *et al.*, 2007, Howell *et al.*, 2011), further indicating the contribution of lymphoid-like structures to a shorter, more aggressive disease.

5.4.2 Meningeal PCR and further investigations

We performed qPCR in order to determine the steady state mRNA levels of cytokine pathway genes. Although it is widely accepted that the steady state mRNA level of a gene does not necessarily reflect its final steady state protein level (Greenbaum *et al.*, 2003), it does directly reflect their degree of transcription and conclusions regarding the expression of the gene may be drawn from qPCR data.

5.4.2.1 Concentration and integrity of RNA

High concentrations of RNA, without protein and phenol/guanidine contamination, could be obtained following meningeal dissection and RNA extraction. The RINs (numbers from 1 to 10) obtained were generally good. The mean RIN obtained was 5.2 ± 0.17, with 5 suggested to be the minimum required for PCR (Fleige and Pfaffl, 2006). However, peaks corresponding to degradation products were observed in the electropherograms obtained, resulting in a RIN of 2.7 for MS311, for example, and a mean RIN of 5.2 and not higher (range 2.7-6.8). RINs varied between cases and it was not possible to take this variation into account for the analysis. The mean RIN obtained in a previous study using RNA extracted from 193 post-mortem human brain tissue samples was 6.8 ± 1.0 (range 2.9-9.2; Durrenberger *et al.*, 2010). We suggest that this difference is due to the region from which samples were taken. The meningeal samples used in the current study are likely to have been exposed to ribonucleases as a result of repeated handling combined with their presence on the surface of cortical blocks, resulting in RNA degradation, whereas the brain

parenchyma samples used in the previous study are likely to have been more protected from ribonucleases.

It has been reported that post-mortem human brain tissue has lower RINs than post-mortem human cardiac and skeletal muscle tissue (Koppelkamm *et al.*, 2011) and that RINs are mainly dependent on the number of times that the tissue has been allowed to warm to enable the tissue to be cut (Sherwood *et al.*, 2011). Tissue obtained from the UK Multiple Sclerosis Tissue Bank is likely to have been allowed to warm (to approximately -10°C) on several occasions for sections to be cut for screening and requests, which could not be avoided, resulting in RINs lower than those expected. Consistent with a previous study, no effect of PMD, age at death or gender was observed in the current study (Sherwood *et al.*, 2011), although another study found significantly higher RINs in men than women as well as a significant negative correlation between age at death and RIN (Durrenberger *et al.*, 2010). Studies investigating the effects of PMD have also yielded conflicting results. Significant negative correlations have been observed (Lipska *et al.*, 2006), whereas other studies showed modest (Ervin *et al.*, 2007) or no correlations (Weis *et al.*, 2007, Durrenberger *et al.*, 2010). Although all cases used in the current study had a PMD of approximately 24 hours or less, it is not possible to discount effects of PMD on the RINs lower than those expected.

5.4.2.2 RT^2 Profiler PCR Array and validation qPCR

Data analysis and regulated genes

Human Inflammatory Cytokines and Receptors arrays were run to profile the expression of 84 key genes involved in inflammation. The advantage of these PCR arrays was that they are a reliable method to profile the expression of a well-researched panel of cytokine pathway genes without making assumptions about which genes we may have expected to be regulated. PCR data analysis was performed using SABiosciences or REST 2009 software or manually, the results of which depended on the method used. The advantage of the randomisation test used by the REST 2009 software was that it made no distributional

assumptions about the data, whereas the *t*-test used by the SABiosciences software assumed a normal distribution and the Kruskal-Wallis test used for manual analysis assumed a non-normal distribution. However, the *t*- and randomisation tests allowed only two groups to be compared simultaneously, resulting in increased probability of a Type 1 error when three comparisons (F+ SPMS v NNC, F- SPMS v NNC and F+ SPMS v F- SPMS) were performed. The Kruskal-Wallis with Dunn's multiple comparisons test, however, allowed all three groups to be compared simultaneously, resulting in a probability of a Type 1 error of 0.05. It was concluded that this latter test was the most appropriate as well as the most stringent, and three genes were found to be upregulated (CXCL13, CXCL9 and IL5RA) and 1 downregulated (CXCL1) in the F+ SPMS group compared to the NNC group and 1 gene upregulated (CXCL9) in the F+ SPMS group compared to the F- SPMS group. This number of regulated genes is perhaps lower than that expected given that the array profiled the expression of 84 genes. We suggest that this is the result of the relatively small group sizes in the current study (*n*=10 per group) and expect a higher number of regulated genes with larger group sizes. This may be necessary due to of a large degree of heterogeneity but is more likely due to the method used for meningeal dissection. Mainly meninges overlying the gyri were dissected, with some meninges lining the sulci, without taking into account the presence or absence of diffuse inflammatory infiltrates and potential lymphoid-like structures, so that sufficient meninges could be obtained. Future work could involve the use of laser capture microdissection to ensure that only areas of meningeal inflammation are dissected. This study is ongoing in this laboratory.

The Kruskal-Wallis with Dunn's multiple comparisons test was also used for manual analysis of validation qPCR data for IFNG and CXCL9. IFNG and CXCL9 were upregulated in the F+ SPMS group compared to both the F- SPMS group and NNC group.

CXCL13

Studies using MS tissue and CSF/serum have suggested important roles for B cells in the pathogenesis of MS as discussed in 1.3.3.2. CXCL13 is a chemokine thought to be required for B cell recruitment to the CNS (Kowarik *et al.*, 2012), although a study in CXCL13-deficient mice with MOG-induced EAE showed the same B cell infiltration in the spinal cord of these animals as in wild type animals (Rainey-Barger *et al.*, 2011). It is also thought to be required for the development of lymphoid organs, together with CCL21 and lymphotoxin-$\alpha_1\beta_2$ (Aloisi and Pujol-Borrell, 2006), by inducing clustering of lymphoid tissue inducer cells that subsequently recruit lymphoid organ components (van de Pavert *et al.*, 2009). Transgenic mice expressing CXCL13 in pancreatic β cells develop lymphoid organs containing B and T cell areas, stromal cells and high endothelial venules (Luther *et al.*, 2000).

The levels of CXCL13 are significantly increased in the CSF of RRMS, PPMS and SPMS patients compared to controls and are correlated with the number of B cells in the CSF, the majority of which express the CXCL13 receptor CXCR5 (Sellebjerg *et al.*, 2009, Sørensen *et al.*, 2002), indicating the significance of CXCL13 and CXCR5 signalling in recruiting B cells to the CNS in MS. The increased levels of CXCL13 in the CSF of progressive MS patients, however, are not a consistent finding (Krumbholz *et al.*, 2006). In RRMS cases, the levels of CXCL13 in the CSF were also correlated with the area of gadolinium-enhancing lesions on MRI and CSF markers of demyelination, axonal damage and IgG production (Sellebjerg *et al.*, 2009). CXCL13 expression has been localised to microglia and infiltrating macrophages/dendritic cells in animal models of CNS infection (Bagaeva *et al.*, 2006, Ramesh *et al.*, 2009) as well as perivascular cuffs and infiltrating immune cells in active lesions in MS, but is not detected in chronic inactive lesions (Krumbholz *et al.*, 2006). It has, however, been detected in lymphoid-like structures in F+ SPMS cases (Serafini *et al.*, 2004). Here we have extended this finding and, using the RT^2 Profiler PCR Arrays, shown that CXCL13 mRNA levels are significantly increased in the meninges of F+ SPMS cases compared to NNCs.

From the above, it is suggested that infiltrating macrophages/dendritic cells may be a source of CXCL13 production in active lesions whereas lymphoid-like structures may be the source in chronic disease with subsequent recruitment of B cells (Krumbholz *et al.*, 2006), although to date no studies have investigated the association between lymphoid-like structure status and levels of CXCL13 in the CSF. CXCR5 is also expressed by T cells following stimulation (Sallusto *et al.*, 1999). It is expressed on T follicular helper cells, which are localised to germinal centres and stimulate the differentiation of B cells into memory B cells and plasma cells (King *et al.*, 2008), and on approximately 20% of central memory T cells, which exist in a resting state and require activation (Kim *et al.*, 2001). This explains the finding that the increased levels of CXCL13 in the CSF of MS patients are correlated with the number of T cells as well as B cells in the CSF, although the function of these T cells remains unclear (Krumbholz *et al.*, 2006). CXCL13 has also been shown to induce upregulation of lymphotoxin-$\alpha_1\beta_2$ on B cells, stimulating the development of follicular dendritic cells present in lymphoid-like structures that secrete further CXCL13, hence establishing a positive feedback loop (Ansel *et al.*, 2000).

We suggest that the increased expression of CXCL13 observed in the meninges of F+ SPMS cases would result in the recruitment of T cells as well as B cells to the meninges by allowing them to respond to the CXCL13 secreted by follicular dendritic cells, in turn resulting in a more inflammatory milieu in the CSF. Further investigation into the role of CXCL13 is ongoing in this laboratory but this gene was not pursued further in the current study.

IL5RA

The IL5RA gene codes for the IL5 receptor, α subunit. IL5 was originally defined as 'T cell-replacing factor' that was secreted from murine T cells and enhanced antibody production by inducing proliferation and differentiation of activated B cells (Takatsu *et al.*, 1980). It also promotes the growth and differentiation of eosinophils (Yokota *et al.*, 1987) and enhances

histamine release from basophils (Lopez *et al.*, 1990). The IL5 receptor is expressed on murine B cell precursors as well as mature B1 cells, eosinophils and basophils (Geijsen *et al.*, 2001). It consists of a unique α subunit that binds IL5 with low affinity and a β subunit that is common to all receptors in this family, which, when associated, form a high affinity receptor (Takaki *et al.*, 1991). Although the role of the IL5 signalling pathway in the pathogenesis of asthma has been extensively investigated (Poon *et al.*, 2012), there does not appear to be a clear role in the pathogenesis of MS. One study investigated potential associations between candidate genes in inflammatory pathways, including IL5RA, and risk of MS. They used novel statistics, namely multifactor dimensionality reduction, to identify epistasis and found a significant three locus interaction between *IL4R* (*Q576R* polymorphism), *IL5RA(-80)* and *CD14(-260)*. This model was used to accurately predict disease status for approximately 76% of cases (Brassat *et al.*, 2006). Although we have shown here, using the RT^2 Profiler PCR Arrays, that IL5RA mRNA levels are significantly increased in the meninges of F+ SPMS cases compared to NNCs, given the overall lack of support for a role for IL5RA in the pathogenesis of MS, we decided not to pursue this gene any further.

CXCL1

CXCL1 is a cytokine that was originally isolated from human melanoma cells (Richmond and Thomas, 1988) also known as growth-related oncogene protein-α or melanoma growth stimulatory activity-α. Its effects are mediated by the receptor CXCR2, which is expressed on all granulocytes, mast cells and monocytes and some CD8+ T cells, NK cells and melanocytes, and include the modulation of angiogenesis, cell motility, inflammation, tumorigenesis and wound healing (Amiri and Richmond, 2003). CXCR2 expression has also been detected on resting and proliferating oligodendrocytes in active WMLs. Proliferating oligodendrocytes were associated with CXCL1-positive reactive astrocytes (Omari *et al.*, 2006), and oligodendrocytes show proliferative and migratory responses to CXCL1 *in vitro* (Tsai *et al.*, 2002). CXCL1 and CXCR2 expression were increased in the spinal cord of mice

with virus-induced demyelination. Inhibition of CXCR2 in these mice resulted in delayed recovery associated with increased demyelination and oligodendrocyte apoptosis (Hosking *et al.*, 2010). Double transgenic mice in which CXCL1 secretion by astrocytes could be induced by the administration of doxycycline showed less severe clinical and pathological MOG-induced EAE, associated with increased remyelination (Omari *et al.*, 2009). These findings suggest a protective role for CXCL1 in preventing oligodendrocyte apoptosis and promoting remyelination. However, a role for CXCR2 signalling in initiating inflammatory demyelinating diseases has also been proposed. Inhibition or genetic deficiency of CXCR2 prevented compromise of BBB integrity and subsequent immune cell infiltration and clinical disease in mice with PLP-induced EAE. This resistance to the development of disease was reversed by the transfer of wild type granulocytes (Carlson *et al.*, 2008), suggesting that CXCR2 signalling is involved in granulocyte activation and/or migration and subsequent compromise of BBB integrity, resulting in entry of immune cells to the CNS and onset of disease. Here we have shown, using the RT^2 Profiler PCR Arrays, that CXCL1 mRNA levels are significantly decreased in the meninges of F+ SPMS cases compared to NNCs.

Given that CXCL1 has been implicated in the initiation of disease, we suggest that the CXCL1 expression detected in the current study using autopsy samples from progressive MS cases was not performing this role but rather its protective role, which is consistent with its decreased expression in the F+ SPMS cases with more severe clinical course. As discussed, this role appears to be dependent on the expression of CXCL1 by astrocytes. In this context, the CXCL1 expression detected in the current study may be in astrocyte end-feet, which, together with the basal lamina, compose the glia limitans and which may have been removed during meningeal dissection. Whether this was the case could be established by performing additional qPCR using the same cDNA samples to detect, for example, aquaporin 4, which is expressed in astrocytes, particularly their end-feet (El-Khoury *et al.*, 2006). However, given that CXCL1 mRNA levels were not significantly decreased in the

meninges of F+ SPMS cases compared to F- SPMS cases, we decided not to pursue this gene any further.

TNF

The role for TNF in the pathogenesis of MS and EAE was discussed in detail in 1.3.3.4. Briefly, studies have suggested a damaging role for sTNF and its TNFR1 signalling pathway and a protective role for tmTNF and its TNFR2 signalling pathway. The TNFR1 signalling pathway results in the transcription of pro-inflammatory genes (Tracey *et al.*, 2008) or apoptotic or necroptotic cell death (Vanlangenakker *et al.*, 2012). Here, under the conditions used for the PrimeTime qPCR Assays, little TNF PCR amplicon was detected; amplification could only be observed at high input cDNA amounts when performing the validation experiment. Hence, it was not possible to compare TNF mRNA levels between groups.

This is in contrast to previous qPCR data obtained in this laboratory, which showed that TNF mRNA levels are significantly increased in the meninges of both F+ SPMS and F- SPMS cases compared to NNCs, with a greater increase in F+ SPMS cases (Gardner *et al.*, 2013). As well as the different method used for qPCR, we suggest that the difference in TNF expression observed between the current and previous studies is also due to the different method used for meningeal dissection. In the current study, mainly meninges overlying the gyri were dissected, with some meninges lining the sulci, whereas in the previous study, mainly meninges lining the sulci were dissected. Given that lymphoid-like structures are present in the meninges but particularly in those of the sulci (Magliozzi *et al.*, 2007, Magliozzi *et al.*, 2010, Howell *et al.*, 2011), it is likely that the meninges dissected in the current study contained mainly diffuse inflammatory infiltrates, with fewer lymphoid-like structures than in the previous study. This will have resulted in a decreased number of the cells with monocyte/macrophage morphology that have been shown to express TNF in inflamed meninges (Gardner *et al.*, 2013) and consequent decreased TNF expression, which was difficult to detect under the conditions used.

IFNG

As for TNF, the role for IFN-γ in the pathogenesis of MS and EAE was also discussed in 1.3.3.4. Until recently, MS was regarded as a Th1 cell-mediated disease (Khoruts *et al.*, 1995) with IFN-γ, the Th1 cell effector cytokine, thought to have a major role in the pathogenesis of disease, although it is now known that it has a broader role. It results in the proliferation and differentiation of naïve T cells into Th1 cells (Imitola *et al.*, 2005) as well as the activation of macrophages/microglia (Vass and Lassmann, 1990, Veroni *et al.*, 2010, Welser-Alves and Milner, 2013). Here we have shown, using PrimeTime qPCR Assays, that IFNG mRNA levels are significantly increased in the meninges of F+ SPMS cases compared to both F- SPMS cases and NNCs.

This is consistent with previous qPCR data obtained in this laboratory, which showed that IFNG mRNA levels are significantly increased in the meninges of F+ SPMS cases compared to NNCs (Gardner *et al.*, 2013). However, the fold change of 2.71 observed in the current study is much lower than the fold change of 30.1 observed in the previous study. We suggest that this difference may be due to the different method used for qPCR; the previous study used QuantiTect Primer Assays (Qiagen), which are not probe-based. However, it is more likely that the difference is again due to the different method used for meningeal dissection, as for TNF. The proposed hypothesis is that cytotoxic and/or pro-inflammatory molecules produced in the inflamed meninges, including TNF and IFN-γ produced by Th1 cells as shown here, diffuse into the cortex from the CSF in the SAS resulting in subpial GMLs, which are associated with inflamed meninges again as shown here. This hypothesis is supported by the model recently developed in this laboratory and further developed in this thesis that shows cortical pathology driven by meningeal inflammation. Acute increased levels of TNF and IFN-γ in the SAS of rats immunised with a subclinical dose of rmMOG resulted in subpial lesions (Gardner *et al.*, 2013). The mechanism of demyelination was proposed to be either direct (Buntinx *et al.*, 2004) or indirect by the production of other

cytotoxic and/or pro-inflammatory molecules in the meninges or the activation of microglia (Mir *et al.*, 2008).

5.4.2.3 CXCL9

CXCL9 may be involved in CNS inflammation

Since a role for IFN-γ in the pathogenesis of MS has been suggested as discussed in 1.3.3.4, interest has arisen in the expression of chemokines inducible by IFN-γ. CXCL9 belongs to a subfamily of chemokines, all members of which are highly inducible by IFN-γ and induce chemotaxis by binding to the G protein-coupled CXCR3 receptor expressed by activated CD4+, mainly Th1 (Sallusto *et al.*, 1998), and CD8+ T cells, memory T cells, NK cells, microglia and dendritic cells (Müller *et al.*, 2007, Müller *et al.*, 2010). Expression of CXCR3, like that of its ligand, is also induced by IFN-γ (Nakajima *et al.*, 2002).

Previous studies have suggested a role for CXCL9 in the pathogenesis of MS and EAE. The levels of CXCL9 are significantly increased in the CSF of MS patients, particularly during relapses, compared to controls (620pg/ml compared to 464pg/ml; Sørensen *et al.*, 1999). CXCL9 expression has been demonstrated in the spinal cord and cerebellum, as well as in the choroid plexus and meninges, of mice with MOG-induced EAE at the peak of neurological deficit, where it is mainly localised to infiltrating mononuclear cells including lesional and perilesional microglia (Carter *et al.*, 2007). In addition, the receptor CXCR3 was found to be expressed by cells in approximately 99% of perivascular cuffs, and CD4+ and CD8+ T cells expressing CXCR3 were enriched in the CSF compared to peripheral blood in MS cases, indicating the functional significance of CXCR3 signalling in recruiting T cells to the CNS in MS (Sørensen *et al.*, 1999). Additionally, CXCL9-deficient mice exhibit decreased CD8+ T cell and NK cell recruitment to the CNS following herpes simplex virus 2 infection, suggesting a functional role for CXCL9 in CNS inflammation. Hence, CXCL9 may represent a novel therapeutic target to reduce inflammation in MS (Thapa *et al.*, 2008). Finally, microarray analysis has shown that CXCL9 mRNA levels are significantly increased

in both GMLs and NAGM of F+ SPMS cases compared to F- SPMS cases and NNCs (unpublished data from this laboratory). Here we have shown, using the RT^2 Profiler PCR Arrays and validating PrimeTime qPCR Assays, that CXCL9 mRNA levels are also significantly increased in the meninges of F+ SPMS cases compared to both F- SPMS cases and NNCs.

CXCL9 mRNA levels are increased in the meninges of F+ SPMS cases

We suggest that meningeal inflammation, consisting of both diffuse inflammatory infiltrates and lymphoid-like structures, and subsequent production of IFN-γ, is a source of increased CXCL9 in F+ SPMS cases resulting in increased concentrations in the CSF. Consistent with CXCL9 being highly inducible by IFN-γ, we showed a correlation between the fold change of IFNG and that of CXCL9 in F+ SPMS cases but not in F- SPMS cases, indicating the significance of CXCL9 in this subset of cases. However, we were not able to detect CXCL9 protein in the meninges of F+ SPMS cases using IF, which may be due to the effect of PMD on protein degradation (Maarouf *et al.*, 2012), the diffusible nature of chemokines or the proposed non-specific nature of the antibody used. The levels of CXCL9 in post-mortem CSF were also below the limit of detection of 31.25pg/ml in the majority of cases. It is likely that this too is due to the effect of PMD on protein degradation, although we attempted to minimise this effect by selecting cases based on PMD. Studies such as that described above that were able to detect CXCL9 in CSF at concentrations of approximately 500pg/ml used lumbar puncture samples, which can be processed immediately with minimal protein degradation. More sensitive methods will be required to detect CXCL9, and to demonstrate significant differences between groups, in the post-mortem CSF samples available from F+ SPMS and F- SPMS cases.

Proposed results of increased CXCL9 mRNA levels

It is hypothesised that the CXCL9 in the CSF/meningeal compartment results in the chemotaxis of activated CD4+ and CD8+ T cells, memory T cells, NK cells and dendritic

cells (Müller *et al.*, 2007, Müller *et al.*, 2010). Consistent with this hypothesis, we showed the presence of large, dense aggregates of CD4+ and CD8+ T cells in potential lymphoid-like structures. Given that the Th1 cells on which CXCR3 is expressed secrete IFN-γ (Dittel, 2008, Zhu *et al.*, 2010), sustained Th1 cell recruitment may be achieved by the induction of CXCL9 expression in surrounding glial cells, although T cell infiltration in the brain parenchyma as well as in the meninges would have been expected were this the case. As CXCR3 has been shown to be expressed by microglia and to mediate chemotaxis in response to CXCL9 *in vitro* (Biber *et al.*, 2002), we also propose that the increased CXCL9 expression in the meninges results in increased numbers of activated macrophages/microglia. Finally, as T cells are involved in the activation and proliferation of B cells by expressing co-stimulatory molecules (King *et al.*, 2008), CXCL9 may have a role in the development of lymphoid-like structures and the subsequent shorter, more aggressive disease (Howell *et al.*, 2011). However, although there appeared to be trends toward younger ages at disease milestones and fewer numbers of years between milestones with increasing fold changes of IFNG and CXCL9, no significant correlations were obtained. Again, we suggest that this is the result of the relatively small group sizes in the current study and expect significant correlations with larger group sizes.

5.4.3 Conclusions

Our finding that severe inflammation and lymphoid-like structures were present in the meninges of F+ SPMS cases and were associated with subpial demyelination and younger ages at disease milestones supports the hypothesis that meningeal inflammation results in increased concentrations of cytotoxic/pro-inflammatory molecules in the CSF, which diffuse into the cortex resulting in cortical GM pathology and a more severe clinical course (Peterson *et al.*, 2001, Reynolds *et al.*, 2011). Our finding that levels of IFNG, CXCL13 and CXCL9 mRNA were increased in the meninges of F+ SPMS cases compared to NNCs is consistent with an inflammatory milieu in the CSF/meningeal compartment. We conclude that the inhibition of CXCL9 would prevent the chemotaxis of T cells to the meninges and the

proposed subsequent activation and proliferation of B cells, development of lymphoid-like structures and shorter, more aggressive disease, and represents a novel therapeutic target for SPMS.

Chapter 6

General discussion

6.1 Cortical GMLs in MS

6.1.2 Subpial cortical GMLs and meningeal inflammation

Our finding that severe inflammation and potential lymphoid-like structures containing large, dense aggregates of B cells were present in the meninges, particularly those lining the sulci, of blocks from F+ SPMS cases is consistent with previous studies using autopsy samples from progressive MS cases that observed diffuse inflammatory infiltrates as well as lymphoid-like structures in the meninges (Guseo and Jellinger, 1975, Kutzelnigg *et al.*, 2005, Magliozzi *et al.*, 2007, Kooi *et al.*, 2009, Magliozzi *et al.*, 2010, Howell *et al.*, 2011, Choi *et al.*, 2012). Potential lymphoid-like structures were associated with extensive subpial demyelination in the current study, again in keeping with these previous studies, in which meningeal inflammation was associated with cortical GM pathology. The presence of lymphoid-like structures in F+ SPMS cases was significantly associated with younger ages at disease milestones. Trends toward fewer numbers of years between disease milestones were also observed in these cases. These findings are consistent with previous studies that showed younger ages at onset, wheelchair use and death as well as a shorter disease duration and fewer numbers of years between onset and progression and progression and death (Magliozzi *et al.*, 2007, Howell *et al.*, 2011). Taken together, findings from this and previous studies support the hypothesis that meningeal inflammation results in increased concentrations of cytotoxic/pro-inflammatory molecules in the CSF, which diffuse from the pial surface into the underlying cortex resulting in cortical GM pathology and a more severe clinical course (Peterson *et al.*, 2001, Reynolds *et al.*, 2011).

6.1.2.1 Cytotoxic/pro-inflammatory molecules

A complete study of the identity of these cytotoxic/pro-inflammatory molecules has not been performed to date. In the current study, we showed increased levels of IFNG, as well as CXCL13 and IL5RA, mRNA and decreased levels of CXCL1 mRNA in the meninges of F+

SPMS cases compared to NNCs. Increased numbers of cells expressing IFNG and increased gene expression of IFNG in the meninges of F+ SPMS cases have been shown previously (Gardner *et al.*, 2013). However, in contrast to this previous study, which also showed increased gene expression of TNF in the meninges of F+ SPMS cases, the levels of TNF mRNA were not sufficient to allow comparison between groups. We suggest that this is due to the different method used for meningeal dissection, which may have resulted in mainly diffuse inflammatory infiltrates with fewer lymphoid-like structures in the meningeal tissue dissected. However, we suggest that the increased gene expression of IFNG and CXCL13, a chemokine that induces chemotaxis of B cells to the CNS (Kowarik *et al.*, 2012), in the meninges of F+ SPMS cases is consistent with an inflammatory milieu in the CSF/meningeal compartment, with diffuse inflammatory infiltrates and lymphoid-like structures suggested to become sources of the cytotoxic/pro-inflammatory molecules that diffuse into the underlying cortex (Aloisi and Pujol-Borrell, 2006, Serafini *et al.*, 2007, Carragher *et al.*, 2008).

We also showed increased levels of CXCL9 mRNA in the meninges of F+ SPMS cases compared to both F- SPMS cases and NNCs. CXCL9 belongs to a subfamily of chemokines that are inducible by IFN-γ. It induces chemotaxis by binding to CXCR3 expressed by activated CD4+ and CD8+ T cells, memory T cells, NK cells, microglia and dendritic cells (Sallusto *et al.*, 1998, Müller *et al.*, 2007, Müller *et al.*, 2010). Consistent with the expression of CXCR3 on T cells, large, dense aggregates of CD4+ and CD8+ T cells were observed in potential lymphoid-like structures. CXCR3 is also expressed by microglia and mediates their chemotaxis in response to CXCL9 (Biber *et al.*, 2002), with CXCL9 expression having been localised to microglia in lesions in mice with MOG-induced EAE at the peak of neurological deficit (Carter *et al.*, 2007). Additionally, as T cells are involved in the activation and proliferation of B cells by expressing co-stimulatory molecules (King *et al.*, 2008), CXCL9 may have a role in the development of lymphoid-like structures, which consist of aggregates of B cells with other immune cells. Hence, we propose that the increased CXCL9 expression

in the meninges of F+ SPMS cases results in increased chemotaxis of T cells to the meninges and proliferation of B cells in the meninges as well as increased chemotaxis of microglia in the underlying cortex following diffusion of CXCL9 from the pial surface. This suggests that the inhibition of CXCL9 would represent a novel therapeutic target for SPMS. Consistent with CXCL9 being inducible by IFN-γ, we showed a correlation between the fold change of IFNG and that of CXCL9 in F+ SPMS cases. Given that IFN-γ has been used in targeted EAE animal models (Kerschensteiner *et al.*, 2004, Merkler *et al.*, 2006, Gardner *et al.*, 2013), we also suggest a role for CXCL9 in pathogenesis in these models.

6.2 Animal model of cortical GM pathology

Despite knowledge of the clinical relevance of cortical GMLs and meningeal inflammation, there is currently no animal model that reliably reproduces the chronic cortical GM pathology observed in MS cases. The development of such a model is important and would allow the investigation of GML pathogenesis and the role of meningeal inflammation, and subsequent identification of potential drug targets for the treatment of MS. It would also allow the investigation of the role of the cytotoxic/pro-inflammatory molecules identified in the current study, including CXCL9.

6.2.1 Subpial cortical GMLs

In this thesis, a recently developed acute model of cortical GM pathology driven by meningeal inflammation (Gardner *et al.*, 2013) was successfully reproduced. The injection of TNF and IFN-γ into the SAS of the sagittal sulcus of asymptomatic animals with an existing cellular/humoral anti-MOG immune response resulted in extensive subpial demyelination. The cortical GMLs observed were similar to the Type III GMLs observed in MS cortex, extending from the pial surface into GM layer III and associated with mild peripheral immune cell infiltration (Peterson *et al.*, 2001, Bø *et al.*, 2003b). However, activated macrophages/microglia, CD4+ and CD8+ T cells and B cells were observed in the meninges and were particularly evident in those overlying areas of subpial demyelination, consistent

with the hypothesis that an inflammatory milieu in the CSF/meningeal compartment can result in subpial cortical GMLs (Peterson *et al.*, 2001, Reynolds *et al.*, 2011). As well as reproducing features of cortical GM pathology in MS, this model also avoids the damage caused by injection into the motor cortex in another targeted EAE model that developed subpial demyelination, which was associated with peripheral immune cell infiltration (Merkler *et al.*, 2006).

6.2.1.1 Microglial activation

The high density of activated macrophages/microglia with an amoeboid morphology observed in areas of subpial demyelination was consistent with both a previous study using this model and with studies of cortical GMLs in MS cases (Peterson *et al.*, 2001, Bø *et al.*, 2003a, Magliozzi *et al.*, 2007), in which they have been shown to be phagocytic and contacting myelin sheaths as well as present in a gradient from the pial surface into GM layers (Magliozzi *et al.*, 2010, Gardner *et al.*, 2013). This has been suggested to be due to the diffusion of pro-inflammatory cytokines from the CSF into the underlying GM layers, with the resulting microglial activation inducing subpial demyelination. There appeared to be a positive correlation between the area of subpial demyelination and the microglial activation in these areas in the current study, similar to that observed previously (Merkler *et al.*, 2006, Gardner *et al.*, 2013). Consistent with the diffusion of pro-inflammatory cytokines and the role of microglial activation, the number of cells with monocyte/macrophage morphology expressing TNF is increased in the meninges and the levels of TNF are increased in the CSF of F+ SPMS cases, with TNF also expressed by microglia in superficial GM (Gardner *et al.*, 2013).

6.2.1.2 Possible mechanisms of subpial cortical GM demyelination

Both an existing cellular/humoral anti-myelin immune response in animals immunised with a subclinical dose of rmMOG and the injection of TNF and IFN-γ (Gardner *et al.*, 2013) are required for the induction of significant meningeal immune cell infiltration, microglial

activation and subpial demyelination. These findings indicate a significant role for the reactivation of myelin-reactive T cells in the CSF/meningeal compartment as well as TNF and IFN-γ in activating meningeal blood vessels, resulting in monocyte/macrophage infiltration (Bartholomäus *et al.*, 2009, Kivisäkk *et al.*, 2009). The increase in meningeal CD4+ and CD8+ T cells with increasing doses of TNF and IFN-γ is consistent with a role for these cytokines in activating the BBB, enabling subsequent immune cell infiltration. The increase in subpial demyelination with increasing doses of TNF and IFN-γ similarly supports a role for these cytokines, consistent with their demyelinating and inflammatory effects *in vitro* and *in vivo* (Simmons and Willenborg, 1990, Aloisi, 2001, Buntinx *et al.*, 2004, Takeuchi *et al.*, 2006, Mir *et al.*, 2008) and validating their use in the current model.

Given that an existing cellular/humoral anti-MOG immune response is required in this model, demyelination may be antibody-mediated. This is dependent on the fixation of complement by anti-MOG antibodies (Piddlesden *et al.*, 1993) and its deposition on myelin sheaths (Storch *et al.*, 1998a), which has been observed in targeted EAE models (Merkler *et al.*, 2006, Gardner *et al.*, 2013). This finding also suggests a role for B cells in the pathogenesis of subpial demyelination, although they were not the most abundant immune cell in the meninges in the current study. Meningeal B cells may function as APCs and increase the activation of T cells (Rodríguez-Pinto, 2005) and may further contribute by secreting cytokines, including IFN-γ (Harris *et al.*, 2005), lymphotoxin and TNF (Bar-Or *et al.*, 2010). A recent study showed that B cells are required for reactivation of myelin-reactive T cells, their cytokine secretion and their subsequent recruitment of further immune cells (Pierson *et al.*, 2014), independent of their production of anti-MOG antibodies (Jagessar *et al.*, 2012, Molnarfi *et al.*, 2013). Alternatively, meningeal B cells may have a regulatory role and secrete the anti-inflammatory cytokine IL10 (Kala *et al.*, 2010) and further experiments will be required to determine whether these cells produce anti-MOG antibodies or are regulatory.

The apparent positive correlation between subpial demyelination and microglial activation described here implicates microglia in the pathogenesis. Microglia may function as APCs and increase the activation of T cells (Aloisi *et al.*, 1999a). They may also express the pro-inflammatory cytokines IL1β and IL6 as well as inducible NOS and produce oxygen radicals (Kuno *et al.*, 2005). However, a protective as well as a damaging role for microglia in MS pathogenesis has been suggested. Two phenotypes have been described to date, with M1 macrophages having a pro-inflammatory phenotype and promoting a Th1 response and M2 macrophages having a regulatory phenotype and promoting a Th2 response (Gordon and Martinez, 2010). Further experiments will be required to determine the phenotype of the macrophages/microglia in the current study. The flavonoid luteolin has been shown to induce phenotype switching of microglia from the M1 to the M2 phenotype (Dirscherl *et al.*, 2010) and hence may be used to inhibit M1 microglia, which it is expected would decrease demyelination.

6.2.2 Lack of chronic cortical GM pathology

Although this model has successfully shown that cortical GM pathology may be driven by meningeal inflammation, its main limitation is the acute nature of the resulting pathology, which is in contrast to the chronic cortical GM pathology and accumulation of chronic cognitive, motor and sensory symptoms in SPMS cases. The area of subpial demyelination and the microglial activation in these areas were significantly greater at 1 week than 2 weeks after injection, which also appeared to be the case for the number of CD4+ and CD8+ T cells and B cells in the meninges. These findings suggest that remyelination had occurred, and that this was associated with a loss of the pro-inflammatory signalling that results in microglial activation and immune cell infiltration. Acute pathology was also observed previously in targeted EAE models, in which inflammation was resolved and remyelination complete by 2 weeks after injection (Merkler *et al.*, 2006, Gardner *et al.*, 2013). Although it resulted in increased extent of pathology, increasing the doses of TNF and IFN-γ injected into the SAS in the current study did not result in increased duration of pathology. This might

have been expected, as the 1µl of cytokines will have been rapidly diluted or catabolised by proteases in the CSF. Additionally, although the rate of CSF flow in the SAS of the sagittal sulcus has not been determined, the rate of CSF bulk flow per whole brain is approximately 2µl per minute, resulting in a turnover rate of approximately 10 times per day (Pardridge, 2011, Chiu *et al.*, 2012), hence the cytokines may have been drained from the injection site. It is likely that chronic pro-inflammatory signalling in the CSF/meningeal compartment is required to achieve chronic microglial activation and chronic subpial demyelination. Increased numbers of OPCs have been found in spinal cord GMLs in MOG-induced EAE, associated with the appearance of remyelinating oligodendrocytes (Reynolds *et al.*, 2002), and increased g-ratios indicative of remyelination have been observed in cortical GMLs in a targeted EAE model at 2 weeks after injection of TNF and IFN-γ (Merkler *et al.*, 2006). Studies have shown that macrophages contribute to remyelination by the phagocytosis of myelin debris, which inhibits OPC differentiation (Robinson and Miller, 1999). Foamy macrophages containing myelin/myelin degradation products express various anti-inflammatory cytokines including IL10 and TGF-β, indicating a regulatory, anti-inflammatory role consistent with the remyelination and associated loss of pro-inflammatory signalling that we suggest are features of the current model.

A previous study using this model also failed to show neuronal loss (Gardner *et al.*, 2013), although transected neurites, apoptotic neurons and synapse loss are found in cortical GMLs (Peterson *et al.*, 2001, Wegner *et al.*, 2006). Neuronal loss is also present in the subpial GMLs observed in F+ SPMS cases, in which it has been suggested to contribute to a shorter, more aggressive disease (Magliozzi *et al.*, 2007, Magliozzi *et al.*, 2010). It is thought to be the result of chronic meningeal inflammation and microglial activation in subpial GMLs and Wallerian degeneration of chronically demyelinated axons (Frischer *et al.*, 2009, Magliozzi *et al.*, 2010). Hence the absence of neuronal loss in this model is the result of the requirement for chronic demyelination and inflammation. The gradient of neuronal loss from the pial surface into GM layers in subpial GMLs in F+ SPMS cases is again consistent with

the diffusion of cytotoxic and/or pro-inflammatory molecules from the chronically inflamed CSF/meningeal compartment into underlying cortical GM layers resulting in chronic microglial activation and subpial demyelination (Magliozzi *et al.*, 2010).

6.2.2.1 Lack of lymphoid-like structures

Although B cell infiltration was confined to the meninges in the current study, consistent with that in MS cases (Frischer *et al.*, 2009), ectopic lymphoid-like structures consisting of aggregates of B cells, some of which are proliferating, together with follicular dendritic cells, plasmablasts/plasma cells and T cells, were not observed, with only isolated meningeal CD4+ and CD8+ T cells and B cells present. However, a chronic inflammatory milieu appears to be required for their development, as well as CXCL13, BAFF and lymphotoxin-$\alpha_1\beta_2$ (Magliozzi *et al.*, 2004, Columba-Cabezas *et al.*, 2006). Hence their absence in the current study is again likely to be due to the acute, rather than chronic, inflammatory milieu resulting from the injection of TNF and IFN-γ. However, given the contribution of lymphoid-like structures to a shorter, more aggressive disease (Magliozzi *et al.*, 2007, Howell *et al.*, 2011), it will be important to develop a model in which these structures are observed.

6.2.3 Evaluating LV vectors

This study then aimed to evaluate LV vectors as a delivery system to achieve a chronic inflammatory milieu in the CSF/meningeal compartment, which we suggest would result in chronic cortical GM myelin and neuronal pathology, and perhaps lymphoid-like structures, in the meninges.

6.2.3.1 Suitability of LV vectors

Long-term, stable expression of eGFP was observed following injection of an LV vector based on HIV-1 pseudotyped with VSV-G and containing the eGFP reporter gene under the transcriptional control of the ubiquitous internal CMV promoter into the SAS of the sagittal sulcus. Expression was observed in the sagittal sulcus and was localised to astrocyte cell

bodies, end-feet and processes and in what appeared to be leptomeningeal cells as well as a small number of pyramidal neurons, consistent with previous studies using similar LV vectors (Jakobsson and Lundberg, 2006, Fedorova *et al.*, 2006, Hendriks *et al.*, 2007). Expression was not localised to macrophages/microglia, in contrast to previous studies (Fedorova *et al.*, 2006, Liu *et al.*, 2006), or in B or T cells. Studies have shown the presence of cells with monocyte/macrophage morphology expressing TNF and T cells expressing IFN-γ in inflamed meninges (Serafini *et al.*, 2007, Magliozzi *et al.*, 2010, Gardner *et al.*, 2013) as well as some microglia expressing TNF in superficial GM in F+ SPMS cases (Gardner *et al.*, 2013), consistent with the increased IFNG mRNA levels in the meninges of F+ SPMS cases compared to NNCs shown in the current study. Hence, although the cellular localisation of eGFP expression here is different to that of TNF and IFN-γ in MS, we suggest that its long-term presence in the sagittal sulcus and the nearby meninges over the superior surface of the cortex would be optimal for achieving a chronic inflammatory milieu in the CSF/meningeal compartment. For example, the injection of a viral vector based on herpes simplex virus type 1 or an adenoviral vector containing the IFNG gene into the cisterna magna resulted in expression in choroidal, ependymal and leptomeningeal cells and increased levels of IFN-γ in the CSF (Furlan *et al.*, 2001, Millward *et al.*, 2007). This is consistent with the increased levels of IFN-γ in the CSF of MS cases (Romme Christensen *et al.*, 2012, Gardner *et al.*, 2013). Although there are no reports of the injection of viral vectors containing the TNF gene into the SAS to date, the findings described here suggest that the LV vector would be suitable for the delivery of TNF and IFN-γ to the SAS.

The absence of cellular or innate immune responses induced by LV proteins (Abordo-Adesida *et al.*, 2005) further supports the suitability of the LV vector for the development of the chronic model of cortical pathology driven by meningeal inflammation. In the current study, microglial activation was most apparent adjacent to the sagittal sulcus and was not significantly increased after injection of the LV vector compared to the vehicle control, suggesting that the microglial activation was a result of an initial, acute innate immune

response to the midline injection. It has been proposed that the immune system recognises only the transgene product and not the capsid or virion, hence this would not be a confounding variable in the chronic model and any inflammation would be the result of the expression of TNF and IFN-γ.

Additionally, although LV vectors have been shown to induce tissue damage in the CNS, characterised by focal areas of necrosis and primary demyelination at the injection site associated with inflammatory infiltrates (Zhao *et al.*, 2003), non-specific demyelination and inflammation were not induced in the current study, even in the presence of an existing cellular/humoral anti-myelin immune response. Again, any tissue damage would hence be the result of TNF and IFN-γ expression and not the LV vector. The transduction efficiency of the LV vector was also unchanged in the presence of an existing immune response, consistent with a previous study (Abordo-Adesida *et al.*, 2005) and indicating that expression of TNF and IFN-γ would be achieved in animals immunised with a subclinical dose of rmMOG as required for the development of this model.

6.2.3.2 Unsuitability of collagen hydrogel

Given that eGFP was expressed over approximately 4mm along the anteroposterior axis, the suitability of delivering the LV vector from a collagen hydrogel to achieve more localised expression was evaluated. This was expected to prevent the extensive diffusion of the LV vector, which would result in a higher concentration of TNF and IFN-γ at the injection site in the chronic model.

The collagen hydrogel delayed expression until 2 weeks after injection and limited its duration, with no expression at 4 weeks after injection. This finding is consistent with a previous study that showed maximal transgene expression at 2 weeks after s.c. implantation, with decreased and absent expression at 4 and 6 weeks respectively (Shin and Shea, 2010). It is likely that the collagen hydrogel initially retains the LV vector, with its

degradation rate and pore size limiting release of the LV vector resulting in delayed expression. The authors of the previous study suggested that the limited duration of expression was the result of clearance of transduced cells by the immune system or a turnover of the transduced cells (Shin and Shea, 2010), although the expression present at later time points in control animals in the current study suggests that this is not the case here. Additionally, microglial activation was not induced by the collagen hydrogel and studies have shown that neither adaptive nor innate immune responses are induced (Gu *et al.*, 2004).

The main limitation of the delivery of the LV vector from the collagen hydrogel is that it did not increase expression at the injection site but increased its spread along the anteroposterior axis, in contrast to the increased expression and decreased spread expected and indeed required in the chronic model. This suggests that the collagen hydrogel used here is not optimised for sustained release in this model but allows rapid release and subsequent spread at later time points. LV vector dilution and drainage from the injection site in the CSF may also explain the absence of expression at later time points.

6.2.4 Further experiments

We suggest that the distribution and duration of expression mediated by the LV vector would be optimal for the development of the chronic model if expression at the injection site could be increased. Given that collagen hydrogels increase the retention and stability of LV vectors, resulting in efficient and localised transgene expression (Shin and Shea, 2010), the use of the collagen hydrogel to deliver the LV vector remains a strategy to limit the spread of expression and hence increase expression at the injection site. However, extensive optimisation of the hydrogel will be required, which may include increasing the collagen content (Premaraj *et al.*, 2006), increasing the relative cross-linker content or immobilising the LV vector to nanoparticles in the hydrogel (Shin and Shea, 2010) to slow degradation and subsequent release.

The production and *in vitro* and *in vivo* evaluation of a bicistronic LV vector containing the genes for TNF and IFN-γ, which will allow the simultaneous expression of the two transgenes by a single LV vector, is ongoing in this laboratory. Given that a tricistronic LV vector containing the genes required for dopamine synthesis has been shown to result in restoration of dopamine levels and motor function for 12 months following intrastriatal injection in a macaque model of Parkinson's disease (Jarraya *et al.*, 2009), we expect that chronic bathing in high concentrations of TNF and IFN-γ of the surface of the brain will be achieved using the bicistronic vector with optimised collagen hydrogel. In order to confirm this, terminal CSF samples will be taken via the cisterna magna and the levels of TNF and IFN-γ measured using ELISAs. We suggest that this will result in chronic meningeal inflammation, microglial activation and subpial demyelination as well as neuronal loss. This chronic pathology in the motor cortex, in which extensive subpial demyelination was observed in the current study, is expected to result in neurological deficits and hence animal behaviour will be evaluated using rotarod and open field activity performance. This model will also allow the evaluation of the role of the cytotoxic/pro-inflammatory molecules identified in the meninges of F+ SPMS cases in the current study, including CXCL9.

6.3 Final conclusions

In this thesis, we have further developed an acute model of cortical GM pathology driven by meningeal inflammation. We have shown that the injection of TNF and IFN-γ into the SAS of animals immunised with a subclinical dose of rmMOG induced acute subpial GMLs. These were similar to the Type III GMLs observed in MS cortex, characterised by immune cell infiltration in the meninges and microglial activation in GMLs. Taken together, our findings from the novel model and post-mortem human tissue studies support the hypothesis that meningeal inflammation results in increased concentrations of cytotoxic/pro-inflammatory molecules in the CSF, which diffuse from the pial surface into the underlying cortex resulting in microglial activation and subpial demyelination. Increased levels of IFNG and CXCL13 mRNA in the meninges of F+ SPMS cases are also consistent with an inflammatory milieu in

the CSF/meningeal compartment, as is the increased level of CXCL9 mRNA, which we suggest results in increased chemotaxis of T cells to the meninges and from which we conclude that CXCL9 represents a novel therapeutic target for SPMS. Increasing the doses of TNF and IFN-γ used in the model did not result in chronic pathology, which we suggest was due to the acute nature of the cytokine delivery. From this we conclude that a chronic inflammatory milieu in the CSF/meningeal compartment is required to achieve chronic microglial activation and subpial demyelination, neuronal loss and perhaps lymphoid-like structures. Hence LV vectors were evaluated as a strategy to achieve chronic cytokine delivery. We suggest that the distribution in the sagittal sulcus and long-term duration of reporter gene expression, in the absence of microglial activation and non-specific demyelination and inflammation, shown here would be optimal for achieving the chronic presence of TNF and IFN-γ in the CSF/meningeal compartment, if expression at the injection site could be increased using a collagen hydrogel, which requires optimisation. We propose that this will result in chronic meningeal inflammation and cortical GM pathology, with subsequent development of neurological deficit. This will allow the evaluation of the role of cytotoxic/pro-inflammatory molecules such as CXCL9. Ultimately it is the aim to reproduce the pathology, clinical course and symptoms of MS that result from progressive GM damage and it is believed that this novel model will prove to be of great benefit for the identification of potential drug targets and the development of therapeutic strategies for the treatment of progressive MS.

Appendix

5’

TTTAAGAAGGAGTATACATATGCGGGGTTCTCATCATCATCATCATCATGGTATGGCTAGCATGACTGG
TGGACAGCAAATGGGTCGGGATCTGTACGACGATGACGATAAGGATCGATGGGGATCCGAGCTCGAG
ATCTGCAGCTGGTACCATGGAATTCTAGGGCAGTTCAGAGTGATAGGACCAGGGTATCCCATCCGGG
CTTTAGTTGGGGATGAAGCAGAGCTGCCGTGCCGCATCTCTCCTGGGAAAAATGCCACGGGCATGGA
GGTGGGTTGGTACCGTTCTCCCTTCTCAAGAGTGGTTCACCTCTACCGAAATGGCAAGGACCAAGATG
CAGAGCAAGCACCTGAATACCGGGGACGCACAGAGCTTCTGAAAGAGACTATCAGTGAGGGAAAGGT
TACCCTTAGGATTCAGAACGTGAGATTCTCAGATGAAGGAGGCTACACCTGCTTCTTCAGAGACCACT
CTTACCAAGAAGAGGCAGCAATGGAGTTGAAAGTAGAATGAGAATTCGAAGCTTGATCCGGCTGCTAA
CAAAGCCCGAAAGGAAGCTGAGTTGGCTGCTGCCACCGCTGAGCAATAACTAGCATAACCCCTTGGG
GCCTCTAAACGGGTCTTGAGGGGTTTTTTGCTGAAAGGAGGAACTATATCCGGATCTGGCGTAATAGC
GAAGAGGCCCGCACCGATCGCCCTTCCCAACAGTTGCGCAGCCTGAATGGCGAATGGGACGCGCCC
TGTAGCGGCGCATTAAGCGCGGCGGGTGTGGTGGTTACGCGCAGCGTGACCGCTACACTTGCCAGC
GCCCTAGCGCCGCTCTTTCGCTTTCTCCCTCTTTCTCGCACGTCGCCGGCTTCCCCGTCAGCTCTAAA
TCGGGGGCTCCCTTTAAGGGTTT

3’

Figure A1. Results of DNA sequencing of transformed *E. coli* colony. DNA sequencing confirmed that the colony of transformed *E. coli* selected for expression of the recombinant protein corresponding to the N-terminal extracellular domain of mouse MOG contained the sequence insert in the vector (orange) flanked by EcoRI (green) and HindIII (red) recognition sequences (restriction sites indicated by arrowheads). The colony also contained the N-terminal polyhistidine sequence (blue) required for subsequent purification with a nickel-chelating resin.

Bibliography

Abordo-Adesida, E., Follenzi, A., Barcia, C., Sciascia, S., Castro, M. G., Naldini, L. and Lowenstein, P. R., 2005. Stability of lentiviral vector-mediated transgene expression in the brain in the presence of systemic antivector immune responses. *Hum Gene Ther*, **16**; 741-51.

Abrahamsson, S. V., Angelini, D. F., Dubinsky, A. N., Morel, E., Oh, U., Jones, J. L., Carassiti, D., Reynolds, R., Salvetti, M., Calabresi, P. A., Coles, A. J., Battistini, L., Martin, R., Burt, R. K. and Muraro, P. A., 2013. Non-myeloablative autologous haematopoietic stem cell transplantation expands regulatory cells and depletes IL-17 producing mucosal-associated invariant T cells in multiple sclerosis. *Brain*, **136**; 2888-903.

Adeeb, N., Deep, A., Griessenauer, C. J., Mortazavi, M. M., Watanabe, K., Loukas, M., Tubbs, R. S. and Cohen-Gadol, A. A., 2013. The intracranial arachnoid mater : a comprehensive review of its history, anatomy, imaging, and pathology. *Childs Nerv Syst*, **29**; 17-33.

Adelmann, M., Wood, J., Benzel, I., Fiori, P., Lassmann, H., Matthieu, J. M., Gardinier, M. V., Dornmair, K. and Linington, C., 1995. The N-terminal domain of the myelin oligodendrocyte glycoprotein (MOG) induces acute demyelinating experimental autoimmune encephalomyelitis in the Lewis rat. *J Neuroimmunol*, **63**; 17-27.

Agresti, C., Bernardo, A., Del Russo, N., Marziali, G., Battistini, A., Aloisi, F., Levi, G. and Coccia, E.M., 1998. Synergistic stimulation of MHC class I and IRF-1 gene expression by IFN-γ and TNF-α in oligodendrocytes. *Eur J Neurosci*, **10**; 2975-83.

Akassoglou, K., Bauer, J., Kassiotis, G., Lassmann, H., Kollias, G. and Probert, L., 1999. Transgenic models of TNF induced demyelination. *Adv Exp Med Biol*, **468**; 245-59.

Akkina, R. K., Walton, R. M., Chen, M. L., Li, Q. X., Planelles, V. and Chen, I. S., 1996. High-efficiency gene transfer into CD34+ cells with a human immunodeficiency virus type 1-based retroviral vector pseudotyped with vesicular stomatitis virus envelope glycoprotein G. *J Virol*, **70**; 2581-5.

Albert, M., Antel, J., Brück, W. and Stadelmann, C., 2007. Extensive cortical remyelination in patients with chronic multiple sclerosis. *Brain Pathol*, **17**; 129-38.

Albulescu, R., Codrici, E., Popescu, I. D., Mihai, S., Necula, L. G., Petrescu, D., Teodoru, M. and Tanase, C. P., 2013. Cytokine patterns in brain tumour progression. *Mediators Inflamm*, **2013**; 979748.

Alcolado, R., Weller, R. O., Parrish, E. P. and Garrod, D., 1988. The cranial arachnoid and pia mater in man: anatomical and ultrastructural observations. *Neuropathol Appl Neurobiol*, **14**; 1-17.

Alexopoulou, L., Kranidioti, K., Xanthoulea, S., Denis, M., Kotanidou, A., Douni, E., Blackshear, P. J., Kontoyiannis, D. L. and Kollias, G., 2006. Transmembrane TNF protects mutant mice against intracellular bacterial infections, chronic inflammation and autoimmunity. *Eur J Immunol*, **36**; 2768-80.

Aloisi, F., De Simone, R., Columba-Cabezas, S. and Levi, G., 1999a. Opposite effects of interferon-gamma and prostaglandin E2 on tumor necrosis factor and interleukin-10 production in microglia: a regulatory loop controlling microglia pro- and anti-inflammatory activities. *J Neurosci Res*, **56**; 571-80.

Aloisi, F., Ria, F., Columba-Cabezas, S., Hess, H., Penna, G. and Adorini, L., 1999b. Relative efficiency of microglia, astrocytes, dendritic cells and B cells in naive CD4+ T cell priming and Th1/Th2 cell restimulation. *Eur J Immunol*, **29**; 2705-14.

Aloisi, F., Ria, F. and Adorini, L., 2000. Regulation of T-cell responses by CNS antigen-presenting cells: different roles for microglia and astrocytes. *Immunol Today*, **21**; 141-7.

Aloisi, F., 2001. Immune function of microglia. *Glia*, **36**; 165-79.

Aloisi, F. and Pujol-Borrell, R., 2006. Lymphoid neogenesis in chronic inflammatory diseases. *Nat Rev Immunol*, **6**; 205-17.

Aloisi, F., Serafini, B., Magliozzi, R., Howell, O. W. and Reynolds, R., 2010. Detection of Epstein-Barr virus and B-cell follicles in the multiple sclerosis brain: what you find depends on how and where you look. *Brain*, **133**; e157.

Alonso, A. and Hernán, M. A., 2008. Temporal trends in the incidence of multiple sclerosis: a systematic review. *Neurology*, **71**; 129-35.

Alvarez, J. I., Cayrol, R. and Prat, A., 2011. Disruption of central nervous system barriers in multiple sclerosis. *Biochim Biophys Acta*, **1812**; 252-64.

Amiguet, P., Gardinier, M. V., Zanetta, J. P. and Matthieu, J. M., 1992. Purification and partial structural and functional characterization of mouse myelin/oligodendrocyte glycoprotein. *J Neurochem*, **58**; 1676-82.

Amiri, K. I. and Richmond, A., 2003. Fine tuning the transcriptional regulation of the CXCL1 chemokine. *Prog Nucleic Acid Res Mol Biol*, **74**; 1-36.
Amsbio, 2013. *Lentiviral Particles.* [online] Available at: <http://www.amsbio.com/Lentivirus.aspx> [Accessed 21 November 2014].
Annibali, V., Ristori, G., Angelini, D. F., Serafini, B., Mechelli, R., Cannoni, S., Romano, S., Paolillo, A., Abderrahim, H., Diamantini, A., Borsellino, G., Aloisi, F., Battistini, L. and Salvetti, M., 2011. CD161(high)CD8+T cells bear pathogenetic potential in multiple sclerosis. *Brain*, **134**; 542-54.
Ansel, K. M., Ngo, V. N., Hyman, P. L., Luther, S. A., Förster, R., Sedgwick, J. D., Browning, J. L., Lipp, M. and Cyster, J. G., 2000. A chemokine-driven positive feedback loop organizes lymphoid follicles. *Nature*, **406**; 309-14.
Applied Biosystems, 2008. *Guide to Performing Relative Quantitation of Gene Expression Using Real-Time Quantitative PCR.* [pdf] Applied Biosystems. Available at: <http://www3.appliedbiosystems.com/cms/groups/mcb_support/documents/generaldocuments/cms_042380.pdf> [Accessed 21 November 2014].
Armengol, M. P., Juan, M., Lucas-Martín, A., Fernández-Figueras, M. T., Jaraquemada, D., Gallart, T. and Pujol-Borrell, R., 2001. Thyroid autoimmune disease: demonstration of thyroid antigen-specific B cells and recombination-activating gene expression in chemokine-containing active intrathyroidal germinal centers. *Am J Pathol*, **159**; 861-73.
Arnett, H. A., Mason, J., Marino, M., Suzuki, K., Matsushima, G. K. and Ting, J. P., 2001. TNF alpha promotes proliferation of oligodendrocyte progenitors and remyelination. *Nat Neurosci*, **4**; 1116-22.
Ascherio, A. and Munger, K. L., 2007. Environmental risk factors for multiple sclerosis. Part I: the role of infection. *Ann Neurol*, **61**; 288-99.
Astier, A. L., Meiffren, G., Freeman, S. and Hafler, D. A., 2006. Alterations in CD46-mediated Tr1 regulatory T cells in patients with multiple sclerosis. *J Clin Invest*, **116**; 3252-7.
Babbe, H., Roers, A., Waisman, A., Lassmann, H., Goebels, N., Hohlfeld, R., Friese, M., Schröder, R., Deckert, M., Schmidt, S., Ravid, R. and Rajewsky, K., 2000. Clonal expansions of CD8(+) T cells dominate the T cell infiltrate in active multiple sclerosis lesions as shown by micromanipulation and single cell polymerase chain reaction. *J Exp Med*, **192**; 393-404.
Badovinac, V. P., Tvinnereim, A. R. and Harty, J. T., 2000. Regulation of antigen-specific CD8+ T cell homeostasis by perforin and interferon-gamma. *Science*, **290**; 1354-8.
Bagaeva, L. V., Rao, P., Powers, J. M. and Segal, B. M., 2006. CXC chemokine ligand 13 plays a role in experimental autoimmune encephalomyelitis. *J Immunol*, **176**; 7676-85.
Banki, K., Colombo, E., Sia, F., Halladay, D., Mattson, D. H., Tatum, A. H., Massa, P. T., Phillips, P. E. and Perl, A., 1994. Oligodendrocyte-specific expression and autoantigenicity of transaldolase in multiple sclerosis. *J Exp Med*, **180**; 1649-63.
Bar-Or, A., Fawaz, L., Fan, B., Darlington, P. J., Rieger, A., Ghorayeb, C., Calabresi, P. A., Waubant, E., Hauser, S. L., Zhang, J. and Smith, C. H., 2010. Abnormal B-cell cytokine responses a trigger of T-cell-mediated disease in MS? *Ann Neurol*, **67**; 452-61.
Baranzini, S. E., Mudge, J., van Velkinburgh, J. C., Khankhanian, P., Khrebtukova, I., Miller, N. A., Zhang, L., Farmer, A. D., Bell, C. J., Kim, R. W., May, G. D., Woodward, J. E., Caillier, S. J., McElroy, J. P., Gomez, R., Pando, M. J., Clendenen, L. E., Ganusova, E. E., Schilkey, F. D., Ramaraj, T., Khan, O. A., Huntley, J. J., Luo, S., Kwok, P. Y., Wu, T. D., Schroth, G. P., Oksenberg, J. R., Hauser, S. L. and Kingsmore, S. F., 2010. Genome, epigenome and RNA sequences of monozygotic twins discordant for multiple sclerosis. *Nature*, **464**; 1351-6.
Bartholomäus, I., Kawakami, N., Odoardi, F., Schläger, C., Miljkovic, D., Ellwart, J. W., Klinkert, W. E., Flügel-Koch, C., Issekutz, T. B., Wekerle, H. and Flügel, A., 2009. Effector T cell interactions with meningeal vascular structures in nascent autoimmune CNS lesions. *Nature*, **462**; 94-8.
Batchelor, P. E., Liberatore, G. T., Wong, J. Y., Porritt, M. J., Frerichs, F., Donnan, G. A. and Howells, D. W., 1999. Activated macrophages and microglia induce dopaminergic sprouting in the injured striatum and express brain-derived neurotrophic factor and glial cell line-derived neurotrophic factor. *J Neurosci*, **19**; 1708-16.
Batoulis, H., Recks, M. S., Addicks, K. and Kuerten, S., 2011. Experimental autoimmune encephalomyelitis--achievements and prospective advances. *APMIS*, **119**; 819-30.
Battistini, L., Piccio, L., Rossi, B., Bach, S., Galgani, S., Gasperini, C., Ottoboni, L., Ciabini, D., Caramia, M. D., Bernardi, G., Laudanna, C., Scarpini, E., McEver, R. P., Butcher, E. C., Borsellino, G. and Constantin, G., 2003. CD8+ T cells from patients with acute multiple sclerosis display selective increase of adhesiveness in brain venules: a critical role for P-selectin glycoprotein ligand-1. *Blood*, **101**; 4775-82.
Beck, J., Rondot, P., Catinot, L., Falcoff, E., Kirchner, H. and Wietzerbin, J., 1988. Increased production of interferon gamma and tumor necrosis factor precedes clinical manifestation in multiple sclerosis: do cytokines trigger off exacerbations? *Acta Neurol Scand*, **78**; 318-23.
Beecham, A. H., Patsopoulos, N. A., Xifara, D. K., Davis, M. F., Kemppinen, A., Cotsapas, C., Shah, T. S., Spencer, C., Booth, D., Goris, A., Oturai, A., Saarela, J., Fontaine, B., Hemmer, B., Martin, C.,

Zipp, F., D'Alfonso, S., Martinelli-Boneschi, F., Taylor, B., Harbo, H. F., Kockum, I., Hillert, J., Olsson, T., Ban, M., Oksenberg, J. R., Hintzen, R., Barcellos, L. F., Agliardi, C., Alfredsson, L., Alizadeh, M., Anderson, C., Andrews, R., Søndergaard, H. B., Baker, A., Band, G. and Baranzini, S. E., 2013. Analysis of immune-related loci identifies 48 new susceptibility variants for multiple sclerosis. **45**; 1353-60.

Ben-Nun, A., Wekerle, H. and Cohen, I. R., 1981. Vaccination against autoimmune encephalomyelitis with T-lymphocyte line cells reactive against myelin basic protein. *Nature*, **292**; 60-1.

Berger, T., Weerth, S., Kojima, K., Linington, C., Wekerle, H. and Lassmann, H., 1997. Experimental autoimmune encephalomyelitis: the antigen specificity of T lymphocytes determines the topography of lesions in the central and peripheral nervous system. *Lab Invest*, **76**; 355-64.

Bernard, C. C., Johns, T. G., Slavin, A., Ichikawa, M., Ewing, C., Liu, J. and Bettadapura, J., 1997. Myelin oligodendrocyte glycoprotein: a novel candidate autoantigen in multiple sclerosis. *J Mol Med (Berl)*, **75**; 77-88.

Bhasin, M., Wu, M. and Tsirka, S. E., 2007. Modulation of microglial/macrophage activation by macrophage inhibitory factor (TKP) or tuftsin (TKPR) attenuates the disease course of experimental autoimmune encephalomyelitis. *BMC Immunol*, **8**; 10.

Biber, K., Dijkstra, I., Trebst, C., De Groot, C. J. A., Ransohoff, R. M. and Boddeke, H., 2002. Functional expression of CXCR3 in cultured mouse and human astrocytes and microglia. *Neuroscience*, **112**; 487-497.

Bjartmar, C., Kidd, G., Mörk, S., Rudick, R. and Trapp, B. D., 2000. Neurological disability correlates with spinal cord axonal loss and reduced N-acetyl aspartate in chronic multiple sclerosis patients. *Ann Neurol*, **48**; 893-901.

Blaževski, J., Petković, F., Momčilović, M., Jevtic, B., Miljković, D. and Mostarica Stojković, M., 2013. High interleukin-10 expression within the central nervous system may be important for initiation of recovery of Dark Agouti rats from experimental autoimmune encephalomyelitis. *Immunobiology*, **218**; 1192-9.

Blömer, U., Naldini, L., Kafri, T., Trono, D., Verma, I. M. and Gage, F. H., 1997. Highly efficient and sustained gene transfer in adult neurons with a lentivirus vector. *J Virol*, **71**; 6641-9.

Bö, L., Mörk, S., Kong, P. A., Nyland, H., Pardo, C. A. and Trapp, B. D., 1994. Detection of MHC class II-antigens on macrophages and microglia, but not on astrocytes and endothelia in active multiple sclerosis lesions. *J Neuroimmunol*, **51**; 135-46.

Bö, L., Geurts, J. J., van der Valk, P., Polman, C. and Barkhof, F., 2007. Lack of correlation between cortical demyelination and white matter pathologic changes in multiple sclerosis. *Arch Neurol*, **64**; 76-80.

Bø, L., Vedeler, C. A., Nyland, H., Trapp, B. D. and Mørk, S. J., 2003a. Intracortical multiple sclerosis lesions are not associated with increased lymphocyte infiltration. *Mult Scler*, **9**; 323-31.

Bø, L., Vedeler, C. A., Nyland, H. I., Trapp, B. D. and Mørk, S. J., 2003b. Subpial demyelination in the cerebral cortex of multiple sclerosis patients. *J Neuropathol Exp Neurol*, **62**; 723-32.

Bonora, M., De Marchi, E., Patergnani, S., Suski, J. M., Celsi, F., Bononi, A., Giorgi, C., Marchi, S., Rimessi, A., Duszyński, J., Pozzan, T., Wieckowski, M. R. and Pinton, P., 2014. Tumor necrosis factor-alpha impairs oligodendroglial differentiation through a mitochondria-dependent process. *Cell Death Differ*.

Boulton, M., Flessner, M., Armstrong, D., Hay, J. and Johnston, M., 1998. Determination of volumetric cerebrospinal fluid absorption into extracranial lymphatics in sheep. *Am J Physiol*, **274**; R88-96.

Bourquin, C., Schubart, A., Tobollik, S., Mather, I., Ogg, S., Liblau, R. and Linington, C., 2003. Selective unresponsiveness to conformational B cell epitopes of the myelin oligodendrocyte glycoprotein in H-2b mice. *J Immunol*, **171**; 455-61.

Brambilla, R., Ashbaugh, J. J., Magliozzi, R., Dellarole, A., Karmally, S., Szymkowski, D. E. and Bethea, J. R., 2011. Inhibition of soluble tumour necrosis factor is therapeutic in experimental autoimmune encephalomyelitis and promotes axon preservation and remyelination. *Brain*, **134**; 2736-54.

Brassat, D., Motsinger, A. A., Caillier, S. J., Erlich, H. A., Walker, K., Steiner, L. L., Cree, B. A., Barcellos, L. F., Pericak-Vance, M. A., Schmidt, S., Gregory, S., Hauser, S. L., Haines, J. L., Oksenberg, J. R. and Ritchie, M. D., 2006. Multifactor dimensionality reduction reveals gene-gene interactions associated with multiple sclerosis susceptibility in African Americans. *Genes Immun*, **7**; 310-5.

Breen, A., Strappe, P., Kumar, A., O'Brien, T. and Pandit, A., 2006. Optimization of a fibrin scaffold for sustained release of an adenoviral gene vector. *J Biomed Mater Res A*, **78**; 702-8.

Breij, E. C., Brink, B. P., Veerhuis, R., van den Berg, C., Vloet, R., Yan, R., Dijkstra, C. D., van der Valk, P. and Bö, L., 2008. Homogeneity of active demyelinating lesions in established multiple sclerosis. *Ann Neurol*, **63**; 16-25.

Brettschneider, J., Czerwoniak, A., Senel, M., Fang, L., Kassubek, J., Pinkhardt, E., Lauda, F., Kapfer, T., Jesse, S., Lehmensiek, V., Ludolph, A. C., Otto, M. and Tumani, H., 2010. The chemokine CXCL13 is a prognostic marker in clinically isolated syndrome (CIS). *PLoS One*, **5**; e11986.

Brink, B. P., Veerhuis, R., Breij, E. C., van der Valk, P., Dijkstra, C. D. and Bö, L., 2005. The pathology of multiple sclerosis is location-dependent: no significant complement activation is detected in purely cortical lesions. *J Neuropathol Exp Neurol*, **64**; 147-55.
Brønnum-Hansen, H., Koch-Henriksen, N. and Stenager, E., 2004. Trends in survival and cause of death in Danish patients with multiple sclerosis. *Brain*, **127**; 844-50.
Brosnan, C. F. and Raine, C. S., 2013. The astrocyte in multiple sclerosis revisited. *Glia*, **61**; 453-65.
Brown, B. D., Sitia, G., Annoni, A., Hauben, E., Sergi, L. S., Zingale, A., Roncarolo, M. G., Guidotti, L. G. and Naldini, L., 2007. In vivo administration of lentiviral vectors triggers a type I interferon response that restricts hepatocyte gene transfer and promotes vector clearance. *Blood*, **109**; 2797-805.
Brown, D. A. and Sawchenko, P. E., 2007. Time course and distribution of inflammatory and neurodegenerative events suggest structural bases for the pathogenesis of experimental autoimmune encephalomyelitis. *J Comp Neurol*, **502**; 236-60.
Brück, W., Schmied, M., Suchanek, G., Brück, Y., Breitschopf, H., Poser, S., Piddlesden, S. and Lassmann, H., 1994. Oligodendrocytes in the early course of multiple sclerosis. *Ann Neurol*, **35**; 65-73.
Brück, W., Porada, P., Poser, S., Rieckmann, P., Hanefeld, F., Kretzschmar, H. A. and Lassmann, H., 1995. Monocyte/macrophage differentiation in early multiple sclerosis lesions. *Ann Neurol*, **38**; 788-96.
Brunner, C., Lassmann, H., Waehneldt, T. V., Matthieu, J. M. and Linington, C., 1989. Differential ultrastructural localization of myelin basic protein, myelin/oligodendroglial glycoprotein, and 2',3'-cyclic nucleotide 3'-phosphodiesterase in the CNS of adult rats. *J Neurochem*, **52**; 296-304.
Buc, M., 2013. Role of regulatory T cells in pathogenesis and biological therapy of multiple sclerosis. *Mediators Inflamm*, **2013**; 963748.
Buntinx, M., Moreels, M., Vandenabeele, F., Lambrichts, I., Raus, J., Steels, P., Stinissen, P. and Ameloot, M., 2004. Cytokine-induced cell death in human oligodendroglial cell lines: I. Synergistic effects of IFN-gamma and TNF-alpha on apoptosis. *J Neurosci Res*, **76**; 834-45.
Burger, D., Steck, A. J., Bernard, C. C. and Kerlero de Rosbo, N., 1993. Human myelin/oligodendrocyte glycoprotein: a new member of the L2/HNK-1 family. *J Neurochem*, **61**; 1822-7.
Burt, R. K., Loh, Y., Cohen, B., Stefoski, D., Balabanov, R., Katsamakis, G., Oyama, Y., Russell, E. J., Stern, J., Muraro, P., Rose, J., Testori, A., Bucha, J., Jovanovic, B., Milanetti, F., Storek, J., Voltarelli, J. C. and Burns, W. H., 2009. Autologous non-myeloablative haemopoietic stem cell transplantation in relapsing-remitting multiple sclerosis: a phase I/II study. *Lancet Neurol*, **8**; 244-53.
Calabrese, M., De Stefano, N., Atzori, M., Bernardi, V., Mattisi, I., Barachino, L., Morra, A., Rinaldi, L., Romualdi, C., Perini, P., Battistin, L. and Gallo, P., 2007. Detection of cortical inflammatory lesions by double inversion recovery magnetic resonance imaging in patients with multiple sclerosis. *Arch Neurol*, **64**; 1416-22.
Calabrese, M., Agosta, F., Rinaldi, F., Mattisi, I., Grossi, P., Favaretto, A., Atzori, M., Bernardi, V., Barachino, L., Rinaldi, L., Perini, P., Gallo, P. and Filippi, M., 2009a. Cortical lesions and atrophy associated with cognitive impairment in relapsing-remitting multiple sclerosis. *Arch Neurol*, **66**; 1144-50.
Calabrese, M., Filippi, M., Rovaris, M., Bernardi, V., Atzori, M., Mattisi, I., Favaretto, A., Grossi, P., Barachino, L., Rinaldi, L., Romualdi, C., Perini, P. and Gallo, P., 2009b. Evidence for relative cortical sparing in benign multiple sclerosis: a longitudinal magnetic resonance imaging study. *Mult Scler*, **15**; 36-41.
Calabrese, M. and Gallo, P., 2009. Magnetic resonance evidence of cortical onset of multiple sclerosis. *Mult Scler*, **15**; 933-41.
Calabrese, M., Rocca, M. A., Atzori, M., Mattisi, I., Bernardi, V., Favaretto, A., Barachino, L., Romualdi, C., Rinaldi, L., Perini, P., Gallo, P. and Filippi, M., 2009c. Cortical lesions in primary progressive multiple sclerosis: a 2-year longitudinal MR study. *Neurology*, **72**; 1330-6.
Calabrese, M., Filippi, M. and Gallo, P., 2010a. Cortical lesions in multiple sclerosis. *Nat Rev Neurol*, **6**; 438-44.
Calabrese, M., Rocca, M. A., Atzori, M., Mattisi, I., Favaretto, A., Perini, P., Gallo, P. and Filippi, M., 2010b. A 3-year magnetic resonance imaging study of cortical lesions in relapse-onset multiple sclerosis. *Ann Neurol*, **67**; 376-83.
Calabrese, M., Poretto, V., Favaretto, A., Alessio, S., Bernardi, V., Romualdi, C., Rinaldi, F., Perini, P. and Gallo, P., 2012. Cortical lesion load associates with progression of disability in multiple sclerosis. *Brain*, **135**; 2952-61.
Caminero, A., Comabella, M. and Montalban, X., 2011. Tumor necrosis factor alpha (TNF-alpha), anti-TNF-alpha and demyelination revisited: an ongoing story. *J Neuroimmunol*, **234**; 1-6.

Carlson, T., Kroenke, M., Rao, P., Lane, T. E. and Segal, B., 2008. The Th17-ELR+ CXC chemokine pathway is essential for the development of central nervous system autoimmune disease. *J Exp Med*, **205**; 811-23.
Carragher, D. M., Rangel-Moreno, J. and Randall, T. D., 2008. Ectopic lymphoid tissues and local immunity. *Semin Immunol*, **20**; 26-42.
Carrigan, K. A., Saurer, T. B., Ijames, S. G. and Lysle, D. T., 2004. Buprenorphine produces naltrexone reversible alterations of immune status. *Int Immunopharmacol*, **4**; 419-28.
Carter, S. L., Müller, M., Manders, P. M. and Campbell, I. L., 2007. Induction of the genes for Cxcl9 and Cxcl10 is dependent on IFN-gamma but shows differential cellular expression in experimental autoimmune encephalomyelitis and by astrocytes and microglia in vitro. *Glia*, **55**; 1728-39.
Chang, A., Staugaitis, S. M., Dutta, R., Batt, C. E., Easley, K. E., Chomyk, A. M., Yong, V. W., Fox, R. J., Kidd, G. J. and Trapp, B. D., 2012. Cortical remyelination: a new target for repair therapies in multiple sclerosis. *Ann Neurol*, **72**; 918-26.
Chertoff, M., Di Paolo, N., Schoeneberg, A., Depino, A., Ferrari, C., Wurst, W., Pfizenmaier, K., Eisel, U. and Pitossi, F., 2011. Neuroprotective and neurodegenerative effects of the chronic expression of tumor necrosis factor alpha in the nigrostriatal dopaminergic circuit of adult mice. *Exp Neurol*, **227**; 237-51.
Chiu, C., Miller, M. C., Caralopoulos, I. N., Worden, M. S., Brinker, T., Gordon, Z. N., Johanson, C. E. and Silverberg, G. D., 2012. Temporal course of cerebrospinal fluid dynamics and amyloid accumulation in the aging rat brain from three to thirty months. *Fluids Barriers CNS*, **9**; 3.
Choi, S. R., Howell, O. W., Carassiti, D., Magliozzi, R., Gveric, D., Muraro, P. A., Nicholas, R., Roncaroli, F. and Reynolds, R., 2012. Meningeal inflammation plays a role in the pathology of primary progressive multiple sclerosis. *Brain*, **135**; 2925-37.
Clements, C. S., Reid, H. H., Beddoe, T., Tynan, F. E., Perugini, M. A., Johns, T. G., Bernard, C. C. and Rossjohn, J., 2003. The crystal structure of myelin oligodendrocyte glycoprotein, a key autoantigen in multiple sclerosis. *Proc Natl Acad Sci U S A*, **100**; 11059-64.
Cockrell, A. S. and Kafri, T., 2007. Gene delivery by lentivirus vectors. *Mol Biotechnol*, **36**; 184-204.
Coebergh, J. A., Roosendaal, S. D., Polman, C. H., Geurts, J. J. and van Woerkom, T. C., 2010. Acute severe memory impairment as a presenting symptom of multiple sclerosis: a clinical case study with 3D double inversion recovery MR imaging. *Mult Scler*, **16**; 1521-4.
Colton, C. A., Snell, J., Chernyshev, O. and Gilbert, D. L., 1994. Induction of superoxide anion and nitric oxide production in cultured microglia. *Ann N Y Acad Sci*, **738**; 54-63.
Columba-Cabezas, S., Griguoli, M., Rosicarelli, B., Magliozzi, R., Ria, F., Serafini, B. and Aloisi, F., 2006. Suppression of established experimental autoimmune encephalomyelitis and formation of meningeal lymphoid follicles by lymphotoxin beta receptor-Ig fusion protein. *J Neuroimmunol*, **179**; 76-86.
Compston, A. and Coles, A., 2002. Multiple sclerosis. *Lancet*, **359**; 1221-31.
Compston, A. and Coles, A., 2008. Multiple sclerosis. *Lancet*, **372**; 1502-17.
Confavreux, C. and Vukusic, S., 2006. The natural history of multiple sclerosis. *Rev Prat*, **56**; 1313-20.
Corcione, A., Casazza, S., Ferretti, E., Giunti, D., Zappia, E., Pistorio, A., Gambini, C., Mancardi, G. L., Uccelli, A. and Pistoia, V., 2004. Recapitulation of B cell differentiation in the central nervous system of patients with multiple sclerosis. *Proc Natl Acad Sci U S A*, **101**; 11064-9.
Cresce, A., Dandu, R., Burger, A., Cappello, J. and Ghandehari, H., 2008. Characterization and real-time imaging of gene expression of adenovirus embedded silk-elastinlike protein polymer hydrogels. *Mol Pharm*, **5**; 891-7.
Dal Bianco, A., Bradl, M., Frischer, J., Kutzelnigg, A., Jellinger, K. and Lassmann, H., 2008. Multiple sclerosis and Alzheimer's disease. *Ann Neurol*, **63**; 174-83.
Damoiseaux, J. G., Döpp, E. A., Calame, W., Chao, D., MacPherson, G. G. and Dijkstra, C. D., 1994. Rat macrophage lysosomal membrane antigen recognized by monoclonal antibody ED1. *Immunology*, **83**; 140-7.
De Jager, P. L., Jia, X., Wang, J., de Bakker, P. I., Ottoboni, L., Aggarwal, N. T., Piccio, L., Raychaudhuri, S., Tran, D., Aubin, C., Briskin, R., Romano, S., International, M. S. G. C., Baranzini, S. E., McCauley, J. L., Pericak-Vance, M. A., Haines, J. L., Gibson, R. A., Naeglin, Y., Uitdehaag, B., Matthews, P. M., Kappos, L., Polman, C., McArdle, W. L., Strachan, D. P., Evans, D., Cross, A. H., Daly, M. J., Compston, A., Sawcer, S. J., Weiner, H. L., Hauser, S. L., Hafler, D. A. and Oksenberg, J. R., 2009. Meta-analysis of genome scans and replication identify CD6, IRF8 and TNFRSF1A as new multiple sclerosis susceptibility loci. *Nat Genet*, **41**; 776-82.
De Stefano, N., Matthews, P. M., Fu, L., Narayanan, S., Stanley, J., Francis, G. S., Antel, J. P. and Arnold, D. L., 1998. Axonal damage correlates with disability in patients with relapsing-remitting multiple sclerosis. Results of a longitudinal magnetic resonance spectroscopy study. *Brain*, **121 (Pt 8)**; 1469-77.

Delarasse, C., Smith, P., Baker, D. and Amor, S., 2013. Novel pathogenic epitopes of myelin oligodendrocyte glycoprotein induce experimental autoimmune encephalomyelitis in C57BL/6 mice. *Immunology*, **140**; 456-64.

Dirscherl, K., Karlstetter, M., Ebert, S., Kraus, D., Hlawatsch, J., Walczak, Y., Moehle, C., Fuchshofer, R. and Langmann, T., 2010. Luteolin triggers global changes in the microglial transcriptome leading to a unique anti-inflammatory and neuroprotective phenotype. *J Neuroinflammation*, **7**; 3.

Dittel, B. N., 2008. CD4 T cells: Balancing the coming and going of autoimmune-mediated inflammation in the CNS. *Brain Behav Immun*, **22**; 421-30.

Dobbie, M. S., Hurst, R. D., Klein, N. J. and Surtees, R. A., 1999. Upregulation of intercellular adhesion molecule-1 expression on human endothelial cells by tumour necrosis factor-alpha in an in vitro model of the blood-brain barrier. *Brain Res*, **830**; 330-6.

Dobson, R., Ramagopalan, S., Davis, A. and Giovannoni, G., 2013. Cerebrospinal fluid oligoclonal bands in multiple sclerosis and clinically isolated syndromes: a meta-analysis of prevalence, prognosis and effect of latitude. *J Neurol Neurosurg Psychiatry*, **84**; 909-14.

Dopp, J. M., Mackenzie-Graham, A., Otero, G. C. and Merrill, J. E., 1997. Differential expression, cytokine modulation, and specific functions of type-1 and type-2 tumor necrosis factor receptors in rat glia. *J Neuroimmunol*, **75**; 104-12.

Durrenberger, P. F., Fernando, S., Kashefi, S. N., Ferrer, I., Hauw, J. J., Seilhean, D., Smith, C., Walker, R., Al-Sarraj, S., Troakes, C., Palkovits, M., Kasztner, M., Huitinga, I., Arzberger, T., Dexter, D. T., Kretzschmar, H. and Reynolds, R., 2010. Effects of antemortem and postmortem variables on human brain mRNA quality: a BrainNet Europe study. *J Neuropathol Exp Neurol*, **69**; 70-81.

Durrenberger, P. F., Fernando, F. S., Magliozzi, R., Kashefi, S. N., Bonnert, T. P., Ferrer, I., Seilhean, D., Nait-Oumesmar, B., Schmitt, A., Gebicke-Haerter, P. J., Falkai, P., Grünblatt, E., Palkovits, M., Parchi, P., Capellari, S., Arzberger, T., Kretzschmar, H., Roncaroli, F., Dexter, D. T. and Reynolds, R., 2012. Selection of novel reference genes for use in the human central nervous system: a BrainNet Europe Study. *Acta Neuropathol*, **124**; 893-903.

Dutta, R., McDonough, J., Yin, X., Peterson, J., Chang, A., Torres, T., Gudz, T., Macklin, W. B., Lewis, D. A., Fox, R. J., Rudick, R., Mirnics, K. and Trapp, B. D., 2006. Mitochondrial dysfunction as a cause of axonal degeneration in multiple sclerosis patients. *Ann Neurol*, **59**; 478-89.

Dutta, R., Chang, A., Doud, M. K., Kidd, G. J., Ribaudo, M. V., Young, E. A., Fox, R. J., Staugaitis, S. M. and Trapp, B. D., 2011. Demyelination causes synaptic alterations in hippocampi from multiple sclerosis patients. *Ann Neurol*, **69**; 445-54.

Dyer, C. A. and Matthieu, J. M., 1994. Antibodies to myelin/oligodendrocyte-specific protein and myelin/oligodendrocyte glycoprotein signal distinct changes in the organization of cultured oligodendroglial membrane sheets. *J Neurochem*, **62**; 777-87.

Ebers, G. C., Bulman, D. E., Sadovnick, A. D., Paty, D. W., Warren, S., Hader, W., Murray, T. J., Seland, T. P., Duquette, P., Grey, T. and et al., 1986. A population-based study of multiple sclerosis in twins. *N Engl J Med*, **315**; 1638-42.

El-Khoury, N., Braun, A., Hu, F., Pandey, M., Nedergaard, M., Lagamma, E. F. and Ballabh, P., 2006. Astrocyte end-feet in germinal matrix, cerebral cortex, and white matter in developing infants. *Pediatr Res*, **59**; 673-9.

Ellison, S. M., Trabalza, A., Tisato, V., Pazarentzos, E., Lee, S., Papadaki, V., Goniotaki, D., Morgan, S., Mirzaei, N. and Mazarakis, N. D., 2013. Dose-dependent neuroprotection of VEGF(1)(6)(5) in Huntington's disease striatum. *Mol Ther*, **21**; 1862-75.

Ervin, J. F., Heinzen, E. L., Cronin, K. D., Goldstein, D., Szymanski, M. H., Burke, J. R., Welsh-Bohmer, K. A. and Hulette, C. M., 2007. Postmortem delay has minimal effect on brain RNA integrity. *J Neuropathol Exp Neurol*, **66**; 1093-9.

Fabry, Z., Waldschmidt, M. M., Hendrickson, D., Keiner, J., Love-Homan, L., Takei, F. and Hart, M. N., 1992. Adhesion molecules on murine brain microvascular endothelial cells: expression and regulation of ICAM-1 and Lgp 55. *J Neuroimmunol*, **36**; 1-11.

Fairweather, D., Frisancho-Kiss, S. and Rose, N. R., 2008. Sex differences in autoimmune disease from a pathological perspective. *Am J Pathol*, **173**; 600-9.

Fedorova, E., Battini, L., Prakash-Cheng, A., Marras, D. and Gusella, G. L., 2006. Lentiviral gene delivery to CNS by spinal intrathecal administration to neonatal mice. *J Gene Med*, **8**; 414-24.

Ferber, I. A., Brocke, S., Taylor-Edwards, C., Ridgway, W., Dinisco, C., Steinman, L., Dalton, D. and Fathman, C. G., 1996. Mice with a disrupted IFN-gamma gene are susceptible to the induction of experimental autoimmune encephalomyelitis (EAE). *J Immunol*, **156**; 5-7.

Ferrer, I., Martinez, A., Boluda, S., Parchi, P. and Barrachina, M., 2008. Brain banks: benefits, limitations and cautions concerning the use of post-mortem brain tissue for molecular studies. *Cell Tissue Bank*, **9**; 181-94.

Festa, E. D., Hankiewicz, K., Kim, S., Skurnick, J., Wolansky, L. J., Cook, S. D. and Cadavid, D., 2009. Serum levels of CXCL13 are elevated in active multiple sclerosis. *Mult Scler*, **15**; 1271-9.

Fisniku, L. K., Chard, D. T., Jackson, J. S., Anderson, V. M., Altmann, D. R., Miszkiel, K. A., Thompson, A. J. and Miller, D. H., 2008. Gray matter atrophy is related to long-term disability in multiple sclerosis. *Ann Neurol*, **64**; 247-54.

Fleige, S. and Pfaffl, M. W., 2006. RNA integrity and the effect on the real-time qRT-PCR performance. *Mol Aspects Med*, **27**; 126-39.

Fletcher, J. M., Lalor, S. J., Sweeney, C. M., Tubridy, N. and Mills, K. H., 2010. T cells in multiple sclerosis and experimental autoimmune encephalomyelitis. *Clin Exp Immunol*, **162**; 1-11.

Foote, A. K. and Blakemore, W. F., 2005. Inflammation stimulates remyelination in areas of chronic demyelination. *Brain*, **128**; 528-39.

Frischer, J. M., Bramow, S., Dal-Bianco, A., Lucchinetti, C. F., Rauschka, H., Schmidbauer, M., Laursen, H., Sorensen, P. S. and Lassmann, H., 2009. The relation between inflammation and neurodegeneration in multiple sclerosis brains. *Brain*, **132**; 1175-89.

Fritzsching, B., Haas, J., König, F., Kunz, P., Fritzsching, E., Pöschl, J., Krammer, P. H., Brück, W., Suri-Payer, E. and Wildemann, B., 2011. Intracerebral human regulatory T cells: analysis of CD4+ CD25+ FOXP3+ T cells in brain lesions and cerebrospinal fluid of multiple sclerosis patients. *PLoS One*, **6**; e17988.

Fujita, T., Yoshimine, T., Maruno, M. and Hayakawa, T., 1998. Cellular dynamics of macrophages and microglial cells in reaction to stab wounds in rat cerebral cortex. *Acta Neurochir (Wien)*, **140**; 275-9.

Furlan, R., Brambilla, E., Ruffini, F., Poliani, P. L., Bergami, A., Marconi, P. C., Franciotta, D. M., Penna, G., Comi, G., Adorini, L. and Martino, G., 2001. Intrathecal delivery of IFN-gamma protects C57BL/6 mice from chronic-progressive experimental autoimmune encephalomyelitis by increasing apoptosis of central nervous system-infiltrating lymphocytes. *J Immunol*, **167**; 1821-9.

Gardinier, M. V., Amiguet, P., Linington, C. and Matthieu, J. M., 1992. Myelin/oligodendrocyte glycoprotein is a unique member of the immunoglobulin superfamily. *J Neurosci Res*, **33**; 177-87.

Gardner, C., Magliozzi, R., Durrenberger, P. F., Howell, O. W., Rundle, J. and Reynolds, R., 2013. Cortical grey matter demyelination can be induced by elevated pro-inflammatory cytokines in the subarachnoid space of MOG-immunized rats. *Brain*, **136**; 3596-608.

Geijsen, N., Koenderman, L. and Coffer, P. J., 2001. Specificity in cytokine signal transduction: lessons learned from the IL-3/IL-5/GM-CSF receptor family. *Cytokine Growth Factor Rev*, **12**; 19-25.

Genain, C. P., Nguyen, M. H., Letvin, N. L., Pearl, R., Davis, R. L., Adelman, M., Lees, M. B., Linington, C. and Hauser, S. L., 1995. Antibody facilitation of multiple sclerosis-like lesions in a nonhuman primate. *J Clin Invest*, **96**; 2966-74.

Genain, C. P., Cannella, B., Hauser, S. L. and Raine, C. S., 1999. Identification of autoantibodies associated with myelin damage in multiple sclerosis. *Nat Med*, **5**; 170-5.

Germann, T., Bongartz, M., Dlugonska, H., Hess, H., Schmitt, E., Kolbe, L., Kölsch, E., Podlaski, F. J., Gately, M. K. and Rüde, E., 1995. Interleukin-12 profoundly up-regulates the synthesis of antigen-specific complement-fixing IgG2a, IgG2b and IgG3 antibody subclasses in vivo. *Eur J Immunol*, **25**; 823-9.

Geurts, J. J., Pouwels, P. J., Uitdehaag, B. M., Polman, C. H., Barkhof, F. and Castelijns, J. A., 2005. Intracortical lesions in multiple sclerosis: improved detection with 3D double inversion-recovery MR imaging. *Radiology*, **236**; 254-60.

Geurts, J. J., Calabrese, M., Fisher, E. and Rudick, R. A., 2012. Measurement and clinical effect of grey matter pathology in multiple sclerosis. *Lancet Neurol*, **11**; 1082-92.

Gillett, A., Marta, M., Jin, T., Tuncel, J., Leclerc, P., Nohra, R., Lange, S., Holmdahl, R., Olsson, T., Harris, R. A. and Jagodic, M., 2010. TNF production in macrophages is genetically determined and regulates inflammatory disease in rats. *J Immunol*, **185**; 442-50.

Gilmore, C. P., Donaldson, I., Bö, L., Owens, T., Lowe, J. and Evangelou, N., 2009. Regional variations in the extent and pattern of grey matter demyelination in multiple sclerosis: a comparison between the cerebral cortex, cerebellar cortex, deep grey matter nuclei and the spinal cord. *J Neurol Neurosurg Psychiatry*, **80**; 182-7.

Gilson, J. and Blakemore, W. F., 1993. Failure of remyelination in areas of demyelination produced in the spinal cord of old rats. *Neuropathol Appl Neurobiol*, **19**; 173-81.

Gitik, M., Reichert, F. and Rotshenker, S., 2010. Cytoskeleton plays a dual role of activation and inhibition in myelin and zymosan phagocytosis by microglia. *Faseb j*, **24**; 2211-21.

Gold, R., Linington, C. and Lassmann, H., 2006. Understanding pathogenesis and therapy of multiple sclerosis via animal models: 70 years of merits and culprits in experimental autoimmune encephalomyelitis research. *Brain*, **129**; 1953-71.

Goldschmidt, T., Antel, J., König, F. B., Brück, W. and Kuhlmann, T., 2009. Remyelination capacity of the MS brain decreases with disease chronicity. *Neurology*, **72**; 1914-1921.

Gonen, O., Catalaa, I., Babb, J. S., Ge, Y., Mannon, L. J., Kolson, D. L. and Grossman, R. I., 2000. Total brain N-acetylaspartate: a new measure of disease load in MS. *Neurology*, **54**; 15-9.

Gordon, S. and Martinez, F. O., 2010. Alternative activation of macrophages: mechanism and functions. *Immunity*, **32**; 593-604.
Gourraud, P. A., Harbo, H. F., Hauser, S. L. and Baranzini, S. E., 2012. The genetics of multiple sclerosis: an up-to-date review. *Immunol Rev*, **248**; 87-103.
Grakoui, A., Donermeyer, D. L., Kanagawa, O., Murphy, K. M. and Allen, P. M., 1999. TCR-independent pathways mediate the effects of antigen dose and altered peptide ligands on Th cell polarization. *J Immunol*, **162**; 1923-30.
Grassi, G., Maccaroni, P., Meyer, R., Kaiser, H., D'Ambrosio, E., Pascale, E., Grassi, M., Kuhn, A., Di Nardo, P., Kandolf, R. and Küpper, J. H., 2003. Inhibitors of DNA methylation and histone deacetylation activate cytomegalovirus promoter-controlled reporter gene expression in human glioblastoma cell line U87. *Carcinogenesis*, **24**; 1625-35.
Greenbaum, D., Colangelo, C., Williams, K. and Gerstein, M., 2003. Comparing protein abundance and mRNA expression levels on a genomic scale. *Genome Biol*, **4**; 117.
Greer, J. M. and Pender, M. P., 2008. Myelin proteolipid protein: an effective autoantigen and target of autoimmunity in multiple sclerosis. *J Autoimmun*, **31**; 281-7.
Grell, M., Douni, E., Wajant, H., Löhden, M., Clauss, M., Maxeiner, B., Georgopoulos, S., Lesslauer, W., Kollias, G., Pfizenmaier, K. and Scheurich, P., 1995. The transmembrane form of tumor necrosis factor is the prime activating ligand of the 80 kDa tumor necrosis factor receptor. *Cell*, **83**; 793-802.
Grell, M., Wajant, H., Zimmermann, G. and Scheurich, P., 1998. The type 1 receptor (CD120a) is the high-affinity receptor for soluble tumor necrosis factor. *Proc Natl Acad Sci U S A*, **95**; 570-5.
Gu, D. L., Nguyen, T., Gonzalez, A. M., Printz, M. A., Pierce, G. F., Sosnowski, B. A., Phillips, M. L. and Chandler, L. A., 2004. Adenovirus encoding human platelet-derived growth factor-B delivered in collagen exhibits safety, biodistribution, and immunogenicity profiles favorable for clinical use. *Mol Ther*, **9**; 699-711.
Guseo, A. and Jellinger, K., 1975. The significance of perivascular infiltrations in multiple sclerosis. *J Neurol*, **211**; 51-60.
Haas, J., Hug, A., Viehover, A., Fritzsching, B., Falk, C. S., Filser, A., Vetter, T., Milkova, L., Korporal, M., Fritz, B., Storch-Hagenlocher, B., Krammer, P. H., Suri-Payer, E. and Wildemann, B., 2005. Reduced suppressive effect of CD4+CD25high regulatory T cells on the T cell immune response against myelin oligodendrocyte glycoprotein in patients with multiple sclerosis. *Eur J Immunol*, **35**; 3343-52.
Haase, C. G., Guggenmos, J., Brehm, U., Andersson, M., Olsson, T., Reindl, M., Schneidewind, J. M., Zettl, U. K., Heidenreich, F., Berger, T., Wekerle, H., Hohlfeld, R. and Linington, C., 2001. The fine specificity of the myelin oligodendrocyte glycoprotein autoantibody response in patients with multiple sclerosis and normal healthy controls. *J Neuroimmunol*, **114**; 220-5.
Hafler, D. A. and Weiner, H. L., 1987. In vivo labeling of blood T cells: rapid traffic into cerebrospinal fluid in multiple sclerosis. *Ann Neurol*, **22**; 89-93.
Hampton, D. W., Innes, N., Merkler, D., Zhao, C., Franklin, R. J. and Chandran, S., 2012. Focal immune-mediated white matter demyelination reveals an age-associated increase in axonal vulnerability and decreased remyelination efficiency. *Am J Pathol*, **180**; 1897-905.
Hansen, T., Skytthe, A., Stenager, E., Petersen, H. C., Brønnum-Hansen, H. and Kyvik, K. O., 2005. Concordance for multiple sclerosis in Danish twins: an update of a nationwide study. *Mult Scler*, **11**; 504-10.
Harris, D. P., Goodrich, S., Gerth, A. J., Peng, S. L. and Lund, F. E., 2005. Regulation of IFN-gamma production by B effector 1 cells: essential roles for T-bet and the IFN-gamma receptor. *J Immunol*, **174**; 6781-90.
Harty, J. T. and Bevan, M. J., 1999. Responses of CD8(+) T cells to intracellular bacteria. *Curr Opin Immunol*, **11**; 89-93.
Hashiguchi, M., Hachimura, S., Ametani, A. and Kaminogawa, S., 2000. Th2 polarization enhanced by oral administration of higher doses of antigen. *Cytotechnology*, **33**; 237-45.
Hauser, S. L., Bhan, A. K., Gilles, F., Kemp, M., Kerr, C. and Weiner, H. L., 1986. Immunohistochemical analysis of the cellular infiltrate in multiple sclerosis lesions. *Ann Neurol*, **19**; 578-87.
Hauser, S. L., Waubant, E., Arnold, D. L., Vollmer, T., Antel, J., Fox, R. J., Bar-Or, A., Panzara, M., Sarkar, N., Agarwal, S., Langer-Gould, A. and Smith, C. H., 2008. B-cell depletion with rituximab in relapsing-remitting multiple sclerosis. *N Engl J Med*, **358**; 676-88.
Hellings, N., Raus, J. and Stinissen, P., 2002. Insights into the immunopathogenesis of multiple sclerosis. *Immunol Res*, **25**; 27-51.
Hendriks, W. T., Eggers, R., Verhaagen, J. and Boer, G. J., 2007. Gene transfer to the spinal cord neural scar with lentiviral vectors: predominant transgene expression in astrocytes but not in meningeal cells. *J Neurosci Res*, **85**; 3041-52.
Heppner, F. L., Greter, M., Marino, D., Falsig, J., Raivich, G., Hövelmeyer, N., Waisman, A., Rülicke, T., Prinz, M., Priller, J., Becher, B. and Aguzzi, A., 2005. Experimental autoimmune encephalomyelitis repressed by microglial paralysis. *Nat Med*, **11**; 146-52.

Hill, K. E., Zollinger, L. V., Watt, H. E., Carlson, N. G. and Rose, J. W., 2004. Inducible nitric oxide synthase in chronic active multiple sclerosis plaques: distribution, cellular expression and association with myelin damage. *J Neuroimmunol*, **151**; 171-9.
Hilton, A. A., Slavin, A. J., Hilton, D. J. and Bernard, C. C., 1995. Characterization of cDNA and genomic clones encoding human myelin oligodendrocyte glycoprotein. *J Neurochem*, **65**; 309-18.
Hjelmström, P., Juedes, A. E., Fjell, J. and Ruddle, N. H., 1998. B-cell-deficient mice develop experimental allergic encephalomyelitis with demyelination after myelin oligodendrocyte glycoprotein sensitization. *J Immunol*, **161**; 4480-3.
Hoban, D. B., Newland, B., Moloney, T. C., Howard, L., Pandit, A. and Dowd, E., 2013. The reduction in immunogenicity of neurotrophin overexpressing stem cells after intra-striatal transplantation by encapsulation in an in situ gelling collagen hydrogel. *Biomaterials*, **34**; 9420-9.
Hofman, F. M., Hinton, D. R., Johnson, K. and Merrill, J. E., 1989. Tumor necrosis factor identified in multiple sclerosis brain. *J Exp Med*, **170**; 607-12.
Horiuchi, M., Itoh, A., Pleasure, D. and Itoh, T., 2006. MEK-ERK signaling is involved in interferon-gamma-induced death of oligodendroglial progenitor cells. *J Biol Chem*, **281**; 20095-106.
Horwitz, M. S., Evans, C. F., McGavern, D. B., Rodriguez, M. and Oldstone, M. B., 1997. Primary demyelination in transgenic mice expressing interferon-gamma. *Nat Med*, **3**; 1037-41.
Hosken, N. A., Shibuya, K., Heath, A. W., Murphy, K. M. and O'Garra, A., 1995. The effect of antigen dose on CD4+ T helper cell phenotype development in a T cell receptor-alpha beta-transgenic model. *J Exp Med*, **182**; 1579-84.
Hosking, M. P., Tirotta, E., Ransohoff, R. M. and Lane, T. E., 2010. CXCR2 signaling protects oligodendrocytes and restricts demyelination in a mouse model of viral-induced demyelination. *PLoS One*, **5**; e11340.
Houtkamp, M. A., de Boer, O. J., van der Loos, C. M., van der Wal, A. C. and Becker, A. E., 2001. Adventitial infiltrates associated with advanced atherosclerotic plaques: structural organization suggests generation of local humoral immune responses. *J Pathol*, **193**; 263-9.
Howell, O. W., Reeves, C. A., Nicholas, R., Carassiti, D., Radotra, B., Gentleman, S. M., Serafini, B., Aloisi, F., Roncaroli, F., Magliozzi, R. and Reynolds, R., 2011. Meningeal inflammation is widespread and linked to cortical pathology in multiple sclerosis. *Brain*, **134**; 2755-71.
Hughes, T. S., Langer, S. J., Johnson, K. W., Chavez, R. A., Watkins, L. R., Milligan, E. D. and Leinwand, L. A., 2009. Intrathecal injection of naked plasmid DNA provides long-term expression of secreted proteins. *Mol Ther*, **17**; 88-94.
Huseby, E. S., Liggitt, D., Brabb, T., Schnabel, B., Ohlén, C. and Goverman, J., 2001. A pathogenic role for myelin-specific CD8(+) T cells in a model for multiple sclerosis. *J Exp Med*, **194**; 669-76.
Iliff, J. J., Wang, M., Liao, Y., Plogg, B. A., Peng, W., Gundersen, G. A., Benveniste, H., Vates, G. E., Deane, R., Goldman, S. A., Nagelhus, E. A. and Nedergaard, M., 2012. A paravascular pathway facilitates CSF flow through the brain parenchyma and the clearance of interstitial solutes, including amyloid beta. *Sci Transl Med*, **4**; 147ra111.
Imbeaud, S., Graudens, E., Boulanger, V., Barlet, X., Zaborski, P., Eveno, E., Mueller, O., Schroeder, A. and Auffray, C., 2005. Towards standardization of RNA quality assessment using user-independent classifiers of microcapillary electrophoresis traces. *Nucleic Acids Res*, **33**; e56.
Imitola, J., Chitnis, T. and Khoury, S. J., 2005. Cytokines in multiple sclerosis: from bench to bedside. *Pharmacol Ther*, **106**; 163-77.
Issazadeh, S., Mustafa, M., Ljungdahl, A., Höjeberg, B., Dagerlind, A., Elde, R. and Olsson, T., 1995. Interferon gamma, interleukin 4 and transforming growth factor beta in experimental autoimmune encephalomyelitis in Lewis rats: dynamics of cellular mRNA expression in the central nervous system and lymphoid cells. *J Neurosci Res*, **40**; 579-90.
Jacobsen, C., Hagemeier, J., Myhr, K. M., Nyland, H., Lode, K., Bergsland, N., Ramasamy, D. P., Dalaker, T. O., Larsen, J. P., Farbu, E. and Zivadinov, R., 2014. Brain atrophy and disability progression in multiple sclerosis patients: a 10-year follow-up study. *J Neurol Neurosurg Psychiatry*.
Jacobsen, M., Cepok, S., Quak, E., Happel, M., Gaber, R., Ziegler, A., Schock, S., Oertel, W. H., Sommer, N. and Hemmer, B., 2002. Oligoclonal expansion of memory CD8+ T cells in cerebrospinal fluid from multiple sclerosis patients. *Brain*, **125**; 538-50.
Jäger, A., Dardalhon, V., Sobel, R. A., Bettelli, E. and Kuchroo, V. K., 2009. Th1, Th17, and Th9 effector cells induce experimental autoimmune encephalomyelitis with different pathological phenotypes. *J Immunol*, **183**; 7169-77.
Jagessar, S. A., Heijmans, N., Bauer, J., Blezer, E. L., Laman, J. D., Hellings, N. and t Hart, B. A., 2012. B-cell depletion abrogates T cell-mediated demyelination in an antibody-nondependent common marmoset experimental autoimmune encephalomyelitis model. *J Neuropathol Exp Neurol*, **71**; 716-28.
Jakobsson, J., Ericson, C., Jansson, M., Björk, E. and Lundberg, C., 2003. Targeted transgene expression in rat brain using lentiviral vectors. *J Neurosci Res*, **73**; 876-85.

Jakobsson, J. and Lundberg, C., 2006. Lentiviral vectors for use in the central nervous system. *Mol Ther*, **13**; 484-93.
Jarraya, B., Boulet, S., Ralph, G. S., Jan, C., Bonvento, G., Azzouz, M., Miskin, J. E., Shin, M., Delzescaux, T., Drouot, X., Hérard, A. S., Day, D. M., Brouillet, E., Kingsman, S. M., Hantraye, P., Mitrophanous, K. A., Mazarakis, N. D. and Palfi, S., 2009. Dopamine gene therapy for Parkinson's disease in a nonhuman primate without associated dyskinesia. *Sci Transl Med*, **1**; 2ra4.
Jersild, C., Svejgaard, A. and Fog, T., 1972. HL-A antigens and multiple sclerosis. *Lancet*, **1**; 1240-1.
Johanson, C. E., Duncan, J. A., Stopa, E. G. and Baird, A., 2005. Enhanced prospects for drug delivery and brain targeting by the choroid plexus-CSF route. *Pharm Res*, **22**; 1011-37.
Johns, T. G., Kerlero de Rosbo, N., Menon, K. K., Abo, S., Gonzales, M. F. and Bernard, C. C., 1995. Myelin oligodendrocyte glycoprotein induces a demyelinating encephalomyelitis resembling multiple sclerosis. *J Immunol*, **154**; 5536-41.
Johns, T. G. and Bernard, C. C., 1997. Binding of complement component Clq to myelin oligodendrocyte glycoprotein: a novel mechanism for regulating CNS inflammation. *Mol Immunol*, **34**; 33-8.
Johns, T. G. and Bernard, C. C., 1999. The structure and function of myelin oligodendrocyte glycoprotein. *J Neurochem*, **72**; 1-9.
Johnston, M., Zakharov, A., Papaiconomou, C., Salmasi, G. and Armstrong, D., 2004. Evidence of connections between cerebrospinal fluid and nasal lymphatic vessels in humans, non-human primates and other mammalian species. *Cerebrospinal Fluid Res*, **1**; 2.
Jurewicz, A., Matysiak, M., Tybor, K., Kilianek, L., Raine, C. S. and Selmaj, K., 2005. Tumour necrosis factor-induced death of adult human oligodendrocytes is mediated by apoptosis inducing factor. *Brain*, **128**; 2675-88.
Kaiko, G. E., Horvat, J. C., Beagley, K. W. and Hansbro, P. M., 2008. Immunological decision-making: how does the immune system decide to mount a helper T-cell response? *Immunology*, **123**; 326-38.
Kala, M., Rhodes, S. N., Piao, W. H., Shi, F. D., Campagnolo, D. I. and Vollmer, T. L., 2010. B cells from glatiramer acetate-treated mice suppress experimental autoimmune encephalomyelitis. *Exp Neurol*, **221**; 136-45.
Kassiotis, G., Pasparakis, M., Kollias, G. and Probert, L., 1999. TNF accelerates the onset but does not alter the incidence and severity of myelin basic protein-induced experimental autoimmune encephalomyelitis. *Eur J Immunol*, **29**; 774-80.
Kawakami, N., Lassmann, S., Li, Z., Odoardi, F., Ritter, T., Ziemssen, T., Klinkert, W. E., Ellwart, J. W., Bradl, M., Krivacic, K., Lassmann, H., Ransohoff, R. M., Volk, H. D., Wekerle, H., Linington, C. and Flügel, A., 2004. The activation status of neuroantigen-specific T cells in the target organ determines the clinical outcome of autoimmune encephalomyelitis. *J Exp Med*, **199**; 185-97.
Kerlero de Rosbo, N., Milo, R., Lees, M. B., Burger, D., Bernard, C. C. and Ben-Nun, A., 1993. Reactivity to myelin antigens in multiple sclerosis. Peripheral blood lymphocytes respond predominantly to myelin oligodendrocyte glycoprotein. *J Clin Invest*, **92**; 2602-8.
Kerschensteiner, M., Stadelmann, C., Buddeberg, B. S., Merkler, D., Bareyre, F. M., Anthony, D. C., Linington, C., Brück, W. and Schwab, M. E., 2004. Targeting experimental autoimmune encephalomyelitis lesions to a predetermined axonal tract system allows for refined behavioral testing in an animal model of multiple sclerosis. *Am J Pathol*, **164**; 1455-69.
Khoruts, A., Miller, S. D. and Jenkins, M. K., 1995. Neuroantigen-specific Th2 cells are inefficient suppressors of experimental autoimmune encephalomyelitis induced by effector Th1 cells. *J Immunol*, **155**; 5011-7.
Kida, S., Pantazis, A. and Weller, R. O., 1993. CSF drains directly from the subarachnoid space into nasal lymphatics in the rat. Anatomy, histology and immunological significance. *Neuropathol Appl Neurobiol*, **19**; 480-8.
Kidd, D., Barkhof, F., McConnell, R., Algra, P. R., Allen, I. V. and Revesz, T., 1999. Cortical lesions in multiple sclerosis. *Brain*, **122 (Pt 1)**; 17-26.
Kim, C. H., Rott, L. S., Clark-Lewis, I., Campbell, D. J., Wu, L. and Butcher, E. C., 2001. Subspecialization of CXCR5+ T cells: B helper activity is focused in a germinal center-localized subset of CXCR5+ T cells. *J Exp Med*, **193**; 1373-81.
King, C., Tangye, S. G. and Mackay, C. R., 2008. T follicular helper (TFH) cells in normal and dysregulated immune responses. *Annu Rev Immunol*, **26**; 741-66.
Kirk, J., Plumb, J., Mirakhur, M. and McQuaid, S., 2003. Tight junctional abnormality in multiple sclerosis white matter affects all calibres of vessel and is associated with blood-brain barrier leakage and active demyelination. *J Pathol*, **201**; 319-27.
Kivisäkk, P., Imitola, J., Rasmussen, S., Elyaman, W., Zhu, B., Ransohoff, R. M. and Khoury, S. J., 2009. Localizing central nervous system immune surveillance: meningeal antigen-presenting cells activate T cells during experimental autoimmune encephalomyelitis. *Ann Neurol*, **65**; 457-69.
Klaver, R., De Vries, H. E., Schenk, G. J. and Geurts, J. J., 2013. Grey matter damage in multiple sclerosis: a pathology perspective. *Prion*, **7**; 66-75.

Kleinewietfeld, M. and Hafler, D. A., 2014. Regulatory T cells in autoimmune neuroinflammation. *Immunol Rev*, **259**; 231-44.
Kohm, A. P., Carpentier, P. A., Anger, H. A. and Miller, S. D., 2002. Cutting edge: CD4+CD25+ regulatory T cells suppress antigen-specific autoreactive immune responses and central nervous system inflammation during active experimental autoimmune encephalomyelitis. *J Immunol*, **169**; 4712-6.
Kolasinski, J., Stagg, C. J., Chance, S. A., Deluca, G. C., Esiri, M. M., Chang, E. H., Palace, J. A., McNab, J. A., Jenkinson, M., Miller, K. L. and Johansen-Berg, H., 2012. A combined post-mortem magnetic resonance imaging and quantitative histological study of multiple sclerosis pathology. *Brain*, **135**; 2938-51.
Kondo, M., Sumino, R. and Okado, H., 1997. Combinations of AMPA receptor subunit expression in individual cortical neurons correlate with expression of specific calcium-binding proteins. *J Neurosci*, **17**; 1570-81.
Konieczny, B. T., Dai, Z., Elwood, E. T., Saleem, S., Linsley, P. S., Baddoura, F. K., Larsen, C. P., Pearson, T. C. and Lakkis, F. G., 1998. IFN-gamma is critical for long-term allograft survival induced by blocking the CD28 and CD40 ligand T cell costimulation pathways. *J Immunol*, **160**; 2059-64.
Kooi, E. J., Geurts, J. J., van Horssen, J., Bø, L. and van der Valk, P., 2009. Meningeal inflammation is not associated with cortical demyelination in chronic multiple sclerosis. *J Neuropathol Exp Neurol*, **68**; 1021-8.
Koppelkamm, A., Vennemann, B., Lutz-Bonengel, S., Fracasso, T. and Vennemann, M., 2011. RNA integrity in post-mortem samples: influencing parameters and implications on RT-qPCR assays. *Int J Legal Med*, **125**; 573-80.
Körner, H., Lemckert, F. A., Chaudhri, G., Etteldorf, S. and Sedgwick, J. D., 1997a. Tumor necrosis factor blockade in actively induced experimental autoimmune encephalomyelitis prevents clinical disease despite activated T cell infiltration to the central nervous system. *Eur J Immunol*, **27**; 1973-81.
Körner, H., Riminton, D. S., Strickland, D. H., Lemckert, F. A., Pollard, J. D. and Sedgwick, J. D., 1997b. Critical points of tumor necrosis factor action in central nervous system autoimmune inflammation defined by gene targeting. *J Exp Med*, **186**; 1585-90.
Kotter, M. R., Zhao, C., van Rooijen, N. and Franklin, R. J., 2005. Macrophage-depletion induced impairment of experimental CNS remyelination is associated with a reduced oligodendrocyte progenitor cell response and altered growth factor expression. *Neurobiol Dis*, **18**; 166-75.
Kowarik, M. C., Cepok, S., Sellner, J., Grummel, V., Weber, M. S., Korn, T., Berthele, A. and Hemmer, B., 2012. CXCL13 is the major determinant for B cell recruitment to the CSF during neuroinflammation. *J Neuroinflammation*, **9**; 93.
Kramann, N., Neid, K., Menken, L., Schlumbohm, C., Stadelmann, C., Fuchs, E., Brück, W. and Wegner, C., 2014. Increased Meningeal T and Plasma Cell Infiltration Is Associated with Early Subpial Cortical Demyelination in Common Marmosets with Experimental Autoimmune Encephalomyelitis. *Brain Pathol*.
Krebs, S., Fischaleck, M. and Blum, H., 2009. A simple and loss-free method to remove TRIzol contaminations from minute RNA samples. *Anal Biochem*, **387**; 136-8.
Krishnamoorthy, G., Lassmann, H., Wekerle, H. and Holz, A., 2006. Spontaneous opticospinal encephalomyelitis in a double-transgenic mouse model of autoimmune T cell/B cell cooperation. *J Clin Invest*, **116**; 2385-92.
Kroepfl, J. F., Viise, L. R., Charron, A. J., Linington, C. and Gardinier, M. V., 1996. Investigation of myelin/oligodendrocyte glycoprotein membrane topology. *J Neurochem*, **67**; 2219-22.
Krumbholz, M., Theil, D., Cepok, S., Hemmer, B., Kivisäkk, P., Ransohoff, R. M., Hofbauer, M., Farina, C., Derfuss, T., Hartle, C., Newcombe, J., Hohlfeld, R. and Meinl, E., 2006. Chemokines in multiple sclerosis: CXCL12 and CXCL13 up-regulation is differentially linked to CNS immune cell recruitment. *Brain*, **129**; 200-11.
Kuenz, B., Lutterotti, A., Ehling, R., Gneiss, C., Haemmerle, M., Rainer, C., Deisenhammer, F., Schocke, M., Berger, T. and Reindl, M., 2008. Cerebrospinal fluid B cells correlate with early brain inflammation in multiple sclerosis. *PLoS One*, **3**; e2559.
Kuhlmann, T., Lingfeld, G., Bitsch, A., Schuchardt, J. and Brück, W., 2002. Acute axonal damage in multiple sclerosis is most extensive in early disease stages and decreases over time. *Brain*, **125**; 2202-12.
Kuhlmann, T., Miron, V., Cui, Q., Wegner, C., Antel, J. and Brück, W., 2008. Differentiation block of oligodendroglial progenitor cells as a cause for remyelination failure in chronic multiple sclerosis. *Brain*, **131**; 1749-58.
Kuno, R., Wang, J., Kawanokuchi, J., Takeuchi, H., Mizuno, T. and Suzumura, A., 2005. Autocrine activation of microglia by tumor necrosis factor-alpha. *J Neuroimmunol*, **162**; 89-96.
Kurtzke, J. F., Dean, G. and Botha, D. P., 1970. A method for estimating the age at immigration of white immigrants to South Africa, with an example of its importance. *S Afr Med J*, **44**; 663-9.

Kutner, R. H., Zhang, X. Y. and Reiser, J., 2009. Production, concentration and titration of pseudotyped HIV-1-based lentiviral vectors. *Nat Protoc*, **4**; 495-505.
Kutzelnigg, A. and Lassmann, H., 2005. Cortical lesions and brain atrophy in MS. *J Neurol Sci*, **233**; 55-9.
Kutzelnigg, A., Lucchinetti, C. F., Stadelmann, C., Brück, W., Rauschka, H., Bergmann, M., Schmidbauer, M., Parisi, J. E. and Lassmann, H., 2005. Cortical demyelination and diffuse white matter injury in multiple sclerosis. *Brain*, **128**; 2705-12.
Kutzelnigg, A., Faber-Rod, J. C., Bauer, J., Lucchinetti, C. F., Sorensen, P. S., Laursen, H., Stadelmann, C., Brück, W., Rauschka, H., Schmidbauer, M. and Lassmann, H., 2007. Widespread demyelination in the cerebellar cortex in multiple sclerosis. *Brain Pathol*, **17**; 38-44.
Langrish, C. L., Chen, Y., Blumenschein, W. M., Mattson, J., Basham, B., Sedgwick, J. D., McClanahan, T., Kastelein, R. A. and Cua, D. J., 2005. IL-23 drives a pathogenic T cell population that induces autoimmune inflammation. *J Exp Med*, **201**; 233-40.
Lassmann, H., Brunner, C., Bradl, M. and Linington, C., 1988. Experimental allergic encephalomyelitis: the balance between encephalitogenic T lymphocytes and demyelinating antibodies determines size and structure of demyelinated lesions. *Acta Neuropathol*, **75**; 566-76.
Lassmann, H., Brück, W. and Lucchinetti, C., 2001. Heterogeneity of multiple sclerosis pathogenesis: implications for diagnosis and therapy. *Trends Mol Med*, **7**; 115-21.
Lassmann, H., 2008. The pathologic substrate of magnetic resonance alterations in multiple sclerosis. *Neuroimaging Clin N Am*, **18**; 563-76, ix.
Lassmann, H. and van Horssen, J., 2011. The molecular basis of neurodegeneration in multiple sclerosis. *FEBS Lett*, **585**; 3715-23.
Lassmann, H., 2012. Cortical lesions in multiple sclerosis: inflammation versus neurodegeneration. *Brain*, **135**; 2904-5.
The Lenercept Multiple Sclerosis Study Group and The University of British Columbia MS/MRI Analysis Group, 1999. TNF neutralization in MS: results of a randomized, placebo-controlled multicenter study. *Neurology*, **53**; 457-65.
Lennon, V. A., Kryzer, T. J., Pittock, S. J., Verkman, A. S. and Hinson, S. R., 2005. IgG marker of optic-spinal multiple sclerosis binds to the aquaporin-4 water channel. *J Exp Med*, **202**; 473-7.
Lewis-Tuffin, L. J., Rodriguez, F., Giannini, C., Scheithauer, B., Necela, B. M., Sarkaria, J. N. and Anastasiadis, P. Z., 2010. Misregulated E-cadherin expression associated with an aggressive brain tumor phenotype. *PLoS One*, **5**; e13665.
Li, W. W., Setzu, A., Zhao, C. and Franklin, R. J., 2005. Minocycline-mediated inhibition of microglia activation impairs oligodendrocyte progenitor cell responses and remyelination in a non-immune model of demyelination. *J Neuroimmunol*, **158**; 58-66.
Lin, W., Kemper, A., Dupree, J. L., Harding, H. P., Ron, D. and Popko, B., 2006. Interferon-gamma inhibits central nervous system remyelination through a process modulated by endoplasmic reticulum stress. *Brain*, **129**; 1306-18.
Linington, C. and Lassmann, H., 1987. Antibody responses in chronic relapsing experimental allergic encephalomyelitis: correlation of serum demyelinating activity with antibody titre to the myelin/oligodendrocyte glycoprotein (MOG). *J Neuroimmunol*, **17**; 61-9.
Linington, C., Bradl, M., Lassmann, H., Brunner, C. and Vass, K., 1988. Augmentation of demyelination in rat acute allergic encephalomyelitis by circulating mouse monoclonal antibodies directed against a myelin/oligodendrocyte glycoprotein. *Am J Pathol*, **130**; 443-54.
Linington, C., Morgan, B. P., Scolding, N. J., Wilkins, P., Piddlesden, S. and Compston, D. A., 1989. The role of complement in the pathogenesis of experimental allergic encephalomyelitis. *Brain*, **112 (Pt 4)**; 895-911.
Lipska, B. K., Deep-Soboslay, A., Weickert, C. S., Hyde, T. M., Martin, C. E., Herman, M. M. and Kleinman, J. E., 2006. Critical factors in gene expression in postmortem human brain: Focus on studies in schizophrenia. *Biol Psychiatry*, **60**; 650-8.
Litzenburger, T., Fässler, R., Bauer, J., Lassmann, H., Linington, C., Wekerle, H. and Iglesias, A., 1998. B lymphocytes producing demyelinating autoantibodies: development and function in gene-targeted transgenic mice. *J Exp Med*, **188**; 169-80.
Liu, J. W., Pernod, G., Dunoyer-Geindre, S., Fish, R. J., Yang, H., Bounameaux, H. and Kruithof, E. K., 2006. Promoter dependence of transgene expression by lentivirus-transduced human blood-derived endothelial progenitor cells. *Stem Cells*, **24**; 199-208.
Livak, K. J. and Schmittgen, T. D., 2001. Analysis of relative gene expression data using real-time quantitative PCR and the 2(-Delta Delta C(T)) Method. *Methods*, **25**; 402-8.
Lopes, C. A. S. and Mair, W. G. P., 1974. Ultrastructure of the outer cortex and thepia mater in man. *Acta Neuropathologica*, **28**; 79-86.
Lopez, A. F., Eglinton, J. M., Lyons, A. B., Tapley, P. M., To, L. B., Park, L. S., Clark, S. C. and Vadas, M. A., 1990. Human interleukin-3 inhibits the binding of granulocyte-macrophage colony-stimulating factor and interleukin-5 to basophils and strongly enhances their functional activity. *J Cell Physiol*, **145**; 69-77.

Lorentzen, J. C., Andersson, M., Issazadeh, S., Dahlman, I., Luthman, H., Weissert, R. and Olsson, T., 1997. Genetic analysis of inflammation, cytokine mRNA expression and disease course of relapsing experimental autoimmune encephalomyelitis in DA rats. *J Neuroimmunol*, **80**; 31-7.
Lovas, G., Szilágyi, N., Majtényi, K., Palkovits, M. and Komoly, S., 2000. Axonal changes in chronic demyelinated cervical spinal cord plaques. *Brain*, **123 (Pt 2)**; 308-17.
Lovato, L., Willis, S. N., Rodig, S. J., Caron, T., Almendinger, S. E., Howell, O. W., Reynolds, R., O'Connor, K. C. and Hafler, D. A., 2011. Related B cell clones populate the meninges and parenchyma of patients with multiple sclerosis. *Brain*, **134**; 534-41.
Lovett-Racke, A. E., Yang, Y. and Racke, M. K., 2011. Th1 versus Th17: are T cell cytokines relevant in multiple sclerosis? *Biochim Biophys Acta*, **1812**; 246-51.
Lucchinetti, C., Brück, W., Parisi, J., Scheithauer, B., Rodriguez, M. and Lassmann, H., 1999. A quantitative analysis of oligodendrocytes in multiple sclerosis lesions - A study of 113 cases. *Brain*, **122**; 2279-2295.
Lucchinetti, C., Brück, W., Parisi, J., Scheithauer, B., Rodriguez, M. and Lassmann, H., 2000. Heterogeneity of multiple sclerosis lesions: implications for the pathogenesis of demyelination. *Ann Neurol*, **47**; 707-17.
Lucchinetti, C. F., Popescu, B. F., Bunyan, R. F., Moll, N. M., Roemer, S. F., Lassmann, H., Brück, W., Parisi, J. E., Scheithauer, B. W., Giannini, C., Weigand, S. D., Mandrekar, J. and Ransohoff, R. M., 2011. Inflammatory cortical demyelination in early multiple sclerosis. *N Engl J Med*, **365**; 2188-97.
Lukic, M. L., Mensah-Brown, E., Galadari, S. and Shahin, A., 2001. Lack of apoptosis of infiltrating cells as the mechanism of high susceptibility to EAE in DA rats. *Dev Immunol*, **8**; 193-200.
Lünemann, J. D., Tintoré, M., Messmer, B., Strowig, T., Rovira, A., Perkal, H., Caballero, E., Münz, C., Montalban, X. and Comabella, M., 2010. Elevated Epstein-Barr virus-encoded nuclear antigen-1 immune responses predict conversion to multiple sclerosis. *Ann Neurol*, **67**; 159-69.
Luther, S. A., Lopez, T., Bai, W., Hanahan, D. and Cyster, J. G., 2000. BLC expression in pancreatic islets causes B cell recruitment and lymphotoxin-dependent lymphoid neogenesis. *Immunity*, **12**; 471-81.
Lyons, J. A., San, M., Happ, M. P. and Cross, A. H., 1999. B cells are critical to induction of experimental allergic encephalomyelitis by protein but not by a short encephalitogenic peptide. *Eur J Immunol*, **29**; 3432-9.
Maarouf, C. L., Beach, T. G., Adler, C. H., Shill, H. A., Sabbagh, M. N., Wu, T., Walker, D. G., Kokjohn, T. A., Roher, A. E. and Arizona, P. D. C., 2012. Cerebrospinal fluid biomarkers of neuropathologically diagnosed Parkinson's disease subjects. *Neurol Res*, **34**; 669-76.
Magalhães, R., Stiehl, P., Morawietz, L., Berek, C. and Krenn, V., 2002. Morphological and molecular pathology of the B cell response in synovitis of rheumatoid arthritis. *Virchows Arch*, **441**; 415-27.
Magliozzi, R., Columba-Cabezas, S., Serafini, B. and Aloisi, F., 2004. Intracerebral expression of CXCL13 and BAFF is accompanied by formation of lymphoid follicle-like structures in the meninges of mice with relapsing experimental autoimmune encephalomyelitis. *J Neuroimmunol*, **148**; 11-23.
Magliozzi, R., Howell, O., Vora, A., Serafini, B., Nicholas, R., Puopolo, M., Reynolds, R. and Aloisi, F., 2007. Meningeal B-cell follicles in secondary progressive multiple sclerosis associate with early onset of disease and severe cortical pathology. *Brain*, **130**; 1089-104.
Magliozzi, R., Howell, O. W., Reeves, C., Roncaroli, F., Nicholas, R., Serafini, B., Aloisi, F. and Reynolds, R., 2010. A Gradient of neuronal loss and meningeal inflammation in multiple sclerosis. *Ann Neurol*, **68**; 477-93.
Magliozzi, R., Serafini, B., Rosicarelli, B., Chiappetta, G., Veroni, C., Reynolds, R. and Aloisi, F., 2013. B-cell enrichment and Epstein-Barr virus infection in inflammatory cortical lesions in secondary progressive multiple sclerosis. *J Neuropathol Exp Neurol*, **72**; 29-41.
Mannie, M., Swanborg, R. H. and Stepaniak, J. A., 2009. Experimental autoimmune encephalomyelitis in the rat. *Curr Protoc Immunol*, **Chapter 15**; Unit 15 2.
Mars, L. T., Saikali, P., Liblau, R. S. and Arbour, N., 2011. Contribution of CD8 T lymphocytes to the immuno-pathogenesis of multiple sclerosis and its animal models. *Biochim Biophys Acta*, **1812**; 151-61.
Matsushita, T., Yanaba, K., Bouaziz, J. D., Fujimoto, M. and Tedder, T. F., 2008. Regulatory B cells inhibit EAE initiation in mice while other B cells promote disease progression. *J Clin Invest*, **118**; 3420-30.
Matute, C., 1998. Characteristics of acute and chronic kainate excitotoxic damage to the optic nerve. *Proc Natl Acad Sci U S A*, **95**; 10229-34.
Mead, R. J., Singhrao, S. K., Neal, J. W., Lassmann, H. and Morgan, B. P., 2002. The membrane attack complex of complement causes severe demyelination associated with acute axonal injury. *J Immunol*, **168**; 458-65.
Merkler, D., Ernsting, T., Kerschensteiner, M., Brück, W. and Stadelmann, C., 2006. A new focal EAE model of cortical demyelination: multiple sclerosis-like lesions with rapid resolution of inflammation and extensive remyelination. *Brain*, **129**; 1972-83.
Merrill, J. E., Ignarro, L. J., Sherman, M. P., Melinek, J. and Lane, T. E., 1993. Microglial cell cytotoxicity of oligodendrocytes is mediated through nitric oxide. *J Immunol*, **151**; 2132-41.

Miller, S. D., Karpus, W. J. and Davidson, T. S., 2010. Experimental autoimmune encephalomyelitis in the mouse. *Curr Protoc Immunol*, **Chapter 15**; Unit 15 1.
Millward, J. M., Caruso, M., Campbell, I. L., Gauldie, J. and Owens, T., 2007. IFN-gamma-induced chemokines synergize with pertussis toxin to promote T cell entry to the central nervous system. *J Immunol*, **178**; 8175-82.
Minagar, A. and Alexander, J. S., 2003. Blood-brain barrier disruption in multiple sclerosis. *Mult Scler*, **9**; 540-9.
Minden, S. L., 2000. Mood disorders in multiple sclerosis: diagnosis and treatment. *J Neurovirol*, **6 Suppl 2**; S160-7.
Mir, M., Tolosa, L., Asensio, V. J., Lladó, J. and Olmos, G., 2008. Complementary roles of tumor necrosis factor alpha and interferon gamma in inducible microglial nitric oxide generation. *J Neuroimmunol*, **204**; 101-9.
Mok, H., Park, J. W. and Park, T. G., 2007. Microencapsulation of PEGylated adenovirus within PLGA microspheres for enhanced stability and gene transfection efficiency. *Pharm Res*, **24**; 2263-9.
Mokhtarian, F., McFarlin, D. E. and Raine, C. S., 1984. Adoptive transfer of myelin basic protein-sensitized T cells produces chronic relapsing demyelinating disease in mice. *Nature*, **309**; 356-8.
Molnarfi, N., Schulze-Topphoff, U., Weber, M. S., Patarroyo, J. C., Prod'homme, T., Varrin-Doyer, M., Shetty, A., Linington, C., Slavin, A. J., Hidalgo, J., Jenne, D. E., Wekerle, H., Sobel, R. A., Bernard, C. C., Shlomchik, M. J. and Zamvil, S. S., 2013. MHC class II-dependent B cell APC function is required for induction of CNS autoimmunity independent of myelin-specific antibodies. *J Exp Med*, **210**; 2921-37.
Mony, J. T., Khorooshi, R. and Owens, T., 2014. MOG extracellular domain (p1-125) triggers elevated frequency of CXCR3+ CD4+ Th1 cells in the CNS of mice and induces greater incidence of severe EAE. *Mult Scler*.
Mosley, K. and Cuzner, M. L., 1996. Receptor-mediated phagocytosis of myelin by macrophages and microglia: effect of opsonization and receptor blocking agents. *Neurochem Res*, **21**; 481-7.
Muller, D. M., Pender, M. P. and Greer, J. M., 2000. A neuropathological analysis of experimental autoimmune encephalomyelitis with predominant brain stem and cerebellar involvement and differences between active and passive induction. *Acta Neuropathol*, **100**; 174-82.
Müller, M., Carter, S. L., Hofer, M. J., Manders, P., Getts, D. R., Getts, M. T., Dreykluft, A., Lu, B., Gerard, C., King, N. J. and Campbell, I. L., 2007. CXCR3 signaling reduces the severity of experimental autoimmune encephalomyelitis by controlling the parenchymal distribution of effector and regulatory T cells in the central nervous system. *J Immunol*, **179**; 2774-86.
Müller, M., Carter, S., Hofer, M. J. and Campbell, I. L., 2010. Review: The chemokine receptor CXCR3 and its ligands CXCL9, CXCL10 and CXCL11 in neuroimmunity--a tale of conflict and conundrum. *Neuropathol Appl Neurobiol*, **36**; 368-87.
Multiple Sclerosis International Federation, 2013. *Atlas of MS 2013.* [pdf] London: Multiple Sclerosis International Federation. Available at: <http://www.msif.org/wp-content/uploads/2014/09/Atlas-of-MS.pdf> [Accessed 13 November 2014].
Mumford, C. J., Wood, N. W., Kellar-Wood, H., Thorpe, J. W., Miller, D. H. and Compston, D. A., 1994. The British Isles survey of multiple sclerosis in twins. *Neurology*, **44**; 11-5.
Munger, K. L., Levin, L. I., Hollis, B. W., Howard, N. S. and Ascherio, A., 2006. Serum 25-hydroxyvitamin D levels and risk of multiple sclerosis. *JAMA*, **296**; 2832-8.
Münzel, E. J. and Williams, A., 2013. Promoting remyelination in multiple sclerosis-recent advances. *Drugs*, **73**; 2017-29.
Nakajima, C., Mukai, T., Yamaguchi, N., Morimoto, Y., Park, W. R., Iwasaki, M., Gao, P., Ono, S., Fujiwara, H. and Hamaoka, T., 2002. Induction of the chemokine receptor CXCR3 on TCR-stimulated T cells: dependence on the release from persistent TCR-triggering and requirement for IFN-gamma stimulation. *Eur J Immunol*, **32**; 1792-801.
Nikodemova, M., Watters, J. J., Jackson, S. J., Yang, S. K. and Duncan, I. D., 2007. Minocycline down-regulates MHC II expression in microglia and macrophages through inhibition of IRF-1 and protein kinase C (PKC)alpha/betaII. *J Biol Chem*, **282**; 15208-16.
Nimmerjahn, A., Kirchhoff, F. and Helmchen, F., 2005. Resting microglial cells are highly dynamic surveillants of brain parenchyma in vivo. *Science*, **308**; 1314-8.
Norrman, K., Fischer, Y., Bonnamy, B., Wolfhagen Sand, F., Ravassard, P. and Semb, H., 2010. Quantitative comparison of constitutive promoters in human ES cells. *PLoS One*, **5**; e12413.
Nylander, A. and Hafler, D. A., 2012. Multiple sclerosis. *J Clin Invest*, **122**; 1180-8.
O'Connor, K. C., Appel, H., Bregoli, L., Call, M. E., Catz, I., Chan, J. A., Moore, N. H., Warren, K. G., Wong, S. J., Hafler, D. A. and Wucherpfennig, K. W., 2005. Antibodies from inflamed central nervous system tissue recognize myelin oligodendrocyte glycoprotein. *J Immunol*, **175**; 1974-82.
O'Connor, P., 2002. Key issues in the diagnosis and treatment of multiple sclerosis. An overview. *Neurology*, **59**; S1-33.

O'Connor, R. A., Prendergast, C. T., Sabatos, C. A., Lau, C. W., Leech, M. D., Wraith, D. C. and Anderton, S. M., 2008. Cutting edge: Th1 cells facilitate the entry of Th17 cells to the central nervous system during experimental autoimmune encephalomyelitis. *J Immunol*, **181**; 3750-4.
O'Keefe, G. M., Nguyen, V. T. and Benveniste, E. N., 1999. Class II transactivator and class II MHC gene expression in microglia: modulation by the cytokines TGF-beta, IL-4, IL-13 and IL-10. *Eur J Immunol*, **29**; 1275-85.
Obradović, D., Kataranovski, M., Dincić, E., Obradović, S. and Colić, M., 2012. Tumor necrosis factor-alfa and interleukin-4 in cerbrospinal fluid and plasma in different clinical forms of multiple sclerosis. *Vojnosanit Pregl*, **69**; 151-6.
Oh, J. W., Schwiebert, L. M. and Benveniste, E. N., 1999. Cytokine regulation of CC and CXC chemokine expression by human astrocytes. *J Neurovirol*, **5**; 82-94.
Olah, M., Amor, S., Brouwer, N., Vinet, J., Eggen, B., Biber, K. and Boddeke, H. W., 2012. Identification of a microglia phenotype supportive of remyelination. *Glia*, **60**; 306-21.
Omari, K. M., John, G., Lango, R. and Raine, C. S., 2006. Role for CXCR2 and CXCL1 on glia in multiple sclerosis. *Glia*, **53**; 24-31.
Omari, K. M., Lutz, S. E., Santambrogio, L., Lira, S. A. and Raine, C. S., 2009. Neuroprotection and remyelination after autoimmune demyelination in mice that inducibly overexpress CXCL1. *Am J Pathol*, **174**; 164-76.
Orton, S. M., Wald, L., Confavreux, C., Vukusic, S., Krohn, J. P., Ramagopalan, S. V., Herrera, B. M., Sadovnick, A. D. and Ebers, G. C., 2011. Association of UV radiation with multiple sclerosis prevalence and sex ratio in France. *Neurology*, **76**; 425-31.
Owens, G. P., Ritchie, A. M., Burgoon, M. P., Williamson, R. A., Corboy, J. R. and Gilden, D. H., 2003. Single-cell repertoire analysis demonstrates that clonal expansion is a prominent feature of the B cell response in multiple sclerosis cerebrospinal fluid. *J Immunol*, **171**; 2725-33.
Panitch, H. S., Hirsch, R. L., Haley, A. S. and Johnson, K. P., 1987. Exacerbations of multiple sclerosis in patients treated with gamma interferon. *Lancet*, **1**; 893-5.
Papadopoulos, D., Pham-Dinh, D. and Reynolds, R., 2006. Axon loss is responsible for chronic neurological deficit following inflammatory demyelination in the rat. *Exp Neurol*, **197**; 373-85.
Papadopoulos, D., Dukes, S., Patel, R., Nicholas, R., Vora, A. and Reynolds, R., 2009. Substantial archaeocortical atrophy and neuronal loss in multiple sclerosis. *Brain Pathol*, **19**; 238-53.
Papadopoulos, D., Rundle, J., Patel, R., Marshall, I., Stretton, J., Eaton, R., Richardson, J. C., Gonzalez, M. I., Philpott, K. L. and Reynolds, R., 2010. FTY720 ameliorates MOG-induced experimental autoimmune encephalomyelitis by suppressing both cellular and humoral immune responses. *J Neurosci Res*, **88**; 346-59.
Pardridge, W. M., 2011. Drug transport in brain via the cerebrospinal fluid. *Fluids Barriers CNS*, **8**; 7.
Patani, R., Balaratnam, M., Vora, A. and Reynolds, R., 2007. Remyelination can be extensive in multiple sclerosis despite a long disease course. *Neuropathol Appl Neurobiol*, **33**; 277-87.
Paterson, P. Y., 1960. Transfer of allergic encephalomyelitis in rats by means of lymph node cells. *J Exp Med*, **111**; 119-36.
Patrikios, P., Stadelmann, C., Kutzelnigg, A., Rauschka, H., Schmidbauer, M., Laursen, H., Sorensen, P. S., Brück, W., Lucchinetti, C. and Lassmann, H., 2006. Remyelination is extensive in a subset of multiple sclerosis patients. *Brain*, **129**; 3165-72.
Paxinos, G. and Watson, C., 1998. *The rat brain in stereotaxic coordinates*. London: Academic Press, Inc.
Penderis, J., Shields, S. A. and Franklin, R. J., 2003. Impaired remyelination and depletion of oligodendrocyte progenitors does not occur following repeated episodes of focal demyelination in the rat central nervous system. *Brain*, **126**; 1382-91.
Périer, O. and Grégoire, A., 1965. Electron microscopic features of multiple sclerosis lesions. *Brain*, **88**; 937-52.
Peterson, J. W., Bö, L., Mörk, S., Chang, A. and Trapp, B. D., 2001. Transected neurites, apoptotic neurons, and reduced inflammation in cortical multiple sclerosis lesions. *Ann Neurol*, **50**; 389-400.
Pfaffl, M. W., Horgan, G. W. and Dempfle, L., 2002. Relative expression software tool (REST) for group-wise comparison and statistical analysis of relative expression results in real-time PCR. *Nucleic Acids Res*, **30**; e36.
Pfaffl, M. W., Tichopad, A., Prgomet, C. and Neuvians, T. P., 2004. Determination of stable housekeeping genes, differentially regulated target genes and sample integrity: BestKeeper--Excel-based tool using pair-wise correlations. *Biotechnol Lett*, **26**; 509-15.
Pham-Dinh, D., Mattei, M. G., Nussbaum, J. L., Roussel, G., Pontarotti, P., Roeckel, N., Mather, I. H., Artzt, K., Lindahl, K. F. and Dautigny, A., 1993. Myelin/oligodendrocyte glycoprotein is a member of a subset of the immunoglobulin superfamily encoded within the major histocompatibility complex. *Proc Natl Acad Sci U S A*, **90**; 7990-4.
Phillips, M. J., Weller, R. O., Kida, S. and Iannotti, F., 1995. Focal brain damage enhances experimental allergic encephalomyelitis in brain and spinal cord. *Neuropathol Appl Neurobiol*, **21**; 189-200.

Piddlesden, S., Lassmann, H., Laffafian, I., Morgan, B. P. and Linington, C., 1991. Antibody-mediated demyelination in experimental allergic encephalomyelitis is independent of complement membrane attack complex formation. *Clin Exp Immunol*, **83**; 245-50.
Piddlesden, S. J., Lassmann, H., Zimprich, F., Morgan, B. P. and Linington, C., 1993. The demyelinating potential of antibodies to myelin oligodendrocyte glycoprotein is related to their ability to fix complement. *Am J Pathol*, **143**; 555-64.
Pierson, E. R., Stromnes, I. M. and Goverman, J. M., 2014. B cells promote induction of experimental autoimmune encephalomyelitis by facilitating reactivation of T cells in the central nervous system. *J Immunol*, **192**; 929-39.
Plane, J. M., Shen, Y., Pleasure, D. E. and Deng, W., 2010. Prospects for minocycline neuroprotection. *Arch Neurol*, **67**; 1442-8.
Polman, C. H., Reingold, S. C., Banwell, B., Clanet, M., Cohen, J. A., Filippi, M., Fujihara, K., Havrdova, E., Hutchinson, M., Kappos, L., Lublin, F. D., Montalban, X., O'Connor, P., Sandberg-Wollheim, M., Thompson, A. J., Waubant, E., Weinshenker, B. and Wolinsky, J. S., 2011. Diagnostic criteria for multiple sclerosis: 2010 revisions to the McDonald criteria. *Ann Neurol*, **69**; 292-302.
Pomeroy, I. M., Matthews, P. M., Frank, J. A., Jordan, E. K. and Esiri, M. M., 2005. Demyelinated neocortical lesions in marmoset autoimmune encephalomyelitis mimic those in multiple sclerosis. *Brain*, **128**; 2713-21.
Poon, A. H., Eidelman, D. H., Martin, J. G., Laprise, C. and Hamid, Q., 2012. Pathogenesis of severe asthma. *Clin Exp Allergy*, **42**; 625-37.
Popescu, B. F., Bunyan, R. F., Parisi, J. E., Ransohoff, R. M. and Lucchinetti, C. F., 2011. A case of multiple sclerosis presenting with inflammatory cortical demyelination. *Neurology*, **76**; 1705-10.
Popescu, B. F. and Lucchinetti, C. F., 2012. Pathology of demyelinating diseases. *Annu Rev Pathol*, **7**; 185-217.
Popovic, N., Schubart, A., Goetz, B. D., Zhang, S. C., Linington, C. and Duncan, I. D., 2002. Inhibition of autoimmune encephalomyelitis by a tetracycline. *Ann Neurol*, **51**; 215-23.
Premaraj, S., Mundy, B. L., Morgan, D., Winnard, P. L., Mooney, M. P. and Moursi, A. M., 2006. Sustained delivery of bioactive cytokine using a dense collagen gel vehicle collagen gel delivery of bioactive cytokine. *Arch Oral Biol*, **51**; 325-33.
Prineas, J. W., Barnard, R. O., Kwon, E. E., Sharer, L. R. and Cho, E. S., 1993a. Multiple-Sclerosis - Remyelination of Nascent Lesions. *Annals of Neurology*, **33**; 137-151.
Prineas, J. W., Barnard, R. O., Revesz, T., Kwon, E. E., Sharer, L. and Cho, E. S., 1993b. Multiple-Sclerosis - Pathology of Recurrent Lesions. *Brain*, **116**; 681-693.
Prineas, J. W., Kwon, E. E., Cho, E. S., Sharer, L. R., Barnett, M. H., Oleszak, E. L., Hoffman, B. and Morgan, B. P., 2001. Immunopathology of secondary-progressive multiple sclerosis. *Ann Neurol*, **50**; 646-57.
Prins, M., Eriksson, C., Wierinckx, A., Bol, J. G., Binnekade, R., Tilders, F. J. and Van Dam, A. M., 2013. Interleukin-1beta and interleukin-1 receptor antagonist appear in grey matter additionally to white matter lesions during experimental multiple sclerosis. *PLoS One*, **8**; e83835.
Probert, L., Akassoglou, K., Pasparakis, M., Kontogeorgos, G. and Kollias, G., 1995. Spontaneous inflammatory demyelinating disease in transgenic mice showing central nervous system-specific expression of tumor necrosis factor alpha. *Proc Natl Acad Sci U S A*, **92**; 11294-8.
Qian, L., Hong, J. S. and Flood, P. M., 2006. Role of microglia in inflammation-mediated degeneration of dopaminergic neurons: neuroprotective effect of interleukin 10. *J Neural Transm Suppl*, 367-71.
Rainey-Barger, E. K., Rumble, J. M., Lalor, S. J., Esen, N., Segal, B. M. and Irani, D. N., 2011. The lymphoid chemokine, CXCL13, is dispensable for the initial recruitment of B cells to the acutely inflamed central nervous system. *Brain Behav Immun*, **25**; 922-31.
Ramagopalan, S. V., Maugeri, N. J., Handunnetthi, L., Lincoln, M. R., Orton, S. M., Dyment, D. A., Deluca, G. C., Herrera, B. M., Chao, M. J., Sadovnick, A. D., Ebers, G. C. and Knight, J. C., 2009. Expression of the multiple sclerosis-associated MHC class II Allele HLA-DRB1*1501 is regulated by vitamin D. *PLoS Genet*, **5**; e1000369.
Ramagopalan, S. V., Handel, A. E., Giovannoni, G., Rutherford Siegel, S., Ebers, G. C. and Chaplin, G., 2011. Relationship of UV exposure to prevalence of multiple sclerosis in England. *Neurology*, **76**; 1410-4.
Ramesh, G., Borda, J. T., Gill, A., Ribka, E. P., Morici, L. A., Mottram, P., Martin, D. S., Jacobs, M. B., Didier, P. J. and Philipp, M. T., 2009. Possible role of glial cells in the onset and progression of Lyme neuroborreliosis. *J Neuroinflammation*, **6**; 23.
Ransohoff, R. M., Kivisäkk, P. and Kidd, G., 2003. Three or more routes for leukocyte migration into the central nervous system. *Nat Rev Immunol*, **3**; 569-81.
Ransohoff, R. M., 2009. Immunology: In the beginning. *Nature*, **462**; 41-42.
Ransohoff, R. M., 2012. Animal models of multiple sclerosis: the good, the bad and the bottom line. *Nat Neurosci*, **15**; 1074-7.

Rasmussen, S., Wang, Y., Kivisäkk, P., Bronson, R. T., Meyer, M., Imitola, J. and Khoury, S. J., 2007. Persistent activation of microglia is associated with neuronal dysfunction of callosal projecting pathways and multiple sclerosis-like lesions in relapsing--remitting experimental autoimmune encephalomyelitis. *Brain*, **130**; 2816-29.

Reboldi, A., Coisne, C., Baumjohann, D., Benvenuto, F., Bottinelli, D., Lira, S., Uccelli, A., Lanzavecchia, A., Engelhardt, B. and Sallusto, F., 2009. C-C chemokine receptor 6-regulated entry of TH-17 cells into the CNS through the choroid plexus is required for the initiation of EAE. *Nat Immunol*, **10**; 514-23.

Reddy, J., Illes, Z., Zhang, X., Encinas, J., Pyrdol, J., Nicholson, L., Sobel, R. A., Wucherpfennig, K. W. and Kuchroo, V. K., 2004. Myelin proteolipid protein-specific CD4+CD25+ regulatory cells mediate genetic resistance to experimental autoimmune encephalomyelitis. *Proc Natl Acad Sci U S A*, **101**; 15434-9.

Redford, E. J., Kapoor, R. and Smith, K. J., 1997. Nitric oxide donors reversibly block axonal conduction: demyelinated axons are especially susceptible. *Brain*, **120 (Pt 12)**; 2149-57.

Regev, L., Ezrielev, E., Gershon, E., Gil, S. and Chen, A., 2010. Genetic approach for intracerebroventricular delivery. *Proc Natl Acad Sci U S A*, **107**; 4424-9.

Reindl, M., Linington, C., Brehm, U., Egg, R., Dilitz, E., Deisenhammer, F., Poewe, W. and Berger, T., 1999. Antibodies against the myelin oligodendrocyte glycoprotein and the myelin basic protein in multiple sclerosis and other neurological diseases: a comparative study. *Brain*, **122 (Pt 11)**; 2047-56.

Rennels, M. L., Gregory, T. F., Blaumanis, O. R., Fujimoto, K. and Grady, P. A., 1985. Evidence for a 'paravascular' fluid circulation in the mammalian central nervous system, provided by the rapid distribution of tracer protein throughout the brain from the subarachnoid space. *Brain Res*, **326**; 47-63.

Reynolds, R., Dawson, M., Papadopoulos, D., Polito, A., Di Bello, I. C., Pham-Dinh, D. and Levine, J., 2002. The response of NG2-expressing oligodendrocyte progenitors to demyelination in MOG-EAE and MS. *J Neurocytol*, **31**; 523-36.

Reynolds, R., Roncaroli, F., Nicholas, R., Radotra, B., Gveric, D. and Howell, O., 2011. The neuropathological basis of clinical progression in multiple sclerosis. *Acta Neuropathol*.

Richmond, A. and Thomas, H. G., 1988. Melanoma growth stimulatory activity: isolation from human melanoma tumors and characterization of tissue distribution. *J Cell Biochem*, **36**; 185-98.

Rieckmann, P., Albrecht, M., Kitze, B., Weber, T., Tumani, H., Broocks, A., Lüer, W., Helwig, A. and Poser, S., 1995. Tumor necrosis factor-alpha messenger RNA expression in patients with relapsing-remitting multiple sclerosis is associated with disease activity. *Ann Neurol*, **37**; 82-8.

Robinson, S. and Miller, R. H., 1999. Contact with central nervous system myelin inhibits oligodendrocyte progenitor maturation. *Dev Biol*, **216**; 359-68.

Rodríguez-Pinto, D., 2005. B cells as antigen presenting cells. *Cell Immunol*, **238**; 67-75.

Rodriguez, E. G., Wegner, C., Kreutzfeldt, M., Neid, K., Thal, D. R., Jürgens, T., Brück, W., Stadelmann, C. and Merkler, D., 2014. Oligodendroglia in cortical multiple sclerosis lesions decrease with disease progression, but regenerate after repeated experimental demyelination. *Acta Neuropathol*, **128**; 231-46.

Romijn, H. J., van Uum, J. F., Breedijk, I., Emmering, J., Radu, I. and Pool, C. W., 1999. Double immunolabeling of neuropeptides in the human hypothalamus as analyzed by confocal laser scanning fluorescence microscopy. *J Histochem Cytochem*, **47**; 229-36.

Romme Christensen, J., Börnsen, L., Hesse, D., Krakauer, M., Sørensen, P. S., Søndergaard, H. B. and Sellebjerg, F., 2012. Cellular sources of dysregulated cytokines in relapsing-remitting multiple sclerosis. *J Neuroinflammation*, **9**; 215.

Romme Christensen, J., Börnsen, L., Khademi, M., Olsson, T., Jensen, P. E., Sørensen, P. S. and Sellebjerg, F., 2013. CSF inflammation and axonal damage are increased and correlate in progressive multiple sclerosis. *Mult Scler*, **19**; 877-84.

Rossi, S., Motta, C., Studer, V., Barbieri, F., Buttari, F., Bergami, A., Sancesario, G., Bernardini, S., De Angelis, G., Martino, G., Furlan, R. and Centonze, D., 2013. Tumor necrosis factor is elevated in progressive multiple sclerosis and causes excitotoxic neurodegeneration. *Mult Scler*.

Roxanis, I., Micklem, K., McConville, J., Newsom-Davis, J. and Willcox, N., 2002. Thymic myoid cells and germinal center formation in myasthenia gravis; possible roles in pathogenesis. *Journal of Neuroimmunology*, **125**; 185-197.

Rubio, J. P., Bahlo, M., Stankovich, J., Burfoot, R. K., Johnson, L. J., Huxtable, S., Butzkueven, H., Lin, L., Taylor, B. V., Speed, T. P., Kilpatrick, T. J., Mignot, E. and Foote, S. J., 2007. Analysis of extended HLA haplotypes in multiple sclerosis and narcolepsy families confirms a predisposing effect for the class I region in Tasmanian MS patients. *Immunogenetics*, **59**; 177-86.

Ruddle, N. H., Bergman, C. M., McGrath, K. M., Lingenheld, E. G., Grunnet, M. L., Padula, S. J. and Clark, R. B., 1990. An antibody to lymphotoxin and tumor necrosis factor prevents transfer of experimental allergic encephalomyelitis. *J Exp Med*, **172**; 1193-200.

Sakuma, T., Barry, M. A. and Ikeda, Y., 2012. Lentiviral vectors: basic to translational. *Biochem J*, **443**; 603-18.

Sallusto, F., Lenig, D., Mackay, C. R. and Lanzavecchia, A., 1998. Flexible programs of chemokine receptor expression on human polarized T helper 1 and 2 lymphocytes. *Journal of Experimental Medicine*, **187**; 875-883.

Sallusto, F., Kremmer, E., Palermo, B., Hoy, A., Ponath, P., Qin, S. X., Förster, R., Lipp, M. and Lanzavecchia, A., 1999. Switch in chemokine receptor expression upon TCR stimulation reveals novel homing potential for recently activated T cells. *European Journal of Immunology*, **29**; 2037-2045.

Salomonsson, S., Jonsson, M. V., Skarstein, K., Brokstad, K. A., Hjelmström, P., Wahren-Herlenius, M. and Jonsson, R., 2003. Cellular basis of ectopic germinal center formation and autoantibody production in the target organ of patients with Sjogren's syndrome. *Arthritis Rheum*, **48**; 3187-201.

Sasaki, M., Lankford, K. L., Brown, R. J., Ruddle, N. H. and Kocsis, J. D., 2010. Focal experimental autoimmune encephalomyelitis in the Lewis rat induced by immunization with myelin oligodendrocyte glycoprotein and intraspinal injection of vascular endothelial growth factor. *Glia*, **58**; 1523-31.

Sawcer, S., Hellenthal, G., Pirinen, M., Spencer, C. C., Patsopoulos, N. A., Moutsianas, L., Dilthey, A., Su, Z., Freeman, C., Hunt, S. E., Edkins, S., Gray, E., Booth, D. R., Potter, S. C., Goris, A., Band, G., Oturai, A. B., Strange, A., Saarela, J., Bellenguez, C., Fontaine, B., Gillman, M., Hemmer, B., Gwilliam, R., Zipp, F., Jayakumar, A., Martin, R., Leslie, S., Hawkins, S., Giannoulatou, E., D'Alfonso, S., Blackburn, H., Martinelli Boneschi, F., Liddle, J., Harbo, H. F., Perez, M. L., Spurkland, A., Waller, M. J., Mycko, M. P., Ricketts, M., Comabella, M., Hammond, N., Kockum, I., McCann, O. T., Ban, M., Whittaker, P., Kemppinen, A., Weston, P., Hawkins, C., Widaa, S., Zajicek, J., Dronov, S., Robertson, N., Bumpstead, S. J., Barcellos, L. F., Ravindrarajah, R., Abraham, R., Alfredsson, L., Ardlie, K., Aubin, C., Baker, A., Baker, K., Baranzini, S. E., Bergamaschi, L., Bergamaschi, R., Bernstein, A., Berthele, A., Boggild, M., Bradfield, J. P., Brassat, D., Broadley, S. A., Buck, D., Butzkueven, H., Capra, R., Carroll, W. M., Cavalla, P., Celius, E. G., Cepok, S., Chiavacci, R., Clerget-Darpoux, F., Clysters, K., Comi, G., Cossburn, M., Cournu-Rebeix, I., Cox, M. B., Cozen, W., Cree, B. A., Cross, A. H., Cusi, D., Daly, M. J., Davis, E., de Bakker, P. I., Debouverie, M., D'Hooghe M, B., Dixon, K., Dobosi, R., Dubois, B., Ellinghaus, D., Elovaara, I., Esposito, F., Fontenille, C., Foote, S., Franke, A., Galimberti, D., Ghezzi, A., Glessner, J., Gomez, R., Gout, O., Graham, C., Grant, S. F., Guerini, F. R., Hakonarson, H., Hall, P., Hamsten, A., Hartung, H. P., Heard, R. N., Heath, S., Hobart, J., Hoshi, M., Infante-Duarte, C., Ingram, G., Ingram, W., Islam, T., Jagodic, M., Kabesch, M., Kermode, A. G., Kilpatrick, T. J., Kim, C., Klopp, N., Koivisto, K., Larsson, M., Lathrop, M., Lechner-Scott, J. S., Leone, M. A., Leppä, V., Liljedahl, U., Bomfim, I. L., Lincoln, R. R., Link, J., Liu, J., Lorentzen, A. R., Lupoli, S., Macciardi, F., Mack, T., Marriott, M., Martinelli, V., Mason, D., McCauley, J. L., Mentch, F., Mero, I. L., Mihalova, T., Montalban, X., Mottershead, J., Myhr, K. M., Naldi, P., Ollier, W., Page, A., Palotie, A., Pelletier, J., Piccio, L., Pickersgill, T., Piehl, F., Pobywajlo, S., Quach, H. L., Ramsay, P. P., Reunanen, M., Reynolds, R., Rioux, J. D., Rodegher, M., Roesner, S., Rubio, J. P., Rückert, I. M., Salvetti, M., Salvi, E., Santaniello, A., Schaefer, C. A., Schreiber, S., Schulze, C., Scott, R. J., Sellebjerg, F., Selmaj, K. W., Sexton, D., Shen, L., Simms-Acuna, B., Skidmore, S., Sleiman, P. M., Smestad, C., Sørensen, P. S., Søndergaard, H. B., Stankovich, J., Strange, R. C., Sulonen, A. M., Sundqvist, E., Syvänen, A. C., Taddeo, F., Taylor, B., Blackwell, J. M., Tienari, P., Bramon, E., Tourbah, A., Brown, M. A., Tronczynska, E., Casas, J. P., Tubridy, N., Corvin, A., Vickery, J., Jankowski, J., Villoslada, P., Markus, H. S., Wang, K., Mathew, C. G., Wason, J., Palmer, C. N., Wichmann, H. E., Plomin, R., Willoughby, E., Rautanen, A., Winkelmann, J., Wittig, M., Trembath, R. C., Yaouanq, J., Viswanathan, A. C., Zhang, H., Wood, N. W., Zuvich, R., Deloukas, P., Langford, C., Duncanson, A., Oksenberg, J. R., Pericak-Vance, M. A., Haines, J. L., Olsson, T., Hillert, J., Ivinson, A. J., De Jager, P. L., Peltonen, L., Stewart, G. J., Hafler, D. A., Hauser, S. L., McVean, G., Donnelly, P. and Compston, A., 2011. Genetic risk and a primary role for cell-mediated immune mechanisms in multiple sclerosis. *Nature*, **476**; 214-9.

Scalfari, A., Neuhaus, A., Degenhardt, A., Rice, G. P., Muraro, P. A., Daumer, M. and Ebers, G. C., 2010. The natural history of multiple sclerosis: a geographically based study 10: relapses and long-term disability. *Brain*, **133**; 1914-29.

Schluesener, H. J., Sobel, R. A., Linington, C. and Weiner, H. L., 1987. A monoclonal antibody against a myelin oligodendrocyte glycoprotein induces relapses and demyelination in central nervous system autoimmune disease. *J Immunol*, **139**; 4016-21.

Schmierer, K., Parkes, H. G., So, P. W., An, S. F., Brandner, S., Ordidge, R. J., Yousry, T. A. and Miller, D. H., 2010. High field (9.4 Tesla) magnetic resonance imaging of cortical grey matter lesions in multiple sclerosis. *Brain*, **133**; 858-67.

Buc, M., 2013. Role of regulatory T cells in pathogenesis and biological therapy of multiple sclerosis. *Mediators Inflamm*, **2013**; 963748.

Haas, J., Hug, A., Viehover, A., Fritzsching, B., Falk, C. S., Filser, A., Vetter, T., Milkova, L., Korporal, M., Fritz, B., Storch-Hagenlocher, B., Krammer, P. H., Suri-Payer, E. and Wildemann, B., 2005. Reduced suppressive effect of CD4+CD25high regulatory T cells on the T cell immune response against myelin oligodendrocyte glycoprotein in patients with multiple sclerosis. *Eur J Immunol*, **35**; 3343-52.

Kohm, A. P., Carpentier, P. A., Anger, H. A. and Miller, S. D., 2002. Cutting edge: CD4+CD25+ regulatory T cells suppress antigen-specific autoreactive immune responses and central nervous system inflammation during active experimental autoimmune encephalomyelitis. *J Immunol*, **169**; 4712-6.

Reddy, J., Illes, Z., Zhang, X., Encinas, J., Pyrdol, J., Nicholson, L., Sobel, R. A., Wucherpfennig, K. W. and Kuchroo, V. K., 2004. Myelin proteolipid protein-specific CD4+CD25+ regulatory cells mediate genetic resistance to experimental autoimmune encephalomyelitis. *Proc Natl Acad Sci U S A*, **101**; 15434-9.

Schneider-Hohendorf, T., Stenner, M. P., Weidenfeller, C., Zozulya, A. L., Simon, O. J., Schwab, N. and Wiendl, H., 2010. Regulatory T cells exhibit enhanced migratory characteristics, a feature impaired in patients with multiple sclerosis. *Eur J Immunol*, **40**; 3581-90.

Schnell, S. A., Staines, W. A. and Wessendorf, M. W., 1999. Reduction of lipofuscin-like autofluorescence in fluorescently labeled tissue. *J Histochem Cytochem*, **47**; 719-30.

Schreiner, B., Heppner, F. L. and Becher, B., 2009. Modeling multiple sclerosis in laboratory animals. *Semin Immunopathol*, **31**; 479-95.

Schroeder, A., Mueller, O., Stocker, S., Salowsky, R., Leiber, M., Gassmann, M., Lightfoot, S., Menzel, W., Granzow, M. and Ragg, T., 2006. The RIN: an RNA integrity number for assigning integrity values to RNA measurements. *BMC Mol Biol*, **7**; 3.

Scolding, N. J., Frith, S., Linington, C., Morgan, B. P., Campbell, A. K. and Compston, D. A., 1989. Myelin-oligodendrocyte glycoprotein (MOG) is a surface marker of oligodendrocyte maturation. *J Neuroimmunol*, **22**; 169-76.

Seewann, A., Kooi, E. J., Roosendaal, S. D., Pouwels, P. J., Wattjes, M. P., van der Valk, P., Barkhof, F., Polman, C. H. and Geurts, J. J., 2012. Postmortem verification of MS cortical lesion detection with 3D DIR. *Neurology*, **78**; 302-8.

Seidlits, S. K., Gower, R. M., Shepard, J. A. and Shea, L. D., 2013. Hydrogels for lentiviral gene delivery. *Expert Opin Drug Deliv*, **10**; 499-509.

Sellebjerg, F., Börnsen, L., Khademi, M., Krakauer, M., Olsson, T., Frederiksen, J. L. and Sørensen, P. S., 2009. Increased cerebrospinal fluid concentrations of the chemokine CXCL13 in active MS. *Neurology*, **73**; 2003-10.

Selmaj, K., Raine, C. S. and Cross, A. H., 1991. Anti-tumor necrosis factor therapy abrogates autoimmune demyelination. *Ann Neurol*, **30**; 694-700.

Serafini, B., Rosicarelli, B., Magliozzi, R., Stigliano, E. and Aloisi, F., 2004. Detection of ectopic B-cell follicles with germinal centers in the meninges of patients with secondary progressive multiple sclerosis. *Brain Pathol*, **14**; 164-74.

Serafini, B., Rosicarelli, B., Franciotta, D., Magliozzi, R., Reynolds, R., Cinque, P., Andreoni, L., Trivedi, P., Salvetti, M., Faggioni, A. and Aloisi, F., 2007. Dysregulated Epstein-Barr virus infection in the multiple sclerosis brain. *J Exp Med*, **204**; 2899-912.

Sharief, M. K. and Hentges, R., 1991. Association between tumor necrosis factor-alpha and disease progression in patients with multiple sclerosis. *N Engl J Med*, **325**; 467-72.

Shen, S., Sandoval, J., Swiss, V. A., Li, J., Dupree, J., Franklin, R. J. and Casaccia-Bonnefil, P., 2008. Age-dependent epigenetic control of differentiation inhibitors is critical for remyelination efficiency. *Nat Neurosci*, **11**; 1024-34.

Sherwood, K. R., Head, M. W., Walker, R., Smith, C., Ironside, J. W. and Fazakerley, J. K., 2011. RNA integrity in post mortem human variant Creutzfeldt-Jakob disease (vCJD) and control brain tissue. *Neuropathol Appl Neurobiol*, **37**; 633-42.

Shields, S. A., Gilson, J. M., Blakemore, W. F. and Franklin, R. J., 1999. Remyelination occurs as extensively but more slowly in old rats compared to young rats following gliotoxin-induced CNS demyelination. *Glia*, **28**; 77-83.

Shin, S., Salvay, D. M. and Shea, L. D., 2010. Lentivirus delivery by adsorption to tissue engineering scaffolds. *J Biomed Mater Res A*, **93**; 1252-9.

Shin, S. and Shea, L. D., 2010. Lentivirus immobilization to nanoparticles for enhanced and localized delivery from hydrogels. *Mol Ther*, **18**; 700-6.

Sim, F. J., Zhao, C., Penderis, J. and Franklin, R. J., 2002. The age-related decrease in CNS remyelination efficiency is attributable to an impairment of both oligodendrocyte progenitor recruitment and differentiation. *J Neurosci*, **22**; 2451-9.

Simmons, R. D. and Willenborg, D. O., 1990. Direct injection of cytokines into the spinal cord causes autoimmune encephalomyelitis-like inflammation. *J Neurol Sci*, **100**; 37-42.

Simpson, S., Jr., Blizzard, L., Otahal, P., Van der Mei, I. and Taylor, B., 2011. Latitude is significantly associated with the prevalence of multiple sclerosis: a meta-analysis. *J Neurol Neurosurg Psychiatry*, **82**; 1132-41.

Sixt, M., Engelhardt, B., Pausch, F., Hallmann, R., Wendler, O. and Sorokin, L. M., 2001. Endothelial cell laminin isoforms, laminins 8 and 10, play decisive roles in T cell recruitment across the blood-brain barrier in experimental autoimmune encephalomyelitis. *J Cell Biol*, **153**; 933-46.

Skulina, C., Schmidt, S., Dornmair, K., Babbe, H., Roers, A., Rajewsky, K., Wekerle, H., Hohlfeld, R. and Goebels, N., 2004. Multiple sclerosis: brain-infiltrating CD8+ T cells persist as clonal expansions in the cerebrospinal fluid and blood. *Proc Natl Acad Sci U S A*, **101**; 2428-33.

Slavin, A. J., Johns, T. G., Orian, J. M. and Bernard, C. C., 1997. Regulation of myelin oligodendrocyte glycoprotein in different species throughout development. *Dev Neurosci*, **19**; 69-78.

Smith, M. E., van der Maesen, K. and Somera, F. P., 1998. Macrophage and microglial responses to cytokines in vitro: phagocytic activity, proteolytic enzyme release, and free radical production. *J Neurosci Res*, **54**; 68-78.

Snyder, D. H., Valsamis, M. P., Stone, S. H. and Raine, C. S., 1975. Progressive demyelination and reparative phenomena in chronic experimental allergic encephalomyelitis. *J Neuropathol Exp Neurol*, **34**; 209-21.

Sørensen, T. L., Tani, M., Jensen, J., Pierce, V., Lucchinetti, C., Folcik, V. A., Qin, S., Rottman, J., Sellebjerg, F., Strieter, R. M., Frederiksen, J. L. and Ransohoff, R. M., 1999. Expression of specific chemokines and chemokine receptors in the central nervous system of multiple sclerosis patients. *J Clin Invest*, **103**; 807-15.

Sørensen, T. L., Roed, H. and Sellebjerg, F., 2002. Chemokine receptor expression on B cells and effect of interferon-beta in multiple sclerosis. *J Neuroimmunol*, **122**; 125-31.

Sospedra, M. and Martin, R., 2005. Immunology of multiple sclerosis. *Annu Rev Immunol*, **23**; 683-747.

Spach, K. M., Blake, M., Bunn, J. Y., McElvany, B., Noubade, R., Blankenhorn, E. P. and Teuscher, C., 2009. Cutting edge: the Y chromosome controls the age-dependent experimental allergic encephalomyelitis sexual dimorphism in SJL/J mice. *J Immunol*, **182**; 1789-93.

Spuler, S., Yousry, T., Scheller, A., Voltz, R., Holler, E., Hartmann, M., Wick, M. and Hohlfeld, R., 1996. Multiple sclerosis: prospective analysis of TNF-alpha and 55 kDa TNF receptor in CSF and serum in correlation with clinical and MRI activity. *J Neuroimmunol*, **66**; 57-64.

Sriram, S. and Steiner, I., 2005. Experimental allergic encephalomyelitis: a misleading model of multiple sclerosis. *Ann Neurol*, **58**; 939-45.

Stefferl, A., Brehm, U., Storch, M., Lambracht-Washington, D., Bourquin, C., Wonigeit, K., Lassmann, H. and Linington, C., 1999a. Myelin oligodendrocyte glycoprotein induces experimental autoimmune encephalomyelitis in the "resistant" Brown Norway rat: disease susceptibility is determined by MHC and MHC-linked effects on the B cell response. *J Immunol*, **163**; 40-9.

Stefferl, A., Linington, C., Holsboer, F. and Reul, J. M., 1999b. Susceptibility and resistance to experimental allergic encephalomyelitis: relationship with hypothalamic-pituitary-adrenocortical axis responsiveness in the rat. *Endocrinology*, **140**; 4932-8.

Steinbrecher, A., Weber, T., Neuberger, T., Mueller, A. M., Pedré, X., Giegerich, G., Bogdahn, U., Jakob, P., Haase, A. and Faber, C., 2005. Experimental autoimmune encephalomyelitis in the rat spinal cord: lesion detection with high-resolution MR microscopy at 17.6 T. *AJNR Am J Neuroradiol*, **26**; 19-25.

Storch, M. K., Piddlesden, S., Haltia, M., Iivanainen, M., Morgan, P. and Lassmann, H., 1998a. Multiple sclerosis: in situ evidence for antibody- and complement-mediated demyelination. *Ann Neurol*, **43**; 465-71.

Storch, M. K., Stefferl, A., Brehm, U., Weissert, R., Wallström, E., Kerschensteiner, M., Olsson, T., Linington, C. and Lassmann, H., 1998b. Autoimmunity to myelin oligodendrocyte glycoprotein in rats mimics the spectrum of multiple sclerosis pathology. *Brain Pathol*, **8**; 681-94.

Storch, M. K., Bauer, J., Linington, C., Olsson, T., Weissert, R. and Lassmann, H., 2006. Cortical demyelination can be modeled in specific rat models of autoimmune encephalomyelitis and is major histocompatibility complex (MHC) haplotype-related. *J Neuropathol Exp Neurol*, **65**; 1137-42.

Stromnes, I. M. and Goverman, J. M., 2006. Passive induction of experimental allergic encephalomyelitis. *Nat Protoc*, **1**; 1952-60.

Sun, D., Tani, M., Newman, T. A., Krivacic, K., Phillips, M., Chernosky, A., Gill, P., Wei, T., Griswold, K. J., Ransohoff, R. M. and Weller, R. O., 2000. Role of chemokines, neuronal projections, and the blood-brain barrier in the enhancement of cerebral EAE following focal brain damage. *J Neuropathol Exp Neurol*, **59**; 1031-43.

Suvannavejh, G. C., Lee, H. O., Padilla, J., Dal Canto, M. C., Barrett, T. A. and Miller, S. D., 2000. Divergent roles for p55 and p75 tumor necrosis factor receptors in the pathogenesis of MOG(35-55)-induced experimental autoimmune encephalomyelitis. *Cell Immunol*, **205**; 24-33.

Takaki, S., Mita, S., Kitamura, T., Yonehara, S., Yamaguchi, N., Tominaga, A., Miyajima, A. and Takatsu, K., 1991. Identification of the second subunit of the murine interleukin-5 receptor: interleukin-3 receptor-like protein, AIC2B is a component of the high affinity interleukin-5 receptor. *EMBO J*, **10**; 2833-8.

Takatsu, K., Tominaga, A. and Hamaoka, T., 1980. Antigen-induced T cell-replacing factor (TRF). I. Functional characterization of a TRF-producing helper T cell subset and genetic studies on TRF production. *J Immunol*, **124**; 2414-22.

Takeuchi, H., Jin, S., Wang, J., Zhang, G., Kawanokuchi, J., Kuno, R., Sonobe, Y., Mizuno, T. and Suzumura, A., 2006. Tumor necrosis factor-alpha induces neurotoxicity via glutamate release from hemichannels of activated microglia in an autocrine manner. *J Biol Chem*, **281**; 21362-8.

Taoufik, E., Tseveleki, V., Chu, S. Y., Tselios, T., Karin, M., Lassmann, H., Szymkowski, D. E. and Probert, L., 2011. Transmembrane tumour necrosis factor is neuroprotective and regulates experimental autoimmune encephalomyelitis via neuronal nuclear factor-kappaB. *Brain*, **134**; 2722-35.

Teuscher, C., Bunn, J. Y., Fillmore, P. D., Butterfield, R. J., Zachary, J. F. and Blankenhorn, E. P., 2004. Gender, age, and season at immunization uniquely influence the genetic control of susceptibility to histopathological lesions and clinical signs of experimental allergic encephalomyelitis: implications for the genetics of multiple sclerosis. *Am J Pathol*, **165**; 1593-602.

Thapa, M., Welner, R. S., Pelayo, R. and Carr, D. J., 2008. CXCL9 and CXCL10 expression are critical for control of genital herpes simplex virus type 2 infection through mobilization of HSV-specific CTL and NK cells to the nervous system. *J Immunol*, **180**; 1098-106.

Thessen Hedreul, M., Gillett, A., Olsson, T., Jagodic, M. and Harris, R. A., 2009. Characterization of Multiple Sclerosis candidate gene expression kinetics in rat experimental autoimmune encephalomyelitis. *J Neuroimmunol*, **210**; 30-9.

Thorley-Lawson, D. A. and Gross, A., 2004. Persistence of the Epstein-Barr virus and the origins of associated lymphomas. *N Engl J Med*, **350**; 1328-37.

Tiscornia, G., Singer, O. and Verma, I. M., 2006. Production and purification of lentiviral vectors. *Nat Protoc*, **1**; 241-5.

Torkildsen, Ø., Stansberg, C., Angelskår, S. M., Kooi, E. J., Geurts, J. J., van der Valk, P., Myhr, K. M., Steen, V. M. and Bø, L., 2010. Upregulation of immunoglobulin-related genes in cortical sections from multiple sclerosis patients. *Brain Pathol*, **20**; 720-9.

Tracey, D., Klareskog, L., Sasso, E. H., Salfeld, J. G. and Tak, P. P., 2008. Tumor necrosis factor antagonist mechanisms of action: a comprehensive review. *Pharmacol Ther*, **117**; 244-79.

Tran, E. H., Hardin-Pouzet, H., Verge, G. and Owens, T., 1997. Astrocytes and microglia express inducible nitric oxide synthase in mice with experimental allergic encephalomyelitis. *J Neuroimmunol*, **74**; 121-9.

Trapp, B. D., Peterson, J., Ransohoff, R. M., Rudick, R., Mörk, S. and Bö, L., 1998. Axonal transection in the lesions of multiple sclerosis. *N Engl J Med*, **338**; 278-85.

Trebst, C., Sørensen, T. L., Kivisäkk, P., Cathcart, M. K., Hesselgesser, J., Horuk, R., Sellebjerg, F., Lassmann, H. and Ransohoff, R. M., 2001. CCR1+/CCR5+ mononuclear phagocytes accumulate in the central nervous system of patients with multiple sclerosis. *Am J Pathol*, **159**; 1701-10.

Tsai, H. H., Frost, E., To, V., Robinson, S., Ffrench-Constant, C., Geertman, R., Ransohoff, R. M. and Miller, R. H., 2002. The chemokine receptor CXCR2 controls positioning of oligodendrocyte precursors in developing spinal cord by arresting their migration. *Cell*, **110**; 373-83.

Tuohy, V. K., Yu, M., Yin, L., Kawczak, J. A. and Kinkel, R. P., 1999. Spontaneous regression of primary autoreactivity during chronic progression of experimental autoimmune encephalomyelitis and multiple sclerosis. *J Exp Med*, **189**; 1033-42.

van de Pavert, S. A., Olivier, B. J., Goverse, G., Vondenhoff, M. F., Greuter, M., Beke, P., Kusser, K., Höpken, U. E., Lipp, M., Niederreither, K., Blomhoff, R., Sitnik, K., Agace, W. W., Randall, T. D., de Jonge, W. J. and Mebius, R. E., 2009. Chemokine CXCL13 is essential for lymph node initiation and is induced by retinoic acid and neuronal stimulation. *Nat Immunol*, **10**; 1193-9.

Van der Goes, A., Kortekaas, M., Hoekstra, K., Dijkstra, C. D. and Amor, S., 1999. The role of anti-myelin (auto)-antibodies in the phagocytosis of myelin by macrophages. *J Neuroimmunol*, **101**; 61-7.

van der Laan, L. J., Ruuls, S. R., Weber, K. S., Lodder, I. J., Döpp, E. A. and Dijkstra, C. D., 1996. Macrophage phagocytosis of myelin in vitro determined by flow cytometry: phagocytosis is mediated by CR3 and induces production of tumor necrosis factor-alpha and nitric oxide. *J Neuroimmunol*, **70**; 145-52.

van der Valk, P. and De Groot, C. J., 2000. Staging of multiple sclerosis (MS) lesions: pathology of the time frame of MS. *Neuropathol Appl Neurobiol*, **26**; 2-10.

van Horssen, J., Brink, B. P., de Vries, H. E., van der Valk, P. and Bø, L., 2007. The blood-brain barrier in cortical multiple sclerosis lesions. *J Neuropathol Exp Neurol*, **66**; 321-8.

van Noort, J. M., van Sechel, A. C., Bajramovic, J. J., el Ouagmiri, M., Polman, C. H., Lassmann, H. and Ravid, R., 1995. The small heat-shock protein alpha B-crystallin as candidate autoantigen in multiple sclerosis. *Nature*, **375**; 798-801.

Vandendriessche, T., Thorrez, L., Acosta-Sanchez, A., Petrus, I., Wang, L., Ma, L., L, D. E. W., Iwasaki, Y., Gillijns, V., Wilson, J. M., Collen, D. and Chuah, M. K., 2007. Efficacy and safety of adeno-associated viral vectors based on serotype 8 and 9 vs. lentiviral vectors for hemophilia B gene therapy. *J Thromb Haemost*, **5**; 16-24.
Vandesompele, J., De Preter, K., Pattyn, F., Poppe, B., Van Roy, N., De Paepe, A. and Speleman, F., 2002. Accurate normalization of real-time quantitative RT-PCR data by geometric averaging of multiple internal control genes. *Genome Biol*, **3**; RESEARCH0034.
Vanlangenakker, N., Vanden Berghe, T. and Vandenabeele, P., 2012. Many stimuli pull the necrotic trigger, an overview. *Cell Death Differ*, **19**; 75-86.
Vartanian, T., Li, Y., Zhao, M. and Stefansson, K., 1995. Interferon-gamma-induced oligodendrocyte cell death: implications for the pathogenesis of multiple sclerosis. *Mol Med*, **1**; 732-43.
Vass, K. and Lassmann, H., 1990. Intrathecal application of interferon gamma. Progressive appearance of MHC antigens within the rat nervous system. *Am J Pathol*, **137**; 789-800.
Vercellino, M., Plano, F., Votta, B., Mutani, R., Giordana, M. T. and Cavalla, P., 2005. Grey matter pathology in multiple sclerosis. *J Neuropathol Exp Neurol*, **64**; 1101-7.
Veroni, C., Gabriele, L., Canini, I., Castiello, L., Coccia, E., Remoli, M. E., Columba-Cabezas, S., Aricò, E., Aloisi, F. and Agresti, C., 2010. Activation of TNF receptor 2 in microglia promotes induction of anti-inflammatory pathways. *Mol Cell Neurosci*, **45**; 234-44.
Viglietta, V., Baecher-Allan, C., Weiner, H. L. and Hafler, D. A., 2004. Loss of functional suppression by CD4+CD25+ regulatory T cells in patients with multiple sclerosis. *J Exp Med*, **199**; 971-9.
Villarroya, H., Marie, Y., Ouallet, J. C., Le Saux, F., Tchélingérian, J. L. and Baumann, N., 1997. Expression of TNF alpha in central neurons of Lewis rat spinal cord after EAE induction. *J Neurosci Res*, **49**; 592-9.
Vincent, A., 2002. Unravelling the pathogenesis of myasthenia gravis. *Nat Rev Immunol*, **2**; 797-804.
Voskuhl, R. R. and Gold, S. M., 2012. Sex-related factors in multiple sclerosis susceptibility and progression. *Nat Rev Neurol*, **8**; 255-63.
Wang, Y., Cooke, M. J., Morshead, C. M. and Shoichet, M. S., 2012. Hydrogel delivery of erythropoietin to the brain for endogenous stem cell stimulation after stroke injury. *Biomaterials*, **33**; 2681-92.
Warren, K. G. and Catz, I., 1993. Autoantibodies to myelin basic protein within multiple sclerosis central nervous system tissue. *J Neurol Sci*, **115**; 169-76.
Wegner, C., Esiri, M. M., Chance, S. A., Palace, J. and Matthews, P. M., 2006. Neocortical neuronal, synaptic, and glial loss in multiple sclerosis. *Neurology*, **67**; 960-7.
Weinstock-Guttman, B., Zivadinov, R., Qu, J., Cookfair, D., Duan, X., Bang, E., Bergsland, N., Hussein, S., Cherneva, M., Willis, L., Heininen-Brown, M. and Ramanathan, M., 2011. Vitamin D metabolites are associated with clinical and MRI outcomes in multiple sclerosis patients. *J Neurol Neurosurg Psychiatry*, **82**; 189-95.
Weis, S., Llenos, I. C., Dulay, J. R., Elashoff, M., Martínez-Murillo, F. and Miller, C. L., 2007. Quality control for microarray analysis of human brain samples: The impact of postmortem factors, RNA characteristics, and histopathology. *J Neurosci Methods*, **165**; 198-209.
Weiss, H. A., Millward, J. M. and Owens, T., 2007. CD8+ T cells in inflammatory demyelinating disease. *J Neuroimmunol*, **191**; 79-85.
Weissert, R., Wallström, E., Storch, M. K., Stefferl, A., Lorentzen, J., Lassmann, H., Linington, C. and Olsson, T., 1998. MHC haplotype-dependent regulation of MOG-induced EAE in rats. *J Clin Invest*, **102**; 1265-73.
Weller, R. O., Galea, I., Carare, R. O. and Minagar, A., 2010. Pathophysiology of the lymphatic drainage of the central nervous system: Implications for pathogenesis and therapy of multiple sclerosis. *Pathophysiology*, **17**; 295-306.
Welser-Alves, J. V. and Milner, R., 2013. Microglia are the major source of TNF-alpha and TGF-beta1 in postnatal glial cultures; regulation by cytokines, lipopolysaccharide, and vitronectin. *Neurochem Int*, **63**; 47-53.
Wilfinger, W. W., Mackey, K. and Chomczynski, P., 1997. Effect of pH and ionic strength on the spectrophotometric assessment of nucleic acid purity. *Biotechniques*, **22**; 474-6, 478-81.
Williams, S. K., Maier, O., Fischer, R., Fairless, R., Hochmeister, S., Stojic, A., Pick, L., Haar, D., Musiol, S., Storch, M. K., Pfizenmaier, K. and Diem, R., 2014. Antibody-mediated inhibition of TNFR1 attenuates disease in a mouse model of multiple sclerosis. *PLoS One*, **9**; e90117.
Willis, S. N., Stadelmann, C., Rodig, S. J., Caron, T., Gattenloehner, S., Mallozzi, S. S., Roughan, J. E., Almendinger, S. E., Blewett, M. M., Brück, W., Hafler, D. A. and O'Connor, K. C., 2009. Epstein-Barr virus infection is not a characteristic feature of multiple sclerosis brain. *Brain*, **132**; 3318-28.
Wong, D. and Dorovini-Zis, K., 1995. Expression of vascular cell adhesion molecule-1 (VCAM-1) by human brain microvessel endothelial cells in primary culture. *Microvasc Res*, **49**; 325-39.
Xie, D., Schultz, R. L. and Whitter, E. F., 1995. The oligodendroglial reaction to brain stab wounds: an immunohistochemical study. *J Neurocytol*, **24**; 435-48.

Yang, L., Lindholm, K., Konishi, Y., Li, R. and Shen, Y., 2002. Target depletion of distinct tumor necrosis factor receptor subtypes reveals hippocampal neuron death and survival through different signal transduction pathways. *J Neurosci*, **22**; 3025-32.

Yokota, T., Coffman, R. L., Hagiwara, H., Rennick, D. M., Takebe, Y., Yokota, K., Gemmell, L., Shrader, B., Yang, G., Meyerson, P. and et al., 1987. Isolation and characterization of lymphokine cDNA clones encoding mouse and human IgA-enhancing factor and eosinophil colony-stimulating factor activities: relationship to interleukin 5. *Proc Natl Acad Sci U S A*, **84**; 7388-92.

Zeis, T., Kinter, J., Herrero-Herranz, E., Weissert, R. and Schaeren-Wiemers, N., 2008. Gene expression analysis of normal appearing brain tissue in an animal model for multiple sclerosis revealed grey matter alterations, but only minor white matter changes. *J Neuroimmunol*, **205**; 10-9.

Zhang, E. T., Richards, H. K., Kida, S. and Weller, R. O., 1992. Directional and compartmentalised drainage of interstitial fluid and cerebrospinal fluid from the rat brain. *Acta Neuropathol*, **83**; 233-9.

Zhao, C., Strappe, P. M., Lever, A. M. and Franklin, R. J., 2003. Lentiviral vectors for gene delivery to normal and demyelinated white matter. *Glia*, **42**; 59-67.

Zhu, J., Yamane, H. and Paul, W. E., 2010. Differentiation of Effector CD4 T Cell Populations. *Annual Review of Immunology*, **28**; 445-489.

Zivadinov, R., Iona, L., Monti-Bragadin, L., Bosco, A., Jurjevic, A., Taus, C., Cazzato, G. and Zorzon, M., 2003. The use of standardized incidence and prevalence rates in epidemiological studies on multiple sclerosis. A meta-analysis study. *Neuroepidemiology*, **22**; 65-74.